

**Zeitschrift:** IABSE reports = Rapports AIPC = IVBH Berichte  
**Band:** 54 (1987)  
**Rubrik:** Session 1: Modelling of material behaviour (advances)

### **Nutzungsbedingungen**

Die ETH-Bibliothek ist die Anbieterin der digitalisierten Zeitschriften auf E-Periodica. Sie besitzt keine Urheberrechte an den Zeitschriften und ist nicht verantwortlich für deren Inhalte. Die Rechte liegen in der Regel bei den Herausgebern beziehungsweise den externen Rechteinhabern. Das Veröffentlichen von Bildern in Print- und Online-Publikationen sowie auf Social Media-Kanälen oder Webseiten ist nur mit vorheriger Genehmigung der Rechteinhaber erlaubt. [Mehr erfahren](#)

### **Conditions d'utilisation**

L'ETH Library est le fournisseur des revues numérisées. Elle ne détient aucun droit d'auteur sur les revues et n'est pas responsable de leur contenu. En règle générale, les droits sont détenus par les éditeurs ou les détenteurs de droits externes. La reproduction d'images dans des publications imprimées ou en ligne ainsi que sur des canaux de médias sociaux ou des sites web n'est autorisée qu'avec l'accord préalable des détenteurs des droits. [En savoir plus](#)

### **Terms of use**

The ETH Library is the provider of the digitised journals. It does not own any copyrights to the journals and is not responsible for their content. The rights usually lie with the publishers or the external rights holders. Publishing images in print and online publications, as well as on social media channels or websites, is only permitted with the prior consent of the rights holders. [Find out more](#)

**Download PDF:** 05.01.2026

**ETH-Bibliothek Zürich, E-Periodica, <https://www.e-periodica.ch>**



## **SESSION 1**

**August 26, 1987 (morning)**

**Modelling of Material Behaviour (Advances)**

**Modélisation du comportement des matériaux (progrès)**

**Modellierung des Materialverhaltens (Fortschritte)**

Chairman: K.H. Gerstle, USA

Invited Lecturers: P.G. Gambarova, Italy  
Modelling of Interface Problems in Reinforced Concrete

T. Tanabe, H. Yoshikawa, Japan  
Constitutive Equations of a Cracked Reinforced Concrete Panel  
by the Damage Tensors and the Reinforcement Tensors



Leere Seite  
Blank page  
Page vide

## Modelling of Interface Problems in Reinforced Concrete

Modélisation des problèmes d'interface dans le béton armé

Mathematische Modelle für Oberflächenprobleme im Stahlbeton

### Pietro G. GAMBAROVA

Prof. of Struct. Eng.  
Politecnico di Milano  
Milan, Italy



Pietro G. Gambarova, born 1941, obtained his Degree in Aeronautical Engineering at the Politecnico di Milano in 1966. He was first interested in Stress Analysis and then in special problems regarding Concrete Mechanics (shear transfer, bond, multiaxial behavior). In 1980 he became Professor of Structural Eng. and is currently Head of the Department of Structural Engineering.

### SUMMARY

Some recent advances in mathematical models are presented for the most important interface problems, which regard plain concrete as well as concrete interacting with the reinforcement. Emphasis is placed on basic phenomena such as aggregate interlock and cracked concrete shear stiffness, steel-to-concrete bond with or without longitudinal splitting, dowel action with or without axial force, transmission of tensile forces across open cracks. Whenever the phenomenological aspects of a problem are clear, constitutive laws are presented and illustrative examples are shown.

### RÉSUMÉ

L'article présente les progrès les plus récents dans la modélisation mathématique des phénomènes d'interface dans le béton armé et non-armé. L'attention est concentrée sur les problèmes de caractère général, comme l'interaction des agrégats dans la transmission du cisaillement, l'adhérence entre l'armature et le béton (avec ou sans le fendage du béton), l'effet de goujons des barres (avec ou sans force axiale), la transmission des forces de traction à travers les fissures ouvertes. Chaque fois que la phénoménologie des problèmes est bien connue, on présente des lois constitutives, ainsi que des exemples.

### ZUSAMMENFASSUNG

Es werden hier die letzten Fortschritte im Bereich der mathematischen Modelle für Oberflächenprobleme im bewehrten und nicht bewehrten Beton vorgestellt. Besondere Aufmerksamkeit wird allgemeinen Fragen geschenkt, unter anderen der Rissuferverzahnung, der Schubsteifigkeit im gerissenen Beton, dem Stahl-Beton-Verbund mit oder ohne Spaltrissen, der Dübelwirkung mit oder ohne Achsialkraft, der Zugkraftübertragung durch offene Risse. Jedesmal, wenn die Phänomenologie der Probleme wohlbekannt ist, werden Grundgesetze und Beispiele zur Erläuterung vorgestellt.



## 1. INTRODUCTION

The Colloquium Delft 87 on Computational Mechanics of Reinforced Concrete comes six years after the Colloquium Delft 81 on Advanced Mechanics of Reinforced Concrete, and though this length of time is relatively short compared to the nearly centennial history of modern concrete, yet the remarkable amount of work done in the past six years makes it possible to draw useful suggestions on future developments of both basic research and applications in the field of concrete and reinforced concrete structures.

As a matter of fact, six years are quite a long period if one thinks of the remarkable growth in the number of scientists investigating the basic aspects of concrete, improving the analysis, developing or refining computational techniques, updating the codes in order to make them more sound and more exhaustive. All this is undeniably favoured by the rapid dissemination of the information through the many magazines, journals and special publications regarding the materials and the structures.

Nevertheless, six years are quite a short period, as already emphasized: as a consequence, fundamental novelties can hardly be expected, since new ideas arise, ripen and develop more slowly than the evolution of computational and investigation techniques, though - of course - the evolution of the latter is a great spur to new ideas.

Before getting to the heart of the problems mentioned in the heading of this paper, it seems useful to remember briefly what has been done so far in the eighties, and even to go back to the inheritance of the previous twenty years.

We have to recognize that in a certain way the inheritance of the sixties lies in the astonishing amount of experimental research work, regarding both the basic behavior of concrete as a structural material (for example, uni-, bi- and tri-axial behavior) and the behavior of the structural elements, either in the working load stage or at collapse. At the same time, some scientists seized the opportunity to examine closely several basic but rather involved aspects of concrete and r.c. structures such as bond, strain softening, microcracking.

The inheritance of the seventies lies in the really remarkable effort to develop and to formulate suitable constitutive laws for describing concrete multiaxial behavior: these laws were devised primarily to be introduced into finite element programs aimed at the analysis of structural elements. As a consequence, often the scientists directed their attention more to the development of semiempirical, computer-oriented constitutive laws, than to the understanding of such basic phenomena as bond, strain softening, cracked concrete shear stiffness, crack formation and propagation. Anyhow, the test results obtained in the sixties and early seventies proved to be an invaluable landmark.

Finally, with regard to the eighties, it is too early to speak of an inheritance, but some indications can be drawn by re-examining briefly the most recurrent topics in the literature. It is easy to recognize that a renewed interest in basic problems has developed, with the twofold purpose of improving our understanding of the phenomena, and of formulating more rational, more realistic and (if possible) simpler constitutive laws.

An examination of the papers published since 1981 in six of the most respected magazines and journals (ASCE Journal of the Mechanical Engineering Division, ASCE Journal of Structural Engineering, Magazine of Concrete Research, ACI Journal, Materials and Structures, Cement and Concrete Research) shows that 77% (Fig. 1a) of the nearly 200 papers on concrete and r.c. structures deal with basic problems, and that 23% deal with the behavior of structural elements (beams, columns, frames, panels, slabs, shells). Furthermore, 1 out of 3 papers dealing with basic problems (Fig. 1b) are aimed at the constitutive laws for solid concrete (multiaxial behavior, failure criteria, impact and fatigue loads, damage theory, endochronic theory, orthotropic models, effects of passive confinement), 1 out of 3

papers are on the so-called interface problems (steel-to-concrete bond, dowel action, aggregate interlock, cracked concrete behavior), 1 out of 4 papers deal with crack formation and propagation (concrete fracture mechanics, continuum damage mechanics, size effect, concrete tensile behavior, strain-softening included). Finally, 1 out of 8 papers are on the rheological behavior of concrete.

The widespread interest in basic problems and constitutive laws is confirmed by the many specialised conferences and symposia, held in the last few years, which have offered many opportunities for the circulation of early results and of not yet fully developed theories. Among others, the following conferences or symposia can be quoted: Bond in Concrete (1982 [1]); Constitutive Laws for Engineering Materials (1983 and 1987 [2,7]); Mechanics of Geomaterials: Rocks, Concretes, Soils (1983 [3]); Application of Fracture Mechanics to Cementitious Composites (1984 [4]); Partial Prestressing: from Theory to Practice (1984 [5]); Creep and Shrinkage of Concrete: Mathematical Modelling (1986 [6]).

At the end of this very rapid and certainly not exhaustive review of the topics investigated over the last six years, one has to admit that - in spite of the remarkable increase of the total number of papers published in the last three years (Fig. 1c) - relatively little attention has been devoted to the behavior of concrete and r.c. structures under severe or even extremum temperature conditions. High temperatures may, for instance, occur in the secondary containment shells of nuclear reactors; on the other hand, very low temperatures are to be expected in the reinforced concrete walls of the cells which are being considered for the storage of electric energy, taking advantage of the superconductivity of huge metallic coils kept at very low temperature (this application of reinforced concrete is however for the years to come!).

Another problem, which is still regarded by many as "non structural", is the problem of durability: nevertheless, since many r.c. or prestressed structures are attaining their design life, structural durability can no longer be underevaluated and should be taken in due consideration in the formulation of constitutive laws.

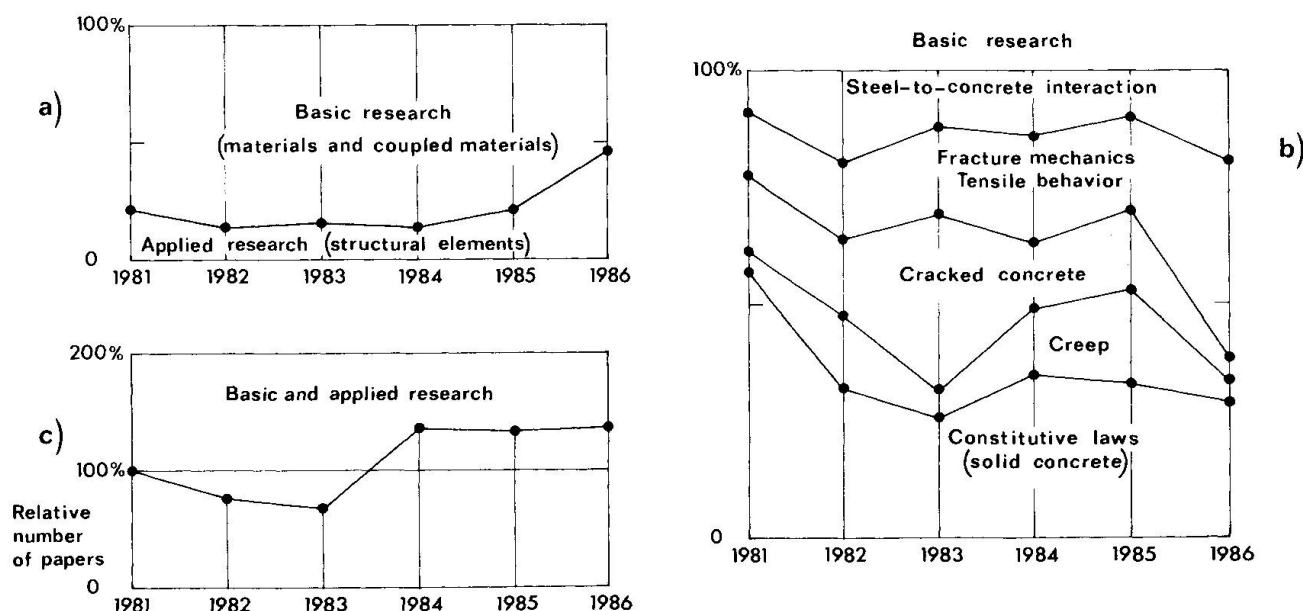


Fig.1 - Statistics regarding the papers published in 6 top journals and magazines (1981-1986) : (a) basic and applied research ; (b) distribution among different topics ; (c) number of published papers with respect to 1981.



## 2. INTERFACE PROBLEMS IN REINFORCED CONCRETE ELEMENTS

As shown in Fig. 1b much effort has also been devoted recently to the so-called interface problems, which are really typical of reinforced concrete. As emphasized by Vintzeleou and Tassios in [8], interface problems are characterized by a variety of aspects which are partly basic and partly structural. Four fundamental lines have been pursued in the study of steel-to-concrete and concrete-to-concrete interfaces.

Steel-to-Concrete Interfaces: Bond. Bond embraces all the phenomena of a chemical and physical nature, which allow the transmission of shear forces between the reinforcement and the concrete: consequently, bond is the very essence of r.c. elements.

As to chemical adhesion and bearing action (this latter characterized by the local crushing of the concrete keys in contact with the bar lugs), bond is essentially a basic problem limited to the two "coupled" materials (concrete and reinforcement, Fig. 2a); as to the mechanical interaction after cover and interspace cracking (due to longitudinal splitting), bond is essentially a structural problem (Fig. 2b), since concrete cover, bar free interspace and stirrup arrangement play a leading role.

Because of the fundamental role of bond, in the working load stage as well as at collapse, the formulation of realistic and reliable constitutive relationships between the bond stress and the bar slip, with or without concrete splitting, is still an important goal to be achieved.

Dowel Action. Dowel action embraces all the mechanical phenomena which permit considerable amounts of shear to be transferred across a crack, because of the local bending and shear stiffness of the bars at the crack interface, and also because of the remarkable stiffness and strength of the concrete, which is highly confined locally, close to the reinforcement. Whenever the shear transfer involves two contiguous structural elements (Fig. 2c) or two different parts of the same element, cast at different times (Fig. 2d), the dowel action is already active in the working load stage; whenever a single element, cast at the same time, is subjected to shear, the resisting contribution of dowel action becomes relevant only in a very advanced stage of the loading process, after the development of tensile or shear cracks (Fig. 2e). The dowel action is essentially a structural problem, but it may be reduced to a material problem once the constitutive laws of the reinforcement are formulated in such a way that concrete cover, bar free interspace and transverse reinforcement are properly introduced, together with the still largely unknown effects of the axial force in the main reinforcement.

Concrete-to-Concrete Interfaces: Aggregate Interlock. Aggregate interlock embraces all the mechanical phenomena which allow the transmission of considerable amounts of shear across a rough, generally open and continuous crack. Of course, in order to have aggregate interlock activated, a suitable confinement action must be provided either by the reinforcement crossing the crack, or by the structural restraints. Should cracking be regular, with parallel and closely spaced cracks (Fig. 2f), aggregate interlock could be considered as a material problem and its constitutive laws could be regarded as a property of (cracked) concrete.

Though the phenomenological aspects of aggregate interlock are well known, either at constant confinement or at constant crack opening, or even at constant restraining stiffness (transverse stiffness), more work has still to be done on spatial cracks, cyclic loads, dynamic behavior of cracked concrete.

Transfer of Tensile Forces across a Crack. As shown in Fig. 1b, a great deal of attention has recently been devoted to concrete fracture mechanics and - more generally - to the tensile behavior of concrete, strain softening included. As emphasized by Bazant in [9], concrete cracking starts as a process distributed over a crack band, because of the discontinuities of the concrete at the micro-

level, and only in an advanced stage does cracking become localized, as a consequence of the release of the energy accumulated within the crack band. The specific fracture energy, as well as the width of the crack band can be regarded as material properties, the latter being a few times (1 to 3) as large as the maximum aggregate size.

Once cracking coalesces into blunt, continuous cracks, new interfaces are formed and the role of these interfaces in transferring tensile forces is a challenging problem. To this end, the analysis of the tensile response of cracked concrete must be extended to localized, continuous and open cracks (a few tenths of a millimeter, Fig. 2h), well beyond the crack width values that are generally investigated with regard to the process zone at the tip of a developing crack (a few thousandths of a millimeter, Fig. 2g).

The formulation of suitable constitutive laws for relatively large values of the crack width may be of great interest in certain problems such as the analysis of the flexural behavior of r.c. beams, since the moment-curvature diagrams are greatly influenced by the transfer of tensile forces in a section during the transition from the 1st uncracked to the 2nd cracked stage.

In the following Sections the different interface problems will be examined and the available constitutive laws will be discussed, as well as the developments in progress and the advances to be expected.

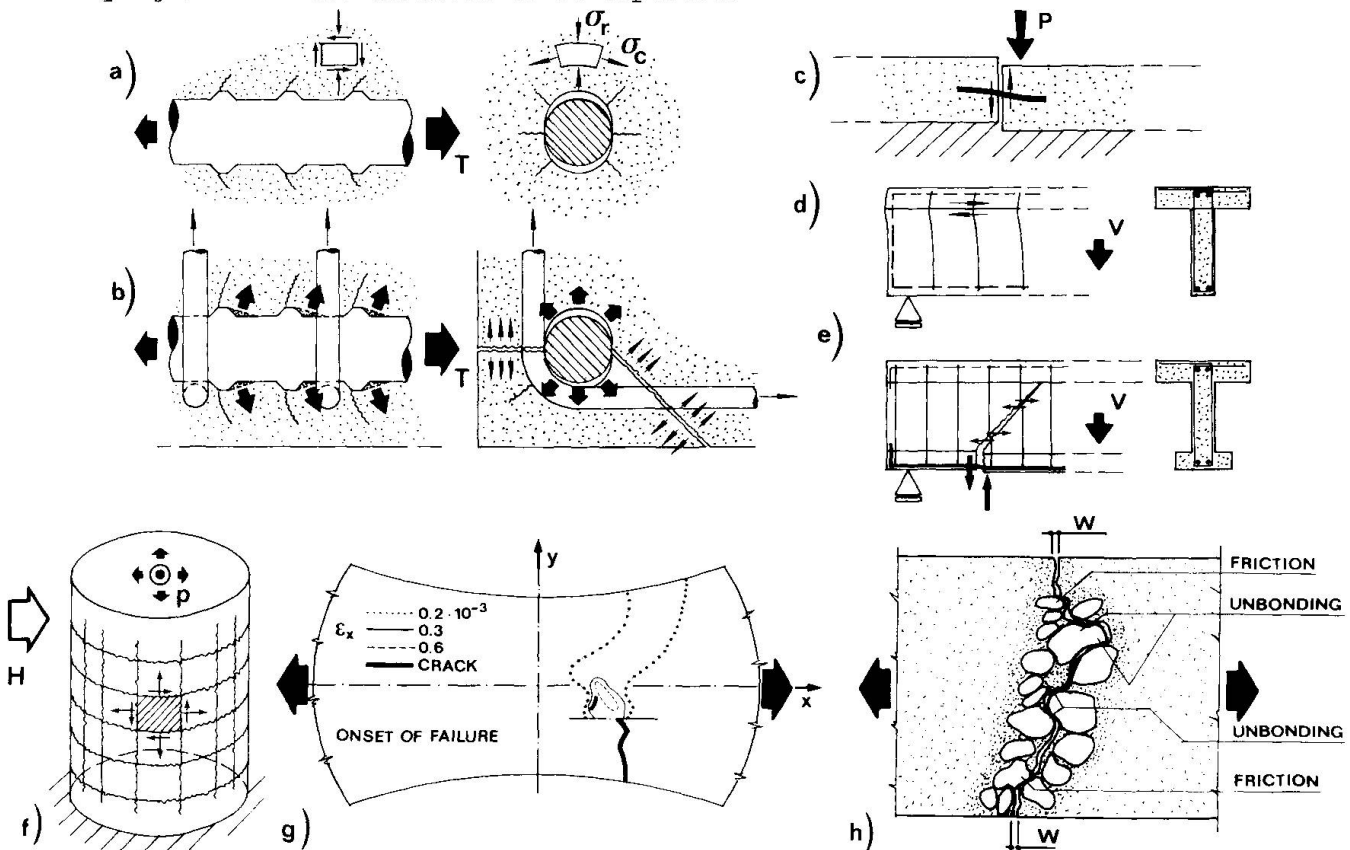


Fig.2 - Various types of interfaces : (a,b) steel-to-concrete bond ; (c,d,e) dowel action ; (f) aggregate interlock ; (g,h) tensile fracture: developing crack (g) [34] and through crack (h) [35].

### 3. BOND

In spite of the great amount of research work done in this area, bond is still a topical subject for different reasons. Primarily this is because of the many parameters involved, but also because of the ongoing improvements in the mechanical prop-





erties of both concrete and steel, as often required by special structures or unusual environmental situations ( $f_{sy} = 500 - 600 \text{ MPa}$ ,  $f'_c > 100 \text{ MPa}$ ). Because of the problems which are still open, the formulation of suitable constitutive relationships is far from definite. As a matter of fact, beside a few well defined main parameters (such as bond stress, confinement stress, shear strain in the concrete and bar slip, interface dilatancy accompanied by longitudinal splitting), many other parameters are involved, either geometrical (concrete cover, bar interspace) or mechanical (transverse reinforcement, loading rate, cyclic loading), physical (temperature of the structure) and technological (casting modalities and type of formwork).

Apart from the technological aspects (which are often very critical, see for instance Schmidt-Thrö, Stöckl, Kluge and Kupfer "Tests on the Bond Behavior of Bars in Slipform Concrete Structures", DAfSt, Heft 378, Berlin, 1986), the basic problems being investigated nowadays are: local bond-slip law (Yankelevsky [13]; Jiang, Shah and Andonian [14]; Lahnert, Houde and Gerstle [36]), bond behavior with transverse and splitting cracks (Tepfers [10]; Gambarova, Rosati and Zasso [11]; Giuriani and Plizzari [12]), effects of lateral pressure (Robins and Standish, MCR, Vol.36, No.129, Dec.1984), temperature (Morley and Royles, MCR, Vol. 35, No.123, June 1983), loading rate (Vos and Reinhardt, Mat. and Structures, Vol. 15, No.85, 1982) and fatigue (Johnston and Zia, Mat. and Struc., Vol.17, No.97, 1984).

Great attention has been lately devoted also to the analysis of bond at the local level, considering the local effects of bar lugs pushing against the concrete, and the individual microcracks originating at bar-to-concrete interface. Generally, complex F.E. programs have been used. Two papers are particularly relevant in the author's opinion, because of the different approaches used in bond analysis. In the first paper (Reinhardt, Blaauwendraad and Vos [15]) the concrete layer (slip layer, Fig. 4) close to a bar is modeled by means of axisymmetric, torus-like elements with nonlinear behavior, whilst the surrounding mass is considered as linearly elastic: transverse microcracking is introduced through a suitable law in tension with a softening branch; a Mohr - Coulomb's failure surface is adopted for compression. In the second paper (Ingraffea, Gerstle, Gergely and Saouma [16]) the transverse cracks are modeled by means of suitable interfaces (the mesh is refined at each loading step, Fig. 3) and a nonlinear fracture mechanics scheme is adopted to model mixed-mode concrete fracture. As an alternative, special tension softening elements are introduced at the interface between a bar and the concrete, wherever a transverse crack may originate.

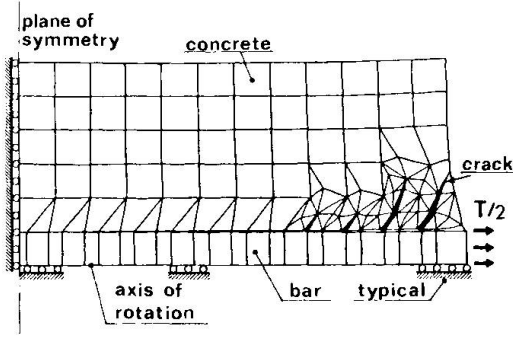
With regard to bond behavior after concrete splitting, we may observe that many tests and several models have been so far devoted to the evaluation of the ultimate force (cracking resistance) in the case of short embedments (i.e. with a limited bond length), with no transverse reinforcement (see for instance Tepfers [10], Fig. 5). On the other hand, much less effort has been made to investigate the effects of longitudinal splitting on bond, when adequate confinement is exerted by the transverse reinforcement.

The cracking resistance  $f_{bc}$  of a short anchorage with no transverse reinforcement lies between the following limits (Fig.5) :

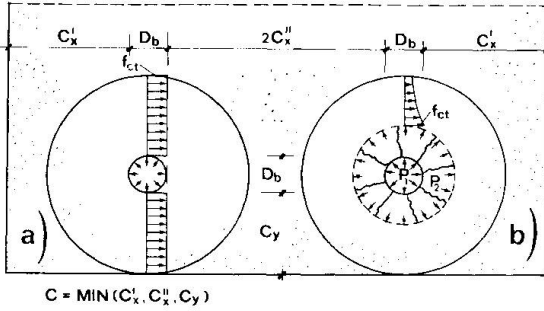
$$f'_{bc} = f_{ct} \frac{c + D_b/2}{1.664 D_b \tan \alpha} \text{ (elasto-cracked model); } f''_{bc} = f_{ct} \frac{2c}{D_b \tan \alpha} \text{ (plastic model)}$$

where  $\alpha$  is the average angle between the transverse cracks in the concrete and the axis of the bar ( $\alpha \approx 45^\circ$ ), and  $f_{ct}$  is the tensile strength of the concrete. As a matter of fact, the test results fall between  $f'_{bc}$  (lower bound) and  $f''_{bc}$  (upper bound) [10].

As soon as the bond stress reaches  $f_{bc}$  at any section of the bar, bond efficiency is guaranteed primarily by the transverse reinforcement (mostly by its bond properties) and by the interaction between bond and confinement stresses at the bar-to-concrete interface; secondly, by the tensile stresses transmitted across



▲ Fig. 3 - Deformed mesh of portion of tension pull-out specimen with four secondary cracks [16].



▲ Fig. 4 - Axisymmetric representation of slip layer (a) and F.E. mesh of a slip layer section (b) [15].

◀ Fig. 5 - Hoop stresses close to a bar according to the perfectly plastic model (a), and to the elasto-cracked model (b) by Tepfers [10].

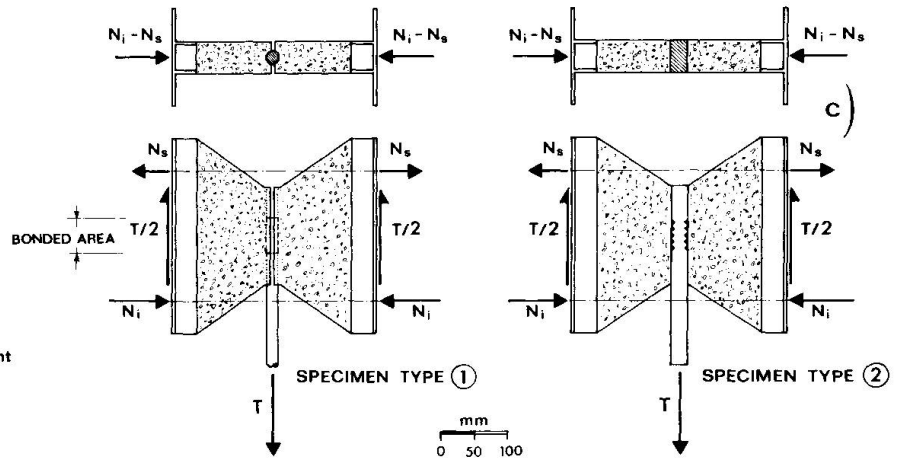
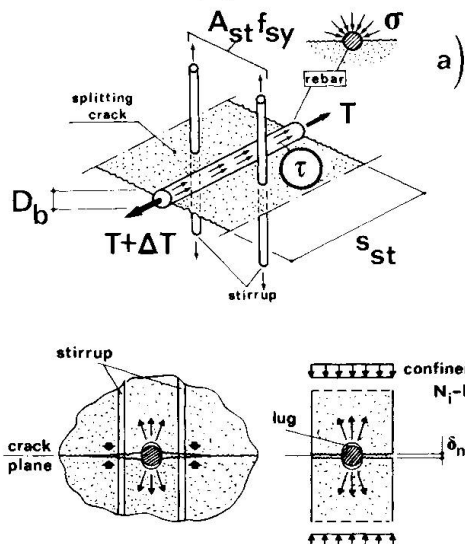


Fig. 6

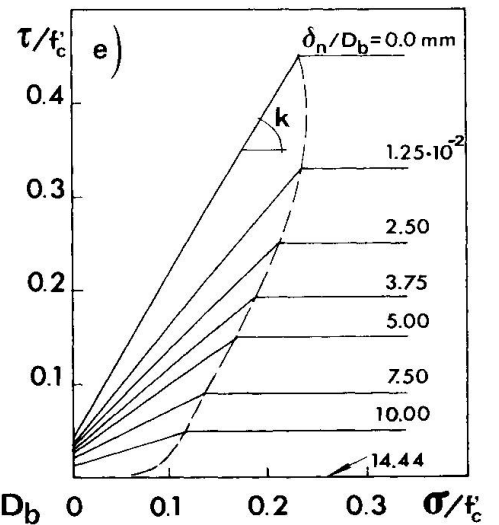
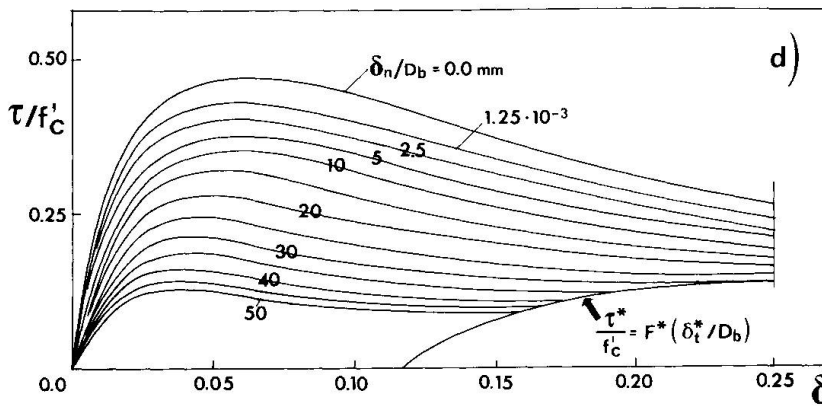


Fig. 6 - (a) Interaction between a longitudinal bar and a two-leg stirrup; (b) Actual splitting crack and idealised splitting crack [11]; (c) Pre-splitted specimens tested in [11] ( $N_s, N_i$  confinement forces); (d) Shear-slip constitutive law; (e) Shear-confinement envelopes.





the plane of the splitting crack. In [11] three series of precracked specimens (Figs. 6b, c) reinforced with a single deformed bar ( $D_b = 18\text{ mm}$ ), and characterised by a short bond length ( $l_b/D_b \approx 3$ ) were subjected to pull-out tests, the crack width being kept constant throughout each test. The local bond-slip relationship (Fig. 6d) was given the following empirical formulation:

$$\frac{\tau}{f'_c} = R(w) \frac{\Delta}{1 + a_1 \Delta + a_2 \Delta^2 + a_3 \Delta^3}, \quad \text{with } \Delta = \delta_t^*/D_b \text{ and } w = \delta_n/D_b,$$

where  $\delta_t^* = \delta_t - \delta_t^0$  is the net bar slip,  $\delta_n$  is the crack opening and  $R, a_1, a_2, a_3, \delta_t^0$  are parameters related to  $\delta_n/D_b$ . The bond-confinement curves at constant crack width (Fig. 6e) were idealised as trilateral envelopes:

$$(\tau/f'_c) = (\tau_0/f'_c) + k(\sigma/f'_c) \quad \text{with } (\tau_0/f'_c) = a_4 - a_5 w, \quad k = a_6 - a_7 \sqrt{w},$$

$$\sigma/f'_c \leq 0.35, \quad \text{where } a_4, a_5, a_6, a_7 \text{ are constants.}$$

Since in structural analysis with F.E. programs it is much more expedient to introduce a comprehensive bond-slip relationship (longitudinal splitting and confinement included) than to push the analysis to such details as local cracking at the bar-to-concrete interface and bar-to-stirrup interaction, further studies on the effects of splitting and on the efficiency of transverse reinforcement are needed (see for instance Giuriani [12]).

#### 4. DOWEL ACTION

The transfer of membrane forces across cracks in r.c. containment vessels, as well as the transfer of shear forces in the partially cracked sections of a r.c. beam are largely based on the dowel action mechanism which accounts for 15 to 35% of the overall shear to be transmitted by the various shear mechanisms (Fig. 7). As a consequence, dowel action is an important interface mechanism, which has essentially structural aspects.

From both a phenomenological and a speculative point of view, the dowel action is characterised by several interesting aspects, which regard: bond, tensile strength of concrete and concrete fracture mechanics, bar-to-stirrup interaction with stirrup tension stiffening.

Since the dowel action is active after concrete cracking, the interaction between the tensile and dowel forces in the main reinforcement should always be taken into due account. As a matter of fact, any variation in the tensile force is accompanied by bond stresses, which produce a complex three-dimensional crack pattern (Fig. 8), consisting of transverse microcracks and longitudinal splitting cracks; cracking in turn modifies the stiffness properties of the concrete embedment of the main reinforcement and further cracking may occur. Nevertheless, should bond failure be due to concrete crushing (pull-out failure: short embedment length, high bond properties, large cover, large stirrup ratio), the local microcracking would not markedly affect the maximum dowel force, as long as the tensile force remains below 80-90% of the pull-out force (Fig. 9a). For long embedments, steel yielding precedes bar pull-out and the tensile force should be better adimensionalized with the yield force (Fig. 9b). The equation of the heavy full-line envelope is given by Soroushian and others in [17]:

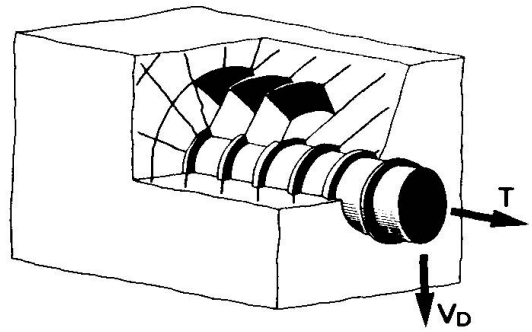
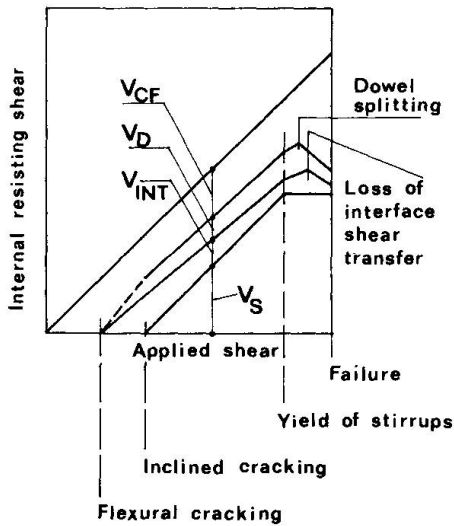
$$V_{Du} = 0.0685 \gamma^2 d^2 f_b + 0.45 f_y d^2 (1 - T^2/T_y^2) / \gamma$$

where:  $\gamma = \sqrt[4]{E_s/K_f d}$ , with  $K_f = 272 \text{ MPa/mm}$  (foundation modulus)

$d$  = dowel bar diameter (mm);  $E_s$  = dowel Young's modulus (MPa)

$f_b = 37.6 \sqrt{f'_c}/\sqrt[3]{d}$  = concrete bearing strength (MPa);  $f_y$  = dowel yield stress (MPa)

$T, T_y$  = axial force in the dowel, axial force at yielding.



► Fig.8 - Crack pattern close to a bar subjected to tension and dowel force.

◄ Fig.7 - Distribution of internal shears in a r.c. beam with web reinforcement.

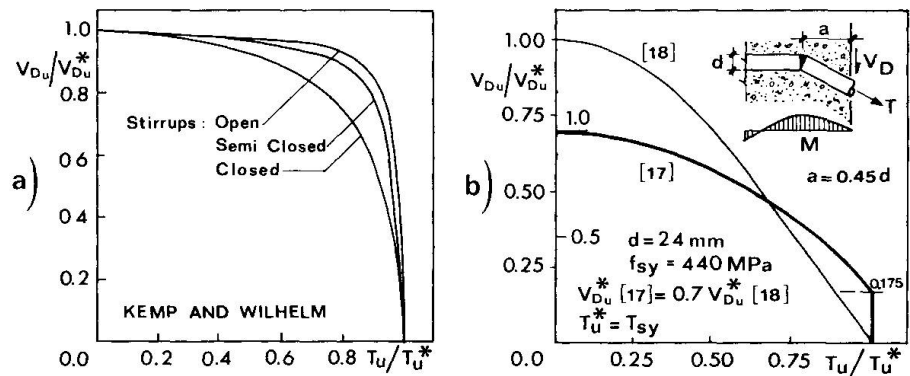
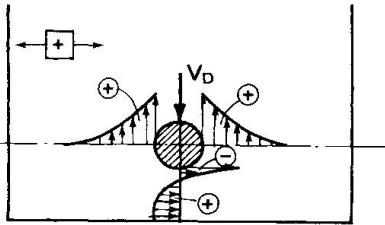


Fig.9 - Failure envelopes for short anchorage lengths (a) : pull-out failure, and for long anchorage lengths (b) : failure due to bar yielding, according to Soroushian et al. [17], and to Vintzeleou and Tassios [18].



▲ Fig.10 - Hoop stresses close to a bar subjected to a dowel force.

▼ Fig.11 - Bending of a bar subjected to dowel action: (a) against concrete cover and (b) against concrete core.

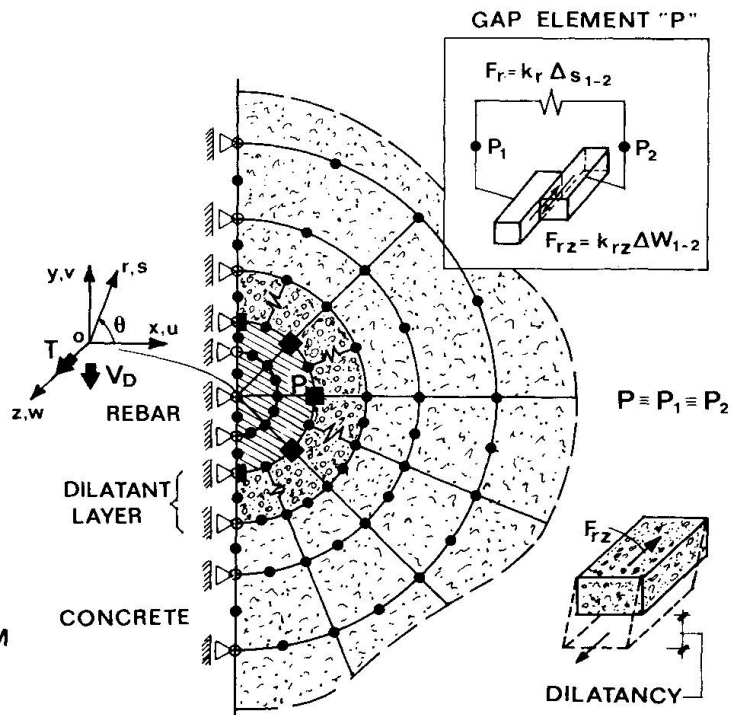
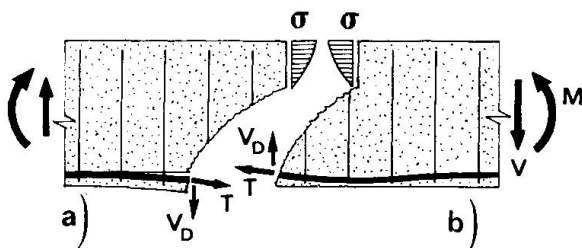


Fig.12 - Possible modelisation of the bar-to-concrete interface.



In Fig. 9b the thin envelope regards the section with the largest bending moment at the verge of plastic collapse (the section is plasticized either in tension or in compression): the dowel strength with no axial force is evaluated according to Vintzeleou and Tassios [18]. The difference between the two envelopes (Fig. 9b) is an indication of the further research work which is still needed in this area.

In case of no transverse reinforcement, with usual bar interspaces and concrete covers, dowel failure is due neither to concrete crushing nor to bar yielding, but to cover and interspace splitting, as shown in [18]. For this purpose, relevant confinement forces can be developed by the interface of the splitting crack (Fig. 10): this fact has been known for some time, but only recent results allow the evaluation of the tensile stresses which can be transferred across really open and continuous cracks (see Sect. 6), having width equal to several tenths of a millimeter.

Most of the research workers in the last 20 years have limited their attention to the maximum dowel force causing concrete splitting (Dulacska, 1972; Paulay, Park and Phillips, 1974; Taylor, 1974; Stanton, 1976), a few have recognized the importance of stirrup arrangement and concrete tensile strength (Baumann and Rüschi, 1970), of the axial force (Kemp and Wilhelm, 1977) and of the need for suitable mathematical models (Johnston and Zia, 1971). Recently, the many test results by Utescher and Herrmann (1983 [20]), and by Paschen and Schönhoff (1983 [21]) have shed further light on the failure of the bars and of the concrete, on the role of the cover, shape and arrangement of the stirrups. These results may hopefully foster the development of exhaustive mathematical models, which - in the writer's opinion - should reduce the complex structural problem to a material problem, through the formulation of suitable constitutive laws for the main reinforcement. To this end, further test results are needed with regard to the interaction between the dowel and the tensile forces, the deflection of a bar inside the concrete mass (Fig. 11), the interaction between the bars and the stirrups.

Numerical analysis may also give a decisive contribution, especially for the study of bar-to-concrete interaction: as an example (Fig. 12), the interface may be modeled by means of (I) a finite element layer with dilatant properties, in order to introduce bond dilatancy due to the wedging effects of the bar lugs; (II) gap-type elements, which transmit a frictional force and bring on a relative slip at the interface; (III) nonlinear, spring-like elements connecting the bar to the outer concrete elements, in order to reproduce the mechanical properties of the concrete embedment, as needed by the modelisation of the dowel action.

## 5. AGGREGATE INTERLOCK

The shear transfer mechanism based on aggregate interlock has been known for a long time in its behavioral aspects, owing to the many test results obtained in the sixties and early seventies. As a consequence of these tests, basic concepts such crack dilatancy (i.e. coupling between shear stress and crack opening, between normal stress and crack slip) and shear-confinement interaction were fully understood, the latter concept being still recently investigated for the purpose of developing new constitutive laws [27].

The remarkable experimental effort has not been matched by a comparable effort in the formulation of rational constitutive laws, because only recently have the properties of aggregate interlock been recognized as material properties. As a matter of fact, the formulation of suitable constitutive laws for cracked concrete became necessary after the concept of smearing the cracks over an entire element was shown to be highly suitable for F.E. analysis.

So far, most of the efforts have been devoted to planar cracks subjected to monotonic loading, in order to formulate the incremental stiffness matrices of a crack

[B], and of cracked concrete (for the symbols see Fig. 13) :

$$\begin{Bmatrix} d\sigma_{nn}^c \\ d\sigma_{nt}^c \end{Bmatrix} = \begin{bmatrix} B_{nn} & B_{nt} \\ B_{tn} & B_{tt} \end{bmatrix} \begin{Bmatrix} d\delta_n \\ d\delta_t \end{Bmatrix} ; \quad \begin{Bmatrix} d\sigma_{nn}^c \\ d\sigma_{tt}^c \\ d\sigma_{nt}^c \end{Bmatrix} = s \begin{bmatrix} B_{nn} & 0 & B_{nt} \\ 0 & 0 & 0 \\ B_{tn} & 0 & B_{tt} \end{bmatrix} \begin{Bmatrix} d\epsilon_n^{cr} \\ d\epsilon_t^{cr} \\ d\gamma_{nt}^{cr} \end{Bmatrix}$$

where:  $d\epsilon_n^{cr} = d\delta_n/s$ ,  $d\gamma_{nt}^{cr} = d\delta_t/s$ ,  $s$  = cracking spacing (to be considered as a state variable, i.e. a function of the strain field and of the reinforcement characteristics, in r.c. elements). Note that [B] is neither positive definite, nor symmetric.

Due to the complexity of the problem (which involves 4 parameters,  $\delta_n$ ,  $\delta_t$ ,  $\sigma_{nn}^c$ ,  $\sigma_{nt}^c$ , in planar cracks), the tests have been mostly performed by decoupling either the interface displacements (tests at constant crack opening, Fig. 14c) or the stresses (tests at constant confinement, Fig. 14d); as a consequence, the constitutive laws proposed so far are mostly based on the total deformation theory, according to the following general formulations:

$$\sigma_{nn}^c = N(\delta_n, \delta_t), \quad \sigma_{nt}^c = T(\delta_n, \delta_t) \quad \text{or} \quad \sigma_{nt}^c = T(\sigma_{nn}^c, \delta_t), \quad \delta_n = \Delta(\sigma_{nn}^c, \delta_t)$$

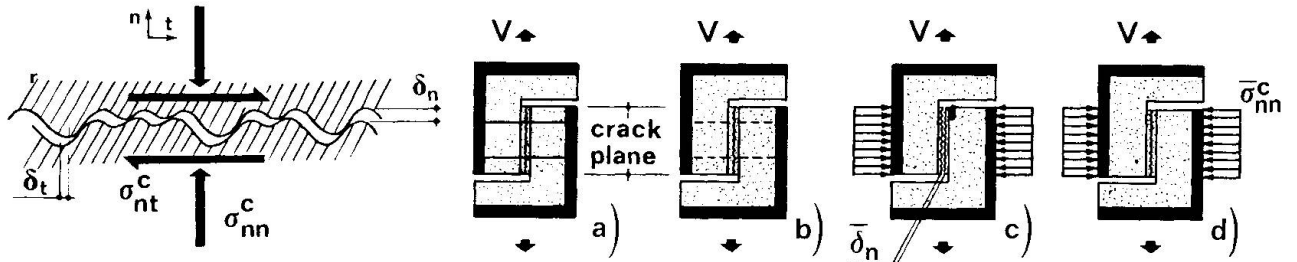
Of course path-independency hardly agrees with the very nature of interface phenomena, but there is little experimental evidence on the importance of aggregate interlock path-dependency.

As to research after Colloquium Delft 81 (for previous research see Bazant and Gambarova, "Rough Cracks in Reinforced Concrete", J. Struc. Div. ASCE, 106 - 1980, pp. 559-582), the following studies are to be cited: test results with constant or variable confinement stiffness (Fig. 14a, b) and Two-Phase Model (Walraven [22]), test results both at constant confinement and at constant crack opening (Fig. 14c, d, Daschner and Kupfer [23]), improvements of Rough Crack Model (Gamborova and Karakoç, see the References quoted in [24] and [25]), test results at constant or variable confinement stiffness (Fig. 14a, b, Millard and Johnson [26]), test results at constant confinement (Fig. 14d) and Dilatancy Factor Model (Divakar, Fafitis and Shah [27]). A further mathematical model which has been successfully applied to the description of aggregate interlock is the so-called Microplane Model (Bazant, Oh, Gambarova, see for instance [28]). Finally, a few engineering models for shear transfer (aggregate interlock and other mechanisms) have been lately proposed (see Perdikaris and White [29], and Yoshikawa and Tanabe [19]).

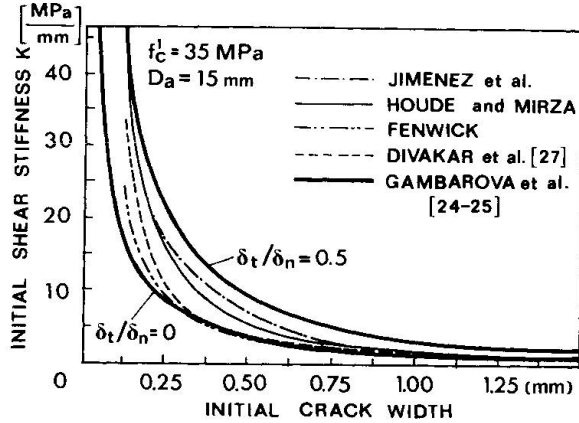
The 4 above-mentioned mathematical models have been thoroughly checked by fitting many of the available test results, and can be considered both realistic and reliable.

### 5.1 Rough Crack Model [24, 25]

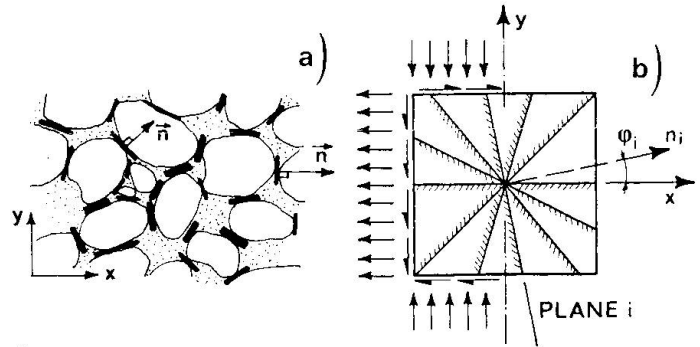
The constitutive laws have a mostly empirical formulation, since they are based on Paulay and Loeber's test results. Nevertheless, the formulation introduces a few general properties to be expected for a crack, such as: (a) the wedging effects of interface asperities make the shear stress mostly dependent on the slip-to-opening ratio  $r = \delta_t/\delta_n$  (this is certainly true for trapezoidal asperities); (b) for small crack openings, the confinement force is not needed (this is certainly true for spherical asperities); (c) for large values of the displacement ratio,  $r$ , the shear stress must exhibit an asymptote, because of microcracking and crushing in the mortar close to the aggregate particles; (d) for large values of the crack opening, the contact at the interface is lost ( $\delta_n > d_a/2$  where  $d_a$  is the maximum aggregate size); (e) the grading of the aggregates matches Fuller's curve. The constitutive laws are as follows:



▲ Fig. 13 - Crack morphology. Fig. 14 - Different specimens for the study of aggregate interlock.

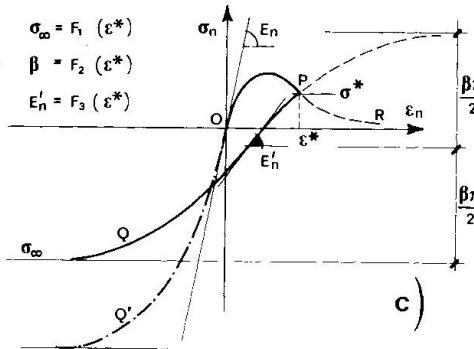
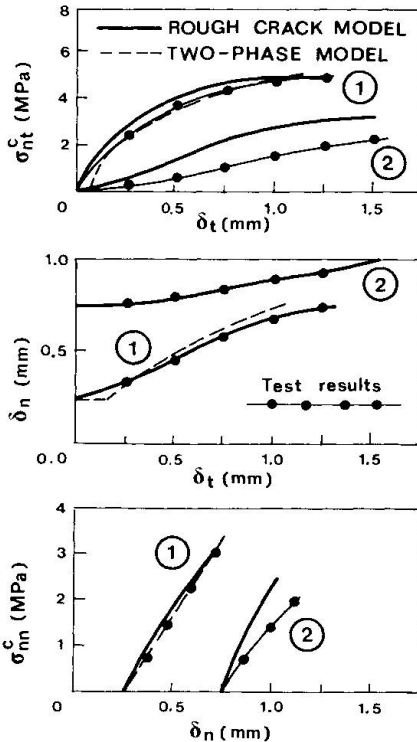


▲ Fig. 16 - Initial shear stiffness according to various tests and analytical models.

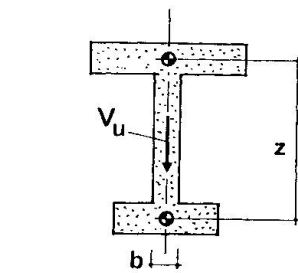
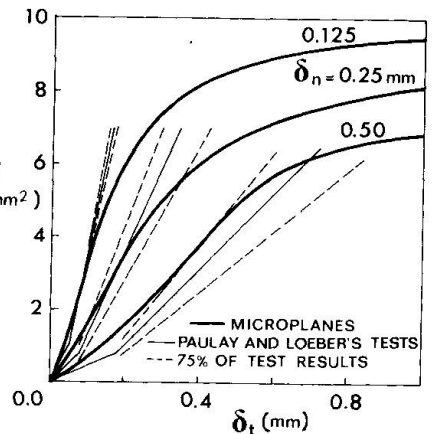


◆ Fig. 15 - Microplane Model: (a) concrete microstructure; (b) microplanes; (c) constitutive law of a microplane [28].

▼ Fig. 17 - Fitting of Millard and Johnson's test results [25, 26].



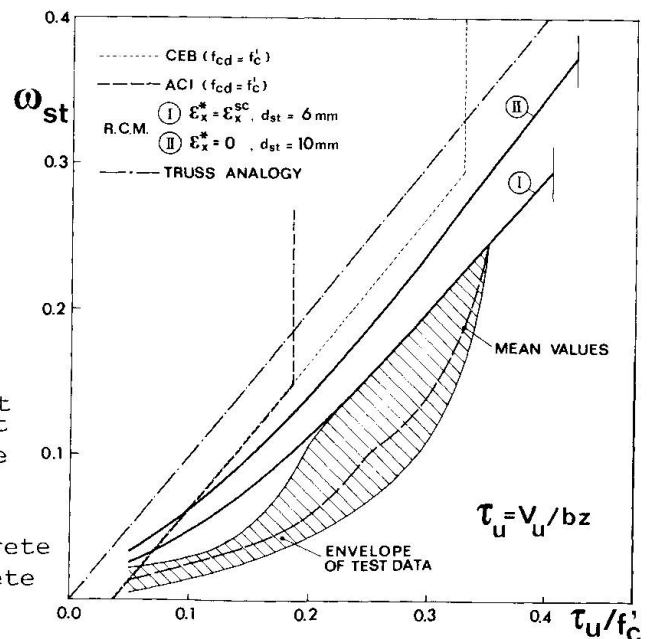
► Fig. 18 - Fitting of Paulay and Loeber's test results [28].



▲ Fig. 19 - Thin-webbed r.c. beams: curves of shear reinforcement degree  $\omega_{st}$  and envelope of test data at collapse due to stirrup yielding [24].

I : prestressed concrete  
II : reinforced concrete

$$\omega_{st} = \rho_{st} (f_{sy}/f'_c)$$



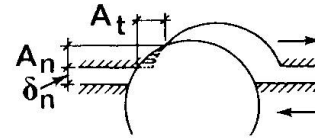
$$\sigma_{nt}^c = \tau_0 (1 - \sqrt{2\delta_n/d_a}) \cdot r \frac{a_3 + a_4 |r|^3}{1 + a_4 r^4}, \quad \sigma_{nn}^c = -a_1 a_2 \sqrt{\delta_n} \frac{r}{(1 + r^2)^{0.25}} \sigma_{nt}^c, \text{ where}$$

$a_1, a_2, a_3$  and  $a_4$  are constants or parameters related to concrete strength  $f'_c$ .

## 5.2 Two-Phase Model [22]

The constitutive laws have a rational formulation based on a few apodictic assumptions: (a) concrete is regarded as a two-phase material, with perfectly stiff spherical inclusions (aggregate particles) and a perfectly plastic matrix (the cement paste); (b) the grading of the aggregates matches Fuller's curve; (c) the active contact areas between the inclusions and the matrix are related to interface displacements, via geometrical relations and taking into account the statistics of aggregate distribution; (d) the compressive contact strength of the matrix is related to concrete strength, while the shear contact strength is linearly related to the compressive contact strength via a constant friction coefficient. The constitutive laws are as follows:

$$\sigma_{nt}^c = \sigma_{pu} (A_n + \mu A_t), \quad \sigma_{nn}^c = \sigma_{pu} (A_t - \mu A_n)$$



where  $A_n$  and  $A_t$  are the averaged contact areas (in the direction  $n$  and  $t$ ) between the inclusions and the matrix,  $\sigma_{pu}$  is the matrix compressive strength ( $\sigma_{pu} = 6.39 f'_c{}^{0.56}$ ) and  $\mu$  is the inclusion-to-mortar friction coefficient ( $\mu = 0.40$ ).

## 5.3 Dilatancy Factor Model [27]

The constitutive laws are empirical since they are based on test results obtained by the Authors, as well as on most of the test results published so far:

$$\sigma_{nt}^c = k_0 \delta_t [1 + (k_0 \delta_t) / (a_1 \sigma_{tp})] \exp[-(2 k_0 \delta_t) / (a_1 \sigma_{tp})]$$

$$\beta = \delta_n / \delta_t = a_2 \exp(-a_3 \delta_t - \sigma_n^{-a_4}) \quad (\beta = \text{dilatancy factor}, \sigma_n = \sigma_{nn}^c)$$

where:  $k_0$  (initial shear stiffness)  $= (\partial \sigma_{nt}^c / \partial \delta_t)_0 = a_5 f'_c{}^{0.193} / \delta_n{}^{1.615}$

$$\sigma_{tp} \text{ (peak shear stress)} = 0.1 f'_c \sqrt{\sum_{i=6,10} a_i (\sigma_n / f'_c)^{i-6}} \text{ with } a_6, \dots, a_{10} = \text{constants.}$$

## 5.4 Microplane Model [28]

The concrete, either solid or cracked, is considered as a system of randomly oriented planes (microplanes: Fig. 15a, b) which are characterized by a uniaxial normal stress-normal strain law; the shear stiffness of the microplanes is disregarded. Although originally developed for the description of the nonlinear behavior and fracture of concrete and rocks (Bazant and Oh, "Microplane Model for Progressive Fracture of Concrete and Rock", J. Engrg. Mech. ASCE, 111 - 1985, pp.559-582; Gambarova and Floris, "Microplane Model for Concrete Subject to Plane Stresses", Nuclear Engrg. and Design, 97 - 1986, pp. 31-48), the Microplane Model has been applied also to describe shear transfer across blunt cracks, by modelling the cracks as "crack bands", with a width equal to maximum aggregate size [28]. Simple asymptotic or exponential laws have been adopted both for loading and unloading (Fig. 15c). The model can describe concrete path-dependency and reorientation of principal stresses with respect to principal strains, and allows easy evaluation of the coefficients of the incremental stiffness matrix.

In Figs. 16, 17 and 18 the curves obtained with the 4 different mathematical models show a very good agreement with test results. Fig. 19 regards the design of





the stirrups in thin-webbed I beams failing in shear due to stirrup yielding [24]: a remarkable saving in reinforcement amount can be achieved, if aggregate interlock is correctly modeled.

## 6. TENSILE FORCES ACROSS AN OPEN CRACK

As already mentioned in Section 2, interest in the tensile properties of concrete has increased very much in recent years, in connection with further investigation on bond, size effect in structural shear strength, comprehensive material models, crack formation and propagation (fracture mechanics, see Reinhardt, Cornelissen and Hordijk [30]). As to this last topic, five parameters are important: Young's modulus at the origin, peak stress (i.e. tensile strength), stress-free crack opening and shape of the descending branch (or the area under the total stress-deformation curve, which is related to the fracture energy), cracking front width (only if the crack band approach is adopted, see Bazant [9, 31]). Within this framework, attention was focused on very small values of the crack opening (generally under 0.10 - 0.15 mm, see the tests by Petersson [32]; Gopalaratnam and Shah [33]; Cedolin, Dei Poli and Iori [34]).

In many important cases, however, the structural engineer has to deal with much wider cracks even under service loads. Very often, large cracked interfaces form due to concrete splitting as in lapped splices, short anchorages with limited transverse pressure, and around the dowels, or to tensile cracking, as in r.c. sections subjected to bending and shear.

In these cases, only the knowledge of the constitutive law  $\sigma(w)$  for relatively large crack openings makes it possible to evaluate the contribution of cracked interfaces to the structural strength. For this purpose, a few very recent tests by Giuriani, Rosati and Tornello [35] may be quoted: as can be observed in Fig. 20 (4th test of a 4 test series), crack width values as large as 0.75 mm were investigated. At  $w = 0.1$  mm (Point C) the tensile strength is close to 0.7 MPa ( $\approx 20\% f_{ct}$ ), while at  $w = 0.7$  mm the tensile strength reduces to 0.1 MPa ( $\approx 2.5 - 3\% f_{ct}$ ). According to these test results, the constitutive law of the crack is tentatively formulated in [35] as follows:  $\sigma = f_{ct}/(C_1 w + C_2)$ , where  $C_1$  and  $C_2$  are constants.

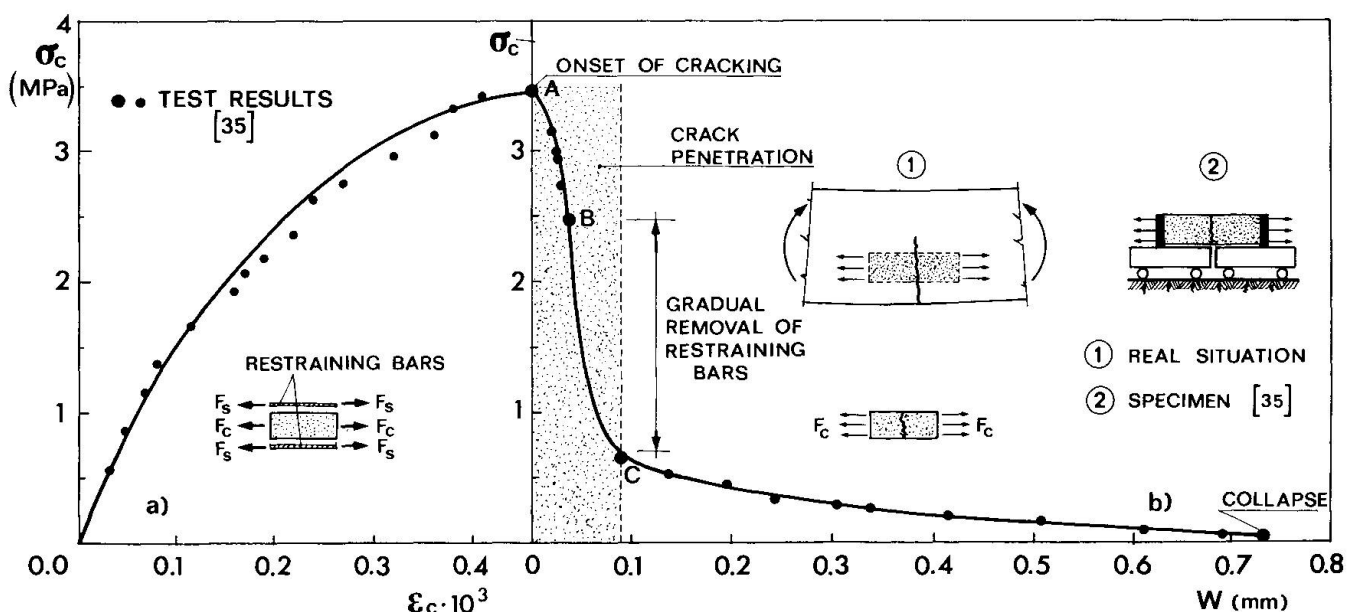


Fig.20 - (a) Stress-strain curve in tension and (b) stress versus crack opening curve for plain concrete [35]. Overall section of the restraining bars:  $A_s = 161 \text{ mm}^2$  (steel); dimensions and area of the section of the concrete specimen:  $b = 50 \text{ mm}$ ,  $h = 60 \text{ mm}$ ,  $A_c = 3000 \text{ mm}^2$ ;  $f'_c = 42 \text{ MPa}$ ;  $d_a$  (maximum aggregate size) = 15 mm.

Though the tensile strength of an open crack is certainly limited, still sizeable forces can be transferred across large cracked interfaces. Because of their contribution to the durability of concrete structures and to the control of concrete cracking, these forces should be taken into account and correctly evaluated.

## 7. CONCLUSION

Interface problems embrace so many different aspects of concrete mechanics that two risks are always involved, a lack of perspective if the research is devoted to one particular topic, and a lack of thoroughness if too many topics are investigated at the same time. Having this in mind, the different interface problems regarding either steel and concrete, or concrete and concrete are here analysed within the more general context of recent research on concrete mechanics.

As to bond behavior up to pull-out failure, to aggregate interlock and to concrete tensile behavior limited to small crack openings, suitable constitutive laws are already available though with lights and shades (particularly in the field of cyclic loads). On the other hand, bond behavior up to and beyond concrete splitting, dowel action and transfer of tensile forces across open cracks require further research work in different directions (monotonic as well as repeated loads, for example). In the end, two goals will be achieved: a better understanding of the different phenomena and a more reliable and sound formulation of the constitutive laws.

## ACKNOWLEDGEMENT

The writer wishes to acknowledge the valuable assistance given by the Graduate Research Associates M. Di Prisco and G.P. Rosati, who participated in screening the literature and in gathering test data as well as numerical results.

The papers here quoted and coauthored by the writer refer to different research programs supported in part by the Italian Ministry of Higher Education (M.P.I.). Helpful discussions with Prof. Z.P. Bazant, S. Dei Poli and T.P. Tassios are gratefully acknowledged.

## REFERENCES

1. BOND IN CONCRETE, Proc. of the Int. Conf. on Bond in Concrete, Paisley College of Technology (Scotland), June 1982, Editor: P. Bartos, Applied Science Publishers, London, 1982.
2. CONSTITUTIVE LAWS FOR ENGINEERING MATERIALS: THEORY AND APPLICATIONS, Proc. of the First Int. Conf. held in Tucson (Arizona, USA), January 1983, Editors: C.S. Desai and R.H. Gallagher, Nat. Science Foundation, Washington, D.C., 1983.
3. MECHANICS OF GEOMATERIALS: ROCKS, CONCRETES, SOILS, Proc. of William Prager Symposium, Evanston (Illinois, USA), September 1983, Editor: Z.P. Bazant, Northwestern University, 1983.
4. APPLICATION OF FRACTURE MECHANICS TO CEMENTITIOUS COMPOSITES, Proc. of NATO Advanced Research Workshop, Evanston (Illinois, USA), September 1984, Editor: S.P. Shah, Northwestern Univ., 1984.
5. PARTIAL PRESTRESSING: FROM THEORY TO PRACTICE, Proc. of NATO Advanced Research Workshop, Saint-Rémy-les-Chevreuse (France), June 1984, Editor: M.Z. Cohn, NATO ASI Series No. 113a-b, 1985.
6. CREEP AND SHRINKAGE OF CONCRETE: MATHEMATICAL MODELING, Proc. of Fourth RILEM Int. Symposium, Evanston (Illinois, USA), August 1986, Editor: Z.P. Bazant, Northwestern University, 1986.
7. CONSTITUTIVE LAWS FOR ENGINEERING MATERIALS: THEORY AND APPLICATIONS, Proc. of the Second Int. Conf. held in Tucson (Arizona, USA), January 1987, Editors: C.S. Desai, E. Krempf, P.D. Kioussis and T. Kundu, Elsevier, New York, 1987.
8. VINTZELEOU E.N. and TASSIOS T.P., "Mechanisms of Load Transfer along Interfaces in Reinforced Concrete: Prediction of Shear Force versus Shear-Displacement Curves", Studi e Ricerche, Vol. 7, Post-Graduate School for the Design of R.C. Structures, Politecnico di Milano, 1985, pp. 121-161.
9. BAZANT Z.P., "Mechanics of Distributed Cracking", Applied Mechanics Review, Vol. 39, No. 5, May 1986, pp. 675-705.
10. TEPPERS R., "Lapped Tensile Reinforcement Splices", Journal of the Structural Division, ASCE, Vol. 108, No. 1, January 1982, pp. 283-301.





11. GAMBAROVA P.G., ROSATI G.P. and ZASSO B., "Test Results and Constitutive Relationships Regarding Steel-to-Concrete Bond after Concrete Splitting", submitted for review and possible publication in *Materials and Structures*, April 1987.
12. GIURIANI E. and PLIZZARI G., "Local Bond-Slip Law after Splitting of Concrete" (in Italian), *Studi e Ricerche*, Vol. 7, Post-Graduate School for the Design of R.C. Structures, Politecnico di Milano, 1985, pp. 57-118.
13. YANKELEVSKY D.Z., "Bond Action between Concrete and a Deformed Bar - A New Model", *ACI Journal*, Tech. Paper No. 82-13, March-April 1985, pp. 154-161.
14. JIANG D.H., SHAH S.P. and ANDONIAN A.T., "Study of the Transfer of Tensile Forces by Bond", *ACI Journal*, Tech. Paper No. 81-24, May-June 1984, pp. 251-259.
15. REINHARDT H.W., BLAAUWENDRAAD J. and VOS E., "Prediction of Bond between Steel and Concrete by Numerical Analysis", *Materials and Structures*, Vol. 17, No. 100, July-August 1984, pp. 311-320.
16. INGRAFFEA A.R., GERSTLE W.H., GERGELY P. and SAOUMA V., "Fracture Mechanics of Bond in Reinforced Concrete", *Journal of Structural Engineering*, ASCE, Vol. 110, No. 4, April 1984, pp. 871-890.
17. SOROUSHIAN P., OBASEKI K., ROJAS M.C. and SIM J., "Analysis of Dowel Bars Acting against Concrete Core", *ACI Journal*, Tech. Paper No. 83-59, July-August 1986, pp. 642-649.
18. VINTZELEOU E.N. and TASSIOS T.P., "Mathematical Models for Dowel Action under Monotonic and Cyclic Conditions", *Magazine of Concrete Research*, Vol. 38, No. 134, March 1986, pp. 13-22.
19. YOSHIKAWA H. and TANABE T., "A Finite Element Model for Cracked Concrete", *Proc. U.S.-Japan Seminar on Finite Element Analysis of R.C. Structures*, ASCE, New York, 1986 (in printing).
20. UTESCHER G. and HERRMANN H., "Tests to Determine the Structural Strength of Round Reinforcing Dowels of Stainless Austenitic Steel Fixed in Concrete" (in German), *DAfSt*, Heft 346, Berlin, 1983, pp. 49-104.
21. PASCHEN H. and SCHÖNHOF T., "Investigations on Shear Connectors Made of Reinforcing Steel Embedded in Concrete" (in German), *DAfSt*, Heft 346, Berlin, 1983, pp. 105-149.
22. WALRAVEN J.C., "Fundamental Analysis of Aggregate Interlock", *Journal of the Structural Division*, ASCE, Vol. 107, No. 11, November 1981, pp. 2245-2270.
23. DASCHNER F. and KUPFER H., "Versuche zur Schubkraftübertragung in Rissen von Normal- und Leichtbeton", *Bauingenieur* 57 (1982), pp. 57-60.
24. DEI POLI S., GAMBAROVA P.G. and KARAKOÇ C., "Aggregate Interlock Role in R.C. Thin-Webbed Beams in Shear", *Journal of Structural Engineering*, ASCE, Vol. 113, No. 1, January 1987, pp. 1-19.
25. DEI POLI S., GAMBAROVA P.G. and KARAKOÇ C., Discussion on the papers "Shear Transfer across Cracks in R.C. due to Aggregate Interlock and to Dowel Action" (MCR, No. 126) and "Shear Transfer in R.C." (MCR, No. 130) by Millard S.G. and Johnson R.P., *Magazine of Concrete Research*, Vol. 38, No. 134, March 1986, pp. 47-51.
26. MILLARD S.G. and JOHNSON R.P., "Shear Transfer across Cracks in Reinforced Concrete due to Aggregate Interlock and to Dowel Action", *Magazine of Concrete Research*, Vol. 36, No. 126, March 1984, pp. 9-21.
27. DIVAKAR M.P., FAFITIS A. and SHAH S.P., "Constitutive Modeling of Rough Interfaces in Sliding Shear", *Trans. of the 2nd Int. Conf. on Constitutive Laws for Engineering Materials: Theory and Applications*, Tucson (Arizona, USA), January 1987, pp. 1027-1034.
28. BAZANT Z.P. and GAMBAROVA P.G., "Crack Shear in Concrete: Crack Band Microplane Model", *Journal of Structural Engineering*, ASCE, Vol. 110, No. 9, September 1984, pp. 2015-2035.
29. PERDIKARIS P.C. and WHITE R.N., "Shear Modulus of Precracked R/C Panels", *Journal of Structural Engineering*, ASCE, Vol. 111, No. 2, February 1985, pp. 270-289.
30. REINHARDT H.W., CORNELISSEN H.A.W. and HORDIJK D.A., "Tensile Tests and Failure Analysis of Concrete", *Journal of Structural Engineering*, ASCE, Vol. 112, No. 11, November 1986, pp. 2462-2477.
31. BAZANT Z.P., "Fracture Mechanics and Strain-Softening of Concrete", *Proc. U.S.-Japan Seminar on Finite Element Analysis of R.C. Structures*, ASCE, New York, 1986 (in printing).
32. PETERSSON P.E., "Crack Growth and Development of Fracture Zones in Plain Concrete and Similar Materials", Report No. TVBM-1006, Lund Institute of Technology, December 1981.
33. GOPALARATNAM V.S. and SHAH S.P., "Softening Response of Plain Concrete in Direct Tension", *ACI Journal*, Tech. Paper No. 82-27, May-June 1985, pp. 310-323.
34. CEDOLIN L., DEI POLI S. and IORI I., "Tensile Behavior of Concrete", *Journal of the Mechanical Engineering Division*, ASCE, to appear in Vol. 113, No. 4, April 1987.
35. GIURIANI E., ROSATI G.P. and TORNELLO M., "Tensile Response of Open Cracks in Plain Concrete", Private Communication, Post-Graduate School for the Design of R.C. Structures, Politecnico di Milano, November 1986.
36. LAHNERT B.J., HOUDE J. and GERSTLE K.H., "Direct Measurement of Slip Between Steel and Concrete", *ACI Journal*, Tech. Paper No. 83-86, November-December 1986, pp. 974-982.

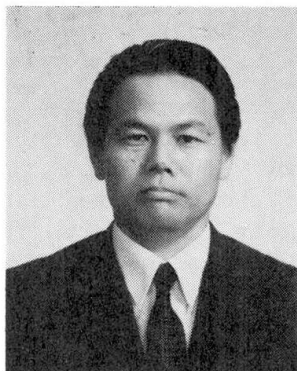
## Constitutive Equations of a Cracked Reinforced Concrete Panel

Equations constitutives d'un panneau en béton armé fissuré

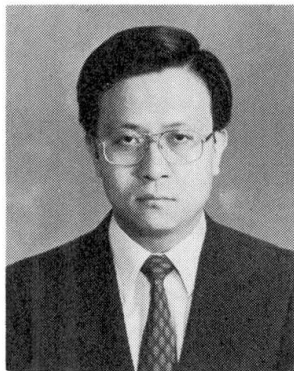
Werkstoffbeziehungen für eine gerissene Stahlbetonscheibe

### Tadaaki TANABE

Professor  
Nagoya University  
Nagoya, Japan



Tadaaki Tanabe, born in 1940, received his Dr. of Eng. at the University of Tokyo. After ten years research work in dams and RC structures of nuclear power stations, he joined the Nagoya University in 1981, was promoted to full Professor in 1984, and was engaged in the research of aseismic design and the thermal stress control of RC structures.



Hiromichi Yoshikawa, born in 1952, received his Dr. of Eng. at the University of Tokyo, involved in research work on the thermal stress analysis of massive concrete, analytical modelling of reinforced concrete members and finite element analysis of RC structures.

### Hiromichi YOSHIKAWA

Senior Research Eng.  
Hazamagumi Co., Ltd.  
Yono-Shi, Saitama,  
Japan

### SUMMARY

Constitutive equations of composite materials of concrete and reinforcement in a twodimensional stress field are developed using damage and reinforcement tensors. The damage tensors are derived for the displacement fields of the frictionless mode at a crack, the contact frictional mode at a crack, and the mixed mode of both from the crack strains which are derived for each displacement field. The experimental results are compared with the theoretical calculations and a reasonable agreement is obtained.

### RÉSUMÉ

Les équations constitutives des matériaux composites de béton et d'armatures sont établies pour un champ de contraintes bi-dimensionnelles, en utilisant les vecteurs de dommage et de renforcement. Les vecteurs de dommage sont obtenus à partir des champs de déplacement dus à l'évolution d'une fissure sans friction, à l'évolution d'une fissure avec friction de contact, et à un mode mixte des deux mentionnés précédemment, à partir des contraintes de fissure qui sont obtenues pour chaque champ de déplacement. Les résultats expérimentaux sont comparés avec les calculs théoriques et une bonne concordance est obtenue.

### ZUSAMMENFASSUNG

Werkstoffbeziehungen von Verbundmaterialien aus Beton und Bewehrung in der zweidimensionalen Spannungsfläche werden entwickelt, wobei von Schadens- und Verstärkungstensoren Gebrauch gemacht wird. Die Schadenstensoren werden für das Verschiebungsfeld von reibungslosen Rissen entwickelt, für den Riss mit Reibung und für gemischte Beanspruchung aus Rissöffnung und Rissverschiebung. Experimente werden mit der Theorie verglichen, wobei befriedigende Übereinstimmung erreicht wird.



## 1. INTRODUCTION

The crack strain method in FEM analysis of a reinforced concrete structure is considered to be a very powerful means to incorporate material nonlinearities of various kinds in calculations. Crack strain in a discontinuous solid is defined in various ways. Powell, Villiers, and Litton [1] as well as Bazant and Gambaroba [2] defined crack strains as the crack width or crack slip divided by the average crack spacing, and expressed total strains as the sum of elastic strains and crack strains. Tanabe and Yamashita have treated a single crack by crack strain expressing it in a function [3]. Yoshikawa and Tanabe [4] defined crack strain in terms of delta function and extended to the case of tension stiffness formulation of reinforced concrete members, showing that crack strain so defined expresses bond slip between reinforcement and concrete.

On the other hand, crack strain has a natural relation to the damage tensor, which expresses the rate of damage of material from the intact condition. The damage tensor expresses material nonlinearity in explicit and simple form which enables the straightforward construction of the nonlinear constitutive equations in a comparatively simple way. In this paper, the fourth rank damage tensor is defined in terms of crack strain and the reinforcement tensor is defined in terms of stress increase due to the reinforcement. The general constitutive equations for the composite material made up of reinforcement and concrete are developed for a two dimensional stress field using these tensors. However, our attention will be limited to monotonic loading, with unloading and reloading excluded.

## 2. DEFINITION OF THE DAMAGE TENSOR FROM THE CRACK STRAINS

The damage tensor of the fourth rank may be defined in the following form to write stress reduction from the intact condition.

$$\Delta \sigma_{ij} = -\varrho_{ijpq}^0 D_{pqmn} \varepsilon_{mn} \quad (2.1)$$

where  $\Delta \sigma_{ij}$  is the reduction of the nominal stress due to damage in the solid from the intact condition. As  $\varrho_{ijpq} = \varrho_{jipq} = \varrho_{jiqp} = \varrho_{ijqp}$ , matrix expression for Eq.(2.1) is written as

$$\{\Delta \sigma\} = -[\varrho]_D [D]_C \{\varepsilon\} \quad (2.2)$$

Similarly, the reinforcement tensor may be written in terms of stress increase from the intact condition due to the reinforcement in concrete as

$$\Delta \sigma_{ij} = \varrho_{ijpq}^* D_{pqmn} \varepsilon_{mn} \quad (2.3)$$

Eq.(2.3) is written in matrix form as

$$\{\Delta \sigma\} = [\varrho]_R [D]_C \{\varepsilon\} \quad (2.4)$$

Using Eq.(2.1) and Eq.(2.3), the general constitutive equation can be derived as

$$\{\sigma\} = [I - \varrho_{D1} - \varrho_{D2} - \dots + \varrho_{R1} + \varrho_{R2} + \dots] [D]_C \{\varepsilon\} \quad (2.5)$$

Stress reduction in concrete from the intact condition is written with the crack strain,  $\{\varepsilon\}_{cr}$ , in the following form as well,

$$\{\Delta \sigma\} = -[D]_C \{\varepsilon\}_{cr} \quad (2.6)$$

Substitution of Eq.(2.6) into Eq.(2.2) yields

$$\{\varepsilon\}_{cr} = [D]_c^{-1} [Q]_b [D]_c \{\varepsilon\} \quad (2.7)$$

Hence, if  $\{\varepsilon\}_{cr}$  or stress reduction  $\{\Delta\sigma\}$  is obtained, the  $[Q]$  can be derived. In other words, if  $\{\varepsilon\}_{cr}$  is obtained in terms of total strain in such a way that

$$\{\varepsilon\}_{cr} = [A] \{\varepsilon\} \quad (2.8)$$

then the damage tensor is obtained as

$$[Q]_b = [D]_c [A] [D]_c^{-1} \quad (2.9)$$

Similarly if the stress increase due to reinforcement is given in terms of total strain in such a way that

$$\{\Delta\sigma\} = [\phi] \{\varepsilon\}, \quad (2.10)$$

the reinforcement tensor is obtained as

$$[Q]_r = [\phi] [D]_c^{-1} \quad (2.11)$$

The form of Eq.(2.5) is directly accommodated in a usual FEM program as the initial strain problem or the initial stress problem.

### 3. TENSION STIFFNESS FORMULATION IN A TWO DIMENSIONAL STRESS FIELD USING CRACK STRAINS

It is known that displacements of a reinforced concrete panel subjected to in-plane loads are highly dependent on the bond characteristics between steel and concrete, the frictional characteristics at cracks, and the material nonlinearities of concrete and steel. In this section, the analytical model for calculating the effect of bond characteristics or tension stiffness effects on deformation is presented. Bond characteristics between steel and concrete are directly related to crack spacing and crack width. For the rigorous analysis of those, we need a fracture theory of concrete. However, we simplify the problem by the assumption that concrete is a linear elastic brittle fracture material in tension and the solution is obtained. Its solution is then modified by coefficients which reflect nonlinearity of the material characteristics.

The experimentally observed relation between the maximum crack spacing,  $l_{max}$ , and the minimum spacing,  $l_{min}$ , for a uniaxially reinforced concrete member suggests that they have a relation of

$$l_{max} = C \cdot l_{min} \quad (3.1)$$

where  $C$  is constant. For instance, Goto has proposed that  $C=2$  [5]. Osaka et.al. proposed that  $C=4$  [6].

Supposing that a new crack initiates when the maximum tensile stress reaches the tensile strength of the concrete,  $f_t$ , and that the crack spacing satisfies the Eq.(3.1), the upper envelop curve of  $l_{max}$  and the lower envelop curve of  $l_{min}$  is obtained uniquely for any arbitrary initial length of  $\ell$ , as the continuous function of applied stress, as shown in Fig.3.1. The function thus obtained decides the analytical expression of the relation between applied stress and crack strains.

If we assume the linear bond slip law for a uniaxially reinforced concrete

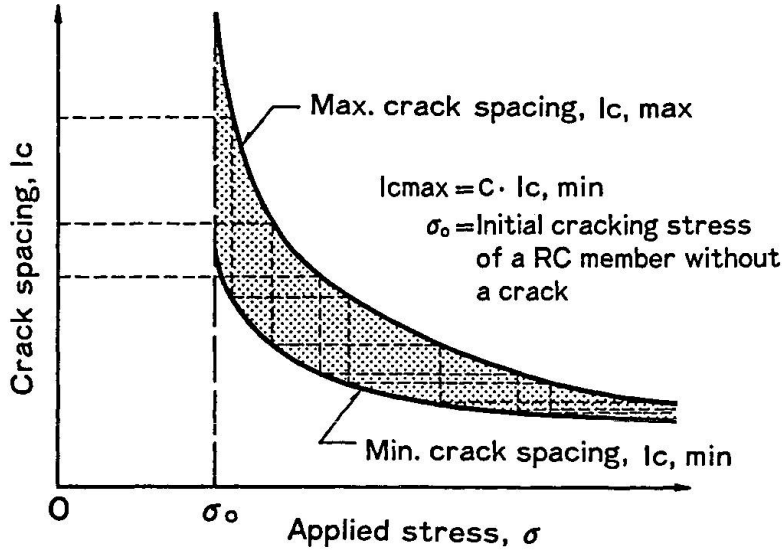


Fig.3.1 Envelope Curves for the Maximum and the Minimum Crack Spacings

member, and the governing equation of bond stress, and bond slip relation as  $d^2g/dx^2 - k g = 0$  [7], where  $g$  is the slip,  $k = (u/u_0)/(g/g_0)$ , and  $u$ ,  $u_0$ ,  $g_0$  are the bond stress, bond strength and the corresponding slip at the maximum bond strength, respectively, and that a crack initiates when concrete stress reaches concrete tensile strength,  $f_t$ , the upper bound envelop curve is expressed as

$$\cosh(\ell_c/b_c) = \frac{\sigma}{\sigma - (1+np)f_t} \quad (3.2)$$

where  $\ell_c$  is half of the crack spacing,  $\sigma$  is the applied uniaxial stress, and  $b_c$  is the parameter that shows bond characteristics and is expressed as  $b_c = \left[ k u_0 s (1+np) / (g_0 A_s E_s) \right]^{-\frac{1}{2}}$ . The notations  $n$ ,  $p$ ,  $s$ , and  $A_s$ , denote the ratio of the Young's Modulus of steel to that of concrete, steel ratio, bar diameter, and sectional area of a bar, respectively.

The lower envelop curve is obtained by substituting  $C \cdot \ell_c$  in  $\ell_c$  of Eq(3.2). Crack strain  $\{\epsilon\}_{cr}$  is defined as the crack width divided by the average crack spacing. As crack width,  $\delta_w$ , equals  $2 b_c \tanh(\ell_c/b_c) \cdot \sigma / p E_s$ ,

$$\epsilon_{cr} = \lambda \frac{\sigma}{p E_s} \quad (3.3)$$

where  $\lambda = \tanh(\mu_c) / \mu_c$ ,  $\mu_c = \ell_c/b_c = \cosh^{-1} \left[ \sigma / \{ \sigma - (1+np) \cdot f_t \} \right]$

Now, the total strain is written as

$$\epsilon = \left( \frac{\lambda + np}{1 + np} \right) \frac{\sigma}{E_s} \quad (3.4)$$

Hence tension stiffness is expressed by the parameter,  $\lambda$ , ( $0 \leq \lambda \leq 1$ ). If  $\lambda = 0$ ,  $\epsilon_{cr} = 0$  and full contribution to tension stiffness from concrete exists, while if  $\lambda = 1$ , then  $\epsilon_{cr} = \sigma / E_s = \epsilon_s$ , steel strain, and no contribution to tension stiffness from concrete exists. The effect of nonlinear characteristics of bond slip law is introduced now by the comparison of the solution with the experimental values. They show that better fitting is obtained if the crack spacing and stress relation is shifted from the upper bound envelop to the lower envelop curve with the increase of applied stress. This modification factor  $\beta$ , which is to be multiplied to the linear solution of crack spacing, is expressed

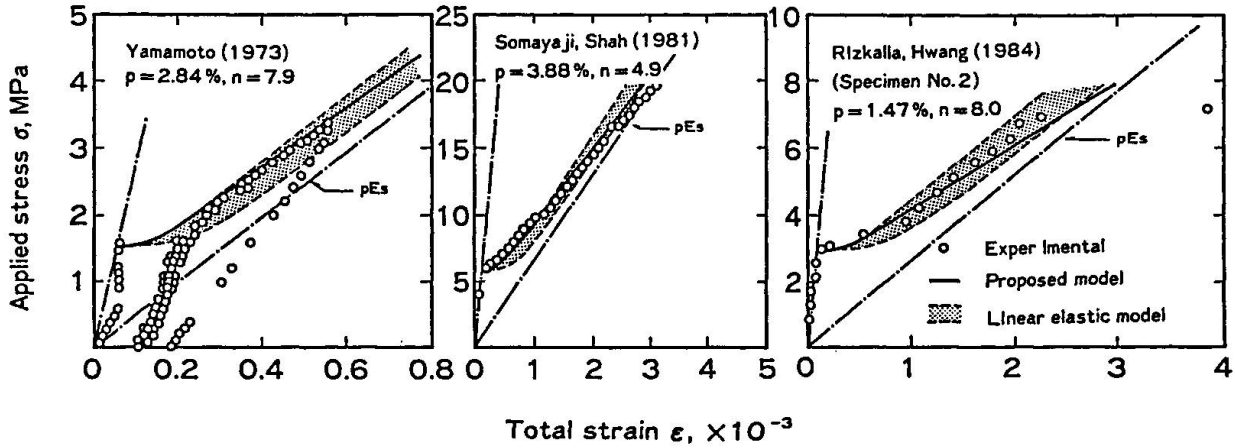


Fig.3.2 Applied Stress and Total Strain Relations in Uniaxial Tension Tests (Ref.8,9,10)

as Eq.(3.5), where  $f_y$  is the yielding stress of a bar,

$$\beta = 1 - C_s \frac{\sigma - (1 + np) f_t}{p f_y - (1 + np) f_t} \quad (3.5)$$

and normalized crack spacing is given as

$$\mu = \ell_c / b_c = \beta \cos h^{-1} \left\{ \frac{\sigma}{\sigma - (1 + np) f_t} \right\} \quad (3.6)$$

The value of  $C_s$  is closely related to the relation of the maximum crack spacing and the minimum spacing, and it seems to take a value between zero and 0.5.

Some numerical example are shown in Fig.3.2 [8][9][10], comparing the analysis with the experimental data of the uniaxially tensioned RC members. In the figure, the shaded area is bounded by the upper and the lower envelop curves. Good agreement is observable from the figures.

We develop now the theory into two dimensional stress field assuming linear bond slip laws. Nonlinearity is again taken into consideration by the similar, but, expanded modification factors,  $\beta_x$  and  $\beta_y$  to the X and Y directions. However, our discussion is limited to cases where cracks are formed in one direction only or to two orthogonal directions in alignment with two orthogonal reinforcement directions, in which case the tension stiffening effects in each direction are treated independently.

Taking out one portion of a cracked panel which is separated by the two cracks as shown in Fig.3.3(a), it is possible to consider that the strips which are the tributary area of both steel reinforcements for the X direction and the Y direction as shown in Fig.3.3(b), independently satisfy the bond slip law along the X and Y directions. The concrete stresses at a square where the strips overlap are then estimated by the similar procedure as we did in the derivation of Eq.(3.2). For the X direction,

$$\sigma_{c,x} = \frac{p_x \sigma_{s,x}}{(1 + np_x)} \left\{ 1 - \frac{\cos h(x / b_{c,x})}{\cos h(\ell_{c,x} / b_{c,x})} \right\} \quad (3.7a)$$

and similarly for the Y direction,

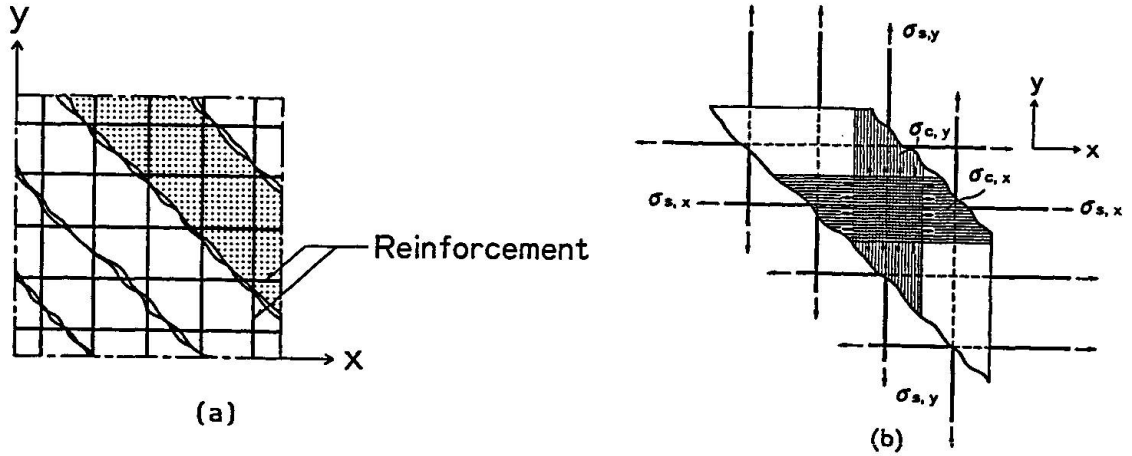


Fig.3.3 A Cracked Reinforced Concrete Panel

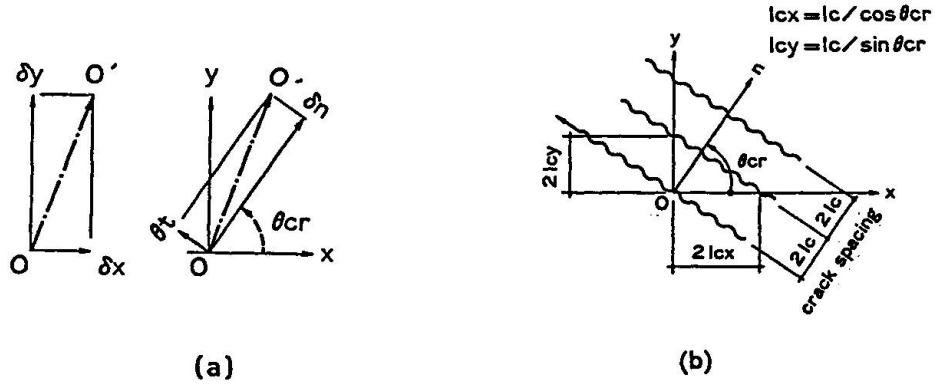


Fig.3.4 Crack Widths to the (x,y) and (n,t) Directions and Crack Spacings of Parallel Cracks

$$\sigma_{c,y} = \frac{p_y \sigma_{s,y}}{(1 + n p_y)} \left\{ 1 - \frac{\cos h(y / b_{c,y})}{\cos h(\ell_{c,y} / b_{c,y})} \right\} \quad (3.7b)$$

where  $\sigma_{s,x}$  and  $\sigma_{s,y}$  are steel stresses at a crack and are equal to the first principal stress of applied stresses from the assumption of lattice structures and  $p_x$  and  $p_y$  are the reinforcement ratios to the X and Y directions. The values  $l_c$  and  $b_c$  with suffix x or y denote the crack spacings and the bond characteristics to the X or Y directions.

The stresses of Eq.(3.7a) and Eq.(3.7b) compose total stresses together with the compressive stress in the concrete struts working to the direction parallel to the cracks. Principal stresses are decided by their stresses. However, in simplicity, the first principal stress may be approximated as

$$\sigma_1 = f_1(\theta) \sigma_{c,x \max} + f_2(\theta) \sigma_{c,y \max} \quad (3.8)$$

$$f_1(\theta) = \cos^n \theta_{cr}, \quad f_2(\theta) = \sin^n \theta_{cr} \quad (3.9a, 3.9b)$$

The value of n of Eq.(3.9) depends on the crack angle, the relative location of reinforcements and so forth, however,  $n=2$  is assumed in this study. The crack spacing and applied stress relation is then expressed as

$$f_1(\theta) \frac{p_x \sigma_{s,x}}{(1 + n p_x)} \left[ 1 - \operatorname{sech} \left( \frac{\ell_c}{b_{c,x} \cos \theta_{cr}} \right) \right] + f_2(\theta) \frac{p_y \sigma_{s,y}}{(1 + n p_y)} \left[ 1 - \operatorname{sech} h \frac{\ell_c}{b_{c,y} \sin \theta_{cr}} \right] = f_t \quad (3.10)$$



Crack widths or slipping off of reinforcements at a crack,  $\delta_x$ ,  $\delta_y$  are then given as

$$\begin{aligned}\delta_x &= 2b_{c,x} \tan h(\ell_{c,x}/b_{c,x}) \frac{\sigma_{s,x}}{p_x E_s} \\ \delta_y &= 2b_{c,y} \tan h(\ell_{c,y}/b_{c,y}) \frac{\sigma_{s,y}}{p_y E_s}\end{aligned}\quad (3.11)$$

On the other hand, the geometry of the crack in Fig.3.4(b) gives the following relation in the (n,t) coordinate system;

$$\begin{Bmatrix} \delta_n \\ \delta_t \end{Bmatrix} = \begin{bmatrix} \cos \theta_{cr} & \sin \theta_{cr} \\ -\sin \theta_{cr} & \cos \theta_{cr} \end{bmatrix} \begin{Bmatrix} \delta_x \\ \delta_y \end{Bmatrix}\quad (3.12)$$

and by definition, crack strain is given as

$$\begin{Bmatrix} \epsilon_n \\ \epsilon_t \end{Bmatrix} = \begin{bmatrix} 1 & 1 \\ -\tan \theta_{cr} & \cot \theta_{cr} \end{bmatrix} \begin{bmatrix} \lambda_x/p_x E_s & 0 \\ 0 & \lambda_y/p_y E_s \end{bmatrix} \begin{Bmatrix} \sigma_{s,x} \\ \sigma_{s,y} \end{Bmatrix} = [S]_{nt} \begin{Bmatrix} \sigma_1 \\ \sigma_2 \end{Bmatrix}\quad (3.13)$$

$$\text{where } [S]_{nt} = \begin{bmatrix} 1 & 1 \\ -\tan \theta_{cr} & \cot \theta_{cr} \end{bmatrix} \begin{bmatrix} \lambda_x/p_x E_s & 0 \\ 0 & \lambda_y/p_y E_s \end{bmatrix} \begin{bmatrix} 1 & 0 \\ 0 & 1 \end{bmatrix}$$

As has been in the uni-dimensional cases, the tension stiffening effect is evaluated by the value of  $\lambda_x$  and  $\lambda_y$ . If  $\lambda_x, \lambda_y = 0$ , full contribution to tension stiffness exists from concrete while if  $\lambda_x, \lambda_y = 1$ , no tension stiffness effect exists, and the transition from  $\lambda_x, \lambda_y = 0$  to  $\lambda_x, \lambda_y = 1$  is dependent on steel stress and other nonlinearity factors, and  $\mu_x, \mu_y$  which are the normalized crack spacings, are modified by the nonlinear factors  $\beta_x$ , and  $\beta_y$ .

Once we obtain the form of Eq.(3.13), it is possible to construct a damage tensor due to cracking. As applied stress  $\{\sigma\}$  equals the sum of  $[D]_s\{\epsilon\}_t$  and  $[D]_c\{\epsilon\}_e$  [11],

$$\{\sigma\}_{cr} = [S][D]_c\{\epsilon\}_e + [S][D]_s\{\epsilon\}_t\quad (3.14)$$

and as total strain,  $\{\epsilon\}_t = \{\epsilon\}_e + \{\epsilon\}_{cr}$ ,  $\{\epsilon\}_e$  being the elastic strain,

$$(I - [S][D]_s)\{\epsilon\}_t = ([S][D]_c + I)\{\epsilon\}_e\quad (3.15)$$

Substitution of  $\{\epsilon\}_e$  of Eq.(3.15) to Eq.(3.14) yields,

$$\{\epsilon\}_{cr} = [A]\{\epsilon\}_t\quad (3.16)$$

where

$$[A] = [S][D]_s + [S][D]_c([S][D]_c + I)^{-1}\quad (3.17)$$

Although we can not obtain the inverse of  $[S]$ , the equation is reduced to the following form,

$$[A] = ([S]^{-1} + [D]_c^{-1})^{-1}([D]_c + [D]_s)\quad (3.18)$$





Then from Eq.(2.9),

$$\{\mathcal{Q}\}_{D_1}^S = \{D\}_c \left[ \{S\}^{-1} + \{D\}_c^{-1} \right]^{-1} (\{D\}_c + \{D\}_s) \{D\}_c^{-1} \quad (3.19)$$

However, the stress increase will give rise to the damage in concrete in the compression zone. Hence, another damage tensor  $\{\mathcal{Q}\}_{D_2}$  should be considered. If we assume the independency of  $\{\mathcal{Q}\}_{D_1}$  and  $\{\mathcal{Q}\}_{D_2}$ ,  $\{\mathcal{Q}\}_{D_2}$  is separately derived and the modified  $\{\mathcal{Q}\}_{D_2}$  discussed in [12] is used in the following discussion. So for the frictionless mode of displacement of a concrete panel the following constitutive equation is derived.

$$\{\sigma\} = (I - \mathcal{Q}_{D_1}^S - \mathcal{Q}_{D_2} + \mathcal{Q}_s) \{D\}_c \{\varepsilon\} = (I - \mathcal{Q}_s) \{D\}_c \{\varepsilon\} \quad (3.20)$$

where  $\{\mathcal{Q}_s\} = \{D_s\} \{D_c\}^{-1}$  from Eq.(2.11).

When we consider the uniaxial condition and neglect the Poisson's ratio of concrete, Eq.(3.19) is reduced to

$$\mathcal{Q}_{D_1} = \frac{1 + \frac{np}{\lambda}}{1 + \frac{np}{\lambda}} \quad (3.21)$$

and the factor  $\lambda$  represents the tension stiffening effect as well. For pure shear loading condition to a panel with equal reinforcement to the X and Y directions, Eq.(3.19) is again reduced to the same equation as

$$\{\mathcal{Q}\}_{D_1} = \begin{bmatrix} \frac{1 + \frac{np}{\lambda}}{1 + \frac{np}{\lambda}} & 0 & 0 \\ 0 & 0 & 0 \\ 0 & 0 & 0 \end{bmatrix} \quad (3.22)$$

The derived constitutive equation is applicable to cases where there is no frictional slip at a crack. This situation can be seen for example in the plane subjected unidirectional load or pure shear load.

In Fig.3.5, the comparison of the experimental data by Vecchio, and Collins [13] is shown with the calculated values. In these figures,  $\lambda_{con}$  denotes the factor to be multiplied to the  $\varepsilon_0$ , the strain that corresponds to the maximum compressive stress of concrete. The figures show the tension stiffness effect as well as the shear rigidity. The agreement is reasonable.

#### 4.CONSTITUTIVE EQUATIONS OF CRACKED RC PANELS FOR THE FRICTIONAL MODE

When the concrete has lateral differential movement of two surfaces at a crack as shown in Fig.4.1, the shear dilatancy and shear friction give rise to complicated problems, and the relations between crack opening,  $\delta_n$ , and crack slip,  $\delta_t$ , versus shear stress,  $\tau_{nt}^c$ , and normal stress,  $\sigma_n^c$ , at a crack are still in argument. Bazant and Ganbaroba [3] discussed the characteristics of this and obtained mathematical expressions for each term of the [B] matrix, the stiffness matrix which relates  $(\sigma_n^c, \tau_{nt}^c)$  and  $(\delta_n, \delta_t)$ , from intuitive consideration of the general properties of crack stiffness satisfying singularity conditions at  $(\delta_n, \delta_t) = (0, 0)$ . Recently, Yoshikawa [14] developed a mathematical expression for the [B] matrix from quite a different angle and successfully identified the term from the regression of experimental data.

Referring to the notation in Fig.4.1, the tangential displacement  $\delta_t$  and normal stress,  $\sigma_n$ , due to the shear stress and shear dilatancy effects are written in the following form.

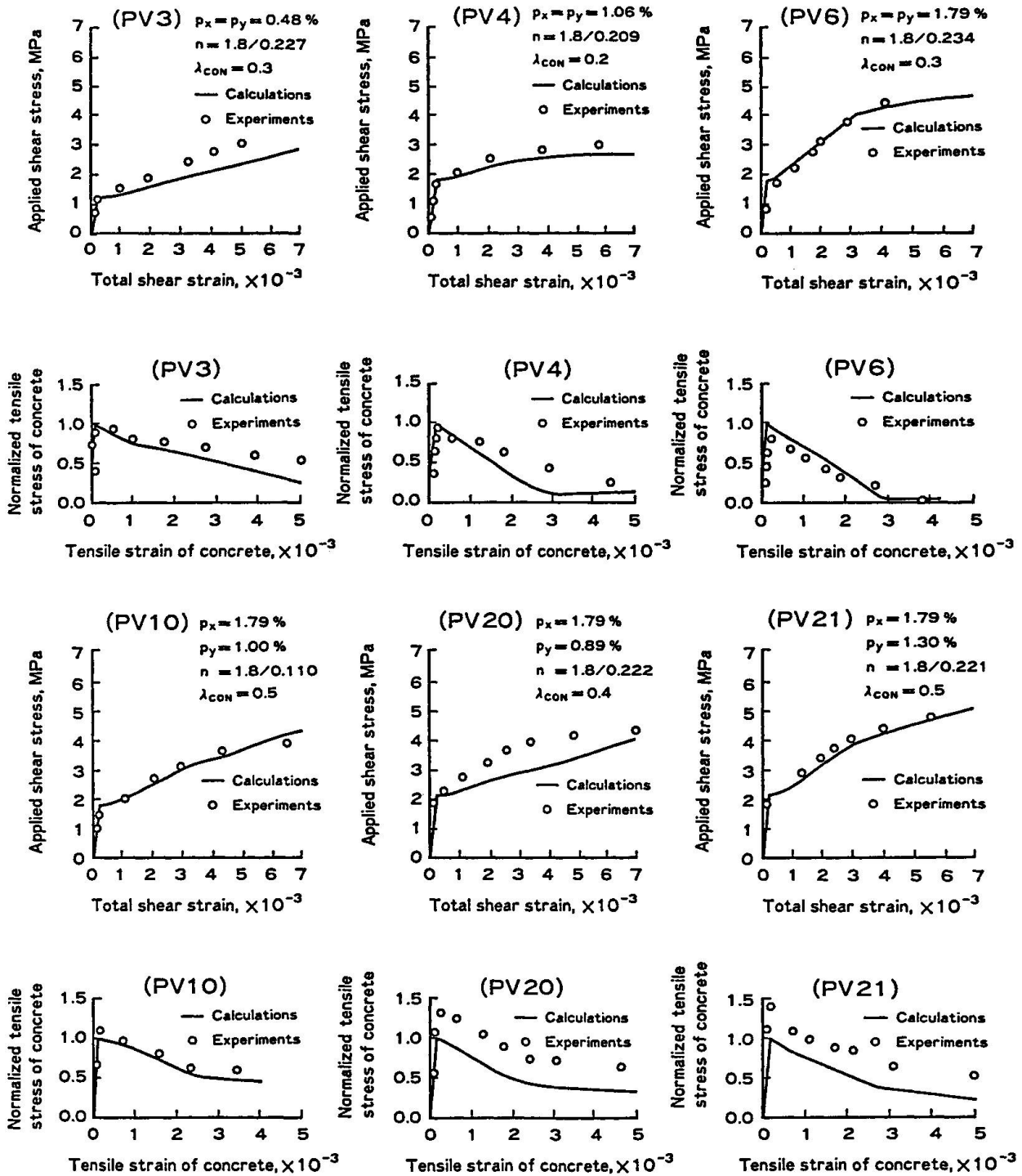


Fig.3.5 Calculated Tension Stiffness Effects and Shear Rigidity Compared with The Experiments by Vecchio and Collins (Ref.13)



$$\begin{aligned}\delta_t &= \delta_t(\tau_{nt}^c, \delta_n) \\ \sigma_n^c &= \sigma_n^c(\tau_{nt}^c, \delta_n)\end{aligned}\quad (4.1)$$

The total differential of  $\delta_t$  and  $\delta_n$  is written as

$$\begin{aligned}d\delta_t &= \frac{\partial \delta_t}{\partial \tau_{nt}^c} \cdot d\tau_{nt}^c + \frac{\partial \delta_t}{\partial \delta_n} \cdot d\delta_n \\ d\sigma_n^c &= \frac{\partial \sigma_n^c}{\partial \tau_{nt}^c} \cdot d\tau_{nt}^c + \frac{\partial \sigma_n^c}{\partial \delta_n} \cdot d\delta_n\end{aligned}\quad (4.2)$$

In Eq.(4.2), the term  $\frac{\partial \tau_{nt}^c}{\partial \delta_n}$  or its inverse do not appear, making the kinematical understanding much easy. However, the form itself is somewhat unusual since one displacement and one stress component are functions of another displacement and stress components. However, the four terms appearing as derivatives of Eq.(4.2) are clearly defined physically.  $(\partial \delta_t / \partial \tau_{nt}^c)_{\delta_n = \text{const}}^{-1} = k_t$  is the shear rigidity at a crack,  $(\partial \delta_t / \partial \delta_n)_{\tau_{nt}^c = \text{const}} = \beta_d'$  is the dilatancy ratio,  $(\partial \sigma_n^c / \partial \delta_n)_{\tau_{nt}^c = \text{const}} = k_n$  is the rigidity to the normal direction of a crack, and  $(\partial \sigma_n^c / \partial \tau_{nt}^c)_{\delta_n = \text{const}} = (-\mu_f)^{-1}$  is the frictional coefficient. These four values are rather easily determined from the comparison of the experimental results.

Eq(4.2). is rewritten in the normal form as,

$$\begin{aligned}d\tau_{nt}^c &= \left[ 1 \quad / \left( \frac{\partial \delta_t}{\partial \tau_{nt}^c} \right) \right] d\delta_t - \left[ \left( \frac{\partial \delta_t}{\partial \delta_n} \right) / \left( \frac{\partial \delta_t}{\partial \tau_{nt}^c} \right) \right] d\delta_n \\ d\sigma_n^c &= \left[ \left( \frac{\partial \sigma_n^c}{\partial \tau_{nt}^c} \right) / \left( \frac{\partial \delta_t}{\partial \tau_{nt}^c} \right) \right] d\delta_t - \left[ \frac{\partial \sigma_n^c}{\partial \delta_n} - \left( \frac{\partial \sigma_n^c}{\partial \tau_{nt}^c} \cdot \frac{\partial \delta_t}{\partial \delta_n} \right) / \left( \frac{\partial \delta_t}{\partial \tau_{nt}^c} \right) \right] d\delta_n\end{aligned}\quad (4.3)$$

or the inverse relation is similarly obtained. Eight different terms of partial derivatives are related to each other as shown in Eq.(4.4).

$$\begin{bmatrix} \frac{\partial \delta_t}{\partial \tau_{nt}^c} & \frac{\partial \delta_t}{\partial \delta_n} \\ -1/\mu_f & k_n \end{bmatrix} \begin{bmatrix} k_t & \frac{\partial \tau_{nt}^c}{\partial \sigma_n^c} \\ \beta_d' & \frac{\partial \sigma_n^c}{\partial \delta_n} \end{bmatrix} = \begin{bmatrix} 1 & 0 \\ 0 & 1 \end{bmatrix}\quad (4.4)$$

As four other partial derivatives are obtained from Eq.(4.4), Eq.(4.3) is rewritten in the form of

$$\begin{bmatrix} d\tau_{nt}^c \\ d\sigma_n^c \end{bmatrix} = k_t \begin{bmatrix} 1 & -(1-\xi)/\beta_d \\ -1/\mu_f & 1/(\mu_f \beta_d) \end{bmatrix} \begin{bmatrix} d\delta_t \\ d\delta_n \end{bmatrix}\quad (4.5)$$

or inversely,

$$\begin{bmatrix} d\delta_t \\ d\delta_n \end{bmatrix} = \frac{1}{\xi k_t} \begin{bmatrix} 1 & (1-\xi)\mu_f \\ \beta_d & \mu_f \beta_d \end{bmatrix} \begin{bmatrix} d\tau_{nt}^c \\ d\sigma_n^c \end{bmatrix}\quad (4.6)$$

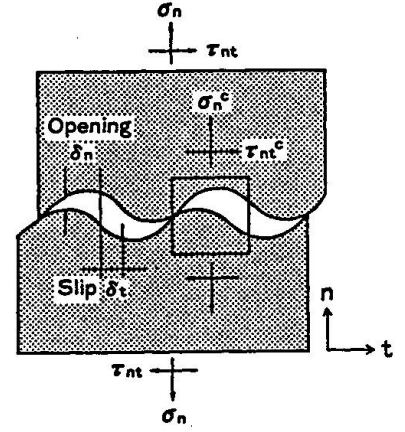


Fig.4.1 Conceptual Figures of Displacements and Stresses at a Crack

Table 4.1 Identification by Yoshikawa of  $k_t$ ,  $k_n$ ,  $\mu_f$ , and  $\beta_d$  Values at A Crack

SHEAR STIFFNESS: $k_t$ [MPa/mm]	CONSTANTS
$k_t = K_{IST} \operatorname{sech}^2 \left\{ \frac{K_o}{\tau_u} (\delta_t - \delta_{t1}) \right\}$ $K_{IST} = a_1 \left( \frac{f_c}{25} \right)^{a_2} \left( \frac{D_a}{16} \right)^{a_3} \delta_n^{-a_4}$ $\delta_{t1} = a_5 \left( \frac{f_c}{25} \right)^{a_6} \left( \frac{D_a}{16} \right)^{a_7} \delta_n^{a_8}$ $\tau_u = \tau_o \frac{a_9}{a_{10} + (\delta_n/D_a)^{a_{11}}}$ $\tau_o = a_{12} f_c$ $K_o = K_{IST} (1 + q)$ $q = \tan h \left( \frac{K_o \delta_{t1}}{\tau_u} \right)$	$a_1 = 3.74, a_2 = 0.60$ $a_3 = 0, a_4 = 0.96$ $a_5 = 1.42, a_6 = 0$ $a_7 = 1.20, a_8 = 1.31$ $a_9 = a_{10} = 0.01$ $a_{11} = 2$ $a_{12} = 0.2 \sim 0.3$ (0.245) $D_a$ : The Maximum Aggregate Size
NORMAL STIFFNESS: $k_n$ [MPa/mm]	CONSTANTS
$K_n = b_1 b_2 (\delta_n - \delta_d \delta_t)^{-(b_2+1)}$	$b_1 = 0.0082$ $b_2 = 0.878$
FRICTIONAL RATIO: $\mu_f$	CONSTANTS
$\mu_f = c_1 \mu_o \exp(c_2 \delta_n)$	$\mu_o = 1.16$ $c_1 = 0.5 \sim 1.5$ $c_2 = 0.61$
DILATANCY RATIO: $\beta_d$	CONSTANTS
$\beta_d = c_3 \beta_o \exp(-c_4 \left  \frac{\sigma_n^c}{f_c} \right )$	$\beta_o = 1.64$ $c_3 = 0.5 \sim 1.5$ $c_4 = 6.42$

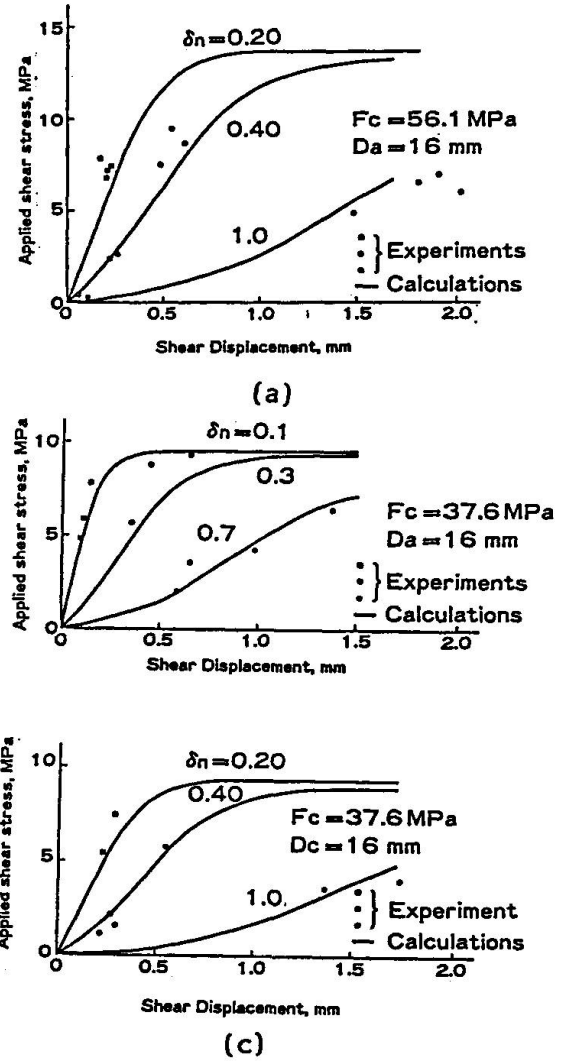


Fig.4.2 The Shear Rigidity at A Crack by Reinhardt and Walraven (Ref.15)

where  $\beta_d = \beta'_d / (1 + \mu_f \beta'_d k_n / k_t)$  and  $\xi = \mu_f \beta_d k_n / k_t$

A detailed discussion of the characteristics of the equation is found in the paper [14]. The identified values by Yoshikawa are shown in Table 4.1 and used in the following numerical calculations.

We will now develop the constitutive equations for the frictional displacement field. We rewrite Eq.(4.5) as the relation of total displacements and total stresses in the following form.

$$\begin{Bmatrix} \tau_{nt}^c \\ \sigma_n^c \end{Bmatrix} = \mu \cdot b_c \begin{bmatrix} A_{11} & A_{12} \\ A_{21} & A_{22} \end{bmatrix} \begin{Bmatrix} \tau_{nt} \\ \epsilon_n \end{Bmatrix} = [A] \begin{Bmatrix} \tau_{nt} \\ \epsilon_n \end{Bmatrix} \quad (4.7)$$

where

$$A_{11} = \frac{1}{\delta_t} \int k_t d \delta_t, \quad A_{12} = \left( \int \left[ k_t (\xi - 1) / \beta_d \right] \cdot d \delta_n \right) / \delta_n, \quad A_{21} = \left( - \int (k_t / \mu_f) d \delta_t \right) / \delta_t$$

$$A_{22} = \left[ \int k_t / (\mu_f \cdot \beta_d) \cdot d \delta_n \right] / \delta_n$$



where  $\mu \cdot b_c$  is the average crack spacing as shown in Eq.(3.5). We transform it for the relation in the global coordinate system using transformation matrices  $T_1$  and  $T_2$  for stress and engineering strain as

$$\{\sigma\} = [T_1]^{-1} [J] [T_2] \{\varepsilon\}_{cr} = [F] \{\varepsilon\}_{cr} \quad (4.8)$$

On the other hand, the concrete portion which does not contain a crack has elastic rigidity and the stress equilibrium at a crack gives the relation,

$$[F] \{\varepsilon\}_{cr} = [D]_c \{\varepsilon\}_e \quad (4.9)$$

The crack strains are derived in terms of total strains from Eq.(4.8) and Eq.(4.9) as

$$\{\varepsilon\}_t = \{\varepsilon\}_{cr} + \{\varepsilon\}_e = ([D]_c^{-1} [F] + I) \{\varepsilon\}_{cr} \quad (4.10)$$

The damage tensor can be derived in the form of Eq.(4.11), referring to Eq.(2.8).

$$[Q]_{D1}^e = [D]_c ([D]_c^{-1} [F] + I)^{-1} [D]_c^{-1} = [D]_c [F] + [D]_c \quad (4.11)$$

If the concrete remains elastic except for the cracked area,  $[Q]_{D1}^e$  of Eq.(4.11) is the only tensor that constitutes the equation; however, as the concrete rigidity is reduced due to the high intensity of compressive stress, we need another damage tensor. Using the series model, total strain is written with the damage strain,  $\{\varepsilon\}_{cd}$ , due to compressive stress as

$$\{\varepsilon\}_t = \{\varepsilon\}_e + \{\varepsilon\}_{cr} + \{\varepsilon\}_{cd} \quad (4.12)$$

and

$$\{\varepsilon\}_{cd} = [D]_c^{-1} [Q]_{D2} [D]_c \{\varepsilon\}_t \quad (4.13)$$

Equation(4.8) with Eq.(4.12) and Eq.(4.13) yields

$$\{\varepsilon\}_{cr} = ([F] + [D]_c)^{-1} [D]_c (I - [D]_c^{-1} [Q]_{D2} [D]_c) \{\varepsilon\}_t \quad (4.14)$$

Hence,

$$[Q]_{D1}^e = [D]_c ([F] + [D]_c)^{-1} (I - [Q]_{D2}) \quad (4.15)$$

The total constitutive equations are derived as

$$\{\sigma\} = (I - Q_{D1}^e - Q_{D2} + Q_R) [D]_c \{\varepsilon\} = (I - Q_R) [D]_c \{\varepsilon\} \quad (4.16)$$

However,  $[Q]_{D1}$  is dependent on  $[Q]_{D2}$ . The applicability of this is examined by comparison with the experiment of panels by Reinhardt and Walraven [15], as shown in Fig.4.2. Agreement seems reasonable.

## 5. CONSTITUTIVE EQUATIONS OF CRACKED RC PANELS FOR THE MIXED MODE

In stress conditions when the crack spacing is comparatively wide and frictional displacement at cracks occurs, the mixed mode of displacement takes place. In other words, the concrete close to the cracks is stressed in compression to the normal direction to a crack surface while the region away from the crack is

stressed in tension. Hence it is considered that the constitutive equation for stress fields of this kind is expressed by the combination of Eq.(3.18) and Eq.(4.16). However, the combination is dependent on a situation which may be classified according to the number of crack orientations, the number of reinforcement orientations, and their relative angles, as the tension stiffening effect in a steel is greatly affected by the occurrence of crossing of cracks in a bar.

In this paper, the following two cases are discussed. The first one is the case in which all cracks are unidirectional. For the cracked reinforced concrete element, the shear forces and normal forces are supposed to be applied. Taking out a representative portion between two cracks it is possible to separate the concrete into two portions, one in which compressive force is working to the normal direction for crack surfaces and the other portion where tensile stress is working to the normal direction for cracked surfaces as shown in Fig.5.1(b).

The transition point of the normal stress from the minus sign (compression) to the plus sign (tension) is again approximated by the linear solution of the governing equation of  $d^2g/d^2\xi - kg = 0$  with boundary conditions of  $\sigma_{s,\xi} = \sigma_{s,\xi}^b$  and  $\sigma_{c,\xi} = \sigma_{c,\xi}^b$  at a crack, where the  $\xi$  direction is normal to crack surfaces. Solving the equation, concrete stress is expressed as

$$\sigma_{c,\xi} = -\frac{s \cdot k}{A_c} \cdot \frac{u_0}{g_0} \left( \frac{\sigma_{s,\xi}^b}{E_s} - \frac{\sigma_{c,\xi}^b}{E_c} \right) \left\{ \cosh \left( \frac{\xi}{b_c} \right) - 1 \right\} \quad (5.1)$$

where  $s$ ,  $u_0$ , and  $g_0$  again denote the perimeter of a bar, the bond strength and the bond slip corresponding to  $u_0$ , respectively, and  $k = (u/u_0)/(g/g_0)$ .  $A_c$  denotes sectional area of tributary concrete section of a bar.

The location where concrete stress changes from compression to tension is written as

$$\xi = b_c \cosh^{-1} C_1$$

$$C_1 = \cosh \left( \frac{\ell_c}{b_c} \right) + A_c \sigma_{c,\xi}^b / \left[ \frac{s k u_0}{g_0} \left( \frac{\sigma_{s,\xi}^b}{E_s} - \frac{\sigma_{c,\xi}^b}{E_c} \right) \frac{b_c^2}{\cosh(\ell_c/b_c)} \right] \quad (5.2)$$

If  $C_1 < 1$ , there exists no tension zone and only the frictional mode exists. However, if  $C_1 > 1$ , the displacement is always in the mixed mode. The portion where concrete is stressed in tension to the  $\xi$  direction, has to be treated as having slip between steel and concrete and its situation is exactly same as the case mentioned in section 3. We separate the concrete portion along the  $\xi$

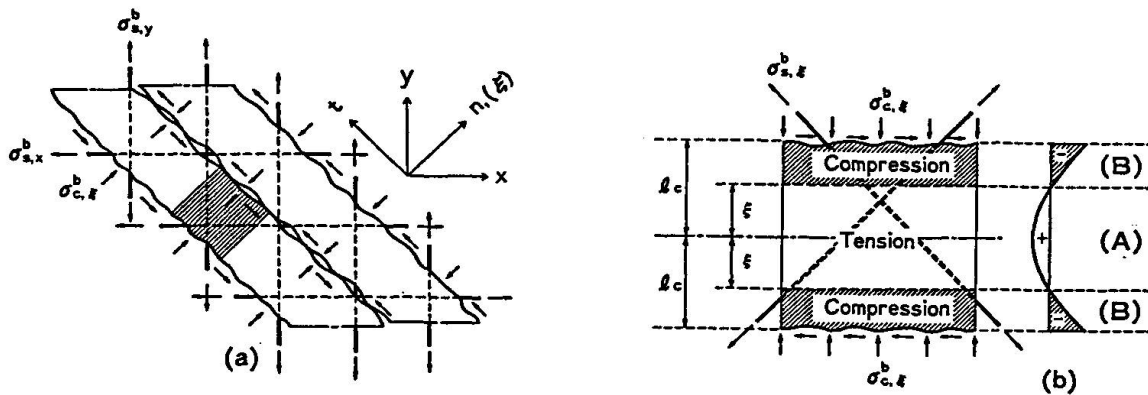


Fig.5.1 Stress Condition at a Crack in the Mixed Mode Displacement Condition



direction to the region A where  $\sigma_\xi$  is in compression and, to the region B where  $\sigma_\xi$  is in tension. The concrete stress is zero at the boundary between A and B. Hence we can consider that the constitutive equation of Eq.(3.20) which considers tension stiffness is applicable in the region A.

The slipping out of a bar at the region A contributes to the crack opening of the region B. Hence the total crack opening,  $\delta_n$ , should be the sum of the contributions from the region A and from the region B.

$$\delta_n = \delta_{n,A} + \delta_{n,B} \quad (5.3)$$

Basing on these consideration, we can develop the constitutive equations for the mixed mode. For the region B, the constitutive equations developed for the frictional mode are applicable. Obviously, at the boundary of two regions, the stress equilibrium should be satisfied. Hence  $\{\sigma\}_A^b = \{\sigma\}_B^b$ , and the total elongation of the portion between two cracks is the sum of the elongation of each region of A and B, and the average strain of the total portion  $\{\epsilon\}_t$  is written as

$$\begin{Bmatrix} \epsilon_n \\ \epsilon_t \\ \gamma_{nt} \end{Bmatrix} = \begin{bmatrix} \eta & 0 & 0 \\ 0 & 1 & 0 \\ 0 & 0 & \eta \end{bmatrix} \begin{Bmatrix} \epsilon_n \\ \epsilon_t \\ \gamma_{nt} \end{Bmatrix}_A + \begin{bmatrix} 1-\eta & 0 & 0 \\ 0 & 0 & 0 \\ 0 & 0 & 1-\eta \end{bmatrix} \begin{Bmatrix} \epsilon_n \\ \epsilon_t \\ \gamma_{nt} \end{Bmatrix}_B = [\eta] \{\epsilon\}_A + [\zeta] \{\epsilon\}_B \quad (5.4)$$

where,  $\eta$  is the fraction to the crack spacing of the length of the area where the concrete is in compression along the  $\xi$  direction and frictionless mode is predominant. This is written in the linear case as

$$\eta = \frac{\xi}{\ell_c} = \frac{1}{\mu_c} \cos h^{-1} C_1 \quad (5.5)$$

As we already have the constitutive equations (3.20) and (4.16) for the regions A and B, Eq.(5.4) is rewritten as

$$\{\epsilon\}_t = [\eta] [D]_c^{-1} (I - [Q]_A)^{-1} \{\sigma\} + [\zeta] [D]_c^{-1} (I - [Q]_B)^{-1} \{\sigma\} \quad (5.6)$$

Hence,

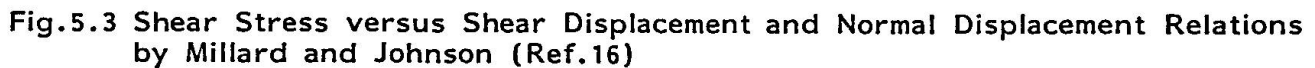
$$\{\sigma\} = [M] \{\epsilon\}_t \quad (5.7)$$

where  $[M] = ([\eta] [D]_c (I - [Q]_A)^{-1} + [\zeta] [D]_c^{-1} (I - [Q]_B)^{-1})^{-1}$

It should be noted that we can not have the frictional mode from the beginning since the crack initiation is always to the principal tensile direction and the first mode should be the frictionless mode. After a small crack width is formed, then the frictional mode or the mixed mode can exist. At the initiation of the first step of the friction mode, the stress equilibrium requires that  $\{\sigma\}_{frictionless} = \{\sigma\}_{friction}$  and the constitutive equation (5.7) of the first step must satisfy this condition.

Experiments corresponding to the mixed mode are very scarce. However, Millard and Jonson [16] carried out this type of experiment using the specimen shown in Fig.5.3(a). They gave rise to a crack at the center of a specimen by applying tensile forces at both ends. Then maintaining the tensile stress, the shear force was applied at the center. The stress condition of concrete will be such that the compressive stress is working at the crack to the normal direction to a crack surfaces while the tensile force is working at the ends to the same direction.

The experimental relations between the shear stress and the shear displacement are shown in comparison with the calculated relations in Fig.5.3(b),(c),(d), and (e). There is some disagreement between them. The calculated values give comparatively softer tendencies compared with the experimental one. These may be due to the assumption of  $\eta=0.5$ . In Fig.5.2, the differences in the shear rigidity due to the extent of the fraction of the region A of the total area were



The only difference from what we derived in the former part of the same section is that shear displacement is affected by the cracks oriented to the X and Y directions. The strain to the normal direction is derived assuming the displacement mode to each direction as the uncoupled mixed mode. Hence,

$$\begin{aligned} [C_M] = & [\eta]_x [D]_c^{-1} (I - \mathcal{Q}_{A,x})^{-1} + [\eta]_y [D]_c^{-1} (I - \mathcal{Q}_{A,y})^{-1} \\ & + [\zeta]_x [M]_x^{-1} + [\zeta]_y [M]_y^{-1} \end{aligned} \quad (5.9)$$

$$\{\eta\}_x = \begin{bmatrix} \eta_x & 0 & 0 \\ 0 & 0 & 0 \\ 0 & 0 & \eta_x \end{bmatrix}, \quad \{\eta\}_y = \begin{bmatrix} 0 & 0 & 0 \\ 0 & \eta_y & 0 \\ 0 & 0 & \eta_y \end{bmatrix}, \quad \{\zeta\}_x = \begin{bmatrix} 1-\eta_x & 0 & 0 \\ 0 & 0 & 0 \\ 0 & 0 & 1-\eta_x \end{bmatrix}, \quad \text{and} \quad \{\zeta\}_y = \begin{bmatrix} 0 & 0 & 0 \\ 0 & 1-\eta_y & 0 \\ 0 & 0 & 1-\eta_y \end{bmatrix}$$

The value of  $\eta_x$  is the fraction of the region where the frictionless mode is



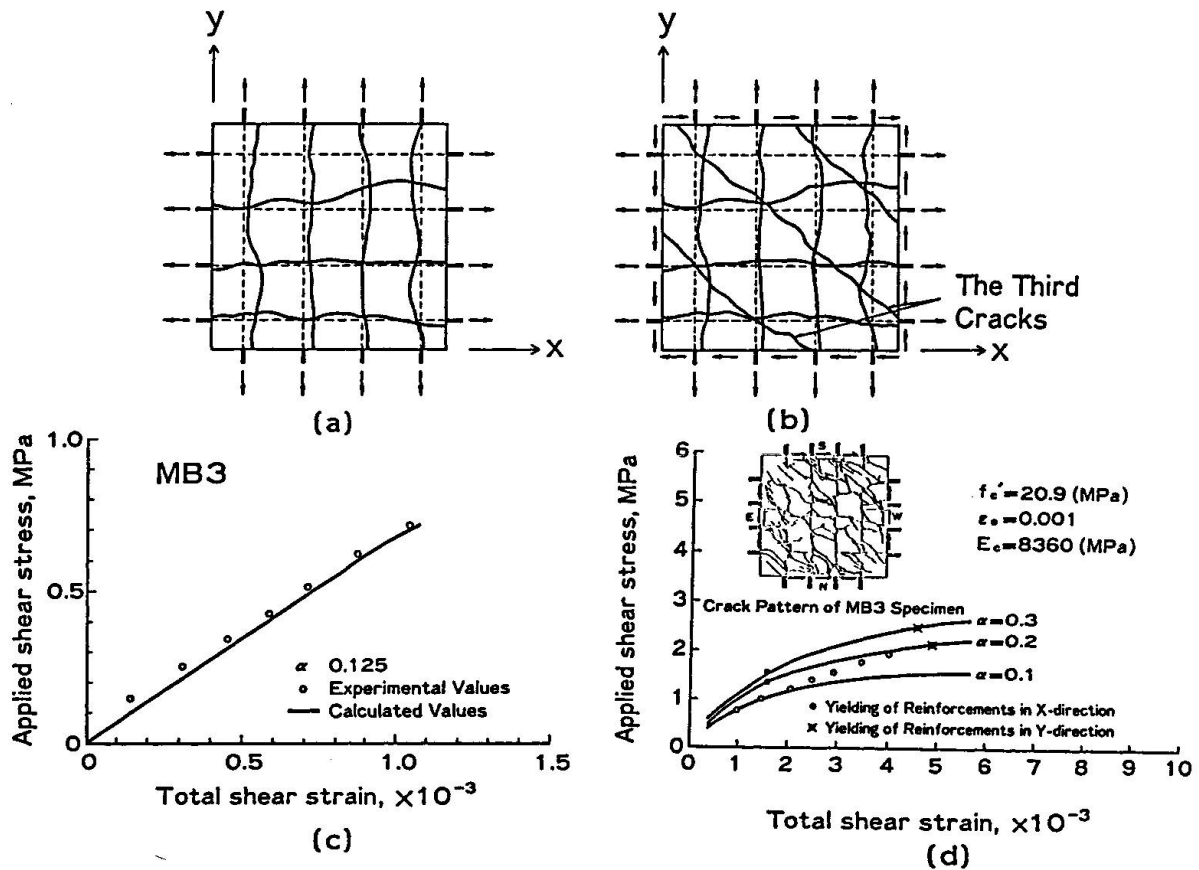


Fig.5.4 Shear Rigidity Before the Formation of Third Cracks and the Ultimate Strength of MB3 Specimen by Oesterie and Russell (Ref.17)

predominant to the total region along the X direction, and  $\eta_y$  is defined similarly along the Y direction.

Oesterie and Russell [17] have carried out experiments applying biaxial tension to specimens in the first stage, giving rise to substantial crack width to the X and Y direction, then applying shear force to the point of failure of the specimens, as shown in Fig.5.4(b). The constitutive Eq.(5.9) is applicable until the third crack is formed to  $135^\circ$  to the X direction. Out of three specimens, two specimens with reinforcement ratios of 0.022 for the X direction and 0.013 for the Y direction were tested by applying loads monotonically. Both showed very similar behavior. For the specimen MB3, crack widths observed at the state when biaxial tension of 5.7 MPa for the X direction and 3.5 MPa for the Y direction were applied were 0.48 mm to the X direction and 0.38 mm to the Y direction, while Eq.(3.20) gives 0.46mm for the X direction and 0.40 mm for the Y direction. The experiments showed that when the shear force was applied maintaining the last tensile stress level constant, the crack width closed in the Y direction and opened wider in the X direction. Eq.(5.9) also gives the same characteristics. The shear strain and applied shear stress relation during that process is given in Fig.5.4(c), comparing the observed values with the calculated values. In the figure,  $\alpha$  is the parameter which was multiplied to the initial Young's Modulus of concrete in the calculation. At 0.7 MPa of applied shear stress, the third crack, oriented  $135^\circ$  to the X direction, has occurred, and some variation in the shear rigidity was observed. At this stage, Eq.(5.9) is not applicable. However, the ultimate strength may be assessed by

Eq.(3.20) reducing the concrete rigidity which is affected by the three directional crackings. The real line shown in the same figure does not have any meaning other than as a mere estimation of the ultimate strength by the frictionless mode. However, the comparison seems to show that equivalent rigidity of concrete at the cracked condition shown in Fig.5.4(d) is almost 3/10 or less of the initial Young's Modulus of concrete.

## CONCLUSION

Constitutive equations of composite material of concrete and reinforcement in two dimensional stress field are developed using damage and reinforcement tensors. The derived damage tensors and reinforcement tensors express rationally the tension stiffness effects affected by the reinforcement ratio, bond slip characteristics between concrete and steel, nonlinear deterioration of concrete in compression, and crack stiffness, in which shear dilatancy and shear friction are incorporated. The damage tensors make the nonlinear calculation much easier owing to the fact that  $\epsilon$  terms can be treated as initial strains or initial stresses to be accommodated in usual FEM programs.

The constitutive equation for the frictional mode is stable and seems quite dependable as we did not meet any numerical divergence due to the instability of the formulation. However, formulation is limited by the number of the crack orientations and if their number is beyond three and cracks are not parallel to reinforcement, we need to develop a formulation which can simulate the tension stiffening effect for that situation.

## ACKNOWLEDGEMENT

Authors express their sincere thanks to Dr. S.Hatanaka, and graduate students, Z.S.Wu and D.R.Lokuliyana for their valuable assistance in the numerical calculations as well as in the preparation of the manuscript.

## REFERENCES

1. Powell, G.H., DE Villiers, I.P., and Lillon, R.W., Implementation of Endochronic Theory for Concrete with Extensions to Include Cracking, SMIRT 5, Vol.M, Berlin, August, 1979, M2/6.
2. Bazant, Z.P., and Gambaroba, P., Rough Cracks in Reinforced Concrete, Journal of the Structural Division, ASCE, Vol.106, No. ST4, pp.819-842, April, 1980.
3. Tanabe, T., Kawasumi, M., and Yamashita, Y., Finite Element Modelling for the Thermal Stress Analysis of Massive Concrete Structures, Proc. of Japan-US Science Seminar on Finite Element Analysis of Reinforced Concrete Structures, Vol.2, pp.75-93, Tokyo, May, 1985.
4. Yoshikawa, H., and Tanabe, T., A Finite Element Model for Cracked Reinforced Concrete Members Introducing Crack Strain Concept, Proc. of Japan-US Science Seminar on Finite Element Analysis of Reinforced Concrete Structures, Vol.2, pp.237-246, May, 1985.
5. Goto, Y., Cracks Formed in Concrete Around Deformed Tension Bars, ACI Journal, Vol.68, No.4, pp.244-251, April, 1971.
6. Ozaka, Y., Ohtsuka, K., and Matsumoto, Y., Cracks Formed in Concrete Prism with Axial Tension Bars under Influence of Drying, Concrete Journal, JCI, Vol.23, No.3, pp.109-119, March, 1985.
7. Yoshikawa, H., and Tanabe, T., An Analytical Study for the Tension Stiffness of Reinforced Concrete Members on the Basis of Bond Slip Mechanism, Proceedings of JSCE, No.366, pp.93-102, V-4, Feb., 1986.



8. Yamamoto, Y., Study on Bond Stress of Reinforcements, Crackings and Restoring Characteristics of Embedded Tension Bars (in Japanese), Taisei Technical Report 6, Technical Research Institute, Taisei Corporation, pp.151-193, 1973.
9. Somayaji, S., and Shah, S.P., Bond Stress Versus Slip Relationship and Cracking Response of Tension Members, ACI Journal, Vol.78, No.3, pp.217-225, May-June, 1981.
10. Rizkalla, S.H., and Hwang, L.S., Crack Prediction for Members in Uniaxial Tension, ACI Journal, Vol.81, No.6, pp.572-579, Nov.-Dec., 1984.
11. Tanabe, T., and Lokuliyana, D.R., Constitutive Equations of a Cracked Reinforced Concrete Panel in Frictionless Mode of Displacements, Proceedings of the 43rd Annual Conference of the JSCE, September, 1987 (to be published).
12. Vecchio, F., and Collins, M.P., Stress-Strain Characteristics of Reinforced Concrete in Pure Shear, Final Report of IABSE Colloquium on Advanced Mechanics of Reinforced Concrete, pp.211-255, Delft, June, 1981.
13. Yoshikawa, H., Analytical Models for the Mechanical Behavior of Reinforced Concrete Members Subjected to Inplane Stresses, Dissertation to University of Tokyo, February, 1987.
14. Reinhardt, H.W., and Walraven, J.C., Cracks in Concrete Subjected to Shear, Journal of the Structural Division, ASCE, Vol.108, No.ST1, pp.207-224, January, 1982.
15. Millard, S.G., and Johnson, R.P., Shear Transfer in Cracked Reinforced Concrete, Magazine of Concrete Research, Vol.37, No.130, pp.3-15, March, 1985.
16. Oesterie, H.G., and Russel, H.G., Shear Transfer in Large Scale Reinforced Concrete Containment Elements, Construction Technology Laboratories, NUREG/CR-1374, April, 1980.

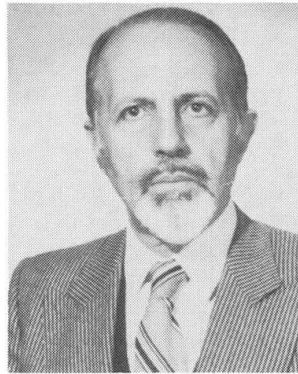
## A Model for Local Crack Behaviour

Modèle de comportement à proximité des fissures

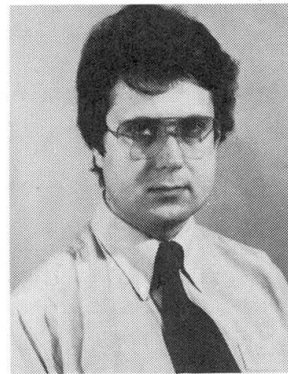
Ein Modell für lokales Rissverhalten

### T.P. TASSIOS

Prof. of Reinforced  
Concrete  
Nat. Techn. Univ.  
Athens, Greece



T.P. Tassios, born 1930, is Professor of Reinforced Concrete at the Nat. Techn. University of Athens. He is currently President of CEB and author of several publications on R.C. non-linear behaviour, mainly under cyclic actions.



### A. SCARPAS

Research Fellow  
Nat. Techn. Univ.  
Athens, Greece

A. Scarpas, born 1956, received his B. Eng. Civil degree from McGill University, Canada and a M. Eng. Civil degree from the University of Canterbury, New Zealand. He is currently completing his Ph.D. dissertation on the Non-Linear Finite Element Analysis of RC Structures at the Nat. Techn. University of Athens.

### SUMMARY

A physical model is proposed for the study of the phenomenon of interface shear transfer in cracked RC. By accounting separately for the contribution of all shear resisting mechanisms at the crack interface, the model can predict both the monotonic and the reversed cyclic response of cracked RC interfaces subjected to a system of in-plane forces.

### RÉSUMÉ

Un modèle physique est proposé pour l'étude du phénomène de transfert des efforts tranchants dans le béton armé fissuré. Prenant en compte séparément la contribution de tous les mécanismes de résistance à l'effort tranchant dans la zone de fissures, le modèle prédit aussi bien la réponse monotonique que cyclique dans les zones de fissures du béton armé soumis à un système de forces dans un plan.

### ZUSAMMENFASSUNG

Ein physikalisches Modell zum Studium der Schubübertragung in Rissen im Stahlbeton wird vorgeschlagen. Dadurch, dass die Beiträge aller Schubübertragungsmechanismen getrennt erfasst werden, kann das Modell das statische wie zyklische Verhalten von Stahlbeton im Scheibenspannungszustand vorhersagen.



## 1. INTRODUCTION

The predominantly non-linear behaviour of R/C members has led many researchers into using the Finite Element Method as a versatile tool to assist in understanding their response. Any accurate R/C finite element analysis must consider the influence of non-linearities. For R/C members, the most pronounced material non-linearity is cracking.

The development of a computer program which accounts automatically for crack formation and propagation and which includes the shear transfer mechanisms across cracks has been undertaken at NTUA [1]. The Discrete Cracking approach has been used, since it was felt that it provides a means of incorporating in the analysis the complex characteristics of the crack interface shear transfer mechanisms and, at the same time, allows the detailed study of the phenomena of crack formation and propagation.

Modelling of the restraining action of the reinforcing bars crossing a crack and of their contribution to the phenomenon of shear transfer at the crack interface is achieved by means of a specially developed "shear transfer" element. Its stiffness has been derived on the basis of the results of a physical model for local crack behaviour. The essence of the model and its unique ability to simulate the interaction between all the shear resisting mechanisms at the crack interface were first presented in Ref. [9].

## 2. SHEAR TRANSFER IN R.C. CRACKS

The shear transfer mechanisms at a R/C cracked interface are identified in Fig. 1. With increasing shear displacements, the wedging action at the crack faces tends to push apart the concrete blocks on each side of the crack. Unless this dilatancy is restrained, very little shear can be transferred. In R.C. cracks the restraint is provided by external normal stresses (if compressive) and by the reinforcement crossing the crack.

From Fig. 1 it becomes apparent that because of the wedging action the reinforcement is tensioned while, at the same time, compressive forces are developed at the crack faces. This plying action of the reinforcement not only restrains crack opening but also enables the development of the friction mechanism at the faces of the crack. In addition, the imposed shear displacements activate the dowel mechanism of the bars which cross the crack. Thus in R.C. cracks, shear transfer results from the combined action of both, friction and the dowel action mechanisms.

## 3. PHYSICAL MODEL FOR LOCAL CRACK BEHAVIOUR

Natural concrete aggregates have an irregular shape and are randomly orientated within the cement paste. Because the strength of aggregates usually exceeds that of the hardened cement paste, cracks intersect the cement paste but run along the surface of the embedded larger aggregate particles, Fig. 2. Hence in modelling the topology of the proposed model, a "saw tooth" idealization appears to be adequate, at least for the purposes of setting up the constitutive equations of the model.

At this stage, no prediction needs to be made with regard to the magnitude of the angle  $\alpha$ , the length and the regularity of the crack teeth. The model can be calibrated with respect to these parameters, on the basis of available experimental results, and refinements can be made to portray their influence on the computed crack behaviour. For example, recent experimental results obtained at NTUA [2] indicate that a realistic estimate for the magnitude and the variation of the crack

angle  $\alpha$  under monotonic loading can be obtained from the relation :

$$w = k * s^{2/3} \quad , (k = 0.6 \text{ to } 0.7) \quad \text{Eq. 1}$$

Only local crack behaviour is to be simulated by both, the proposed "physical" model and the corresponding "shear transfer" finite element. Within the context of the Finite Element Method, shear transfer along the length of a discrete crack spanning through concrete elements, can be simulated by the inclusion of a number of "shear transfer" elements connecting the nodes at opposite faces of the crack line [1], [6].

On a local basis and depending on whether the opposite crack faces come into contact or not, the corresponding cracked regions will be termed in the following as "one - side closed" and "fully open", respectively.

### 3.1 Locally Fully Open Crack

Considering the cracked concrete section shown in Fig. 3(a), to an imposed magnitude of crack slip  $s$  corresponds a crack width  $w$ . If the two concrete blocks are assumed to displace as rigid bodies without rotation, then, all points along the upper crack face displace from their original (before cracking) positions along a vector parallel and equal to the vector  $AA'$ . The same is true for two points along the reinforcing bar, one at each face of the crack.

Following a kinematic analysis, vector  $AA'$  can be analysed into components parallel and transverse to the reinforcing bar axis, Fig. 3(a). Hence, the net bar elongation  $w'$  can be expressed in terms of the crack opening displacement  $w$  and the imposed shear displacement  $s$  as :

$$w' = w \sin \theta - s (\tan \alpha \sin \theta + \cos \theta) \quad \text{Eq. 2(a)}$$

and the net bar dowel displacement  $s'$  as :

$$s' = w \cos \theta - s (\tan \alpha \cos \theta - \sin \theta) \quad \text{Eq. 2(b)}$$

Knowledge of these steel displacements allows the determination of the corresponding bond  $B$  and dowel  $D$  forces developed by the reinforcement at the face of the crack (Fig. 3(b)) by means of formalistic sub-models that have been developed on the basis of extensive theoretical and experimental work [2].

A particular characteristic of this model is that to each shear slip displacement  $s$  corresponds a whole range of possible crack width  $w$  values, Fig. 4. However, out of these displacements there exists a unique one for which the overall static equilibrium of the element (see also Fig.5) :

$$f(\Delta V, \Delta N) = 0 \quad \text{Eq. 3}$$

is satisfied. The algorithm of Fig. 6 presents the successive steps for the computation of response of the proposed crack model to imposed shear displacements. Details can be found in [1] and [3].

### 3.2 Locally One-Side Closed Crack

In the case when the value of  $w$  required for equilibrium is equal to  $2s \tan \alpha$ , the crack becomes "one-side closed". Now and because of the wedging action of the crack faces, the upper concrete block slides along the crack teeth, Fig. 7(a).





Following a kinematic analysis, the bar pull-out can be computed as :

$$w' = s(2\tan\alpha\sin\theta - \cos\theta) \quad \text{Eq. 4(a)}$$

and the dowel-displacement as :

$$s' = s(2\tan\alpha\cos\theta + \sin\theta) \quad \text{Eq. 4(b)}$$

In Fig. 7(b) the external and internal forces for the case of an "one-side closed" crack are identified. Comparison of this model with the "fully open" one reveals that in the former, two additional actions, namely, friction and concrete contact forces participate in shear resistance.

Because of the dependance of friction stresses on both the normal stresses acting on the interface and the magnitude of the imposed frictional slip, the magnitude of the friction force  $F$  can be determined by means of an appropriate frictional constitutive law (see e.g.[7]).

As shown in the algorithm of Fig. 8, for the computation of the response of an "one-side closed" crack model, a trial-and-error numerical procedure is followed for the determination of the values of friction force  $F$  and concrete contact force  $R$ , which fulfill the overall static equilibrium of the crack element.

#### 4. LOCAL CRACK MODEL FOR MESH REINFORCED CONCRETE

Based on the same principles and techniques, a similar model has been developed [1] [4] for the study of the response of cracked interfaces in concrete elements reinforced with a rectangular mesh, Fig. 9.

#### 5. NUMERICAL APPLICATIONS

For the application of the proposed physical "Local Crack" model to the study of both, monotonic and reversed cyclic shear transfer along cracked interfaces, a computer program was developed. For any given increment of slip  $\Delta s_i$ , the program automatically determines whether the crack is "fully open" or "one - side closed". Using the algorithms of Figs. 6 and 8, the shear force  $V_i$  corresponding to the imposed crack slip  $s_i = s_{i-1} + \Delta s_i$  is computed. By means of this program, the response of cracked concrete elements reinforced with steel bars and subjected to monotonic or reversed cyclic loading histories was studied.

The dramatic increase in shear carrying capacity of a R.C. element (of length 200 mm and width 100 mm, reinforced with two parallel bars) as a result of the increase in bar inclination  $\theta$  from 45 to 135 degrees is shown in Fig. 10(a). Both the stiffness and the shear carrying capacity increase abruptly after closing of the crack (i.e. one-side closed model) and the engagement of the much stiffer friction mechanism. The improved control of crack width as the inclination of the bar increases is shown in Fig. 10(b). On a qualitative basis, the results of Fig. 10 compare very favourably with Walraven's experimental results (8).

Axial force plays a major role in determining crack behaviour, Fig. 11, since, depending on its magnitude and direction, participation of the friction mechanism in carrying a significant portion of the externally imposed shear may be accelerated, delayed or even completely annihilated (e.g. for large tensile forces). The significance of bar diameter is shown in the same figure. Larger bar diameter implies larger participation of the bond and the dowel mechanisms in resisting the imposed shear at the cracked interface.



For an element reinforced with a single bar, reversed cyclic loading resulted to a severe reduction in stiffness as early as the second half of the first cycle, while the response became very soft at low load levels, Fig. 12(a). Since the stiffness of all involved mechanisms reduces with cycling, a continuous increase of crack width was observed, Fig. 12(b).

Less pronounced appeared to be the influence of bar inclination on the shear carrying capacity of a cracked element (of length 200 mm and width 100 mm) reinforced with two layers of mesh reinforcement, Fig. 13. Nevertheless, as  $\theta$  increased, better control of crack opening was achieved. Here again, significant appeared to be the influence of both the bar diameter and the axial load, Fig. 14.

## 6. CONCLUSIONS

The physical modelling of a reinforced crack, supported by detailed sub-models of the intervening shear transfer mechanisms, is a versatile analytical tool in describing the structural behaviour of particular interfaces (e.g. precast connections) and of cracks through R.C. elements in general.

## 7. REFERENCES

1. SCARPAS A., Numerical Simulation of Cracking in R/C Structures. Ph.D. Thesis, (Supervised by T.P. Tassios), Dept. of Civil Engineering, NTUA, Athens. (in preparation)
2. VINTZELEOU E.N., Mechanisms of Load Transfer along Reinforced Concrete Interfaces under Monotonic and Cyclic Actions. Ph.D. Thesis, (Supervised by T.P. Tassios), Dept. of Civil Engineering, NTUA, Athens, Dec. 1984. (in Greek)
3. PAPAMAKARIOS A., Modelling of Shear Transfer through Singly Reinforced Cracked Concrete Interfaces. Diploma Thesis Dissertation, (Supervised by A. Scarpas and T.P. Tassios), Dept. of Civil Engineering, NTUA, Athens, Sept. 1982. (in Greek)
4. THEOPHANOPOULOS N., Modelling of Shear Transfer through Cracks in Mesh Reinforced Concrete. Diploma Thesis Dissertation, (Supervised by A. Scarpas and T.P. Tassios), Dept. of Civil Engineering, NTUA, Athens, June 1983. (in Greek)
5. POUANGARE H., Modelling of Shear Transfer in Cracks of Reinforced Concrete, Diploma Thesis Dissertation, (Supervised by A. Scarpas and T.P. Tassios), Dept. of Civil Engineering, NTUA, Athens, June 1986. (in Greek)
6. LAMBROPOULOS N., Discrete Cracking Analysis of Reinforced Concrete Members, Diploma Thesis Dissertation, (Supervised by A. Scarpas), Dept. of Civil Engineering, NTUA, Athens, Feb. 1986. (in Greek)
7. TASSIOS T.P., VINTZELEOU E., Concrete to Concrete Friction. (to be published in the Journal of ASCE, Structural Division).
8. WALRAVEN J.C., Aggregate Interlock : A Theoretical and Experimental Analysis. Ph.D. Thesis, Delft University of Technology, Delft, 1980.
9. TASSIOS T.P., VINTZELEOU E., Shear Force-Displacements Characteristics of Prestressed Connections. Proc. of the RILEM-CEB-CIB Symposium on the Mechanical & Insulating Properties of Joints of Precast R/C Elements, Athens, Sept. 1978.

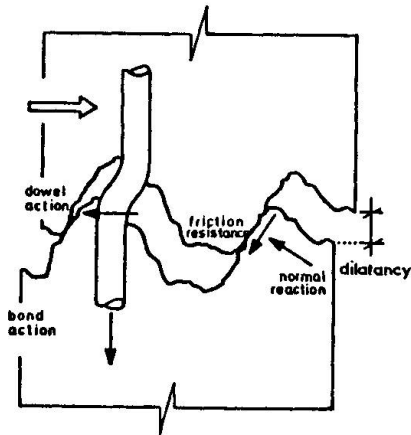


Fig. 1: Shear transfer mechanisms at the crack interface.

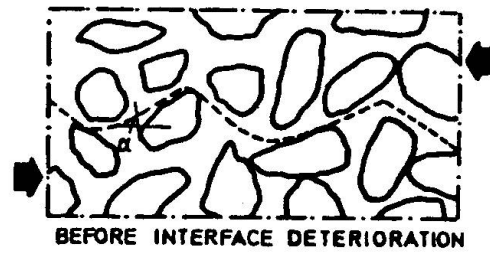
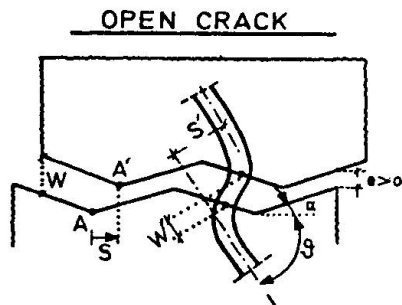
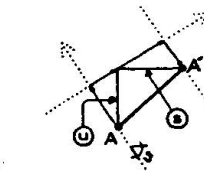


Fig. 2: Formation of the "concrete teeth"



KINEMATIC  
CONDITIONS:  $W' = f(W, S, \theta)$   
(a)  $S' = f(W, S, \theta)$



FORCE EQUILIBRIUM:

$$f_h(D, B, V, N, \theta) = 0$$

$$f_v(D, B, V, N, \theta) = 0$$

- EXTERNAL FORCES  $N, V$
- MOBILISED RESISTANCES  $D = D(S')$   
 $B = B(W)$

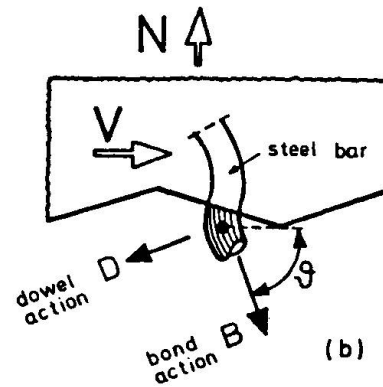


Fig. 3: "Open" crack model

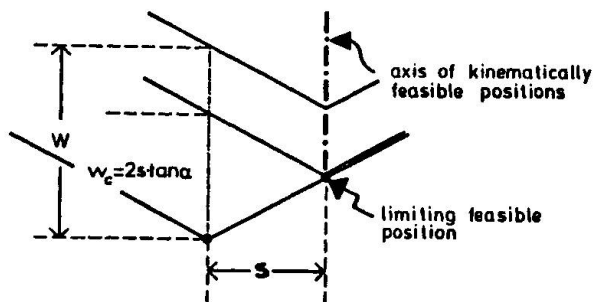


Fig. 4: Feasible equilibrium positions for the "Open" crack model

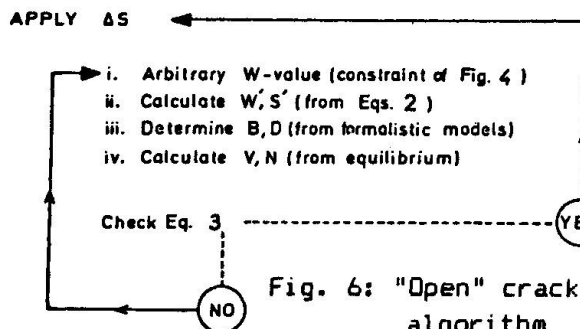
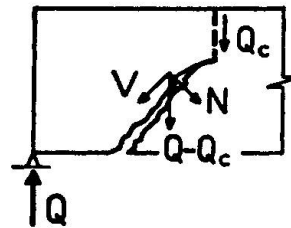


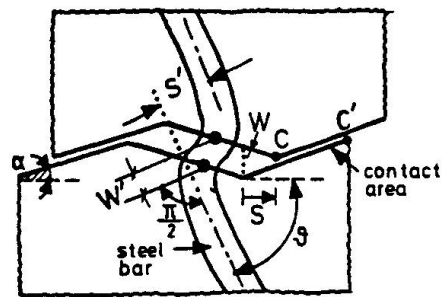
Fig. 6: "Open" crack algorithm



$$f(\Delta V, \Delta N) = \Delta V - \Delta N = 0$$

Fig. 5: Differential relationship for the equilibrium of internal forces along an inclined crack

# ONE SIDE CLOSED CRACK



KINEMATIC CONDITIONS:

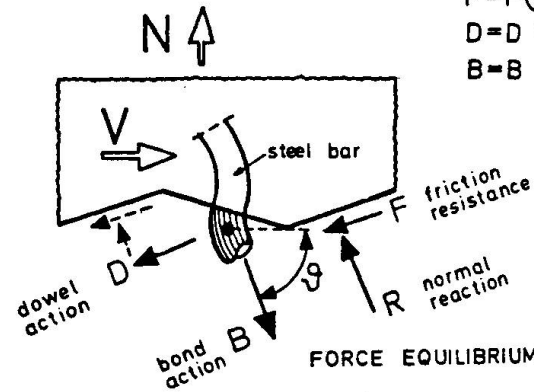
$$\begin{aligned} w' &= s(2 \tan \alpha \cdot \sin \theta - \cos \theta) \\ s' &= s(2 \tan \alpha \cdot \cos \theta + \sin \theta) \end{aligned}$$

(a)

Fig. 7: "One-Side Closed" crack model

- EXTERNAL FORCES  $N, V$
- MOBILISED RESISTANCES  $R$

$$\begin{aligned} F &= F(R, S) \\ D &= D(S') \\ B &= B(W) \end{aligned}$$



(b)

FORCE EQUILIBRIUM:

$$\begin{aligned} f_h(D, B, F, R, V, N, \theta) &= 0 \\ f_v(D, B, F, R, V, N, \theta) &= 0 \end{aligned}$$

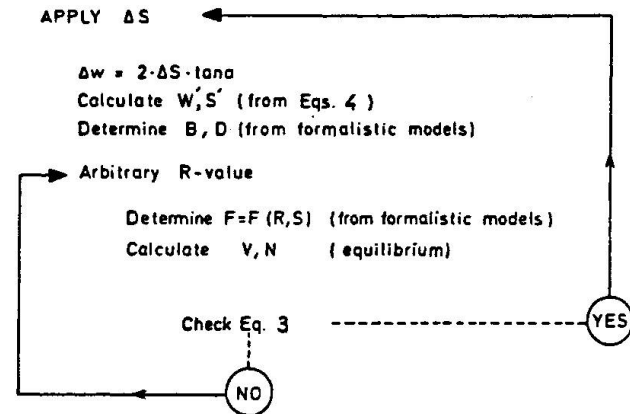


Fig. 8: "One-Side Closed" crack algorithm

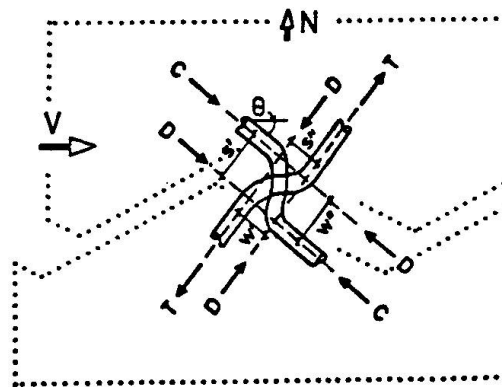
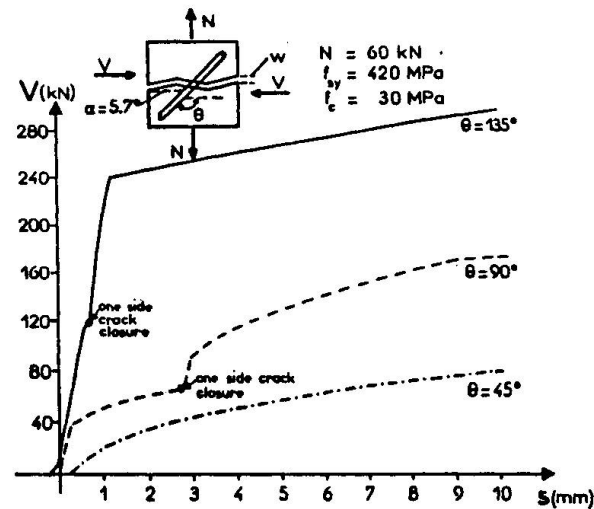
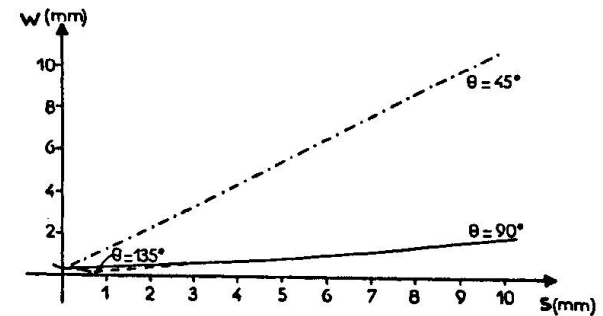


Fig. 9: Modeling of shear transfer through cracks in mesh R.C.



(a)



(b)

Fig. 10: Influence of the variation of bar inclination  $\theta$  on : (a) the response characteristics of a reinforced crack (b) the corresponding crack width  $w$

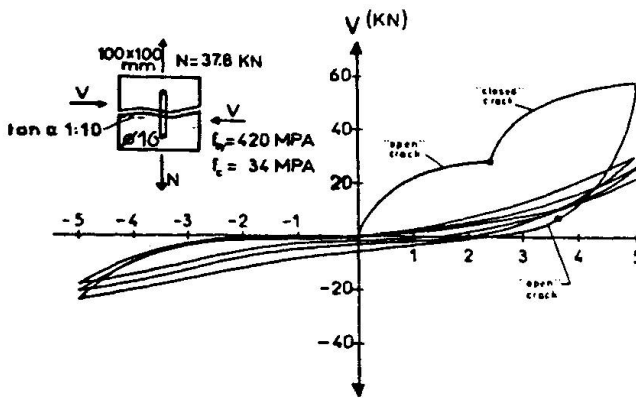


Fig. 12(a): Crack behaviour under reversed cyclic loading

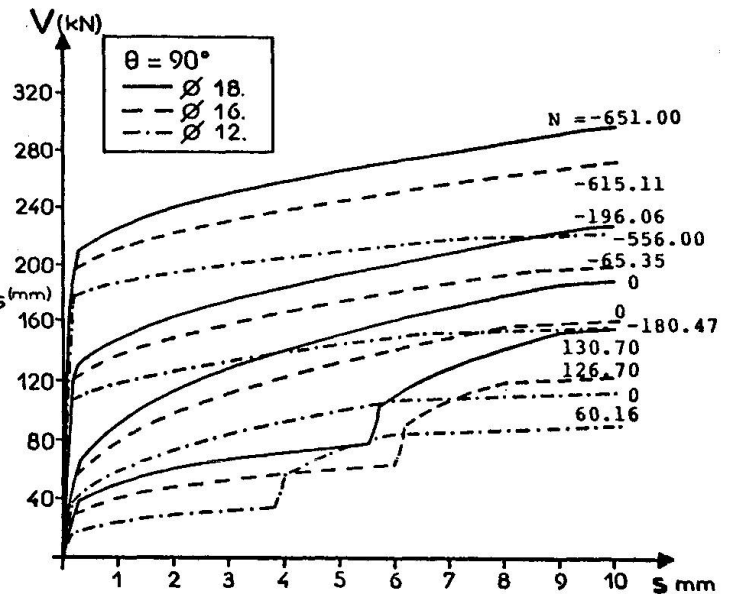


Fig. 11: Influence of the variation of bar diameter and axial force on the response characteristics of a reinforced crack

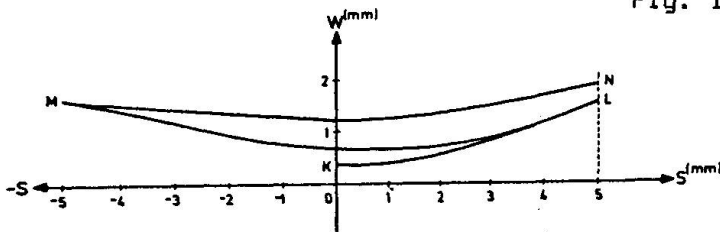


Fig. 12(b): Increase of crack width due to reversed cyclic loading.

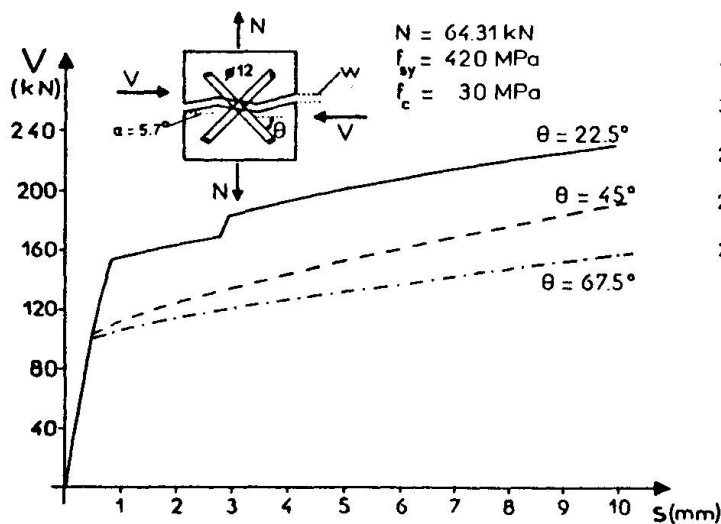


Fig. 13: Influence of the variation of bar inclination  $\theta$  on the response characteristics of mesh reinforced cracks

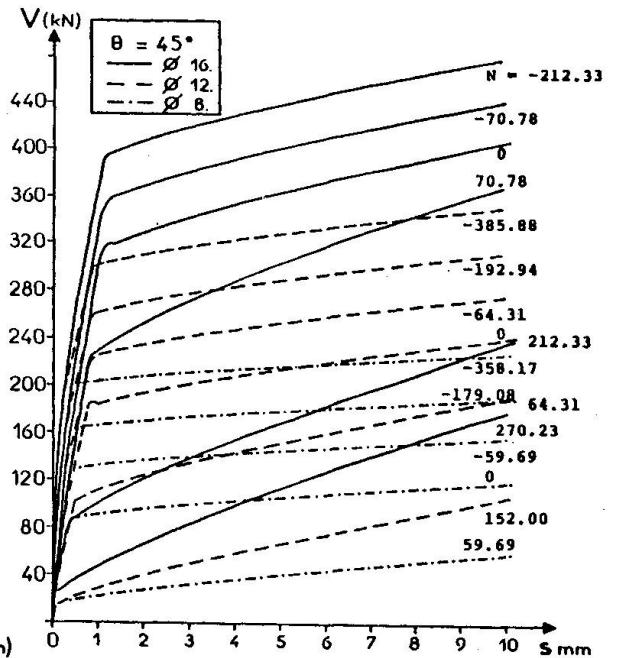


Fig. 14: Influence of the variation of axial force and bar diameter on the response characteristics of mesh reinforced cracks.

## Shear Resistance of Cracked Concrete Subjected to Cyclic Loading

Résistance au cisaillement de béton fissuré, soumis à un chargement répété

Die Schubtragfähigkeit von gerissenem Beton bei zyklischer Belastung

### Arjan F. PRUIJSSERS

Research Engineer  
Delft Univ. of Techn.  
Delft, The Netherlands



Arjan F. Puijssers, born 1958, received his M.Sc. degree at Delft Univ. of Techn. in 1982. Presently he is working in the Stevin Laboratory as a research engineer on the shear resistance of cracked reinforced concrete.

### SUMMARY

The shear resistance of cracked concrete depends upon the roughness of the crack surfaces and the dowel action of the embedded reinforcing bars. For reinforced concrete, the static crack-opening path is described using Walraven's aggregate interlock model. Results of 'high-cycle low-amplitude' tests with repeated shear loading are presented, showing that the crack behaviour can be described quasi-statically. Furthermore, 'low-cycle high-amplitude' experiments on cracked plain concrete are simulated with an extended version of Walraven's model.

### RÉSUMÉ

La résistance au cisaillement d'un béton fissuré dépend de la rugosité des surfaces intérieures des fissures et de l'effet de goujon de l'armature. Pour le béton armé le cheminement de l'apparition des fissures sous un chargement statique est décrit à l'aide du modèle de Walraven sur l'interpénétration des granulats. Les résultats d'essais de nombreux cycles de faible amplitude, avec un effort tranchant répété montrent que le comportement des fissures peut être décrit comme étant quasiment statique. Des essais avec un nombre restreint de cycles de grande amplitude sont simulés avec une version développée du modèle de Walraven.

### ZUSAMMENFASSUNG

Die Schubtragfähigkeit von gerissenem Beton hängt von der Rauigkeit der Rissoberflächen und der Dübelsteifigkeit der Bewehrung ab. Für die statische Schubbeanspruchung von Rissen in bewehrtem Beton lässt sich das allmähliche Anwachsen der Rissverformungen mit dem Modell von Walraven erklären, das auf der Rauigkeit der Rissoberflächen beruht. Versuche mit einer sehr oft wiederholten Schubbelastung zeigten, dass das Verhalten der Risse quasi-statisch beschrieben werden kann. Für Risse, die durch eine sehr hohe zyklische Belastung beansprucht werden, kann die Schädigung der Rissoberflächen mit einer zyklischen Version des Modells von Walraven berechnet werden.



## 1. INTRODUCTION

The problem of designing large-scale concrete structures, such as offshore platforms and nuclear containment vessels, with sufficient safety against failure is based upon the idealization of the structure as an assembly of simple structural members. The response of these members to applied loads can be investigated in experimental programs. The interactions between the elements and their redistribution of the loads can be simulated in numerical programs.

Due to tensile stresses caused by the applied loads and restrained deformations the concrete members will be cracked. Therefore, the concrete structure will respond in a highly non-linear manner to severe loading conditions such as earthquakes, wave attacks, collisions. Hence, the problem of designing complex concrete structures is shifted towards a thorough understanding of the response of the simple elements to cyclic loading conditions. The behaviour of a simple member, such as a membrane element, largely depends upon the resistance of the existing cracks to the in-plane stresses. Due to redistribution of the applied loads the crack faces are forced to slide over each other, thus transmitting shear stresses. The resistance of the cracks to shear sliding is mainly caused by the roughness due to the aggregate particles which are protruding from the crack plane. This mechanism, called aggregate interlock, is physically understood for static shear loads. Experimental and theoretical work of Walraven [1,2] provided a physical model describing static shear transfer in plain concrete. In reinforced concrete members the embedded bars crossing the cracks contribute to the transfer of shear stress due to dowel action.

This paper focusses on the behaviour of a cracked membrane element subjected to repeated and reversed in-plane shear stresses. Walraven's static model will be adapted to the case of cyclic shear loading. This study is part of the Concrete Mechanics research project sponsored by the Netherlands Centre for Civil Engineering Research, Recommendations and Codes (CUR).

## 2. IN-PLANE SHEAR TRANSFER

### 2.1 Introduction

Experiments with cyclic shear loads, including those conducted by White et al [3], Laible et al. [4], Jimenez et al [5] and Mattock [6], were tied to the behaviour of nuclear reactor vessels. Therefore, the experimental parameters were a large crack width ( $\delta_n > 0.5$  mm), a small number of cycles ( $N = 15-100$ ) and a high shear stress in proportion to the crack width. This type of test is called 'low-cycle high-amplitude'. The lack of information with respect to cyclic shear loading is therefore restricted to a relatively low shear stress, i.e. the 'high-cycle low-amplitude' experiments. This paper will report on this type of test, which focusses on wind and wave attack on offshore structures. As appeared from those tests, the increase in crack displacements may be as small as  $10^{-6}$  mm/cycle, which is far less than the numerical accuracy of any mathematical model. Therefore, in this study the response of an element to 'high-cycle' fatigue is considered to be quasi-static taking into account the number of cycles to failure. In practice, a structure will be subjected to a few cycles with high amplitude shear loads after endurance of a large number of cycles with low amplitude shear loads. The response of an element to the high cyclic shear load can be calculated with an extended version of Walraven's model. However, the load history and the crack displacements due to the 'low-amplitude' cycles must be the input in the calculation.

Therefore, the analysis reported here is split into three parts. First, the static response of a crack to shear loads is described. Then, the response during the low-amplitude cycles is treated quasi-statically. Finally, Walraven's model

plain concrete is adapted to the case of cyclic loading in such a way that the load history can be neglected.

## 2.2 Static shear loading

For the case of static shear loading, Walraven's two-phase model describes the physical reality with a high degree of accuracy. In general, a crack runs through the matrix, but along the perimeters of the rigid aggregate particles. In the model the particles are considered as rigid spheres embedded in a rigid-plastic matrix with a yielding strength  $\sigma_{pu}$ . For a single particle it is shown that due to the shear sliding of the crack faces a contact area develops between the particle and the matrix material of the opposing crack plane. See Fig. 1.

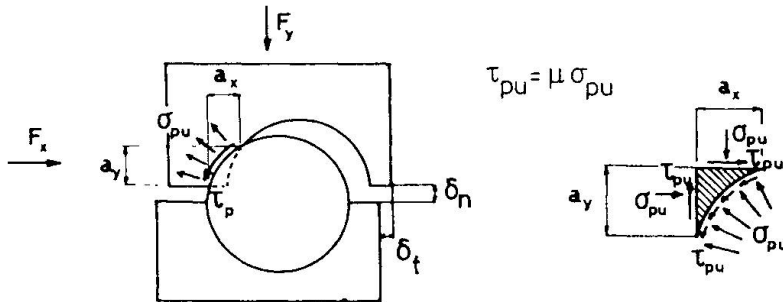


Fig. 1. Formation of the contact area for a single particle

According to Fig. 1, and taking into account all particles in the crack plane, the following constitutive equations can be formulated:

$$\tau_{ai} = \sigma_{pu} (\Sigma a_y + \mu \Sigma a_x) \quad (1)$$

$$\sigma_{ai} = \sigma_{pu} (\Sigma a_x - \mu \Sigma a_y) \quad (2)$$

The total contact areas can be analytically calculated for given crack displacements and maximum particle size. Walraven performed tests on plain concrete push-off specimens to derive expressions for  $\sigma_{pu}$  and  $\mu$ . From the experimental results it was found that  $\mu$  equals 0.4 and  $\sigma_{pu}$  can be calculated according to:

$$\sigma_{pu} = 6.39 f_{ccm}^{0.56} \quad (3)$$

Apart from the test series with plain concrete push-off specimens Walraven also performed tests on reinforced specimens. Now the embedded reinforcing bars perpendicularly crossing the crack plane contribute to the shear resistance according to Rasmussen's formula [7]. It was found [8]:

$$\tau_{exp} = \tau_{ai} + \tau_d \quad (4)$$

with

$$\tau_d = \frac{5}{3} \cdot \gamma \cdot \rho \sqrt{f_{ccm} f_{sy} (1 - \alpha^2)} \quad ; \quad \alpha = \frac{\sigma_s}{f_{sy}} \quad ; \quad \gamma = \sqrt{\frac{\delta_t}{\delta_{ni}}} \leq 1$$

Based upon the mechanism of dowel action the crack opening path for reinforced specimens is a function of the concrete strength, the steel strength and the initial crack width [8]. Experimental results of Walraven [1], Millard [9] and Mattock [6] yielded the following formulation:

$$\delta_t = \sqrt{\frac{\delta_{ni} f_{sy}}{2 f_{ccm}}} (\delta_n - \delta_{ni})^{\frac{2}{3}} \quad (5)$$

Initially the crack opening path is determined by eq. (5) for increasing shear





stress (See Fig. 2a.). According to eq. (4) the dowel action reaches its maximum value for  $\delta_t$  equal to  $\delta_{ni}$ . At the onset of a decrease in the contribution of aggregate interlock to the shear transfer the crack opening path follows the path for a constant  $\tau_{ai}$  according to Walraven's model. Figure 2b-c. presents the comparison between the calculated paths and some typical crack opening paths for Walraven's and Millard's tests.

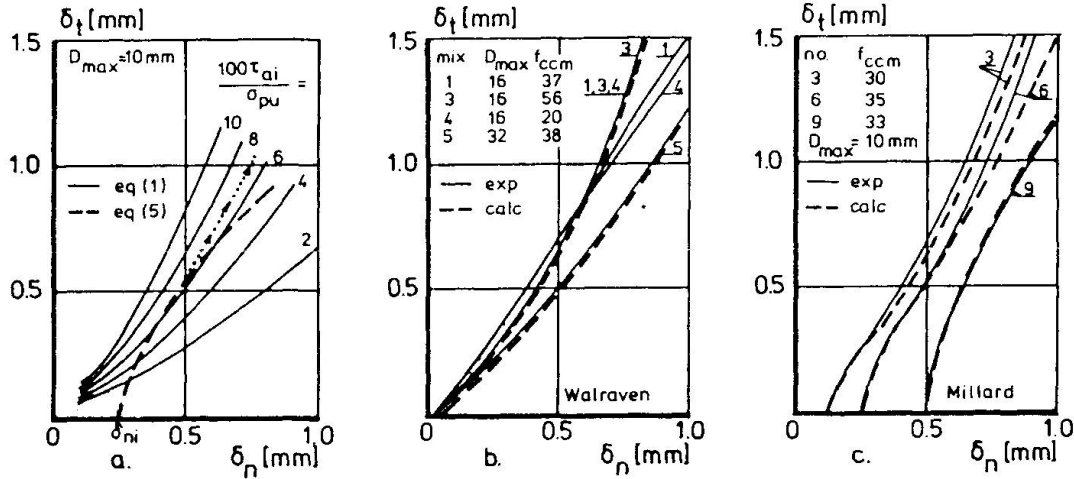


Fig. 2. Crack-opening paths according to the equations (1) and (5).

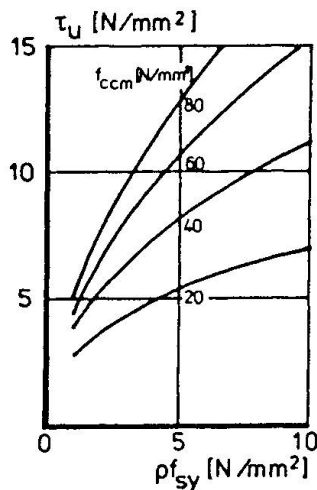


Fig. 3. The ultimate shear stress according to eq. (6) [10].

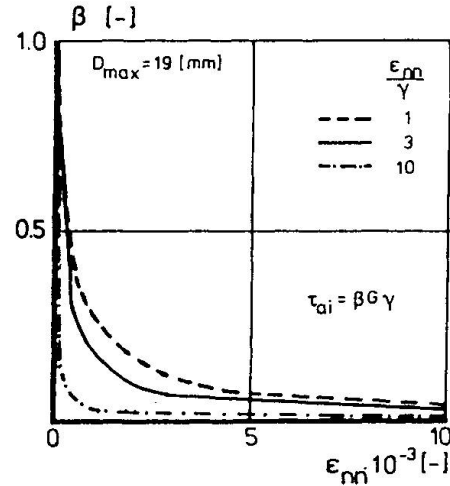


Fig. 4. Shear retention factor according to Walraven's model [13].

The ultimate shear stress for reinforced specimens can be calculated according to eq. (6) [10]. This expression was derived empirically on basis of 88 test results [1,10,11,12]. The relation between the mechanical reinforcement ratio and the shear strength is shown in Fig. 3.

$$\tau_u = a (\rho f_{sy})^b \quad (6)$$

with  $a = 0.822 f_{ccm}^{0.406}$        $b = 0.159 f_{ccm}^{0.303}$

In numerical programs of the smeared crack type a shear retention factor  $\beta$  is commonly used to account for the shear softening in cracks. Based upon Walraven's model an expression (eq. 7) was derived [13] (See Fig. 4). Although eq. (7) is an improvement of the relations derived by Rots [14] and Bazant et al [15] it is not possible to model the crack behaviour using one parameter  $\beta$ . Firstly, the interaction between strain - and shear softening must be taken into account. Secondly, the contribution of dowel action must be implemented.

$$\beta = \frac{1}{P \epsilon_{nn} + 1} \quad \text{with } P = \frac{2500}{D_{\max}^{0.14} \left[ 0.76 - 0.16 \frac{\epsilon_{nn}}{\gamma} \left\{ 1 - \exp\left(1 - 6 \frac{\gamma}{\epsilon_{nn}}\right) \right\} \right]} \quad (7)$$

### 2.3 Cyclic shear loading; high-cycle low-amplitude

The study reported in this paper comprises 42 'high-cycle low-amplitude' tests on push-off specimens with 8 mm diameter bars perpendicularly crossing the crack plane (See Fig. 5). The variables were:

- the concrete strength  $f_{ccm} = 51, 70$  [N/mm<sup>2</sup>] ( $D_{\max} = 16$  mm, Fuller curve)
- initial crack width  $\delta_{ni} = 0.01$ -0.10 mm
- number of bars  $n = 4$ -6 (1.12-1.68 %)
- number of cycles  $N = 118$ -931731
- applied stress level:  $\tau_m = 0.45$ -0.90  $\tau_u$

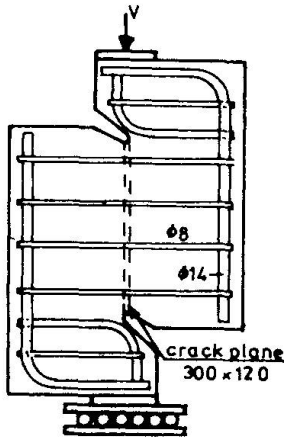


Fig. 5 Push-off specimen [12].

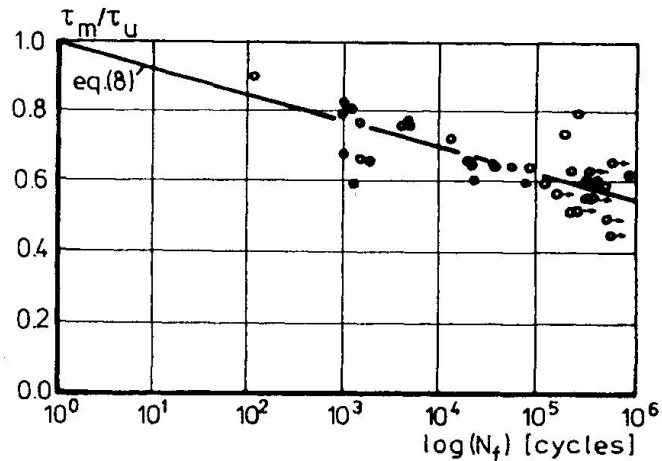


Fig. 6. The  $\tau_m/\tau_u$ -log( $N_f$ )-relation [12].

All the specimens were precracked. The tests were performed load-controlled with a sinusoidal signal with 60 cycles/min. The applied stress varied between 0.3 N/mm<sup>2</sup> and  $\tau_m$  (repeated loading). A complete description of the test results is given in [12]. Fig. 6 presents the relation between the applied stress level and the number of cycles to failure. This relation is approximated by the empirical relation:

$$\frac{\tau_m}{\tau_u} = 1 - 0.073 \log(N_f) \quad (8)$$

Some typical test results are presented in the Figs. 7-8. It was observed that for increasing stress-levels the increments of the crack-displacements per cycle

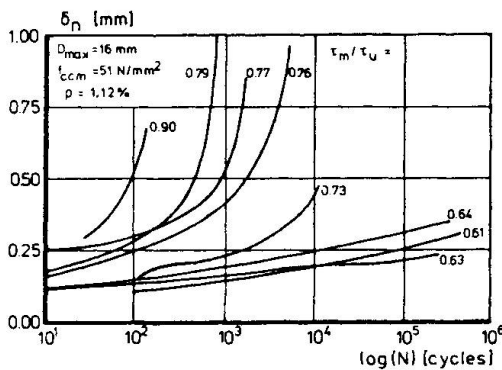


Fig. 7. The  $\delta_n$ -log( $N$ ) relation for given stress-levels.

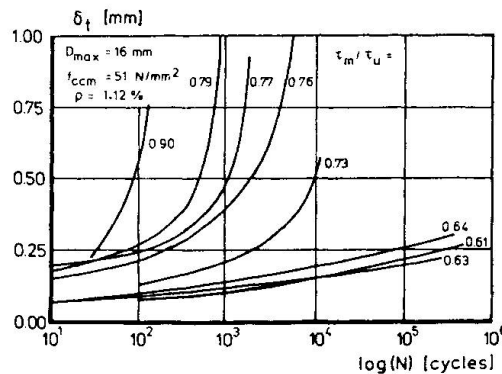


Fig. 8. The  $\delta_t$ -log( $N$ ) relation for given stress-levels.



also increase. It appeared that, as for the static case, the crack opening paths were determined by a constant shear stress due to aggregate interlock. As a consequence, the contribution of dowel action also remained constant. From eq. (4) it is known that both aggregate interlock and dowel action are approximately proportional to  $2\sqrt{f_{ccm}}$ . However, no measurable decrease of the concrete strength due to fatigue was found from the test results. This was probably due to the fact that the matrix material, highly stressed in a previous cycle, deteriorated in a subsequent cycle. Therefore, unaffected matrix material was then deformed to obtain the contact areas between matrix and particles. The high loading rate with respect to the crack width could be another important factor.

Based upon the experimental observations it can be concluded that the 'high-cycle' crack behaviour can be treated statically. Provided that suitable empirical expressions describing the relations in Figs. 7-8 are available, the crack-displacements can be calculated for a given number of cycles. With eq. (1) the most favourable crack opening direction can be determined.

#### 2.4 Cyclic shear loading; 'low-cycle high amplitude'

In this Section the model is restricted to the crack behaviour in plain concrete, so that the transfer of stresses across a crack depends upon the mechanism of aggregate interlock. For the case of a few load cycles with a relatively high applied shear stress the crack displacements per cycle are considerably larger than the numerical accuracy of a mathematical model. Hence, for this case an extended version of Walraven model can be used. In [1] Walraven already gave a qualitative description of cyclic loading tests performed by Laible [16] using his two-phase model. In [17] this idea was worked out numerically, taking into account the actual deformations caused by 100 particles. The contact area of each particle was determined using ten points situated in the contact zone (See Fig. 9). Now eqs. (1)-(2) become ( $j = 1-100$ ):

$$\tau_{ai} = \sigma_{pu} (\Sigma a_{y,j} + \mu \Sigma a_{x,j}) \quad (9)$$

$$\sigma_{ai} = \sigma_{pu} (\Sigma a_{x,j} - \mu \Sigma a_{y,j}) \quad (10)$$

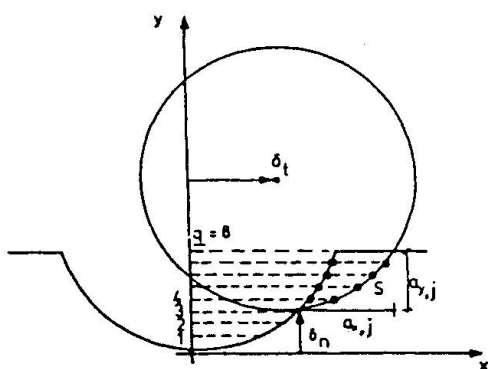


Fig. 9. Extended two-phase model of Walraven [17]

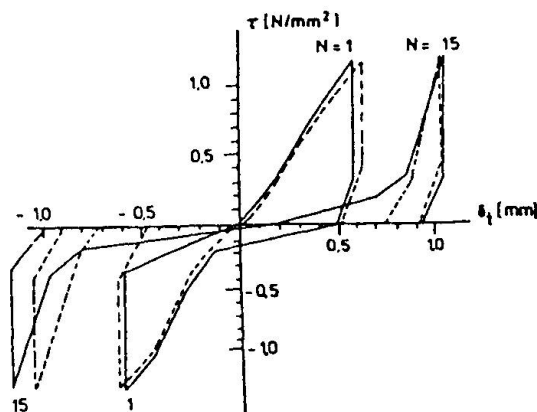


Fig. 10. Calculated and experimental result for Laible's test A1 [17]

Laible performed 'high-amplitude' tests on precracked plain concrete push-off specimens, for which the normal restraint stiffness was obtained by means of external bars. The experimental result of test A1 was predicted quite satisfactorily (See Fig. 10). To find the unknown material parameters, the model was fitted to the first static cycle:  $\mu$  equal to 0.2 and the contact area reduced by 25 percent. In agreement with the experimental results of the 'low-amplitude' tests, the matrix strength was kept constant for each cycle. In the calculation

the normal restraint stiffness was prescribed according to the experimental results.

This model can be used to perform a sensitivity analysis of the shear stiffness for various parameters, such as initial crack width, normal restraint stiffness and different stress levels. However, the model is too complex for implementation in a finite element program.

A major problem inherent in the physical behaviour of the crack and in this extended model is the fact, that the load history must be taken into account. In consequence, it cannot be used with a quasi-static description of previous 'low-amplitude' cycles.

Therefore, the extended two-phase model of Walraven [17] is simplified assuming that for each particle the 'load history' goes back as far as the last increment of the crack width and the deformation caused by the last displacement increment of the previous cycle [18]. Now, the contact area can be determined analytically, using the intersection points of three circles (See Fig. 11). These circles represent:

- Circle 1: deformation before the last crack width increment
- Circle 2: particle position for the momentary displacements
- Circle 3: end deformation of the previous load cycle.

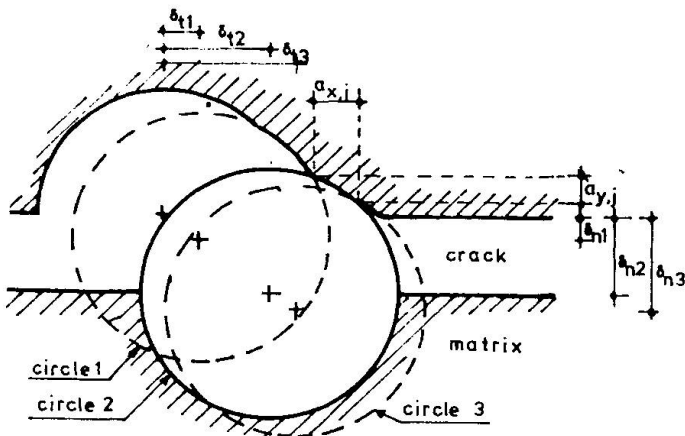


Fig. 11. Simplified calculation of contact zone

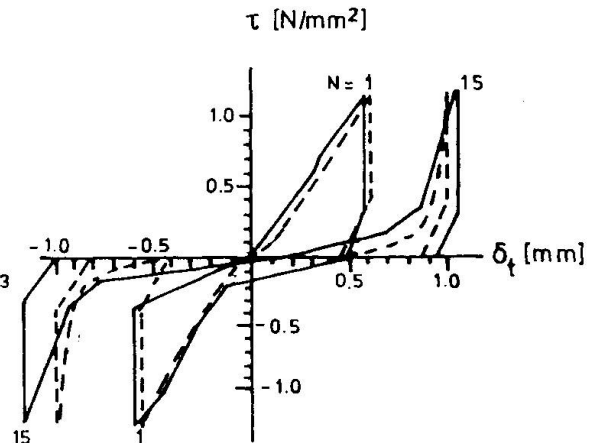


Fig. 12. Predicted result for test A1 neglecting most of the load history

Fig. 12 presents the calculated response for Laible's test A1 using the simplified model. It appeared that the experimental result can be simulated neglecting most of the load history. Therefore, the simplified model can be used in combination with preceding 'low-amplitude' cycles.

## 2.4 Concluding remarks

- Shear transfer in cracked reinforced concrete is based upon the mechanism of aggregate interlock and dowel action.
- Crack behaviour can be treated quasi-statically for the case of repeated 'high-cycle low-amplitude' shear loading.
- The extended model of Walraven can be used to simulate 'high-amplitude' tests.
- For implementation in numerical programs the number of particles must be reduced to a maximum of three.
- Apart from implementation of the extended aggregate interlock model the cyclic response of the mechanism of dowel action must be described in order to predict the shear resistance of reinforced cracks subjected to cyclic shear loading.



### 3. NOTATION

$D_{max}$ = maximum particle diameter [mm]	$\delta_n, \delta_t$ = crack width, shear slip [mm]
$N$ = number of cycles	$\epsilon_{nn}, \gamma$ = normal, shear deformation
$a, b, P, \alpha, \gamma$ = empirical parameters	$\tau, \sigma$ = shear, normal stress [N/mm <sup>2</sup> ]
$f_{ccm}$ = cube crushing strength [N/mm <sup>2</sup> ]	$\beta$ = shear retention factor
$f_{sy}$ = steel yield strength [N/mm <sup>2</sup> ]	$\mu$ = coefficient of friction
$a_x, a_y$ = projected contact areas [mm <sup>2</sup> ]	$\rho$ = reinforcement ratio

### 4. REFERENCES

1. Walraven, J.C., Aggregate interlock, a theoretical and experimental analysis, Dissertation, Delft Univ. of Technology, Oct. 1980
2. Walraven, J.C., Vos, E., Reinhardt, H.W., Experiments on shear transfer in cracks in concrete, Part I: Description of results, Stevin Report 5-79-3, Delft Univ. of Techn., 1979.
3. White, R.N., Holley, M.J., Experimental studies of membrane shear transfer, ASCE-1972 ST, pp 1835-1865.
4. Laible, J.P., White, R.N., Gergely, P., Experimental investigation of seismic shear transfer in concrete nuclear containment vessels, ACI SP-53-9, pp 203-226
5. Jimenez, R., White, R.N., Gergely, P., Cyclic shear and dowel action models in reinforced concrete, ASCE May 1982 ST, pp 1106-1123.
6. Mattock, A.H., Cyclic shear transfer and type of interface, ASCE Oct. 1981 ST, pp 1945-1964.
7. Rasmussen, B.H., The carrying capacity of transversely loaded bolts and dowels embedded in concrete, Bygningssstatistiske Meddelelser, Vol 34, No. 2, 1963
8. Pruijssers, A.F., The effect of reinforcing bars upon the shear transfer in a crack in concrete, Delft Univ. of Technology, (in preparation)
9. Millard, S.G., Johnson, R.P., Shear transfer across cracks in reinforced concrete due to aggregate interlock and dowel action, Mag. of Concrete Research, Vol. 36, No. 126, 1984, pp. 9-21
10. Walraven, J.W., Frenay, J.W., Pruijssers, A.F., Influence of concrete strength and load history on the shear friction capacity of concrete members, PCI (to be published in Jan/Feb 1987).
11. Frenay, J.W., Shear transfer across a single crack in reinforced concrete under sustained loading, Part I: Experiments, Stevin Report 5-85-5, Delft Univ. of Techn., 1985.
12. Pruijssers, A.F., Liqui Lung, G., Shear transfer across a crack in concrete subjected to repeated loading, Experimental results: Part I, Stevin Report 5-85-12, Delft University of Technology, 1985, pp. 178.
13. Pruijssers, A.F., Description of the stiffness relation for mixed-mode fracture problems in concrete using the rough-crack model of Walraven, Stevin Report 5-85-2, Delft Univ. of Technology, 1985, pp. 36.
14. Rots, J.G., Kusters, G.M.A., Nauta, P., Variabele reductiefactor voor de schuifweerstand van gescheurd beton, TNO-IBBC Report BI-84-33, 1984.
15. Bazant, Z.P., Gambarova, P., Rough cracks in reinforced concrete, ASCE Journal of the Structural Division, Vol. 106, 1980, pp. 819-842.
16. Laible, J.P., An experimental investigation of interface shear transfer and applications in the dynamic analysis of nuclear containment vessels, Thesis, 1973, pp. 343.
17. Walraven J.C., Kornverzahnung bei zyklischer Belastung, Mitteilungen aus dem Inst. fur Massivbau der Techn. Hochschule Darmstadt, Heft 38, 1986, p. 45-58.
18. Pruijssers, A.F., Shear transfer across a crack in concrete subjected to repeated loading, Part II: analysis of results (in preparation).

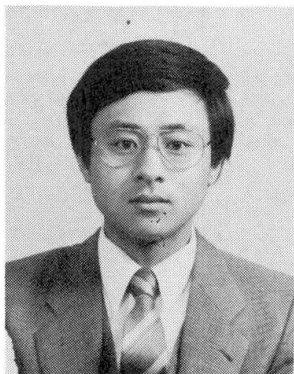
## Contact Density Model for Cracks in Concrete

Modèle de densité de contact pour les fissures dans le béton

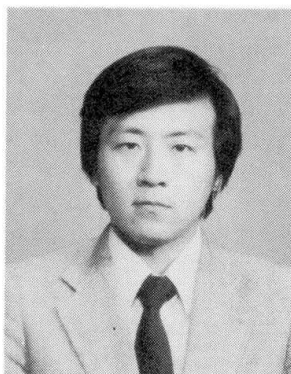
Kontaktdichte-Modell für Risse in Beton

### Baolu LI

Graduate Student  
University of Tokyo  
Tokyo, Japan



Baolu Li, born in 1960, received his BSc from Tongji University in China. Since 1985, he has been a graduate student of the University of Tokyo. His research interest is in the crack problems of concrete in general.



### Koichi MAEKAWA

Assoc. Professor  
University of Tokyo  
Tokyo, Japan

Koichi Maekawa, born in 1957, received his BSc and Dr. Eng. from the University of Tokyo. He is interested in material, structural nonlinearity and the finite element analysis of reinforced concrete.

### SUMMARY

A new proposal for the contact density function representing both geometrical roughness and mechanical rigidity of crack surfaces in concrete was introduced. A simple stress transfer model for cracks which is applicable to non-proportional and cyclic loading paths, was derived by combining the concept of elasto-plasticity with the proposed contact density function.

### RÉSUMÉ

L'article propose une fonction de densité de contact représentant les irrégularités géométriques et la rigidité mécanique des surfaces de fissures dans le béton. Un modèle simple de transfert de contraintes pour les fissures, lequel est applicable à des systèmes de charges cycliques et non-proportionnels, est dérivé en combinant le concept élasto-plastique avec la fonction de densité de contact proposée.

### ZUSAMMENFASSUNG

Ein neuer Vorschlag für die Kontakt-Dichtefunktion, welche die geometrischen und mechanischen Widerstände der Rissfläche in Beton berücksichtigt, wird eingeführt. Ein einfaches Schubübertragungsmodell, das sich für statische und wiederholte Belastungen eignet, wurde abgeleitet, indem man Elasto-Plastizität mit der Kontakt-Dichtefunktion kombinierte.





## 1. INTRODUCTION

This paper describes the establishment of the path-dependent stress transfer model across cracks in concrete. When a shear slip  $\delta$  occurs along a single crack, the resultants are the transferred shear stress  $\tau$  parallel to a crack, compressive stress  $\sigma$  and crack opening  $\omega$  normal to the crack plane. When we expect precise structural analysis by finite element methods [1], two stress components  $\tau$  and  $\sigma$  shall be formulated under the given deformation  $\delta$  and  $\omega$  respectively. Many researches have been done on problems of the shear transfer in concrete crack [1,2]. However, most of the mathematical models mainly deal with so-called monotonic loading history. A simple but reasonable model of shear transfer in concrete crack taking into account of path-dependency including cyclic loading is still lacking. Without any simple and unified concepts for stress transfer, it might be very difficult to formulate the path-dependent computational model with wide applicability.

In the past, a few physical models have been proposed from a view point of crack contact surface of crack. Buyukozturk [3] represented the shape of crack surface using a simple function. Walravan [4] idealized the crack surface as a set of circular aggregates. These models simulate the stress transfer mechanism by taking into account the anisotropic crack surface geometry. On the other hand, Bazant et.al [5] introduced the microplane model assuming infinite uniaxial struts which stand on microplanes isotropically arranged in a crack band. These approaches are considered reasonable for establishing the path-dependent model, but the elasto-plastic behavior, the shear dilatancy and the direction of transferred stress under cyclic loads have not been explained by a unified concept with reasonable accuracy.

The authors introduced a contact density function representing both geometrical roughness and mechanical rigidity of crack contact surfaces in concrete. Combining the concept of elasto-plasticity with the proposed density function, a simple stress transfer model considering path-dependency including cyclic loading was proposed and computational constitutive equations were derived.

## 2. EFFECTIVE CONTACT DENSITY MODEL

### 2.1 Modeling of Crack Geometry and Stress Transfer

As illustrated in Fig.1, unit area of the crack surface was idealized as a set of infinite potential contact planes with different directional angle  $\theta$ , where counterclockwise direction from y axis is defined as positive. Then the initial area of potential contact planes  $dA(\theta)$ , whose directions are between  $\theta$  and  $\theta+d\theta$ , is defined by the contact density function  $\rho$  as follows.

$$dA(\theta) = A_t \rho(\theta) d\theta \quad \int_{-\frac{\pi}{2}}^{\frac{\pi}{2}} \rho(\theta) d\theta = 1 \quad (1)$$

where,  $A_t$  is total area of crack surface and a constant.

Strictly speaking, the direction of contact plane and/or  $\rho(\theta)$  should be a function of crack deformation  $(\omega, \delta)$  as shown in Fig.1. But, the crack deformation is much smaller when compared with the size of crack roughness. Therefore it can be assumed that the density function  $\rho(\theta)$  is not affected by the history of crack deformation  $(d\omega, d\delta)$ .

Let us consider the mechanism of stress transfer. The stress  $(\tau, \sigma)$  transferred



across a crack must be in equilibrium with total forces acting on the crack surfaces which are in contact with each other. We can define  $\sigma_{con}(\theta)(\geq 0)$  as the contact stress acting on the contact plane at the directional angle  $\theta$  (See Fig.1). The stress transferred  $(\tau, \delta)$  can be derived as follows.

$$\begin{aligned} \tau &= \int_{-\pi/2}^{\pi/2} R1(\delta, \omega, \theta) d\theta = \int A_t \sigma_{con}(\delta, \omega, \theta) \sin \theta_s(\delta, \omega, \theta) K(\delta, \omega, \theta) \rho(\theta) d\theta \\ \sigma &= \int_{-\pi/2}^{\pi/2} R2(\delta, \omega, \theta) d\theta = \int A_t \sigma_{con}(\delta, \omega, \theta) \cos \theta_s(\delta, \omega, \theta) K(\delta, \omega, \theta) \rho(\theta) d\theta \quad (2) \end{aligned}$$

where,  $\sigma$  and  $\omega$  are defined as positive in compression and crack opening respectively.  $\theta_s$  is a directional angle of contact stress acting on the negative side as defined in Fig.1. The crack opening reduces the actual contact area from the initial state. The value of  $K$  in Eq.(2) is the reduction factor and  $KdA(\theta)$  is the effective contact area.

Eq.(2) is the basic constitutive equation for the proposed contact density model. The computational constitutive equations are completed when simple and appropriate functions,  $\sigma_{con}$ ,  $\theta_s$ ,  $K$  and  $\rho$  which are mentioned above are formulated under arbitrary crack deformation paths  $(d\delta, d\omega)$ .

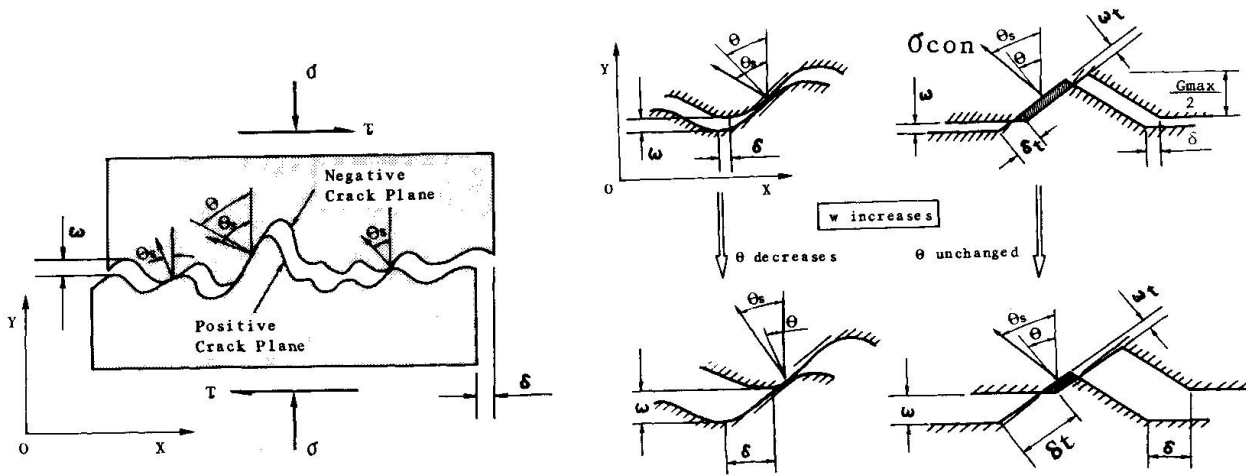


Fig.1 Idealization of Crack Contact

## 2.2 Mechanical Modeling

The contact stress  $\sigma_{con}(\theta)$  is generated when the positive and negative planes with direction  $\theta$  are met together. Hence, it may be reasonable to adopt the relative displacement parallel and normal to the contact plane as the parameters influencing the  $\sigma_{con}$ ,  $\theta_s$ ,  $K$  and  $\rho$ .

$$\begin{aligned} \delta_t(\delta, \omega, \theta) &= \delta \cos \theta + \omega \sin \theta \\ \omega_t(\delta, \omega, \theta) &= \delta \sin \theta - \omega \cos \theta \end{aligned} \quad (3)$$

where,  $\omega_t$  is positive definite at closing. Increasing shear slip under the fixed crack opening causes the contact of potential planes with greater values of  $\theta$ , followed by the contact of planes with smaller  $\theta$ . Then, the relative



slip  $\delta t$  on each contact plane is observed as shown in Fig.1 or Fig.2. Because of the existence of friction, the direction of contact stress  $\theta_s$  tilts from the normal direction of the contact plane  $\theta$ . When the slip direction varies, the discontinuous change of  $\theta_s$  occurs and results in the discontinuous rotation of transferred stress direction ( $\tau/\sigma$ , See Fig.2). As shown in Fig.3, however, the observed stress direction under the fixed crack opening varies continuously even when the applied shear stress and slip direction are changed. i.e.

$$\theta_s(\delta, \omega, \theta) = \theta \quad (4)$$

where, only the so-called interlock mechanism is taken into consideration. Strictly speaking, the test result shown in Fig.3 is not necessarily suitable because the slip reversal along each contact plane is not so great as to decide the micro-model of  $\theta_s$ , but this can not be discussed further due to lack of test results. We should recognize that Eq.(4) is the approximation of the first step.

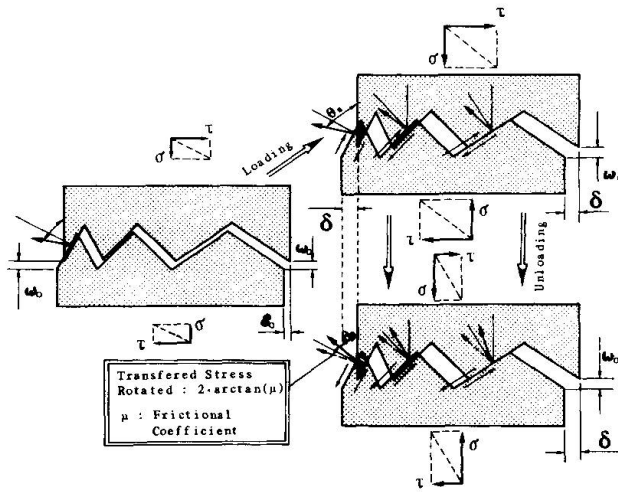


Fig.2 Direction of Contact Stress and Crack Contact Plane

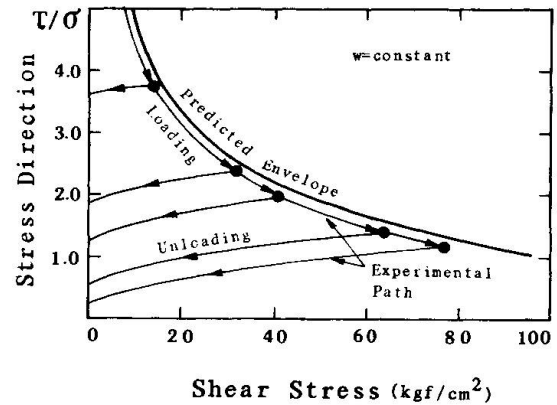


Fig.3 Direction of Stress Transfer under Cyclic Loading

When the representative roughness  $G_{max}$  is idealized as shown in Fig.1, the ratio of effective contact area  $K$  is simply assumed as,

$$K(\delta, \omega, \theta) = 1 - \frac{2\omega}{G_{max}} \quad (5)$$

where,  $G_{max}$  of normal strength concrete is the maximum size of coarse aggregate. In the case of structural analysis, the value of  $\omega$  is much smaller than  $G_{max}$ . Therefore the value of  $K$  is approximately equal to unity. Eq.(5) plays an important role only for extreme cases such as large crack opening or mortar.

Path-dependent and cyclic behavior of stress transfer has a close correlation with the constitutive model concerned with contact stress  $\theta_{con}$ . The total shear slip under fixed crack width (0.1-1mm) can be divided into elastic and plastic shear slip components as shown in Fig.4. But the elastic deformation has very small contribution to the total shear slip. We may adopt the most simple perfectly elasto-plastic formulation as a relationship between contact stress  $\sigma_{con}$  and closing displacement  $\omega t$  as shown in Fig.5.

$$\sigma_{con}(\delta, w, \theta) = E [\omega_t - \omega_{tp}] \quad , \quad \text{when } \omega_t > \omega_{tp} \quad (6-1)$$

$$= 0 \quad , \quad \text{when } \omega_t \leq \omega_{tp}$$

$$\omega_{tp} = \int d\omega_{tp}(\theta) \quad (6-2)$$

$$d\omega_{tp}(\theta) = d\omega_t(\theta), \text{ if } \omega_t = \omega_{t \max} > \omega_{lim} \text{ and } d\omega_t > 0, \text{ else}$$

$$= 0$$

where,  $E$  represents stiffness around contact planes and  $\omega_{lim}$  is the elastic limit defined as 0.004cm. The path-dependency is introduced to the model by the plastic displacement distribution  $\omega_{tp}(\theta)$  in each direction, namely,  $\omega_{tp}(\theta)$  memorizes the past loading history. Substituting Eq.(3)-(6) into Eq.(2), we have functions  $R1$  and  $R2$  concerning  $\theta$  and stiffness matrix as follows.

$$R1(\delta, w, \theta) = m(\delta \sin \theta - w \cos \theta - \omega_{tp}) \left(1 - \frac{2w}{G_{max}}\right) \sin \theta \rho(\theta)$$

$$R2(\delta, w, \theta) = m(\delta \sin \theta - w \cos \theta - \omega_{tp}) \left(1 - \frac{2w}{G_{max}}\right) \cos \theta \rho(\theta)$$

$$\begin{Bmatrix} d\tau \\ d\sigma \end{Bmatrix} = \begin{pmatrix} D_{11} & D_{12} \\ D_{21} & D_{22} \end{pmatrix} \begin{Bmatrix} d\delta \\ dw \end{Bmatrix} \quad D_{ij} = \int_{-\pi/2}^{\pi/2} \frac{\partial R_i}{\partial x_j} d\theta \quad (7)$$

where,  $m = A_t \cdot E$ ,  $x_1 = \delta$  and  $x_2 = w$ . The value of  $m$  represents the average rigidity around contact planes and is considered to be affected by the compressive strength  $f_c'$ . Since the conceptual coefficient  $m$  and contact density function  $\rho$  cannot be directly determined by experiments, those values are decided by comparing the derived analytical results with experimental ones as follows (See Fig.5 and Fig.6).

$$m = 20500 f_c' \frac{1}{3}$$

$$\rho(\theta) = 0.5 \cos \theta \quad (8)$$

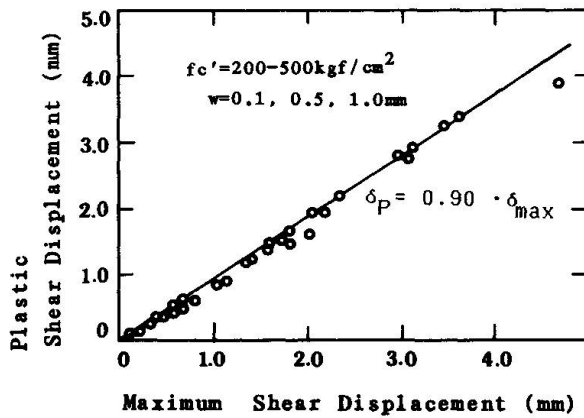


Fig.4 Plastic Shear Component

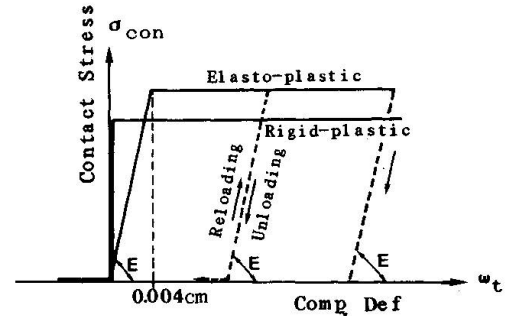


Fig.5 Model of Contact Stress.

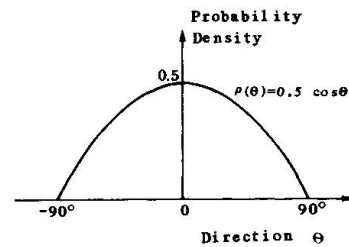


Fig.6 Model of Contact Density Function



### 3. EXPERIMENTAL VERIFICATION

The stress transferred across a crack is calculated by integrating R1 and R2 over the direction of  $\theta$  and along a deformation path ( $d\delta, d\omega$ ) in Eq.(2). However, we must rely on the numerical integration as summarized in Appendix. The cyclic response of stress transfer under fixed crack width of 0.300mm which was obtained by authors experimentally is shown in Fig.7. Similarly, the shear transfer under various crack widths are shown in Fig.8. Using the proposed model the overall cyclic behavior of stress transfer, the shear stiffness change under various crack widths and correlation of  $\tau$  and  $\sigma$ , that is, direction of stress transfer ( $\tau/\sigma$ ) are fairly simulated. The basic modelings regarding the plastic hysteresis of the contact stress and contact density function have a great effect on the overall response as shown in Fig.7 and Fig.8.

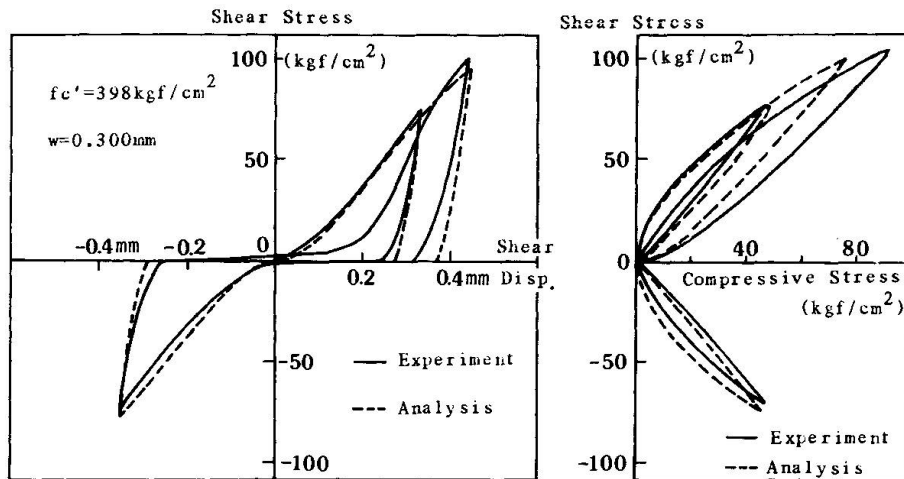


Fig.7 Cyclic Stress Transfer under Constant Crack Width

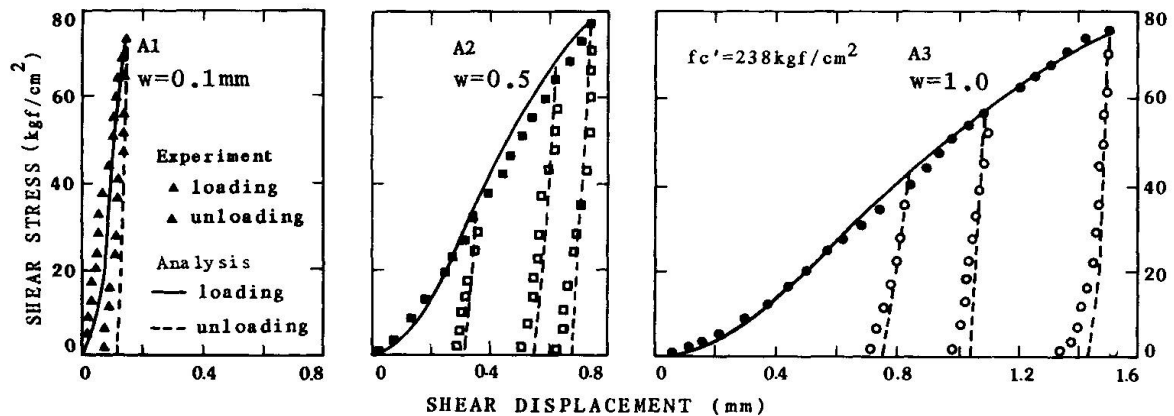


Fig.8 Shear Transfer Stiffness under Various Crack Width

In order to check the effect of loading path on the stress evaluation, the authors adopted the step type deformation paths on ( $\delta, \omega$ ) space as shown in Fig.9(a). When shear displacement is kept constant and the crack width increases, the sustained shear stress decreases rapidly (See Fig.9(b)). When shear slip increases again under another unchanged crack width, the shear stiffness varies differently from the monotonic loading where the crack width is fixed throughout. The corresponding relation between compressive and shear stresses is shown in Fig.9(c), from which we can find the cyclic response

similar to the loading and reloading path in Fig.7. Here, the analytical model succeeds in explaining this path-dependent behavior. Path B in Fig.9(a) includes crack closing history due to increasing confining stress under a certain shear displacement. The numerically integrated solution predicts the actual response fairly (See Fig.9(d)). But compared with the monotonic loading cases, we can see the decrease in precision. The simple perfectly elastoplastic model for contact stress may be responsible for the difference in analytical results from experimental values. Further research on more realistic cyclic model for contact stress will be necessary for the better agreement.

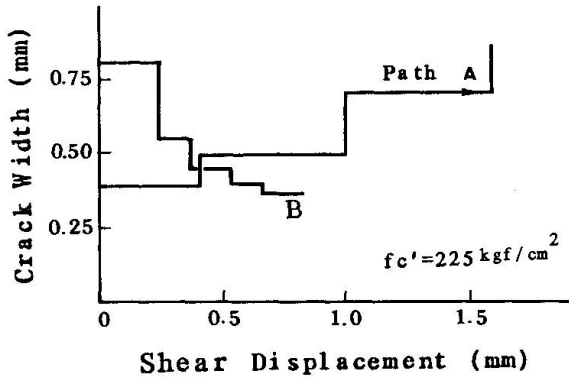
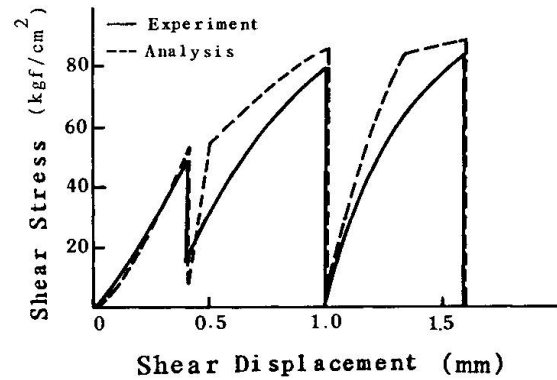
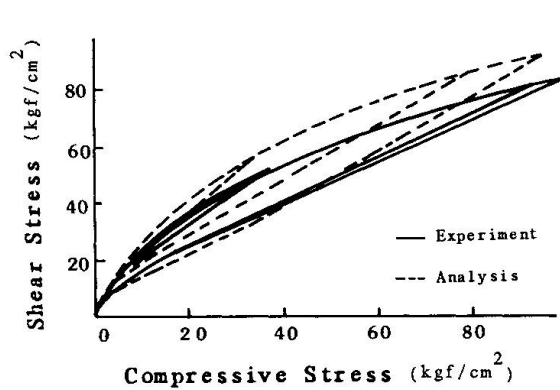
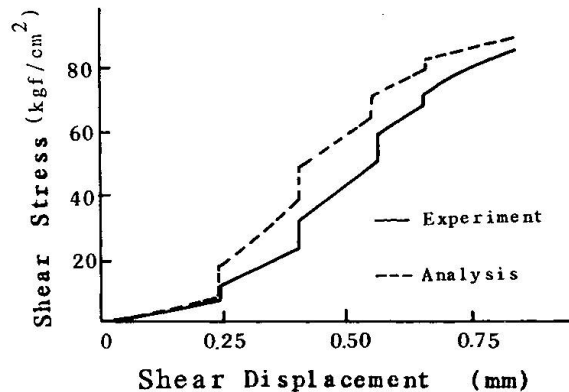


Fig.9(a) Step-type Loading path


Fig.9(b)  $\tau$ - $\delta$  relation of Path A

Fig.9(c)  $\tau$ - $\sigma$  relation of Path A

Fig.9(d)  $\tau$ - $\delta$  relation of Path B

The microscopic idealization for the contact stress and density function is indirectly verified, but the effective ratio  $K$  has very small contribution to the overall behavior mentioned above, accordingly, we adopted the stress transfer across a crack in mortar as an extreme case for experimental verification. The stress transferred in mortar under constant crack width is shown in Fig.10 with analytical results, where some characteristic values of  $G_{max}$  for mortar are used for trial, because we can not define the maximum size of coarse aggregate in mortar. When we select the roughness index  $G_{max}$  of 1.7mm using the same functions as  $\rho$  and  $\sigma_{con}$ , this model gives us fair agreement with experimental result. In other words, the crack surface condition of mortar is assumed to be represented by the similar contraction of concrete crack asperity. The same discussion holds even in the case of lightweight concrete [6].

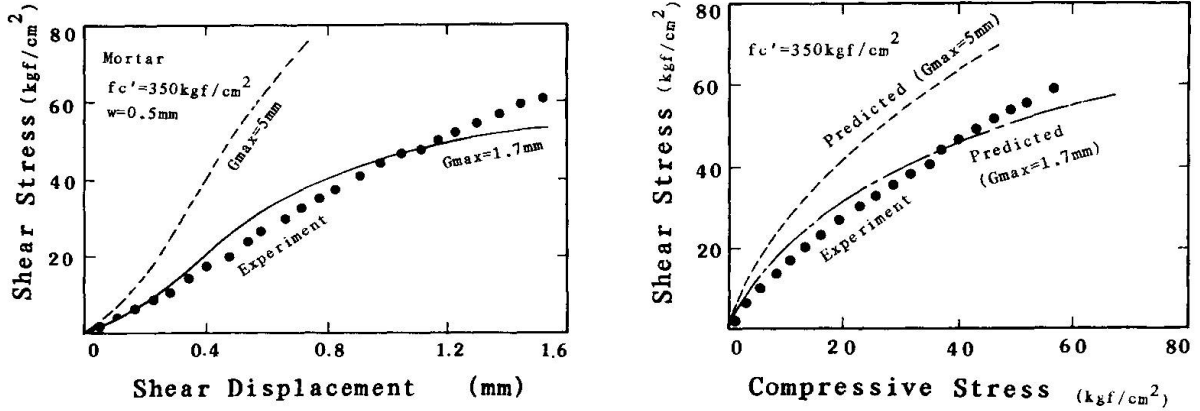


Fig.10 Stress Transfer across a Crack in Mortar

#### 4. APPLICATION OF INTEGRATED CONSTITUTIVE EQUATIONS ON MONOTONIC LOADING

##### 4.1 Analytical Integration and Verification

The proposed stress transfer model requires the double integral on the directional angle and deformation path, however, the analytical integration can be easily carried out on the monotonic loading path. Here, the strict definition of monotonic loading is made as the deformation path ( $d\delta, d\omega$ ) on which the increment of contact stress  $d\sigma_{con}(\theta)$  in every direction is zero or positive. For simplicity, we assume that the rigid-plastic model for the contact stress  $\sigma_{con}$  neglecting the elastic component of deformation as shown in Fig.5, and that the ratio of effective contact area  $K(\delta, \omega, \theta)$  is unity as discussed in Chapter 2. Accordingly, the integrands in Eq.(2) become zero when  $\omega(\theta) < 0$  or  $-\pi/2 < \theta < \tan^{-1}(\omega/\delta)$ . Within the subdomain where the touch of potential contact planes occurs when  $\omega(\theta) > 0$ , the functions  $R_1$  and  $R_2$  in Eq.(2) are converted to trigonometric functions. Using the effective domain of integration  $\tan^{-1}(\omega/\delta) < \theta < \pi/2$ , we have

$$\tau = k \frac{\delta^2}{\omega^2 + \delta^2}, \quad k = 18 f_c'^{\frac{1}{3}} \quad (\text{kgf/cm}^2)$$

$$\sigma = k \left[ \frac{\pi}{2} - \tan^{-1}\left(\frac{\omega}{\delta}\right) - \frac{\omega \delta}{\omega^2 + \delta^2} \right] \quad (9)$$

Eq.(9) is a simplified particular solution of the original path-dependent constitutive model, however, it gives us exactly the same prediction as that by the original model verified by the experimental results under constant crack width (See envelopes of Fig.7 and Fig.8).

Considering actual loading paths produced in RC structures, however, the constant crack width condition used for experimental verification is not popular, but the crack width normally opens according to the increase of shear slip and/or shear stress. As an example of model verification for monotonic loading path similar to that produced in actual RC structural elements, it may be acceptable to take up a loading path with constant  $\tau/\omega$ , where crack width increases according to the shear loading. Relationships between  $(\tau-\delta)$ ,  $(\tau-\sigma)$  and  $(\omega-\delta)$  measured from test result together with the predictions by the particular integral solution are shown in Fig.11. The shear stiffness

$(d\tau/d\delta)\tau/\omega$  decreases monotonically, not similar to the change of stiffness  $(d\tau/d\delta)\omega$  under the fixed crack width, and are predicted accurately.

The simple expression shown in Eq.(9) enables us to understand the properties of the proposed original model. There exists an ultimate shear strength if a suitable confining stress is provided to keep the crack opening unchanged. This shear strength is not affected by the crack width,

$$\lim_{\delta \rightarrow \infty} \tau = \lim_{\delta \rightarrow \infty} \left[ k \frac{\delta^2}{\omega^2 + \delta^2} \right] = k = 18 f_c'^{\frac{1}{3}} \quad (10)$$

The simplified model would lose its accuracy if crack opening becomes larger, but the crack width not greater than 1mm could be considered the upper limit in general. The fact that the shear strength under fixed crack width is not affected by crack width, has also been observed experimentally by Paulay [7].

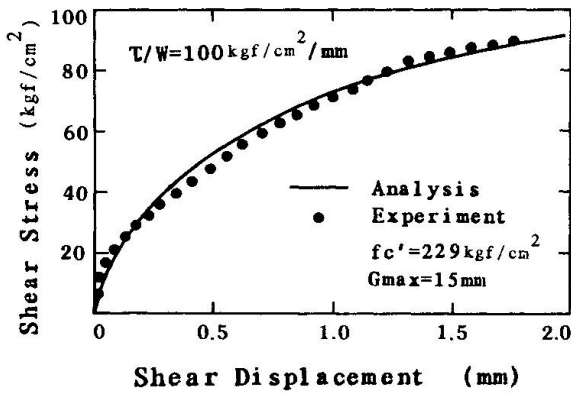


Fig.11(a)  $\tau$ - $\delta$  Relation

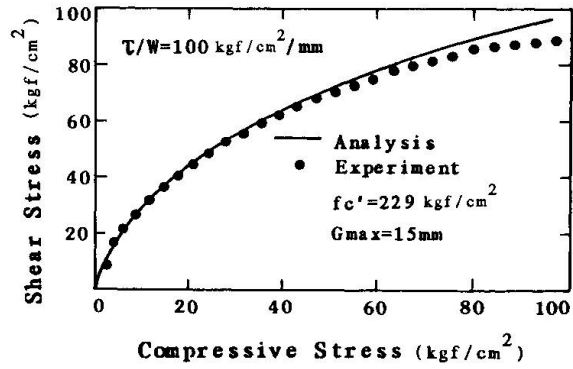


Fig.11(b)  $\tau$ - $\sigma$  Relation

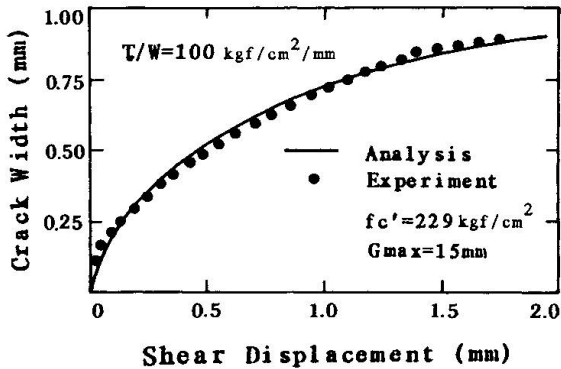


Fig.11(c) Deformational Path under Changing Crack Width Path

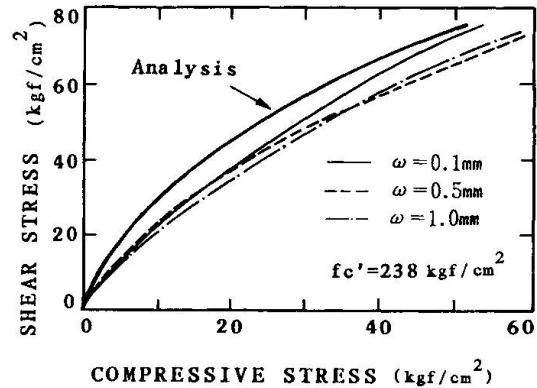


Fig.12  $\tau$ - $\sigma$  Relation under Constant Crack Width

Furthermore, another interesting mechanism for the stress transfer on monotonic loading is derived from Eq.(9). Both  $\tau$  and  $\sigma$  in Eq.(9) are functions of  $(\omega/\delta)$ , then, we have

$$\tau = \tau(\sigma) \quad \text{or} \quad \sigma = \sigma(\tau) = k \left[ \frac{\pi}{2} - \tan^{-1} \sqrt{\frac{k}{\tau} - 1} - \frac{\sqrt{\frac{k}{\tau} - 1}}{\frac{k}{\tau}} \right] \quad (11)$$





Eq.(11) means that there exists a unique correlation between  $\tau$  and  $\sigma$  when the plastic deformation proceeds. If crack width is kept constant, the confining stress increases with shear stress. Actually, this relation does not depend on the crack deformation ( $\delta, w$ ) and can be predicted accurately by Eq.(11) as shown in Fig.12. From a view point of the theory of plasticity, we can recognize Eq.(11) as a loading function, in which stress components must satisfy when the plastic deformation flows. In the case of constant compressive stress loading path, we can observe the perfectly elasto-plastic behavior between shear stress and displacement as shown in Fig.13, where very rigid shear modulus is followed by the plastic plateau under constant shear stress. Fig.13 shows experimental loading paths and plastic flowing stress point on which crack deformations proceed rapidly. Experimentally obtained points corresponding to plastic flow coincide with the envelope given by Eq.(11) with a good accuracy.

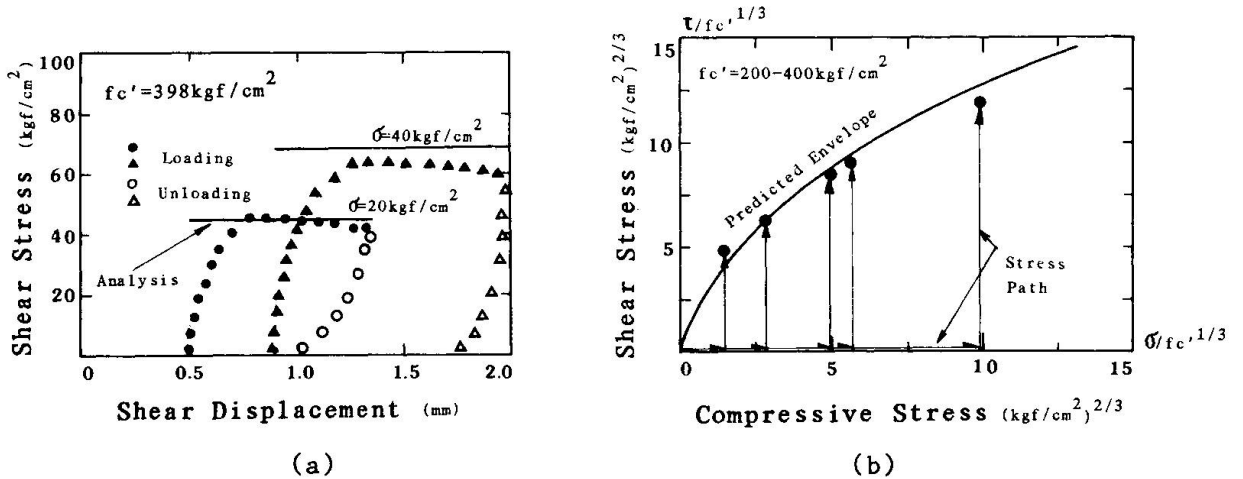


Fig.13 (a)  $\tau$ - $\delta$  relation and (b) Shear Strength Under Constant Compression

#### 4.2 Application to Smeared Crack Analysis

Let us evaluate average stiffness of an element including a number of parallel cracks. In the smeared crack procedure, the discontinuous crack deformation is considered smeared out within the total length or volume of the element considered and represented by the average strains as,

$$\gamma_{cr} = \frac{\delta}{L}, \quad \epsilon_{cr} = \frac{w}{L} \quad (12)$$

where,  $L$  is the characteristic length, and the average crack spacing depends on the bond characteristics between concrete and reinforcement. Substituting Eq.(12) into Eq.(9), we get

$$\tau = k \frac{\gamma_{cr}^2}{\epsilon_{cr}^2 + \gamma_{cr}^2}, \quad k = 18 f_c'^{1/3} \text{ (kgf/cm}^2\text{)} \quad (13)$$

$$\sigma = k \left[ \frac{\pi}{2} - \tan^{-1} \left( \frac{\epsilon_{cr}}{\gamma_{cr}} \right) - \frac{\epsilon_{cr} \gamma_{cr}}{\epsilon_{cr}^2 + \gamma_{cr}^2} \right]$$

where, we can find an interesting fact that the characteristic length does not appear in the above equations. This cancellation means that average stiffness of finite elements with cracks is not affected by the numbers of cracks, and is convenient for structural analysis. The authors use Eq.(13) for analysis of reinforced concrete plates subjected to in-plane loads.



## 5. CONCLUDING REMARKS

The path-dependent stress transfer across cracks in concrete can be simply predicted by a physical model, which is completed regarding the geometrical asperity of cracked plane by using a suitable contact distribution density function and a simple assumption of perfect elasto-plasticity in contact area. The proposed model which is capable of dealing with cyclic and non-proportional loadings was verified by experimental data. It was checked that the derived constitutive equations can be applied to structural analysis with reasonable accuracy.

The formulated constitutive equations adopt double integral along the loading path and over the contact direction, accordingly, require some numerical integration schemes in general. However, along the so-called monotonic loading path, we can easily find the particular solution derived from the original model analytically. The relationship between compressive and shear stresses acting on a crack plane is found to be mathematically unique and independent on the crack deformation under monotonic loading, and its validity was proved by experimental results.

In expanding the proposed model for a single crack to the computational model for finite elements including distributed cracks, smeared crack procedure is available whereas the characteristic length of crack spacing is generally required. However, this length affected by the bond property and other factors does not explicitly appear when we evaluate the average stiffness of elements with cracks using the integrated stress transfer model derived in this research. As a computational model, this can be applied widely.

## ACKNOWLEDGMENTS

The authors are grateful to Prof.H.Okamura and Mr.J.Izumo, University of Tokyo, for their active discussion and some technical suggestions. They also would like to express their gratitude to MITUBISHI foundation and Grand-in-Aid No. 61420035 for scientific research of the Ministry of Education for providing financial support.

## REFERENCES

1. State-of-the-art Report on Finite Element Analysis of Reinforced Concrete, ASCE Publication, 1984.
2. Bazant, Z.P. and Gambarova, P., "Rough Cracks in Reinforced Concrete", ST4, ASCE, Apr., 1980.
3. Fardis, M.N. and Buyukozturk, O., "Shear Transfer Model for Reinforced Concrete", ASCE, EM2, Apt., 1979.
4. Walraven, J.C. and Reinhardt, H.W., "Theory and Experiments of The Mechanical Behavior of Cracks in Plain and Reinforced Concrete Subjected to Shear Loading", Heron, Vol.26, No.1A, 1981.
5. Bazant, Z.P. and Gambarava, P., "Crack shear in Concrete: Crack Bond Microplane Model", Journal of the Structural Engineering, ASCE, Vol.110, No.9, Sep., 1984.
6. Lim, T.B. and Li, B.L. and Maekawa, K., "Mixed-Mode Strain-Softening Model for Shear Fracture Band on Concrete Subjected to In-plane Shear and Normal Compression", International Conference on Computational Plasticity, Spain, Apr., 1987.
7. Paulay, T. and Leober, P.J., "Shear Transfer by Aggregate Interlock", Shear in Reinforced Concrete, ACI, SP-42, Volume 1, 1974.



## APPENDIX NUMERICAL INTEGRATION ALGORITHM

The stress components are obtained by conducting numerical integration of Eq.(2) with respect to directional angle  $\theta$ . The following algorithm shows the accepted scheme of calculating stresses along an arbitrary crack deformation path. The crack deformation under any stress history can be easily found by the iterative calculus of Newton Raphson Method. The domain of the directional integral is divided into  $N$  pieces. The loop A in Fig.14 means the directional integral. In each direction, the plastic contact displacement  $\omega_{tp}$  is determined and stored in memory, by which the path-dependency is taken into account in this model. The values of integrands  $R1$  and  $R2$  in Eq.(2) are stored respectively. The loop B gives the path-dependent displacement integral.

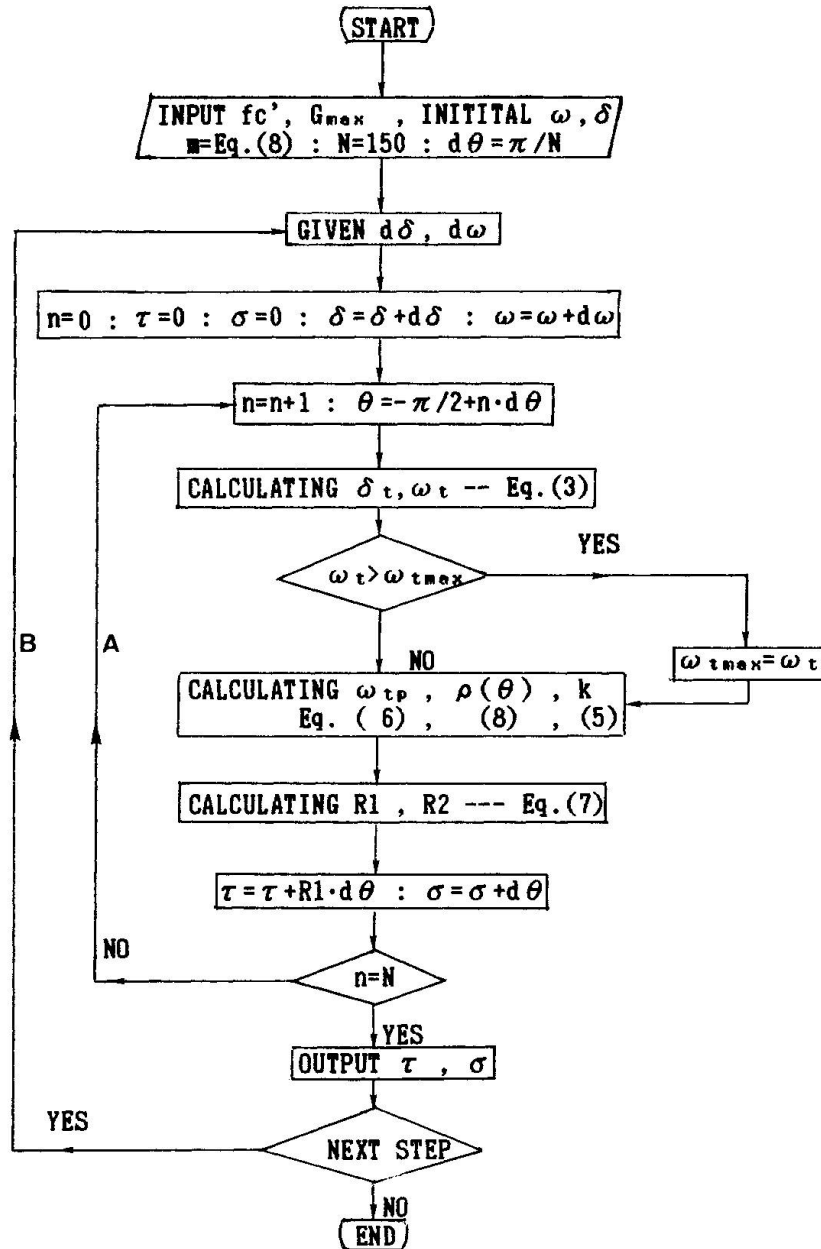


Fig.14 Numerical Integral Algorithm of Proposed Stress Transfer Model

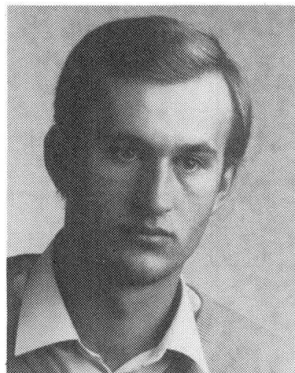
## Material Model for Cracked Reinforced Concrete

Modèle du matériau pour le béton armé fissuré

Ein Materialmodell für gerissenen Stahlbeton

### Johann KOLLEGGER

Res. Assistant  
University of Kassel  
Kassel, FRG



Johann Kollegger, born 1956 in Austria, received his master of Eng. degree at Berkeley in 1980 and his Dipl.-Ing. degree at TU Graz, Austria, in 1981. Since 1983 he is research assistant at the University of Kassel, FRG.



Gerhard Mehlhorn, born 1932, received his Dipl.-Ing. degree in 1959 in Dresden. He worked from 1959-1965 as a design engineer. He joined the TH Darmstadt in 1965, got his Dr. degree in 1970 and became professor there in 1972. Since 1983 he is professor of Civil Engineering at the University of Kassel.

### Gerhard MEHLHORN

Professor  
University of Kassel  
Kassel, FRG

### SUMMARY

A material model for the analysis of cracked reinforced concrete surface structures is developed based on recent experimental work. The constitutive model employs the smeared crack concept, i.e. only average material stresses are considered at an integration point. A new formulation for the reduction of the compressive strength of cracked concrete is proposed. A refined procedure for the evaluation of tension stiffening is also presented.

### RÉSUMÉ

Sur la base de nouveaux essais un modèle du matériau est proposé pour le calcul des structures bidimensionnelles en béton armé. Dans ce modèle du matériau le concept de fissuration homogénéisée est utilisé, c'est à dire que seules les tensions et torsions moyennes au point d'intégration sont considérées. Une définition nouvelle pour la réduction de la résistance à la compression du béton fissuré est proposée. Une méthode très élaborée pour déterminer les tensions de traction dans le béton fissuré est aussi présentée.

### ZUSAMMENFASSUNG

Auf der Grundlage neuer experimenteller Untersuchungen wird ein Materialmodell für die Berechnung von Stahlbetonflächentragwerken entwickelt. Im Materialmodell wird das Konzept verschmierter Rißbildung verwendet, d.h. es werden nur mittlere Spannungen und Verzerrungen am Integrationspunkt berücksichtigt. Zur Reduzierung der Druckfestigkeit gerissenen Betons wird eine neue Formulierung vorgeschlagen. Eine verfeinerte Methode zur Ermittlung der Zugspannungen im gerissenen Beton wird ebenfalls vorgestellt.



## 1. INTRODUCTION

In the analysis of reinforced concrete surface structures cracking of concrete usually causes the main nonlinearities in the structural response. Many different formulations for the numerical treatment of cracked reinforced concrete have been presented in the literature. Differences exist in the treatment of

- the reduction of the concrete compressive strength after cracking (reduction according to Vecchio and Collins [12, 13] versus no reduction),
- the tension stiffening effect (as a property of concrete or as a property of reinforcement),
- the crack direction (fixed cracks versus rotating cracks), and of
- the magnitude of the shear modulus of cracked concrete.

In order to gain more experimental data on the behavior of cracked reinforced concrete under plane stress loading conditions, experiments have been carried out at the University of Kassel [6, 7] and at the University of Toronto [5]. All panels were subjected to uniform stress states. The strains in the panels were measured over lengths which included several cracks. The stress-strain relationships from these tests represent the average behavior of reinforced concrete specimens. Thus they are directly applicable to Finite Element analyses where the smeared crack concept is employed. The results of our experimental investigation led to improvements in the computational treatment of cracked reinforced concrete, which will be presented in this paper.

## 2. CRACKED CONCRETE

### 2.1 Reduction of concrete compressive strength

#### 2.1.1 Description of the problem

The biaxial strength envelope by Kupfer, Hilsdorf and Rüschi [8] is often used as failure surface for uncracked concrete. The biaxial strength envelope is shown in Fig. 1 and regions of compressive failure (concrete crushing) and tensile failure (tensile splitting) are indicated. If a reinforced concrete panel, which is reinforced in direction of the applied tensile stress  $f_1$  only, as shown in Fig. 1, is subjected to load path 1, failure will be due to crushing of concrete when the applied compressive stress reaches the concrete compressive strength, which is a function of the simultaneously acting tensile stress in concrete. If the applied load follows load path 2 of Fig. 1 the concrete will crack once the failure surface is reached. Upon cracking the average concrete tensile stress  $f_{c1}$  decreases. After cracking tensile concrete stresses exist only in the concrete struts between the cracks. The released tensile stresses are taken up by the reinforcement.

If it is assumed that the panel of Fig. 1 is sufficiently reinforced so that a failure of the reinforcement is prevented, crushing of the cracked concrete will govern the failure. But which criterion for the compressive strength of cracked concrete should be used? Is the strength of the cracked concrete equal to the cylinder crushing strength  $f'_c$ , as for example assumed by Milford and Schnobrich [9]? Or is the strength of cracked concrete a function of the transverse strain  $\epsilon_1$  as proposed by Vecchio and Collins [12, 13]? Or should the concrete compressive strength of cracked concrete be generally reduced by 20 % as recommended by Schlaich and Schäfer [11]?

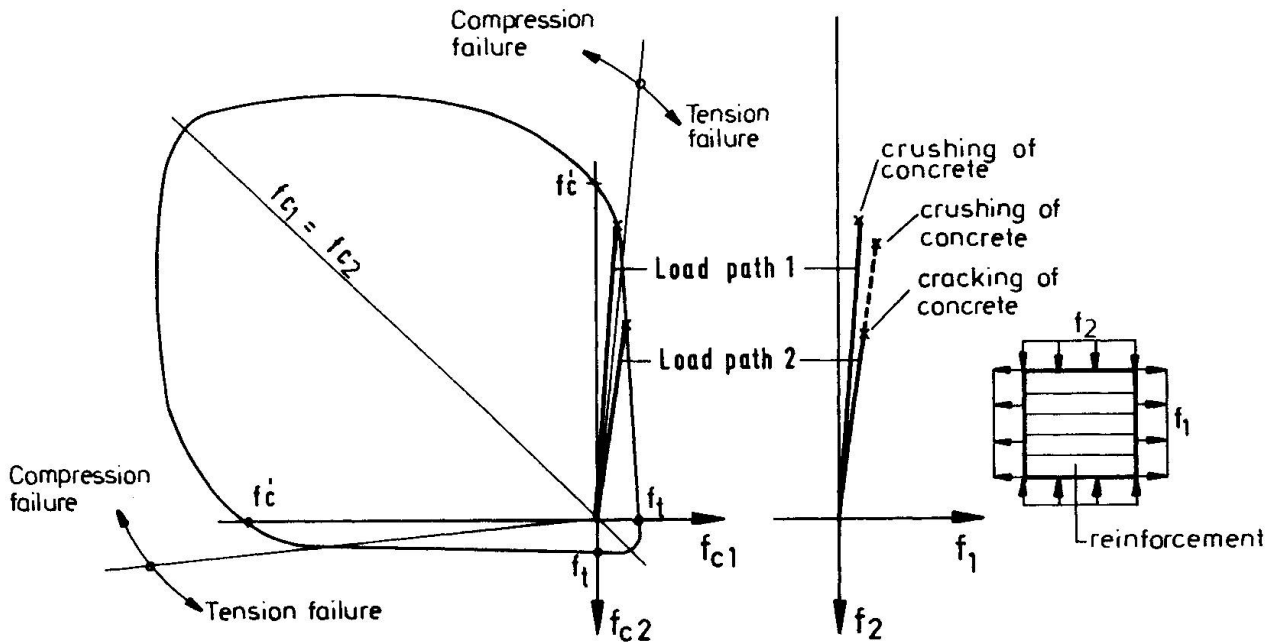


Fig.1 Biaxial concrete strength and RC panel subjected to tension and compression

### 2.1.2 Experimental results

In order to answer these questions a series of fifty panels is being tested at the University of Kassel and eight panels were tested at the University of Toronto. The detailed experimental results will be given in [5, 7]. Here, only the major conclusions regarding the compressive strength of cracked concrete will be summarized.

The maximum reduction of the concrete compressive strength in both series was around 20 to 25 %. The results of the Toronto tests [5] are compared with the phenomenological relationship for the reduction of the concrete compressive strength based on experimental results obtained by Vecchio and Collins [12] in Fig. 2. The relationship suggested by Vecchio and Collins considerably underestimates the observed concrete strengths of this series, as is shown in Fig. 2.

In cracked concrete transverse stresses exist in the concrete struts, which will be further investigated in section 2.2. The biaxial failure stresses of the reinforced concrete panels [5] are compared in Fig. 2 with the biaxial strength envelope of Kupfer et al. [8]. Three panels tested by Vecchio and Collins [12], which failed due to concrete crushing, have also been included in Fig. 2. Considering that average stresses in reinforced concrete panels are compared with results obtained on plain concrete specimens (200 mm x 200 mm x 50 mm) by Kupfer et al. in Fig. 2, good agreement of the biaxial failure stresses can be noted.

Kupfer et al. [8] report that specimens subjected to combined tension and compression behaved similarly to the specimens loaded in biaxial compression as long as the ratio of the applied stresses  $f_1/-f_2$  was less than 1/15; with a stress ratio  $f_1/-f_2$  equal to 1/10 tensile splitting failures occurred (see Fig.2). These observations are also in good agreement with the results of the panel test series; the panels failed due to concrete crushing and the corresponding stress ratios at failure are in the compression failure region of the tests by Kupfer et al. If the reinforcement does not fail tension failure is not possible in a



reinforced concrete panel. If the tensile stress in the concrete exceeds the cracking strength, a crack forms and the tensile stress is released. This explains why failures of reinforced concrete panels have to occur in the compression failure region of Fig. 2, unless the ultimate strength of the panel is governed by the load carrying capacity of the reinforcement in tension.

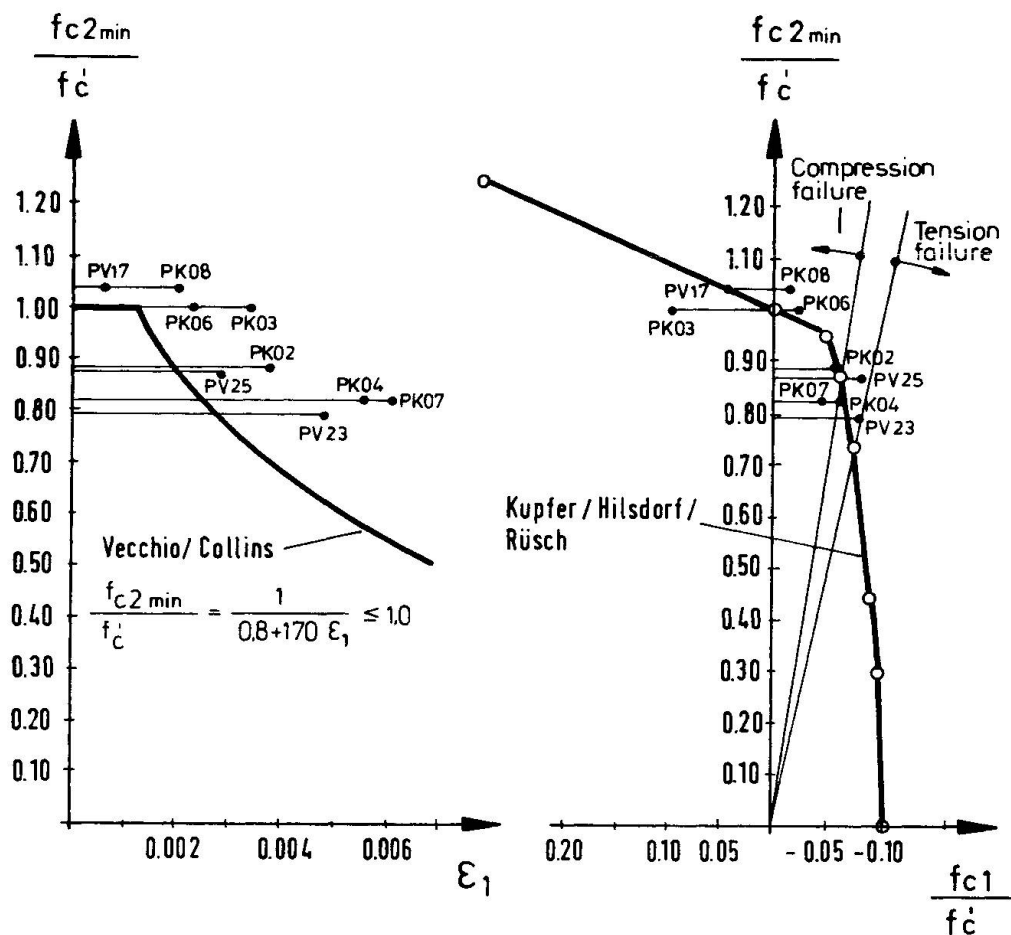


Fig.2 Compressive strength of concrete as a function of transverse strain and transverse stress

### 2.1.3 Proposed formulation

Based on the experimental results of Fig. 2 which are in agreement with the findings reported in [7] it is proposed to reduce the concrete compressive strength as a function of the simultaneously acting transverse stress. Fig. 3 shows how for a given stress  $f_{c1}$  the minimum compressive stress  $f_{c2}$  is found from the biaxial failure envelope. The strain corresponding to the peak stress  $f_{c2\min}$  is determined from the equation  $\epsilon_{c2\min} = \epsilon'_c * f_{c2\min} / f'_c$ .



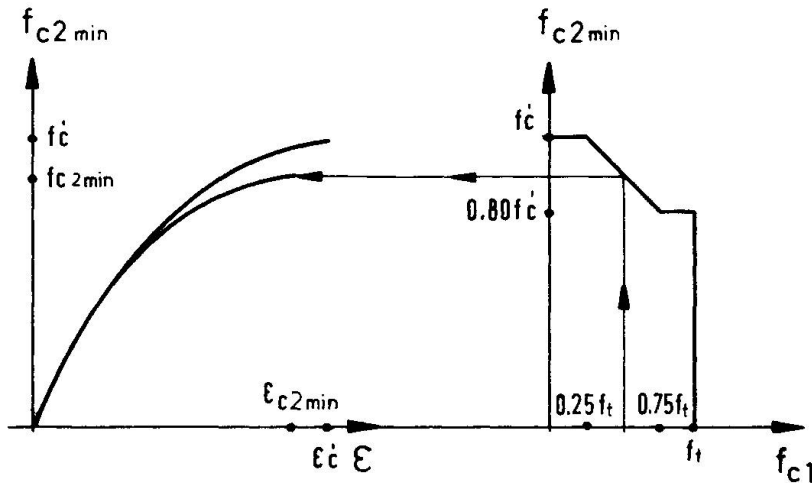


Fig.3 Proposed reduction of compressive strength for cracked concrete

## 2.2 Tension stiffening

### 2.2.1 General considerations

When formulating a material model for reinforced and prestressed concrete structures for either loading conditions, the realistic modelling of the stiffness after cracking deserves special attention. The inclusion of a realistic tension stiffening model is generally very important in the analysis of reinforced concrete shell structures which might be endangered by a stability failure. If the minimum concrete compressive stress is a function of the transverse stress, as outlined in section 2.1, a careful evaluation of the tensile concrete stresses is even more crucial.

### 2.2.2 Tension stiffening for coinciding principal tensile strain and reinforcement directions

The results of a tension test [5] are shown in Fig. 4. The response of the bare bar and the reinforced concrete specimen are compared in this figure. Multiplying the stress difference of the two curves times the reinforcement ratio yields the tension stiffening curve of Fig. 5. While the concrete is free of stress at the cracks, between the cracks tensile stresses are transferred from the steel to the concrete by bond action. The tensile stress shown in Fig. 5 is the average concrete stress of the specimen. Experimental data on tension stiffening of panels for varying reinforcement ratios and different reinforcement properties is given in [5, 6]. All tension stiffening curves for coinciding principal tensile strain and reinforcement direction are of a shape similar to Fig. 5. After cracking the average concrete tensile stress drops gradually to a certain stress level. Tension stiffening vanishes once the yield strength of the reinforcement at a crack is reached. However, even if the reinforcement yields at a crack, between the cracks the concrete still carries tensile stresses.

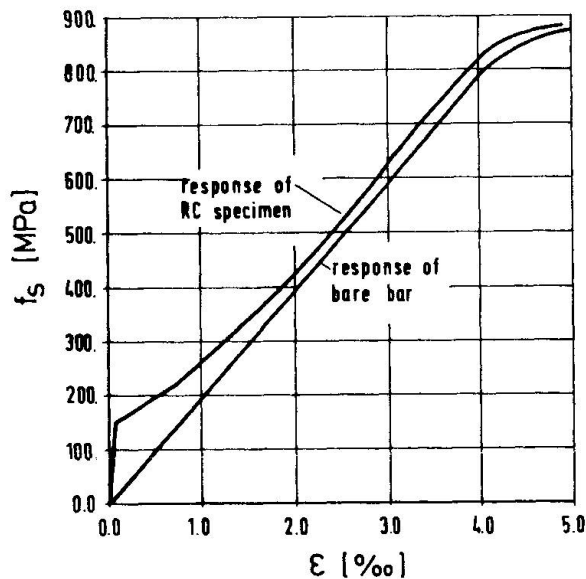


Fig.4 Results of tension test

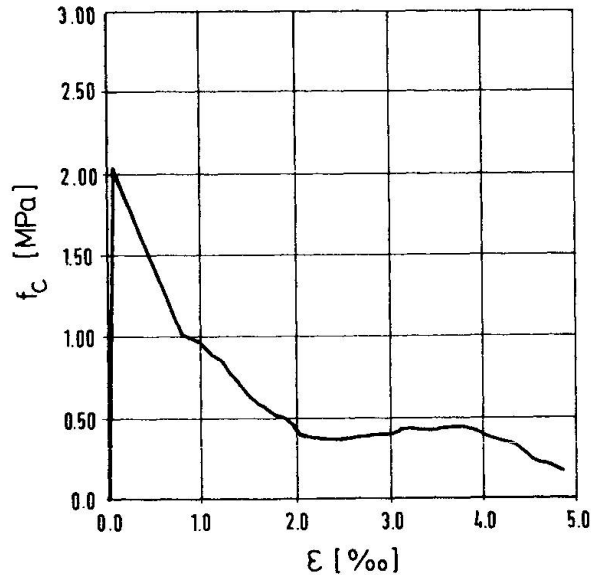


Fig.5 Tension stiffening curve

### 2.2.3 Tension stiffening for arbitrary angles between principal tensile strain and reinforcement directions

An evaluation of test results reported by Röder [10] and Vecchio and Collins [12] showed that the angles between the principal tensile strain and reinforcement direction do not have a noticeable influence on the tension stiffening, if tension stiffening is considered in the reinforcement direction [6]. This observation proved to be in good agreement with panel tests [5], where it was also noticed that the crack spacing did not depend on the angles between principal tensile strain and reinforcement directions, if the crack spacing was measured in the reinforcement directions.

It is suggested to evaluate the tension stiffening in the reinforcement directions and then to transform the concrete tensile stresses to the principal strain direction. A numerical example for this procedure is given in section 4.1.

### 2.2.4 Additional transverse stresses in concrete struts

Additional transverse tensile or compressive stresses may exist in the concrete struts due to strain compatibility of reinforcement and concrete. On precracked panels subjected to compressive stresses  $f_2$  the formation of these transverse stresses will be explained. Fig. 6 shows a panel where the reinforcement is inclined by  $45^\circ$  with respect to the applied stress. In a similar experiment [5] compressive stresses developed in the reinforcement when the loading was applied. Compressive steel stresses can only exist if they are balanced by tensile concrete stresses. Since the panel is precracked tensile stresses cannot be transferred across the cracks. But between the cracks tensile stresses exist as is indicated in Fig. 6.

If the reinforcement is oriented orthogonal to the applied stress (Fig. 7) compressive transverse stresses develop in the concrete struts, because the transverse deformation of the concrete struts, caused by Poisson's ratio and dilatation effects, is restrained by the reinforcement.

In order to evaluate the transverse stresses in the concrete struts the stresses in the reinforcement within a strut are determined from the principal compressive strain  $\epsilon_2$ , the transverse strain in the strut  $\nu \cdot \epsilon_2$  and the angle  $\theta$ . The steel stresses are then transformed to the direction 1. Because of equilibrium in the transverse direction, the concrete stress has to be equal to the trans-

formed steel stress. The transverse concrete stresses are neither uniform over the width nor over the height of the strut (Figs. 6 and 7). In order to account for this fact the transverse concrete stresses have to be scaled down by a factor, which depends on the reinforcement properties. This transverse stress in the concrete strut is added to the stress caused by tension stiffening. This stress is then used to determine the compressive strength of cracked concrete as described in section 2.1.

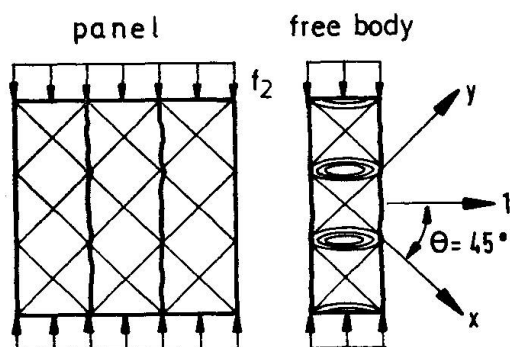


Fig.6 Transverse tensile stresses in concrete struts

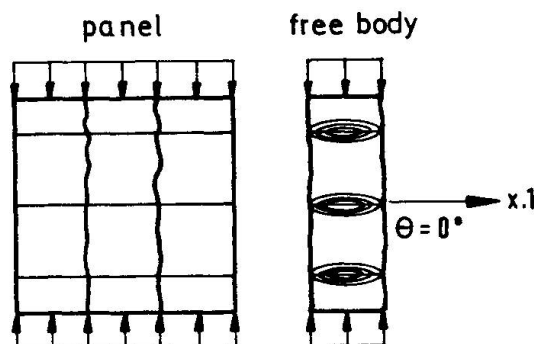


Fig.7 Transverse compressive stresses in concrete struts

### 2.3 Reorientation of principal strain direction

The numerical algorithm used to account for a reorientation of the principal strain direction is the "rotating crack model" by Akbar and Gupta [1]. Progressive cracking, or changes in the crack direction are considered in this model assuming that the crack direction is always normal to the direction of the maximum principal tensile strain. This assumption is in good agreement with experimental results as is shown by a sequence of pictures (Figs. 8 to 11) of a panel test, carried out by the first named author. The panel, which was reinforced in the x-direction only, was subjected to tensile stresses in the x-direction and shear stresses. Initially the cracks formed in a direction normal to the principal tensile stress in concrete (Fig. 8). Upon increased loading the tips of the cracks turned into a new direction, the original cracks became smaller and new cracks opened (Fig. 9). When the ultimate strength of the panel was reached (Fig. 10), the original cracks were closed and the failure of the panel was governed by an uncontrolled opening of the new cracks. The rotating crack model would describe the behavior of this panel by a rotation of the original concrete struts (Fig. 8) by approximately 45° into the final position. With the rotating crack approach the overall behavior of reinforced concrete panels can be captured better than with any fixed crack model. How complicated the actual behavior of the panel was, is shown in the close-up picture in Fig. 11. The crack pattern of Fig. 11 could probably not even be reproduced by the most sophisticated discrete crack models. But for the global analysis of shell structures the rotating crack model is a simple and efficient method to account for changes in the crack direction.

Using the rotating crack model the principal strain directions are updated in each iteration, i.e. the maximum principal strain is always orthogonal to the crack. From this follows that the shear strain is always zero. Therefore, no shear modulus has to be retained when the rotating crack model is used.

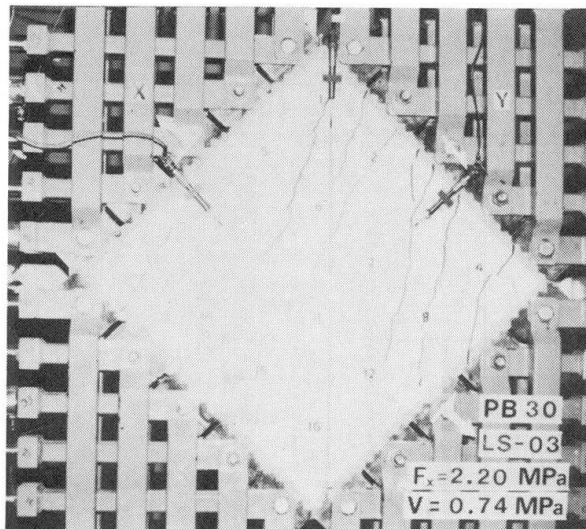


Fig.8 Panel PB30 LS-03

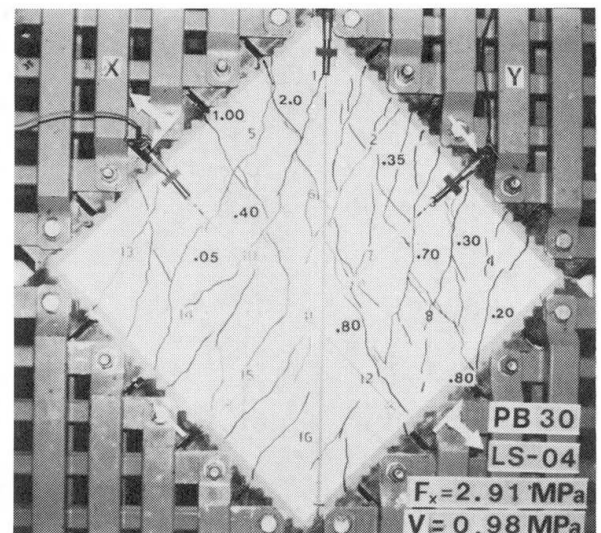


Fig.9 Panel PB30 LS-04

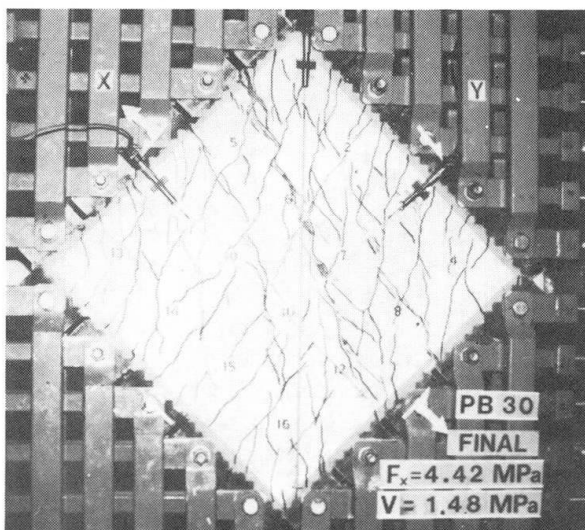


Fig.10 Panel PB30 FINAL

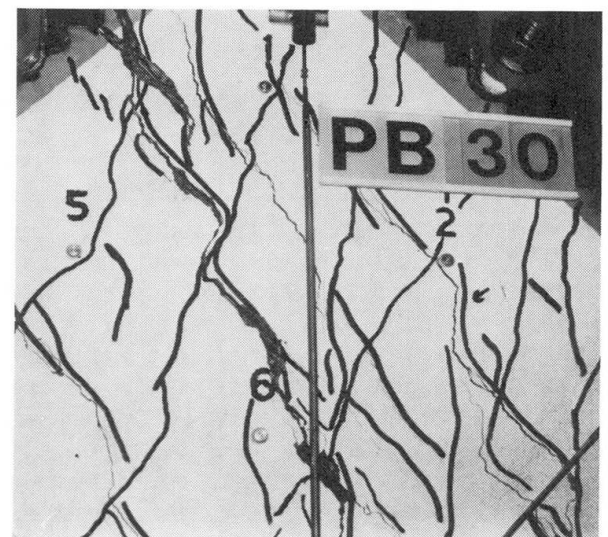


Fig.11 Detail of panel PB30

### 3. UNCRACKED CONCRETE

Uncracked concrete is modelled by Figueiras' plasticity model [4]. For the geometrically and physically nonlinear analysis of reinforced concrete shell structures the finite element code SEGNID [2] is used. The solution capabilities of the program as well as the available element library are described in [3].

## 4. EXAMPLES

### 4.1 Panels subjected to tension

The response of a panel subjected to tensile stresses in direction of the reinforcement is shown in Fig. 12. The stress-strain relationship of this example is qualitatively similar to the actual experiment shown in Fig. 4. The same response is obtained for tension stiffening models which evaluate concrete stresses as a function of the principal tensile strain  $\epsilon_1$  and as a function of

the strain in the reinforcement direction  $\epsilon_x$ . Tension stiffening vanishes when the yield strain of the reinforcement  $\epsilon_x = 0,002$  is reached.

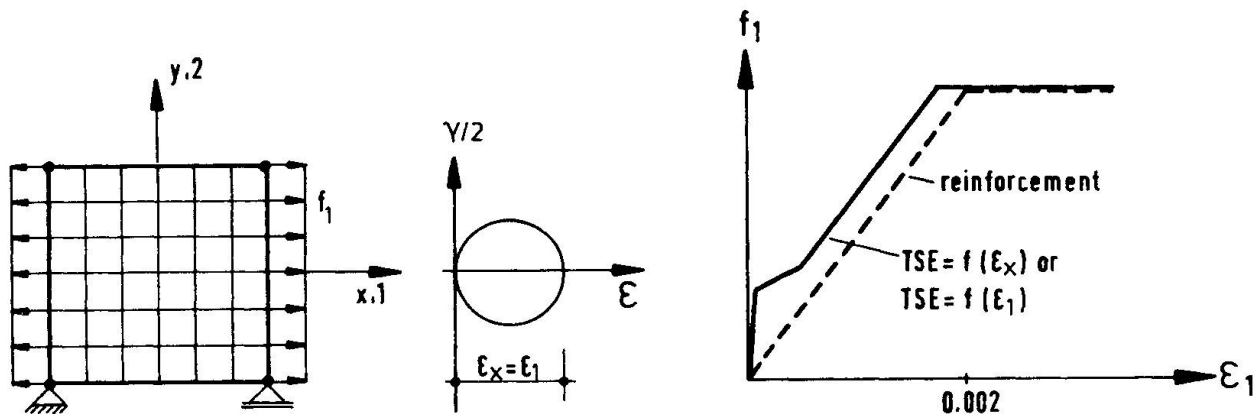


Fig.12 Panel subjected to tension in reinforcement direction

If the reinforcement is rotated by 45 degrees with respect to the applied tensile stress then different responses are obtained for tension stiffening formulations as a function of  $\epsilon_x$  and  $\epsilon_1$ . This is shown in Fig. 13, where it has been assumed that the concrete is infinitely stiff in compression. In the case that the tension stiffening depends on the strain orthogonal to the crack, the tensile stresses vanish when a strain of  $\epsilon_1 = 0.002$  is reached. If tension stiffening is considered in the reinforcement directions, the stiffening effect of the tensile stresses in the concrete would be noticeable until the reinforcements will yield at  $\epsilon_x = \epsilon_y = 0.002$ . A strain of 0.002 in the reinforcement directions corresponds to a principal tensile strain  $\epsilon_1 = 0.004$ , as is indicated by the Mohr's circle of strain in Fig. 13. This example shows that the actual tension stiffening is considerably underestimated, if tension stiffening is associated with the principal tensile strain direction.

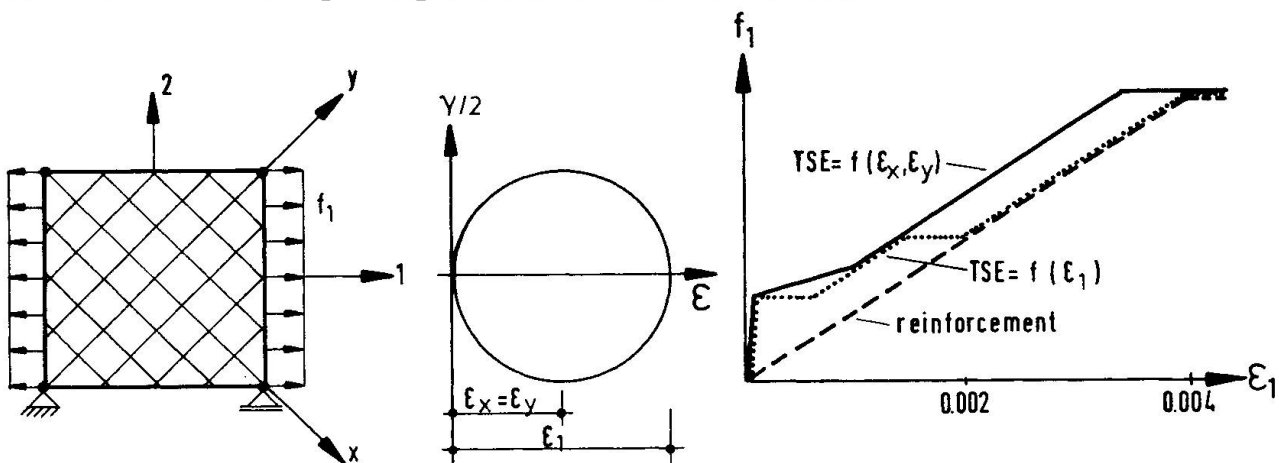


Fig.13 Panel subjected to tension at an angle of 45° with respect to reinforcement

#### 4.2 Panel subjected to tension and compression

The properties of panel PK04 [5] which was subjected to biaxial tensile and compressive stresses are shown in Fig. 14. In the experiment the tensile stresses were applied first up to a stress of  $f_1 = 5.4$  MPa. The tension was kept at this level when the compression was applied. The principal strains of experiment and analysis as a function of the applied compressive stress are compared in Fig. 15.





In the analysis one four node plane stress element was used as shown in Figs.12 and 13. The concrete compressive strength was reduced according to Fig. 3. At failure the effective concrete strength of the analysis was  $0.80 f'_c$ . This compares well with the maximum concrete strength of the experiment which turned out to be equal  $0.82 f'_c$  (Fig. 2). The reduction of the concrete compressive strength as suggested by Vecchio and Collins (Fig. 2) would yield an effective concrete strength of only  $0.56 f'_c$ .

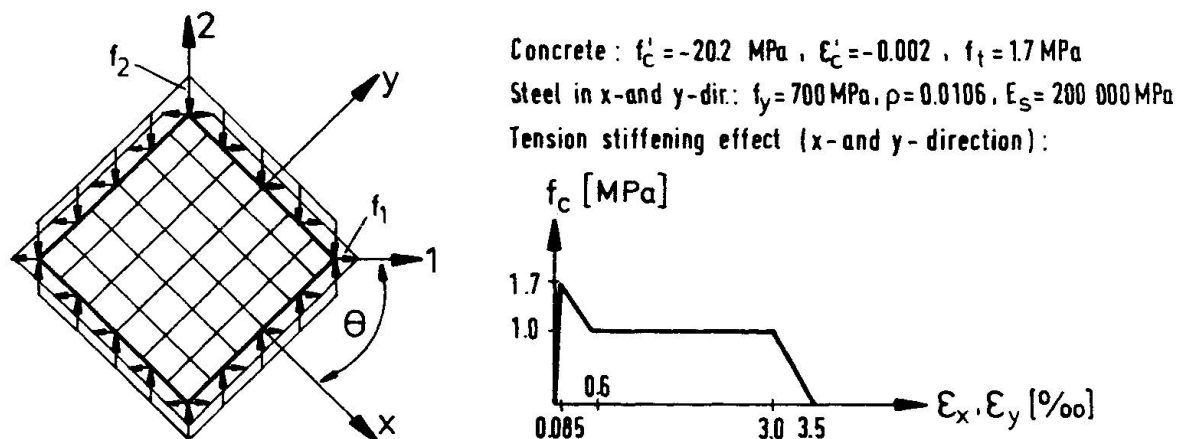


Fig.14 Loading and properties of panel PK04

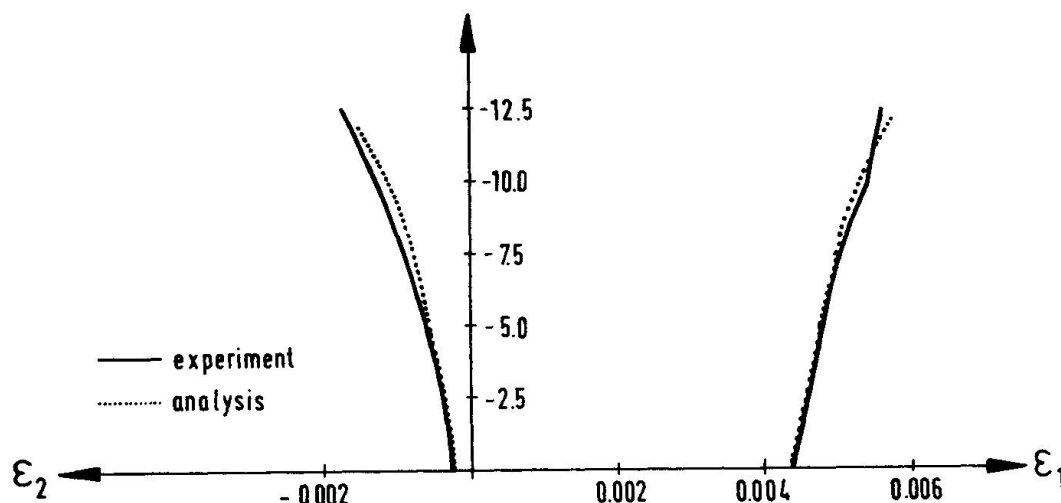


Fig.15 Stress-strain response of panel PK04

#### 4.3 Panel subjected to shear

Panel PV19 was tested by Vecchio and Collins in pure shear. The reinforcement of the panel in the y-direction was weaker than in the x-direction (Fig. 16). Therefore the principal strain direction  $\theta$ , which should be 45 degrees before cracking, changes after cracking as a function of the applied load. Fig. 17 shows that the rotating crack model is able to reproduce the stress-strain response of the test specimen. The failure load of the rotating crack model is 5 % higher than in the experiment. An analysis with a fixed crack model would overestimate the experimental failure load by 30 % (Fig. 17). In [12] the failure of the panel is attributed to concrete crushing. But the analysis reveals that the failure occurs, when the second reinforcement starts to yield.

Assuming an elastic-perfectly plastic stress-strain relationship for the reinforcement, the determinant of the stiffness matrix becomes zero at this load stage.

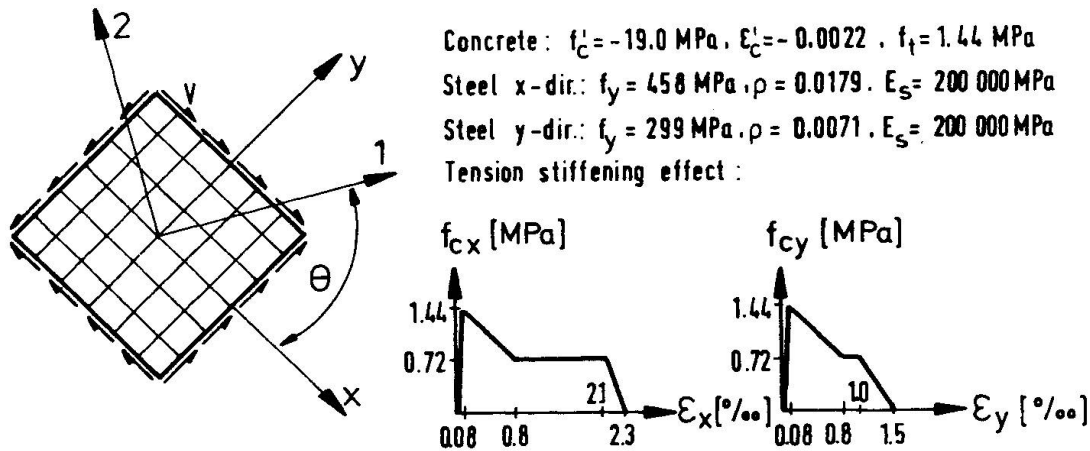


Fig.16 Loading and properties of panel PV19

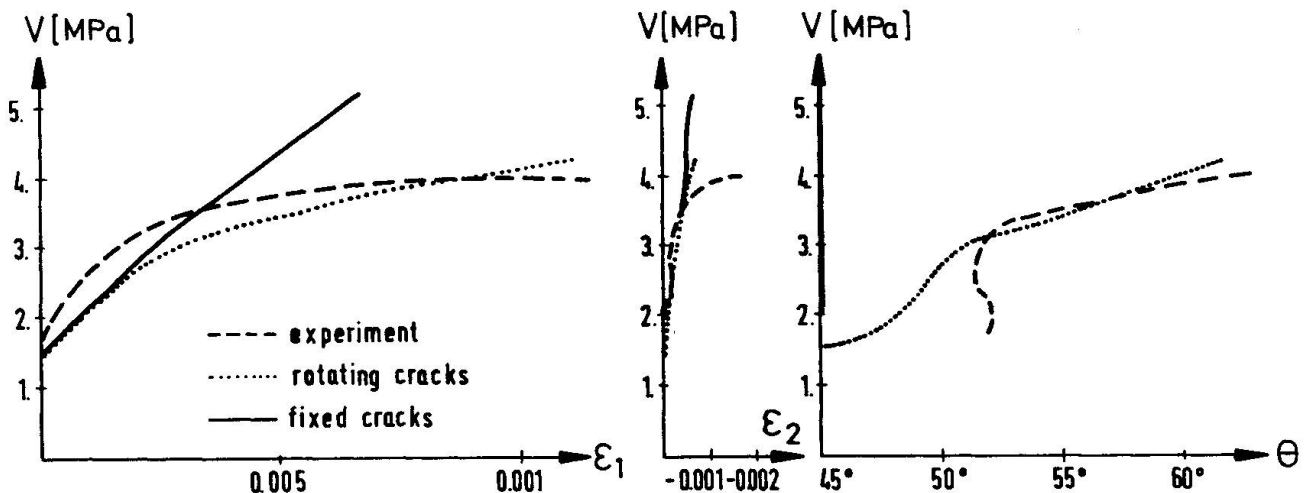


Fig.17 Stress-strain response of panel PV19

## 5. CONCLUSIONS

In the proposed material model the concrete compressive strength is a function of the simultaneously acting transverse stress. Therefore, the accurate evaluation of tensile stresses in cracked concrete is important. Based on experimental research a realistic procedure for the determination of tensile stresses in cracked concrete has been presented. It is believed that the presented formulation for cracked reinforced concrete will prove to be very effective in the nonlinear analysis of complex shell structures.

## ACKNOWLEDGEMENTS

The financial support of this investigation by the Deutsche Forschungsgemeinschaft is appreciated. The authors are very thankful to Professor Collins and the Department of Civil Engineering of the University of Toronto for providing the opportunity to do experimental work at their Civil Engineering Laboratories.





## REFERENCES

- [1] AKBAR, H. and GUPTA, A.: Membrane Reinforcement in Concrete Shells - Design versus Nonlinear Behavior, Department of Civil Engineering, North Carolina State University at Raleigh, January 1985.
- [2] DINGES, D.: Vergleichende Untersuchungen von Stahlbetonflächentragwerken unter Berücksichtigung physikalischer und geometrischer Nichtlinearitäten (Comparative Investigations of Reinforced Concrete Surface Structures Considering Physical and Geometrical Nonlinearities), Dissertation, Technical University of Darmstadt, 1987.
- [3] DINGES, D., SCHULZ, J.U., KOLLEGGGER, J. and MEHLHORN, G.: SEGNID - Finite Elemente Programm zur Berechnung geometrisch und physikalisch nichtlinearer Strukturen (Finite Element Program for the Analysis of Geometrically and Physically Nonlinear Structures), Forschungsbericht Nr. 4 aus dem Fachgebiet Massivbau, Gesamthochschule Kassel, 1987.
- [4] FIGUEIRAS, J.A.: Ultimate Load Analysis of Anisotropic and Reinforced Concrete Plates and Shells, Ph.D. Thesis, Department of Civil Engineering, University College of Swansea, September 1983.
- [5] KOLLEGGGER, J., COLLINS, M.P. and MEHLHORN, G.: Tension- and Tension-Compression Tests on Reinforced Concrete Elements, Department of Civil Engineering, University of Toronto, will be published in 1987.
- [6] KOLLEGGGER, J., GÜNTHER, G. and MEHLHORN, G.: Zug- und Zug-Druckversuche an Stahlbetonscheiben (Tension- and Tension-Compression Tests on Reinforced Concrete Panels), Forschungsbericht Nr. 1 aus dem Fachgebiet Massivbau, University of Kassel, 1986.
- [7] KOLLEGGGER, J. and MEHLHORN, G.: Druckversuche an Stahlbetonscheiben (Compression Tests on Reinforced Concrete Panels), Forschungsbericht aus dem Fachgebiet Massivbau der Gesamthochschule Kassel, to be published in 1987.
- [8] KUPFER, H., HILSDORF, H.K. and RÜSCH, H.: Behavior of Concrete Under Biaxial Stresses, Journal of the American Concrete Institute, August 1969, pp. 656-666.
- [9] MILFORD, R.V. and SCHNOBRICH, W.C.: Nonlinear Behavior of Reinforced Concrete Cooling Towers, Civil Engineering Studies, University of Illinois at Urbana-Champaign, May 1984.
- [10] RÖDER, F.K.: Versuchsergebnisse zum Kraftverlauf in schräg zum Riß angeordneten Bewehrungsstäben (Experimental Results on the Force Distribution in Reinforcement Bars Inclined with Respect to the Crack), Forschungsbericht Nr. 23, Institut für Massivbau, Technical University of Darmstadt, 1974.
- [11] SCHLAICH, J. and SCHÄFER, K.: Zur Druck-Querzug-Festigkeit des Stahlbetons (On the Compression-Transverse Tensile-Strength of Reinforced Concrete), Beton- und Stahlbetonbau, 3/1983, pp. 73-78.
- [12] VECCHIO, F. and COLLINS, M.P.: The Response of Reinforced Concrete to In-Plane and Normal Stresses, Department of Civil Engineering, Publication 82-03, University of Toronto, March 1982.
- [13] VECCHIO, F. and COLLINS, M.P.: The Modified Compression-Field Theory for Reinforced Concrete Elements Subjected to Shear, Journal of the American Concrete Institute, March-April 1986, pp. 219-231.

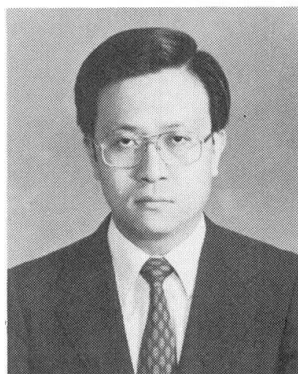
## An Analytical Model for Frictional Shear Slip of Cracked Concrete

Modèle analytique pour l'étude du glissement par friction et cisaillement de béton  
fissuré

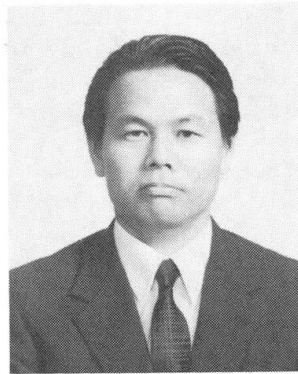
Ein Rechenmodell für die Rissreibung in Beton

### Hiromichi YOSHIKAWA

Senior Research Eng.  
Techn. Res. Inst.  
Hazamagumi, Japan



Hiromichi Yoshikawa, born in 1952, got his Dr. of Eng. at the University of Tokyo, involved in the research works on the thermal stress analysis of concrete, analytical modelling of reinforced concrete members and finite element analysis of RC structures at Hazamagumi Construction Company.



Tadaaki Tanabe, born in 1940, got his Dr. of Eng. at the University of Tokyo. After ten years research work in dams and RC structures of nuclear power stations, at the Central Research Institute of Electric Power Industry, he joined the Nagoya University in 1981, was promoted to full Professor in 1984, and was engaged in the research of aseismic design and the thermal stress control of RC structures.

### Tadaaki TANABE

Prof. of Civil Eng.  
Nagoya University  
Nagoya, Japan

### SUMMARY

Analytical formulation of a constitutive equation for a single crack is made and modelling of four basic coefficients are discussed. Numerical simulation and comparisons with test results indicate that the proposed model can represent essential characteristics such as nonlinear shear transfer, aggregate interlock and crack dilatancy, and satisfactorily predicts experimentally observed results. Finally, the constitutive matrix is presented for concrete containing regularly distributed cracks.

### RÉSUMÉ

La formulation analytique d'une équation constitutive pour une fissure simple est proposée et un modèle basé sur quatre coefficients est présenté. Une simulation numérique et des comparaisons avec des résultats d'essais montre que le modèle proposé peut représenter les caractéristiques essentielles telles que le transfert d'efforts tranchants non-linéaires, l'influence des agrégats et l'évolution des fissures. Il prédit de façon satisfaisante les résultats expérimentaux observés. Finalement la matrice constitutive est présentée pour un béton contenant des fissures distribuées de façon régulière.

### ZUSAMMENFASSUNG

Ein Vierparameter-Werkstoffgesetz für den Einzelriss wird analytisch formuliert. Mittels numerischer Berechnungen und Vergleichs mit Versuchsergebnissen wird gezeigt, dass das Werkstoffgesetz die wichtigsten Merkmale wiedergibt, wie nichtlineare Schubübertragung, Rissdilatanz und Kornverzahnung. Zum Schluss wird das Werkstoffgesetz für Beton mit regelmässig verteilten Rissen gegeben.



## 1. INTRODUCTION

It has been long recognized that cracks in concrete have a significant effect on the mechanical response of reinforced concrete. This requires construction of an analytical model representing a single crack for nonlinear analysis of reinforced concrete members. The authors develop a constitutive equation that relates relative discontinuous displacements (shear slip and crack opening) and applied shear and normal stresses on crack surfaces of concrete in a state of plane stress.

In this paper, the formulation of a basic constitutive equation and modeling of the four coefficients contained in the constitutive matrix are described. Numerical examinations demonstrate that the shear stress-shear displacement relation exhibits highly nonlinear behavior and is quite sensitive to vertical constraint such as the normal displacement (crack width) and extensional stiffness of reinforcement across a crack. Numerical comparisons indicate satisfactory agreement with available test data.

The authors propose a constitutive model that can reflect such typical characteristics as shear transfer due to aggregate interlock, coupling effect (crack dilatancy and frictional contact slip) and path-dependence. Moreover, this model can easily be incorporated into conventional finite element codes without a great deal of revision by means of damage mechanics as well as crack strain method, which have been developed by Tanabe and his coworkers ([1]-[4], [17]-[19]).

## 2. BASIC EQUATIONS FOR STRESS-DISPLACEMENT RELATIONS

When expressing the mechanical behavior on the crack surface in a state of plane stress (Fig. 1), the relation between the shear stress  $\tau_{nt}^c$ , the normal stress  $\sigma_n^c$ , the relative shear displacement (slip)  $\delta_t$  and the relative normal displacement (crack opening)  $\delta_n$  may be generally assumed in the form:

$$\begin{Bmatrix} d\tau_{nt}^c \\ d\sigma_n^c \end{Bmatrix} = \begin{bmatrix} B_{tt} & B_{tn} \\ B_{nt} & B_{nn} \end{bmatrix} \begin{Bmatrix} d\delta_t \\ d\delta_n \end{Bmatrix}, \quad \{d\sigma_c\} = [B]\{d\delta\} \quad (1)$$

in which  $B_{tt}$  and  $B_{nn}$  are the crack stiffness, and  $B_{tn}$  and  $B_{nt}$  function as off-diagonal terms ([5], [6]). Identifying all the terms in the matrix of  $[B]$  is a major objective of this paper, although no fully established formulation for Eq.1 has been attained yet.

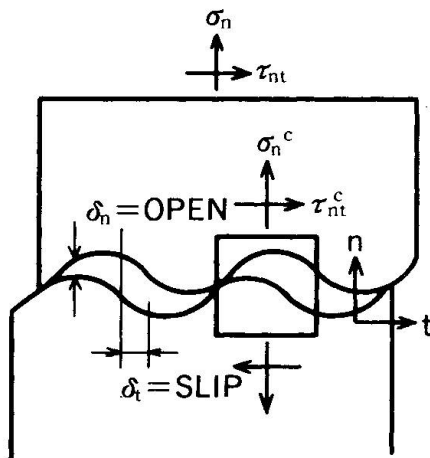


Fig. 1 Stresses and Discontinuous Displacements in a Single Crack

Examining experimental observations offered by many researchers, the following relations may be deduced. The shear displacement (shear slip) is affected by not only the applied shear stress but also the normal displacement (crack opening). The normal stress (always compressive) is of course determined by the normal displacement and also induced by the application of the shear stress especially when the crack opening is restrained. Consequently, the relations among these four variables can be expressed as follows:

$$\begin{aligned}\delta_t &= \delta_t(\tau_{nt}^c, \delta_n) \\ \sigma_n^c &= \sigma_n^c(\delta_n, \tau_{nt}^c)\end{aligned}\quad (2)$$

Differentiating each of Eq. 2 by making use of the chain rule, then,

$$d\delta_t = \frac{\partial \delta_t}{\partial \tau_{nt}^c} d\tau_{nt}^c + \frac{\partial \delta_t}{\partial \delta_n} d\delta_n, \quad d\sigma_n^c = \frac{\partial \sigma_n^c}{\partial \delta_n} d\delta_n + \frac{\partial \sigma_n^c}{\partial \tau_{nt}^c} d\tau_{nt}^c \quad (3)$$

is obtained. Here, we introduce the four coefficients defined by the differential derivatives appeared in Eq. 3 such that:

$$k_t \equiv \left(\frac{\partial \delta_t}{\partial \tau_{nt}^c}\right)^{-1}, \quad k_n \equiv \frac{\partial \sigma_n^c}{\partial \delta_n}, \quad \mu_f \equiv \left(\frac{-\partial \sigma_n^c}{\partial \tau_{nt}^c}\right)^{-1}, \quad \beta_d \equiv \left(\frac{\partial \delta_t}{\partial \delta_n}\right)^{-1}, \quad \beta_d' \equiv \frac{\partial \delta_n}{\partial \delta_t} \quad (4)$$

in which  $k_t$  = the shear stiffness,  $k_n$  = the normal stiffness,  $\beta_d$ ,  $\beta_d'$  = the dilatancy ratio and  $\mu_f$  = the frictional coefficient, respectively, all of which are defined in the tangential (incremental) form. Then, substituting the four coefficients into Eq. 3 leads to the following constitutive relation in the matrix form.

$$\begin{Bmatrix} d\delta_t \\ d\sigma_n^c \end{Bmatrix} = \begin{bmatrix} \frac{1}{k_t} & \frac{1}{\beta_d'} \\ -\frac{1}{\mu_f} & k_n \end{bmatrix} \begin{Bmatrix} d\tau_{nt}^c \\ d\delta_n \end{Bmatrix} \quad (5)$$

Note that in both vectors in Eq. 5 stress components and their corresponding displacement components are mixed, which may stem from the coupling effect between opposite crack surfaces. This important but cumbersome mechanical behavior can be represented by the above derived equations, which seems quite different from conventional types of stress-strain relations for continuum solid mechanics.

By modifying the form of Eq. 5 into the usual form as Eq. 1, the following equation is obtained.

$$\begin{Bmatrix} d\tau_{nt}^c \\ d\sigma_n^c \end{Bmatrix} = k_t \begin{bmatrix} 1 & -(1-\xi)\frac{1}{\beta_d'} \\ -\frac{1}{\mu_f} & \frac{1}{\mu_f \beta_d'} \end{bmatrix} \begin{Bmatrix} d\delta_t \\ d\delta_n \end{Bmatrix} \quad (6), \quad \begin{Bmatrix} d\delta_t \\ d\delta_n \end{Bmatrix} = \frac{1}{\xi k_t} \begin{bmatrix} 1 & (1-\xi)\mu_f \\ \beta_d & \mu_f \beta_d \end{bmatrix} \begin{Bmatrix} d\tau_{nt}^c \\ d\sigma_n^c \end{Bmatrix} \quad (7)$$

where  $\xi$  is a nondimensional parameter calculated from the four coefficients such that:

$$\xi = \mu_f \beta_d' \frac{k_n}{k_t} \quad (8)$$

Eqs. 6 and 7 appear to be asymmetric and the matrix [F] becomes singular when  $\xi=0$  and is guaranteed positive definite under the condition that  $\xi>0$ .

It should be noted that the proposed model, Eq. 7, includes Heuze and Barbour's formula [8] (called "uncoupled approach") as a special case when  $\xi=1$  and that ASCE's comment (made in Chapter 5 of Ref. [5]) that the term  $F_{tn}$  in the matrix [F] is very unlikely, corresponds to Eq. 7 assuming  $\xi=1$ . Eq. 7 when  $\xi=0$  is reduced to slip-dilatancy model by Bažant and Tsubaki [7] if solid concrete between cracks is assumed rigid.



### 3. MODELING OF THE FOUR COEFFICIENTS

It is expected that the four coefficients introduced in the previous section are not constant quantities but vary depending on applied stresses and displacements as well as concrete strength, size of aggregate and roughness of crack. Thus, sophisticated modeling for  $k_t$ ,  $k_n$ ,  $\beta_d$  and  $\mu_f$  is required, being represented as nonlinear functions of state-variables and concrete properties. This is described subsequently, making use of experimental data presently available from existing literature.

**Shear Stiffness  $k_t$ :** According to experimental observations, in the initial shear load, rather free slippage occurs on the cracked plane which is not in close contact, and further application of the shear stress makes the cracks stiffer due to firm contact (aggregate interlock). Finally, the shear stress levels off approaching the ultimate shear strength. This behavior can be represented by a hyperbolic curve such that:

$$\tau_{nt}^c = \tau_u \cdot \frac{\tanh \left\{ \frac{K_0}{\tau_u} (\delta_t - \delta_{t1}) \right\} + q}{1 + q} \quad (9)$$

$$k_t = K_{IST} \cdot \text{sech}^2 \left\{ \frac{K_0}{\tau_u} (\delta_t - \delta_{t1}) \right\} \quad (10)$$

$$\text{where, } K_0 = K_{IST} (1 + q), \quad q = \tanh \left( \frac{K_0}{\tau_u} \delta_{t1} \right) \quad (11)$$

in which  $K_{IST}$  denotes the maximum shear stiffness (expressed in MPa/mm) in the shear displacement  $\delta_{t1}$  (in mm) and  $\tau_u$  is the maximum shear strength (in MPa), which are illustrated in Fig. 2. The values of  $K_0$  and  $q$  can be calculated from  $K_{IST}$ ,  $\delta_{t1}$  and  $\tau_u$  by Eq. 11. Thus, the shape of a curve for shear slippage is characterized by means of these three values, which are considered to be significantly influenced by the normal displacement  $\delta_n$  and material property. The following expressions are identified by regression analysis from experimental data ([9]–[13]).

$$K_{IST} = 3.74 \left( \frac{f_c}{25} \right)^{0.60} \delta_n^{-0.96} \quad (12)$$

$$\delta_{t1} = 1.42 \left( \frac{D_a}{16} \right)^{-1.20} \delta_n^{1.31} \quad (13)$$

$$\tau_u = \frac{0.01}{0.01 + \left( \frac{\delta_n}{D_a} \right)^2} \tau_0, \quad \tau_0 = (0.2 \sim 0.3) f_c \quad (14)$$

( $f_c$ :MPa,  $D_a$ :mm,  $\delta_n$ :mm)

where  $f_c$  is the compressive strength of concrete (in MPa),  $D_a$  is the maximum aggregate size (in mm) and  $\tau_0$  is the shear strength of uncracked concrete (in MPa) interpreted as limiting value of asymptote for  $\tau_u$  when  $\delta_n \rightarrow 0$ . Empirical formula for  $\tau_u$  is taken from Ref.[6].

**Normal Stiffness  $k_n$ :** The relation between the normal stress and the normal displacement exhibits the simpler behavior as indicated in Fig. 3. Thus, the  $\sigma_n^c \sim \delta_n$  relation and the normal stiffness  $k_n$  can be represented in the form:

$$(15) \quad -\sigma_n^c = b_1 (\delta_n - \beta_d \delta_t)^{-b_2} \quad (15)$$

$$(16) \quad k_n = b_1 b_2 (\delta_n - \beta_d \delta_t)^{-(b_2 + 1)} \quad (16)$$

in which  $b_1$  and  $b_2$  are material constants. Although these constants are supposed to be dependent on concrete strength and aggregate size, this is not clarified due to the scarcity of test data. According to the authors' experiment,  $b_1=0.0082$  and  $b_2=0.878$  were obtained [14].

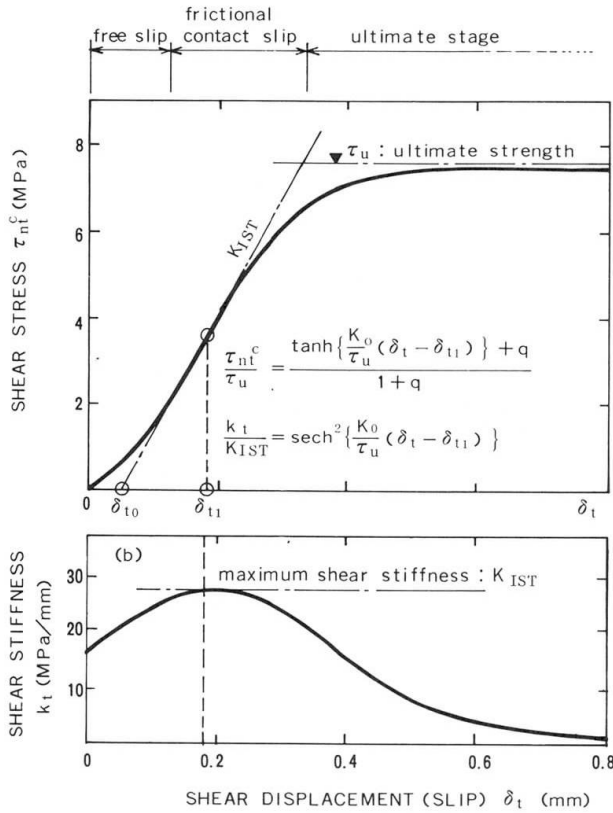


**Fig. 2 Idealization for Shear Behavior, (a) Shear Stress ~ Shear Displacement Relation, (b) Tangential Shear Stiffness (An Example for a Case of  $\delta_{t1}=0.18$  mm,  $K_{IST}=27$  MPa/mm,  $\tau_u=7.5$  MPa)**

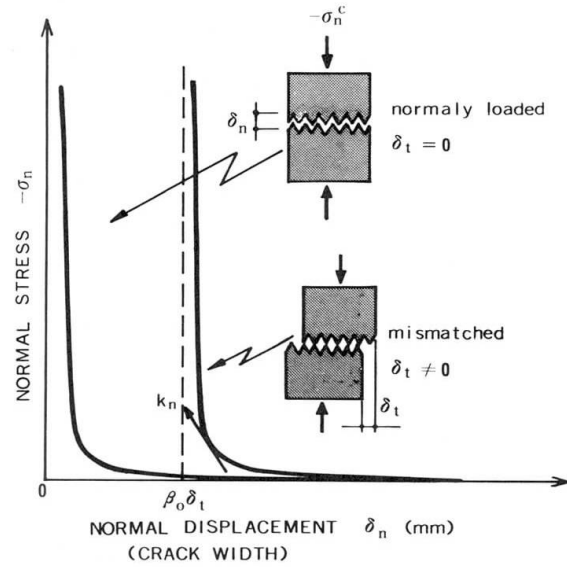


**Fig. 3 Idealization for Relation of Normal Stress and Normal displacement**

Dilatancy Ratio  $\beta_d$  and Frictional Coefficient  $\mu_f$ : Even though crack dilatancy and frictional slip have been experimentally recognized and pointed out as important characteristic accompanying discontinuities, no fully successful model seems to have been attained in the past. The dilatancy ratio is defined as the ratio of  $\delta_n$  and  $\delta_t$  at constant  $\sigma_n^c$  ( $<0$ ), the following expression is obtained using experimental data (Yoshikawa [14]), as shown in Fig. 4.

$$\mu_f = 1.16 \exp(0.61 \delta_n) \quad (17)$$

The frictional coefficient  $\mu_f$  is, on the other hand, described as the ratio of  $-\sigma_n^c$  and  $\tau_{nt}^c$  at constant  $\delta_n$ , which is found to be:

$$\beta_d = 1.64 \exp(-6.42 \left| \frac{\sigma_n^c}{f_c} \right|) \quad (18)$$

from test results ([9], [14], [15]) as shown in Fig. 5.

Figs. 4 and 5 indicate that experimentally obtained results display large fluctuations of up to  $\pm 50\%$ . Hence, constants of  $c_1$  for  $\mu_f$  and  $c_3$  for  $\beta_d$ , both of which vary 0.5 to 1.5, are introduced for the present to compensate for the



uncertainty of these two coefficients. This implies a need for further refinement of proposed expressions, Eqs. 17 and 18, as well as for carrying out more extensive experimental works.

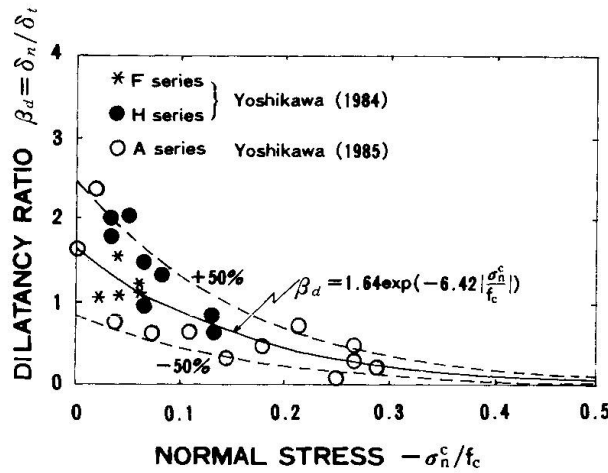


Fig. 4 Experimental Data for Dilatancy Ratio  $\beta_d$  and Obtained Regression Curve

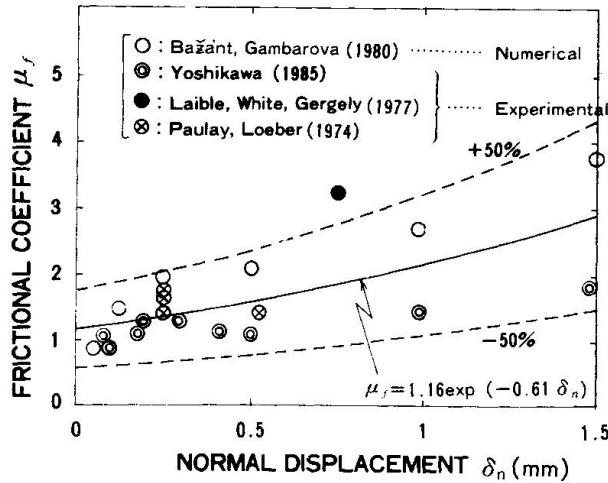


Fig. 5 Experimental Data for Frictional Coefficient  $\mu_f$  and Obtained Regression Curve

All of the expressions for the four coefficients by the authors are summarized in Table-1. The shear stiffness  $k_t$  among others reveal the most complicated expressions requiring twelve material constants,  $a_1 \sim a_{12}$ , which seem to be inevitable because of the complexity of shear transfer mechanism.

Table 1 Proposed Expressions for the Four Basic Coefficients and Experimentally Obtained Constants

SHEAR STIFFNESS : $k_t$ [MPa/mm]	CONSTANTS	NORMAL STIFFNESS : $k_n$ [MPa/mm]	CONSTANTS
$k_t = K_{IST} \operatorname{sech}^2 \left\{ \frac{K_0}{\tau_u} (\delta_t - \delta_{t1}) \right\}$		$k_n = b_1 b_2 (\delta_n - \beta_d \delta_t)^{-(b_1+1)}$	$b_1 = 0.0082$ $b_2 = 0.878$
$K_{IST} = a_1 \left( \frac{f_c}{25} \right)^{a_2} \left( \frac{D_a}{16} \right)^{a_3} \delta_n^{-a_4}$	$a_1 = 3.74, a_2 = 0.60$ $a_3 = 0, a_4 = 0.96$	<b>FRICTIONAL RATIO : <math>\mu_f</math></b>	<b>CONSTANTS</b>
$\delta_{t1} = a_5 \left( \frac{f_c}{25} \right)^{a_6} \left( \frac{D_a}{16} \right)^{-a_7} \delta_n^{a_8}$	$a_5 = 1.42, a_6 = 0$ $a_7 = 1.20, a_8 = 1.31$	$\mu_f = c_1 \mu_0 \exp(c_2 \delta_n)$	$\mu_0 = 1.16$ $c_1 = 0.5 \sim 1.5$ $c_2 = 0.61$
$\tau_u = \tau_0 \frac{a_9}{a_{10} + (\delta_n/D_a)^{a_{11}}}, \tau_0 = a_{12} f_c$	$a_9 = a_{10} = 0.01$ $a_{11} = 2$	<b>DILATANCY RATIO : <math>\beta_d</math></b>	<b>CONSTANTS</b>
$K_0 = K_{IST} (1 + q), q = \tan h \left( \frac{K_0 \delta_{t1}}{\tau_u} \right)$	$a_{12} = 0.2 \sim 0.3$ (0.245)	$\beta_d = c_3 \beta_0 \exp \left( -c_4 \left  \frac{\sigma_n^c}{f_c} \right  \right)$	$\beta_0 = 1.64$ $c_3 = 0.5 \sim 1.5$ $c_4 = 6.42$



#### 4. NUMERICAL SIMULATION AND COMPARISONS WITH TEST RESULTS

Fig. 6 depicts schematic descriptions of shear stress and normal stress, being represented as functions of displacements,  $\delta_t$  and  $\delta_n$ , which are computed from the authors' proposed model. Shown in Fig. 7 are variations of the shear stress under the condition that  $D_a=25\text{mm}$  and  $f_c=25\text{MPa}$  or  $40\text{MPa}$ . It may be concluded that these figures reveal the realistic nonlinear relations among the four state-variables,  $\tau_{nt}^c$ ,  $-\sigma_n^c$ ,  $\delta_t$  and  $\delta_n$ , and that obtained numerical results well conform to actually observed behavior.

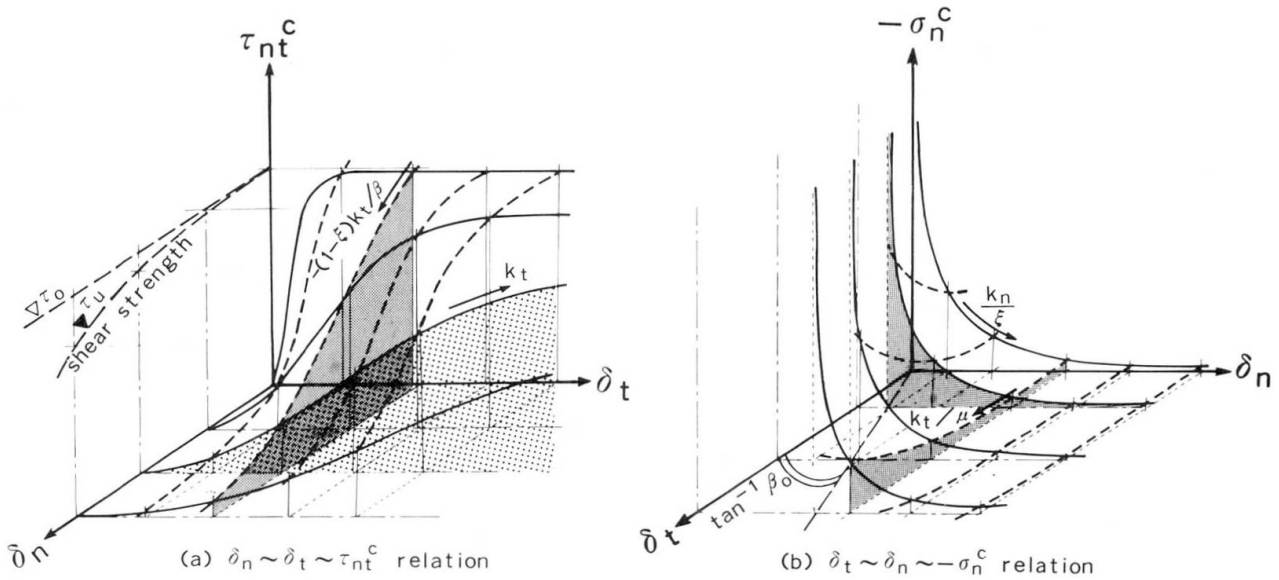


Fig. 6 Schematic Descriptions of Shear and Normal Stresses being Represented as Functions of Shear and Normal Displacements

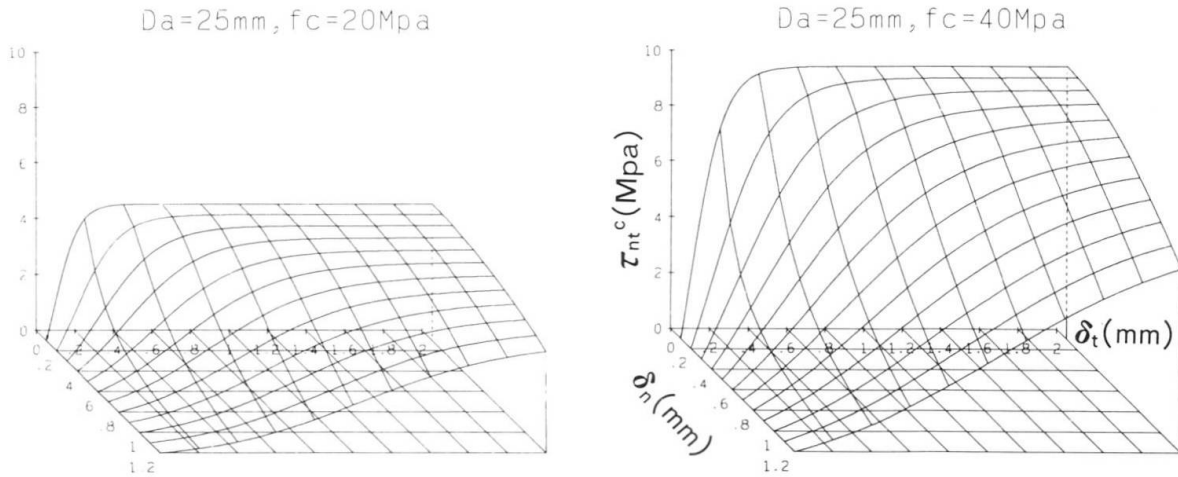


Fig. 7 Relationship between Shear Stress  $\tau_{nt}^c$  and Displacements  $\delta_n$  and  $\delta_t$  (Effect of Concrete Strength on Shear Behavior)



Fig. 8 shows relations of two variables among  $\tau_{nt}^c$ ,  $-\sigma_n^c$ ,  $\delta_t$  and  $\delta_n$ , in which fixed normal displacements (crack width)  $\delta_{n0}$  are chosen as a parameter in Fig. 8 a), b) and fixed normal stress  $-\sigma_{n0}^c$  is a parameter in Fig. 8 c).

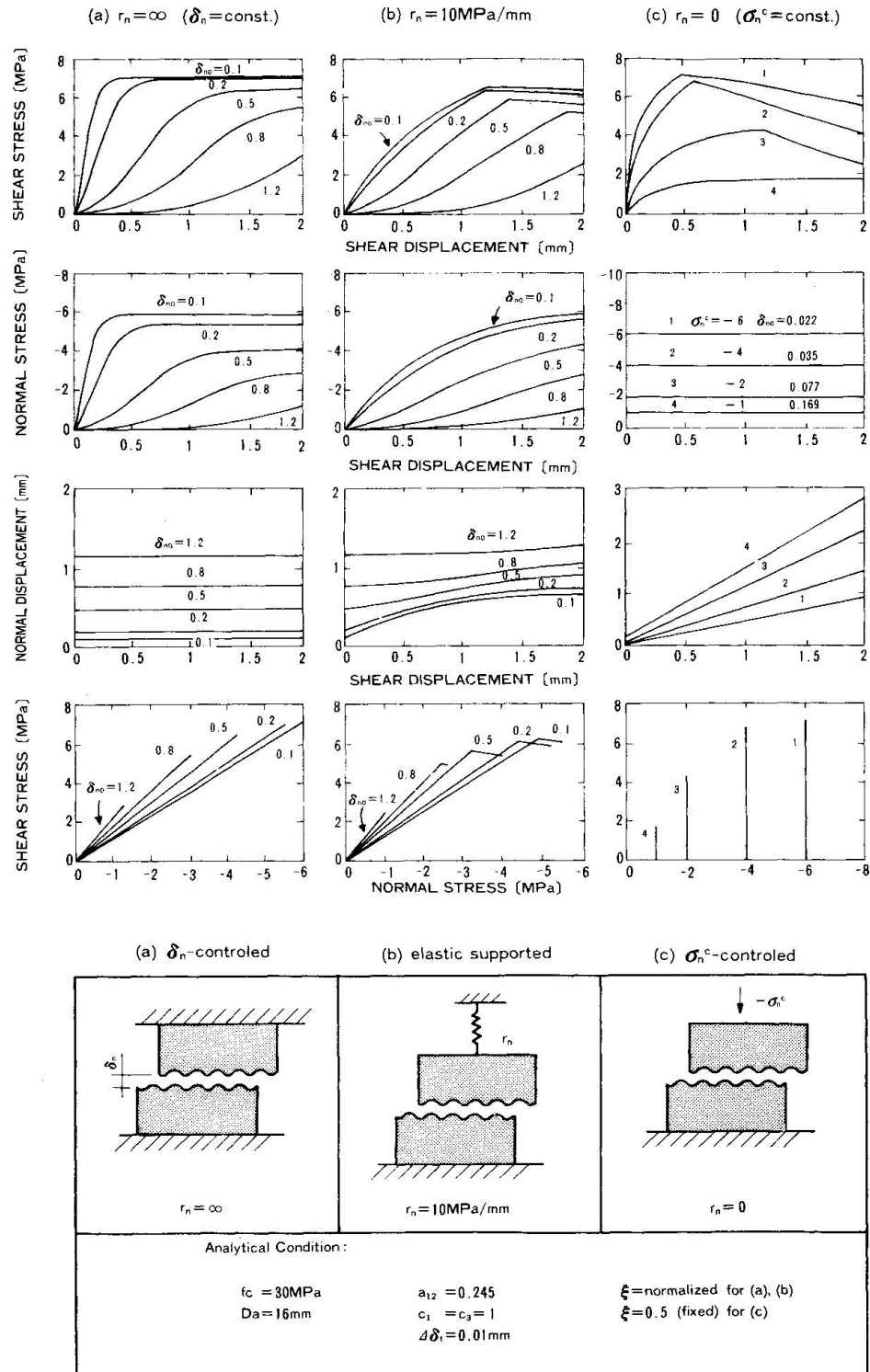
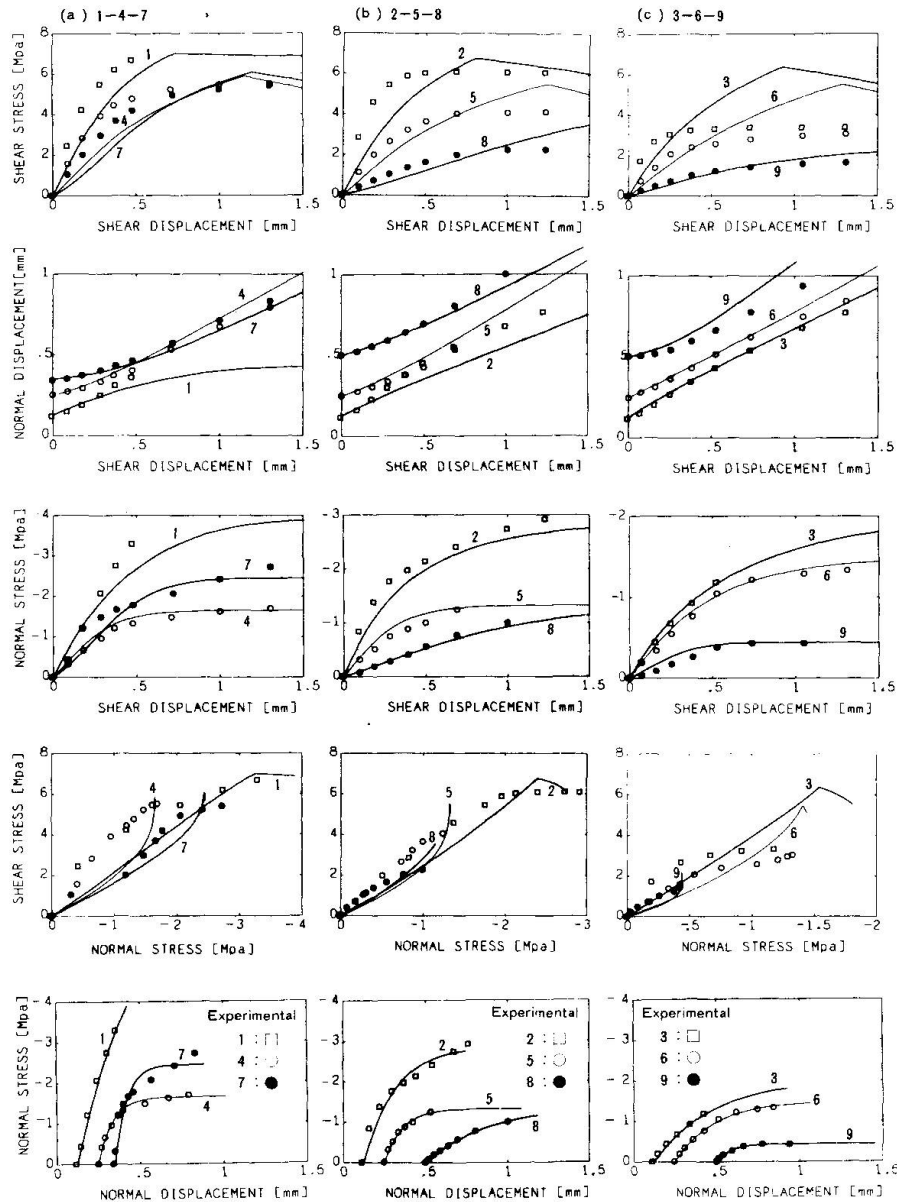


Fig. 8 Numerical Demonstration for Relations of Two Variables between  $\tau_{nt}^c$ ,  $-\sigma_n^c$ ,  $\delta_t$  and  $\delta_n$

In calculations, linear elastic spring is arranged in the direction normal to the crack surface, whose extensional stiffness is  $r_n$  (expressed in MPa/mm). The magnitude of the spring stiffness  $r_n$  determines the constraint condition such that  $\delta_n$  remains to be constant when  $r_n = \infty$  (Fig. 8 a)) and that  $-\sigma_n^c$  is a constant value when  $r_n = 0$  (Fig. 8 c)), and  $r_n$  assumed in Fig. 8 b) exists in-between (where  $r_n = 10$  MPa/mm is assumed). A series of drawings in Fig. 8 indicates that

### Direct Shear Tests by Millard, Johnson (1985)



### Analytical Condition

$\xi$	$a_{12}$	$c_1$	$c_3$	Initial crack width $\delta_{n0}$ (mm)			Concrete
0.5	0.245	1	0.5	□ 1 : 0.125	□ 2 : 0.125	□ 3 : 0.125	$f_c = 30\text{MPa}$ $D_a = 16\text{mm}$
				○ 4 : 0.25	○ 5 : 0.25	○ 6 : 0.25	
				● 7 : 0.35	● 8 : 0.50	● 9 : 0.50	

Fig. 9 Comparison of Calculated Values With Experimental Data (Millard and Johnson [16])



transmission of the shear stress along the crack surface is very sensitive to the constraint condition perpendicular to the crack surface. It is demonstrated that the shear stress is always accompanied by an increase of the crack opening ( $d\delta_n > 0$ ), otherwise compressive normal stress is induced ( $d\sigma_n^c < 0$ ) if the crack opening is restrained by the elastic spring.

Numerical comparison with observed data from Millard and Johanson's work [16] is shown in Fig. 9, where 9 specimens were tested with different initial crack width  $\delta_{n0}$  and different stiffness of reinforcement crossing a crack. Fig. 9 indicates that numerical values calculated from the proposed model are in relatively good agreement with experimental results.

## 5. CONCRETE WITH REGULARLY DISTRIBUTED CRACKS

We consider now a reinforced concrete panel (or wall, shell) that is carrying in-plane stresses, where regularly distributed cracks are gradually generated due to excessive tensile stress. The proposed constitutive equation prepared for a single crack can be applied to such a cracked reinforced panel, utilizing the crack strain concept.

Letting  $L_c$  be crack spacing (a distance between two adjacent cracks), the expression for a crack strain vector in a state of plane stress can be made as follows:

$$\{d\epsilon_{cr}\}^T = \{d\epsilon_n^{cr} \quad d\epsilon_t^{cr} \quad d\gamma_{nt}^{cr}\} = \frac{1}{L_c} \{d\delta_n \quad 0 \quad d\delta_t\} \quad (19)$$

assuming crack strains due to shear slip and crack opening are distributed evenly over the control area. Yoshikawa and Tanabe [4] mathematically derived the above equation using Dirac's delta function and its derivative.

The discontinuous displacements (shear slip and crack opening) given by Eq. 7 are substituted into Eq. 19, then, one has:

$$\{d\epsilon_{cr}\} = \frac{1}{\xi k_t L_c} \begin{bmatrix} \mu_f \beta d & 0 & \beta d \\ 0 & 0 & 0 \\ (1 - \xi) \mu_f & 0 & 1 \end{bmatrix} \begin{Bmatrix} d\sigma_n^c \\ d\sigma_t^c \\ d\tau_{nt}^c \end{Bmatrix} = [F] \{d\sigma_c\} \quad (20)$$

in which  $\{d\sigma_c\}$  means applied stress vector having its three components,  $d\sigma_n^c$ ,  $d\sigma_t^c$  and  $d\tau_{nt}^c$ , and the matrix  $[F]$  denotes such that:

$$[F] = \frac{1}{\xi k_t L_c} \begin{bmatrix} \mu_f \beta d & 0 & \beta d \\ 0 & 0 & 0 \\ (1 - \xi) \mu_f & 0 & 1 \end{bmatrix} \quad (21)$$

Here, it is assumed that the total strain  $\{d\epsilon\}$  is expressed by the sum of the crack strain,  $\{d\epsilon_{cr}\}$ , and the elastic/plastic strain between cracks,  $\{d\epsilon_{sc}\}$ , namely:

$$\{d\epsilon\} = \{d\epsilon_{sc}\} + \{d\epsilon_{cr}\} \quad (22)$$

Letting  $[D_c]$  be the stiffness matrix of the uncracked part of concrete (solid concrete), then the constitutive equation of uncracked concrete is expressed by the following usual form:

$$\{d\sigma_c\} = [D_c] \{d\varepsilon_{sc}\} = [D_c] (\{d\varepsilon\} - \{d\varepsilon_{cr}\}) \quad (23)$$

Then, the relation of applied stress and total strain is obtained by eliminating crack strain from Eqs. 20 and 23. This is:

$$\{d\sigma_c\} = ([I] + [D_c][F])^{-1} [D_c]\{d\varepsilon\} \quad (24)$$

in which  $[I]$  is a unit matrix.

Finally, the constitutive matrix  $[D^*]$  expressing overall stiffness of cracked concrete is written as follows:

$$[D^*] = [\psi][D_c] \quad (25)$$

where,  $[\psi] = ([I] + [D_c][F])^{-1}$

In the above equation, the nondimensional matrix  $[\psi]$  is considered to express the magnitude of degradation of cracked concrete due to discontinuous displacements (shear slip and crack opening) in addition to plasticity of solid concrete. This implies that nonlinear behavior of cracked concrete can be represented by means of a single constitutive matrix so-obtained, which may readily be applied to finite element analyses only if difficulty in treating unsymmetric matrix is overcome.

## 6. CONCLUDING REMARKS

The proposed model successfully reflects such typical characteristics of a crack in concrete as aggregate interlocking, crack dilatancy and frictional slip. Numerical simulation suggests that off-diagonal terms in the constitutive matrix characterized by dilatancy ratio and frictional coefficient play an important role in the shear transfer mechanism according to constraint conditions normal to the crack direction. Although this behavior has been recognized as coupling effect or cross effect by experimental works, very few analytical models were proposed.

One advantage of the authors' model is that the derived stiffness matrix of cracked concrete can readily be incorporated into existing finite element codes, requiring no additional isolated interelements. This decreases computational costs especially when large-scale reinforced concrete structures like nuclear facilities are dealt with.

The study of the tension stiffening effect is beyond the scope of the present paper, because this effect is observed in the completely different crack mode. A mathematical model for the tension stiffening based on analytical formulation taking bond-slip mechanism into consideration has been proposed in the authors' recent works ([17]-[19]).

We call the crack mechanism discussed in this paper the F-mode (frictional contact slip mode), while the tensile cracking mode where the tension stiffening effect must be taken into consideration is referred to as the S-mode (nonfrictional separation mode). In actual reinforced concrete structures, both of these crack modes are mixed. Hence, A further study is needed to combine both crack modes.



## REFERENCES

- [ 1 ] Tanabe, T. and Yoshikawa, H., A Finite Element Model for Cracked Reinforced Concrete Structures Introducing Crack Strain Concept, Proceedings of JCI Colloquium on Finite Element Analysis of RC Structures, Dec., 1984, pp. 65~72, (in Japanese).
- [ 2 ] Tanabe, T. and Yoshikawa, H.: A study on Constitutive Equations of a Cracked Reinforced Concrete Panel by the Damage and Reinforcement Matrices, the Colloquium on Computational Mechanics of Concrete Structures, IABSE, August, 1987.
- [ 3 ] Ishikawa, M., Yoshikawa, H. and Tanabe, T.: The Constitutive Model in Terms of Damage Tensor, Japan-US Joint Seminar on finite Element Analysis of Reinforced Concrete Structures, May, 1985, pp. 93~104, (Approved for publication by ST Division, ASCE).
- [ 4 ] Yoshikawa, H. and Tanabe, T., A Finite Element Model for Cracked Reinforced Concrete Members Introducing Crack Strain Concept, Japan-US Joint Seminar on Finite Element Analysis of Reinforced Concrete Structures, May, 1985, pp. 214~225, (Approved for publication by ST Division, ASCE).
- [ 5 ] The Task Committee on Finite Element Analysis of Reinforced Concrete Structures of the Structural Division Committee on Concrete and Masonry Structures: State-of-the-Art Report on Finite Element Analysis of Reinforced Concrete, ASCE, New York, 1981.
- [ 6 ] Bazant, Z.P., and Gambarova, P.: Rough Cracks in Reinforced Concrete, Journal of the Structural Division, ASCE, Vol. 106, No. ST4, April, 1980, pp. 819~842.
- [ 7 ] Bazant, Z.P. and Tsubaki, T.: Slip-Dilatancy Model for Cracked Reinforced Concrete, Journal of the Structural Division, ASCE, Vol. 106, No. ST9, Sept., 1980, pp. 1947~1966.
- [ 8 ] Heuze, F.E., and Barbour, T.G.: New Models for Rock Joints and Interfaces, Journal of the Geotechnical Engineering Division, ASCE, Vol. 108, No. GT5, May, 1982, pp. 757~776.
- [ 9 ] Paulay, T., and Loeber, P.J.: Shear Transfer by Aggregate Interlock, SP42, American Concrete Institute, 1974, pp. 1~15.
- [ 10 ] Houde, J. and Mirza, M.S., Investigation of Shear Transfer Across Cracks by Aggregate Interlock, Reserach Report No. 72-06, Ecole Polytechnique de Montreal, Department of Genie Civil, Division de Structures, 1972.
- [ 11 ] Fenwick, R.C. and Paulay, T.: Mechanisms of Shear Resistance of Concrete Beams, Journal of the Structural Division, ASCE, Vol. 94, No. ST10, October, 1968, pp. 2325~2350.
- [ 12 ] Reinhardt, H.W., and Walraven, J.C.: Cracks in Concrete Subject to Shear, Journal of the Structural Division, ASCE, Vol. 108, No. ST1, Jan., 1982, pp. 207~224.
- [ 13 ] Yamada, K.: A Study on the Design of RC Containment for Nuclear Power Stations with Particular Reference to Rationalization of RC Shell Elements against Shear Forces, Special Report of the Technical Research Institute of Maeda Construction Co., Ltd., No. 22-1, March, 1982 (in Japanese).
- [ 14 ] Yoshikawa, T.: Analytical Models for the Mechanical Behavior of Reinforced Concrete Members subjected to In-Plane Stresses, thesis presented to the University of Tokyo in 1986 required for the degree of Doctor of Engineering (in Japanese).
- [ 15 ] Laible, J.P., White, R.N., and Gergely, P.: Experimental Investigation of Shear Transfer Across Cracks in Concrete Nuclear Containment Vessels, SP-53, American Concrete Institute, 1977, pp. 203~226.
- [ 16 ] Millard, S.G., and Johnson, R.P.: Shear Transfer in Cracked Reinforced Concrete, Magazine of Concrete Research, Vol. 37, No. 130, March, 1985, pp. 3~15.
- [ 17 ] Yoshikawa, H. and Tanabe, T.: An Analytical Study on the Tension Stiffness and Constitutive Equations for Cracked Reinforced Concrete Members, International Symposium on Fundamental Theory of Reinforced and Prestressed Concrete, September 18-20, 1986, Nanjing Institute of Technology, Nanjing, China, pp. 1106~1113.
- [ 18 ] Yoshikawa, H. and Tanabe, T.: An Analytical Study of the Tension Stiffness of Reinforced Concrete Members on the Basis of Bond-Slip Mechanism, Transactions of the Japan Concrete Institute, Vol. 8, JCI, 1986, pp. 473~480.
- [ 19 ] Tanabe, T. and Yoshikawa, H.: Tension Stiffness and Constitutive Equation of a Cracked Reinforced Concrete Panel in the Plane Stress State, Transactions of the Japan Concrete Institute, Vol. 8, JCI, 1986, pp. 457~464.

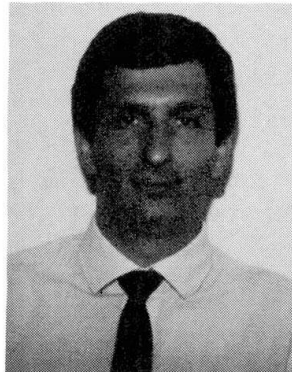
## Constitutive Laws of Structural Concrete for Application to Nonlinear Analysis

Lois constitutives du béton armé et précontraint et application à l'analyse non-linéaire

Werkstoffgesetze des Stahlbetons für die Anwendung auf nichtlineare Berechnungen

### M.Z. COHN

Prof. of Civil Eng.  
University of Waterloo  
Waterloo, ON, Canada



### P. RIVA

Res. Assist.  
University of Waterloo  
Waterloo, ON, Canada

### SUMMARY

This is the first of a two-part study on a practice-oriented approach to the non-linear analysis based on a lumped-plasticity concept and realistic constitutive laws for structural concrete. The approach consists of developing moment-curvature-rotation relations for reinforced, prestressed and partially prestressed concrete sections, starting from accurate descriptions of natural laws for concrete in tension and compression, as well as for ordinary and prestressing reinforcements. Resulting relations enable prediction of the section response under monotonic loading throughout all behaviour states up to failure.

### RÉSUMÉ

Cette contribution est la première partie d'une étude orientée vers l'analyse non-linéaire basée sur la notion de 'concentration de la plasticité' et des lois constitutives réalistes pour le béton. L'approche consiste à développer des relations moment-courbure-rotation pour le béton armé, précontraint et partiellement précontraint, en partant des expressions correctes pour les courbes caractéristiques du béton en traction et compression, ainsi que pour les armatures ordinaires et précontraintes. Les relations qui en résultent permettent d'étudier le comportement des sections sous charges monotones en passant progressivement par tous les états jusqu'à la rupture.

### ZUSAMMENFASSUNG

Dies ist der erste Teil einer zweiteiligen Studie über eine praxisorientierte Methode, die es erlaubt, auf Grund eines diskreten Plastizitätsmodells und realistischen Werkstoffgesetzes eine nichtlineare Berechnung von Betonelementen durchzuführen. Es werden Beziehungen zwischen dem Moment, der Krümmung und der Verdrehung bei bewehrten, vorgespannten und teilweise vorgespannten Betonquerschnitten entwickelt. Den Ausgangspunkt bilden dabei genaue Beschreibungen des Verhaltens von Beton unter Druck und Zug sowohl für eine schlaife als auch für eine vorgespannte Bewehrung. Die vorgestellten Ergebnisse ermöglichen eine Vorhersage des Verhaltens des Querschnittes bei konstanter Last unter allen Bedingungen bis zum Versagen.





## 1. INTRODUCTION

This study is an extension of some earlier investigations on the nonlinear analysis of structural concrete sections [1,2,3,4], aiming at more reliable techniques for the nonlinear analysis of hyperstatic structures, with particular reference to the inelastic states. Parallel efforts are reported in [5,6,7,8] and elsewhere. Considerable work has been devoted to the section response at the cracking and post-cracking states, including the effect of tension-stiffening [9,10,11].

Recent studies on partial prestressing and nonlinear analysis [12,13] suggest that it is possible to develop flexural theories that realistically account for the material behaviour, equally apply to reinforced, prestressed and partially prestressed concrete (R.C., P.C., and P.P.C., respectively), and continuously describe all load-deformation states, including cracking, service, yielding, and the ultimate state.

The paper presents a constitutive model for structural concrete sections that has the above features and will serve as a basis for further developments in the nonlinear analysis of hyperstatic structures based on the "lumped-plasticity" model [14,15,16,17].

## 2. ANALYTICAL MODEL

### 2.1 Assumptions

- (1) Quasi-static (monotonic, non-repeated, non-reversible) loading.
- (2) Negligible shear effects.
- (3) Planarity of sections (linear strain distribution).
- (4) Known natural stress-strain relationships (analytical, experimental, etc.)
- (5) Mono-axial stress-strain laws valid for section analysis.

For the cracked states the section considered (B) is the middle of an element (AC) of length  $\ell_c$ , equidistant to the neighbouring cracks, as shown in Fig. 1.

Moments are assumed to be constant over the length of the element  $\ell_c$ .

### 2.2 Material Constitutive Laws

For brevity, the adopted constitutive relations are summarized in Figs. 2 - 4, along with the relevant notation and equations.

Figs. 2a and 2b illustrate the  $\sigma_c - \epsilon_c$  and  $\sigma_{ct} - \epsilon_{ct}$  equations for the concrete in compression [1] and tension [10], respectively.

Fig. 3 shows the stress-strain curves and their analytical expressions for ordinary and prestressing steels, adapted from [1].

Figs. 4a and 4b illustrate the assumed bond-slip relations  $\tau_{bs} - s_s$  and  $\tau_{bp} - s_p$  for ordinary and prestressing steels, respectively [18].

### 2.3 Compatibility Equations

We consider a typical element AB with cross section strain, stress distribution and notation in Fig. 5. Since for the cracked section the neutral axis and rotation axis do not coincide, the compatibility conditions are expressed in terms of the latter, with corresponding ordinates related by  $z = y - (y_G - z')$ :

$$u_{cB} = \phi(z+z_0)/2 ; \quad u_{sB} = \phi(d_s - z' - z_0)/2 ; \quad u_{pB} = \phi(d_p - z' - z_0)/2 \quad (1)$$

Strains in the reinforcing and prestressing steels are expressed with consideration of the bond effects as:

$$\epsilon_{sB} = 2u_{sB}/\ell_c + \Delta\epsilon_s ; \quad \epsilon_{pB} = f_{pe}/E_p + 2u_{pB}/\ell_c + \Delta\epsilon_p \quad (2)$$

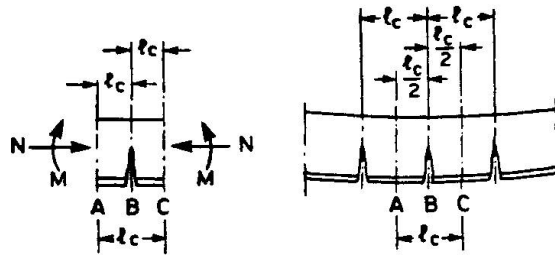


Fig. 1

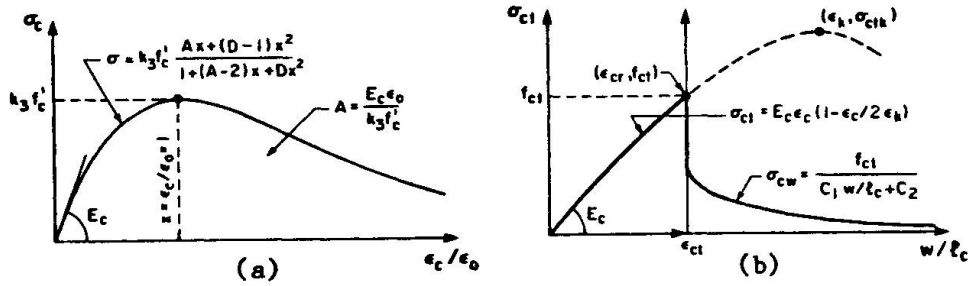


Fig. 2

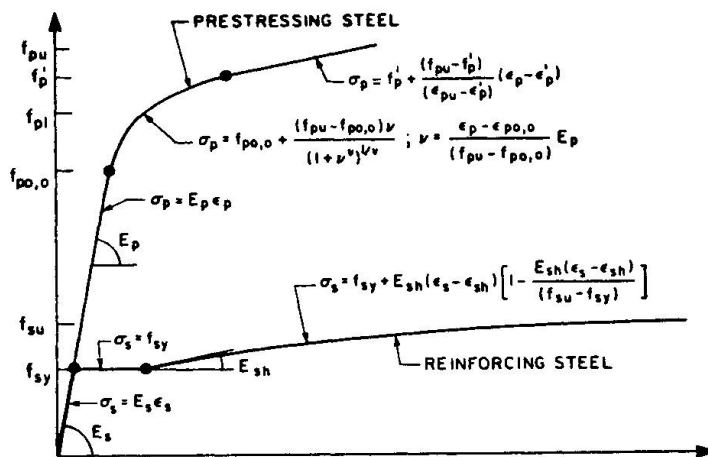


Fig. 3

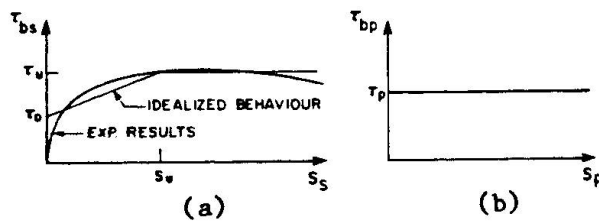


Fig. 4

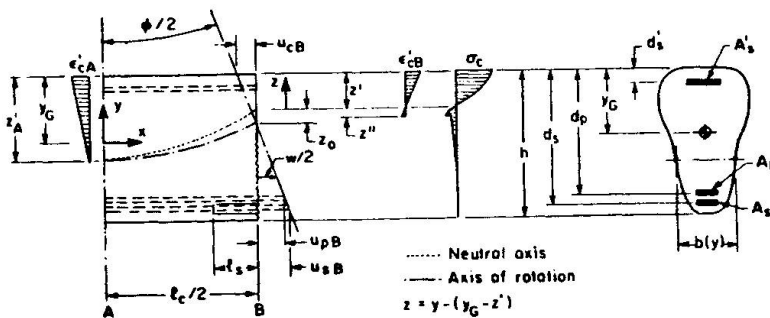


Fig. 5



where  $l_c$  is the crack spacing,  $2u_{sB}/l_c$  and  $2u_{pB}/l_c$  are the average deformations of  $A_s$  and  $A_p$ , respectively, and  $\Delta\epsilon_s$ ,  $\Delta\epsilon_p$  are the strain contributions of the tension-stiffening effect.

With the bond-slip constitutive laws in Fig. 4, expressions for  $\Delta\epsilon_s$  and  $\Delta\epsilon_p$  may be obtained for various behaviour states.

(a) Partial bar slip ( $l_s < l_c/2$ ): Denoting as  $l_s$  the bar length over which slip takes place, it can be shown that [19]:

$$\Delta\epsilon_s = -2u_{sB}/l_c + \alpha \left[ \frac{z}{t} \frac{2\alpha l_s}{l_c} + \frac{\epsilon''}{\alpha} \right] \frac{\sinh(2\alpha l_s/l_c)}{2\alpha l_s/l_c} \quad (3)$$

where  $\alpha = \sqrt{\tau_1 l_c^2 / E_s D_s}$ ;  $t = \tau_1 l_c / \tau_0$ ;  $\epsilon'' \approx \epsilon_{sA} = \epsilon_{cr}(h - z'_A)/(d_s - z'_A)$ ; and  $a_s$  is related to  $u_{sB}$  by the equation:

$$\cosh(2\alpha l_s/l_c) = 1 + [2u_{sB}/l_c - \epsilon''(1 - l_s/l_c)]/[2/t + \epsilon'' l_c/2\alpha^2 l_s] \quad (3')$$

(b) Full bar slip and moderate cracking ( $l_s = l_c/2$  and  $w_s \leq 2s_u$ ): Denoting as  $w_s$  the crack width at the reinforcing steel level and the slip limit (Fig. 4) as  $s_u$ ,  $\Delta\epsilon_s$  may be expressed as [19]:

$$\Delta\epsilon_s = (2/t + \epsilon''/\alpha^2) \left[ \alpha \frac{\cosh\alpha - 1}{\sinh\alpha} \right] - \frac{\epsilon''}{2} \alpha \frac{\cosh\alpha}{\sinh\alpha} + \frac{2u_{sB}}{l_c} \left( \frac{\alpha \cosh\alpha}{\sinh\alpha} - 1 \right) \quad (4)$$

(c) Extensive cracking ( $w_s > 2s_u$ ):

$$\Delta\epsilon_s = (\tau_{su}/E_s)(l_c/D_s) \quad (5)$$

(d) Prestressing steel contribution:

$$\Delta\epsilon_p = (\tau_p/E_p)(l_c/D_p) \quad (6)$$

where  $D_s$  and  $D_p$  are the diameters of a reinforcing steel bar and of a prestressing tendon, respectively.

Consideration of the strain distributions at sections A and B in Fig. 5 enables the longitudinal displacement in the cracked section to be expressed as [9]:

$$u_{cB}(z) = \int_0^{l_c/2} \epsilon_c(x, z) dx = \epsilon_{cB}(z) l_c/2 \gamma(z) \quad (7)$$

where  $\epsilon_{cB}$  is the concrete strain at a fibre  $z$  of the cracked section and  $\gamma(z)$  is the ratio between the concrete strain and the average deformation, i.e.,  $\gamma(z) = (l_c/2) \epsilon_{cB}(z) / \int_0^{l_c/2} \epsilon_c(x, z) dx$ .

The concrete strain  $\epsilon_{cB}$  may be obtained from (1) and (7):

$$\epsilon_{cB}(z) = \phi z f / l_c \quad (8)$$

where  $\phi/l_c$  is the average compression of the element and  $f = \gamma(z)(z+z_0)/z$  is a parameter related to the strain distribution variation between sections A and B [9]. These distributions also allow the definition of the distance  $z_0$  between the neutral axis and the rotation axis of the cracked section (Fig. 5). The resulting expressions are:

$$f = 2z_A'^2 / (z_A'^2 + z'^2) \quad \text{and} \quad z_0 = z'^2 (z_A' - z') / (z_A'^2 + z'^2) \quad (9)$$

Relation (8) also allows the strain in the compression reinforcement to be expressed as:

$$\epsilon_{sB}' = (\phi/l_c)(z' - d_s') f \quad (10)$$

## 2.4 Equilibrium Equations

Expressing the strain equations (7), (8) and (10) as functions of the average curvature  $\bar{\phi} = \phi/\ell_c$  through relations (1), and adopting the appropriate  $\sigma - \epsilon$  constitutive laws for concrete and steels (Section 2.2), the equilibrium equations and  $M - \bar{\phi}$  constitutive law may be formulated.

The equilibrium equations, referred to the centroid of the gross cross section, are:

$$N = \int_0^{z'} \sigma_{CB}^+ b dz + A_s \sigma_{sB}^+ + \int_{-z''}^0 \sigma_{CB}^- b dz + \int_{-(h-z')}^{-z''} \sigma_{CB}^-(w) b dz - A_s \sigma_{sB} - A_p \sigma_{pB} \quad (11)$$

$$M = \int_0^{z'} \sigma_{CB}^+ [z + (y_G - z')] b dz + A_s \sigma_{sB}^+ [y_G - d_s'] + \int_{-z''}^0 \sigma_{CB}^- [z + (y_G - z')] b dz + \int_{-(h-z')}^{-z''} \sigma_{CB}^-(w) [z + (y_G - z')] b dz + A_s \sigma_{sB} [d_s - y_G] + A_p \sigma_{pB} [d_p - y_G] \quad (12)$$

In equations (11) and (12)  $b = b(z)$ ,  $\epsilon = \epsilon(z)$ ,  $\sigma = \sigma(\epsilon)$  and  $w = w(z)$ ; the term in  $w$  is due to the constitutive law adopted for the concrete in tension, based on experimental results reported in [20]. Further tests in progress at Politecnico di Milano, Milano, Italy, seem to confirm this law and the values of related constants [10].

Finally, the crack width may be expressed as:

$$w(z) = w_s(z - z'') / (d_s - z' - z'') \quad (13)$$

where the crack width at the reinforcing steel level is:

$$w_s = [(\phi/\ell_c)(d_s - z' - z_0) - \epsilon_{sA}(1 - \ell_s/\ell_c) - \epsilon_{sB}\ell_s/\ell_c] \ell_c \quad (14)$$

We note that the adopted constitutive law for concrete in tension, Fig. 2a, is appropriate for predicting the overall behaviour of cracked sections, but is not suitable for the accurate investigation of the local response around the crack tip.

## 2.5 Computational Features

A general computer program, MOCURO (MOment-CURvature-ROtation) has been developed in order to automatically handle the governing conditions of section response at all loading states. Any symmetrical concrete section with up to fifteen layers of mild and/or prestressing steel, under either positive or negative bending, may be analyzed. The program accepts any experimental, analytical or assumed point-by-point constitutive laws.

Each point of the  $M - \bar{\phi}$  constitutive law is determined by imposing the curvature and solving the equilibrium equation (11) by an iterative procedure. During the phase of partial slip, the length  $\ell_s$  is imposed and the curvature is given by equation (3').

## 3. PARAMETRIC STUDY

### 3.1 Governing Parameters

A parametric study has been conducted in order to ascertain the influence of the basic parameters that govern the  $M - \bar{\phi}$  constitutive law.

Material characteristics have been assumed constant throughout the study and their influence on the  $M - \bar{\phi}$  relation has not been investigated.



By reference to material laws and definitions in Figs. 2, 3 and 4, the numerical constants used in computations are identified in Table 1.

Table 1

CONCRETE COMPRESSION		$f'_c = 40 \text{ MPa}$ $E_c = 29930 \text{ MPa}$	$\epsilon_o = 0.00264$ $A \approx 2.5$	$0 \approx 0.362$ [1] $k = 0.8$
CONCRETE TENSION		$f_{cr} = 4.5 \text{ MPa}$	$c_2 = 2$ $c_1 / \epsilon_c = 12000$	[10]
MILD STEEL		$f_{sy} = 400 \text{ MPa}$ $E_s = 200000 \text{ MPa}$	$f_{su} = 600 \text{ MPa}$ $\epsilon_{su} = 7\%$	[22]; $\epsilon_{sh} = 1\%$ [21] $E_{sh} = 6500 \text{ MPa}$
MILD STEEL BOND		$\tau_o = 3 \text{ MPa}$	$\tau_{su} = 10 \text{ MPa}$ $s_u = 0.5 \text{ mm}$	[18]
PRESTRESSING STEEL		$f_{pop} = 1300 \text{ MPa}$ $E_r = 190000 \text{ MPa}$ [STELCO]	$f_{p1} = 1580 \text{ MPa}$ , $\epsilon_p = 1\%$ [22]; $f_{pu} = 1860 \text{ MPa}$ , $\epsilon_{pu} = 3.5\%$	$f'_p = 17.40 \text{ MPa}$ $\epsilon'_p = 1.9\%$
PRESTRESSING STEEL BOND		$\tau_p = 4 \text{ MPa}$ [23]		

Major parameters are related to the problem geometry and include (1) the net reinforcement index,  $\omega$ ; (2) the mixed reinforcement index,  $\gamma$ ; (3) the degree of prestressing,  $\kappa$ ; (4) the lateral steel percentage,  $\rho$ ; (5) the crack spacing,  $\ell_c$ ; and (6) the section shape.

Parameters  $\omega$  and  $\gamma$  essentially reflect the ultimate flexural behaviour of concrete sections [4] and are redefined accordingly as follows:

$$\omega = (A_s f_{su} + A_p f_{pu} - A_s f_{su}) / (b d f'_c) \quad (15)$$

$$\gamma = (A_p f_{pu}) / (A_p f_{pu} + A_s f_{su}) \quad (16)$$

These definitions ensure that the ultimate moments of R.C. and P.C. sections with the same  $\omega$  are identical; if strain-hardening of the reinforcing steel is negligible, definitions (15) and (16) coincide with those given in [4].

Parameter  $\bar{\kappa}$  is defined as [4]:

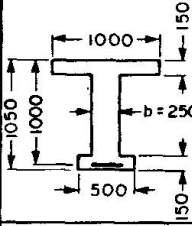
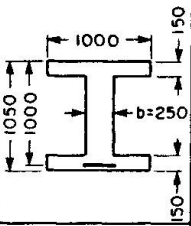
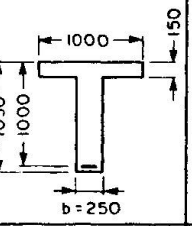
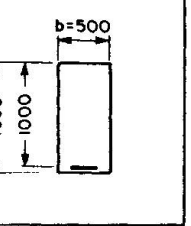
$$\bar{\kappa} = f_{pe} / f_{pa} \quad (17)$$

where  $f_{pe}$  and  $f_{pa}$  are the effective and maximum allowable prestressing stresses, respectively.

### 3.2 Numerical Simulation Program

A set of 24 numerical tests on four section shapes, identified as A, B, C and D in Table 2, has been performed in order to study the influence of the aforementioned geometric parameters. The stirrups area and spacing, as well as the degree of prestressing  $\kappa$  ( $\kappa = 1$ ), have been assumed constant in all the tests. For sections A and C both positive and negative moments have been considered. In all cases studied the yielding point is assumed to correspond to  $\epsilon_s = \epsilon_{sy} = 0.2\%$  or  $\Delta \epsilon_p = \epsilon_{sp} = 0.2\%$ .

Table 2

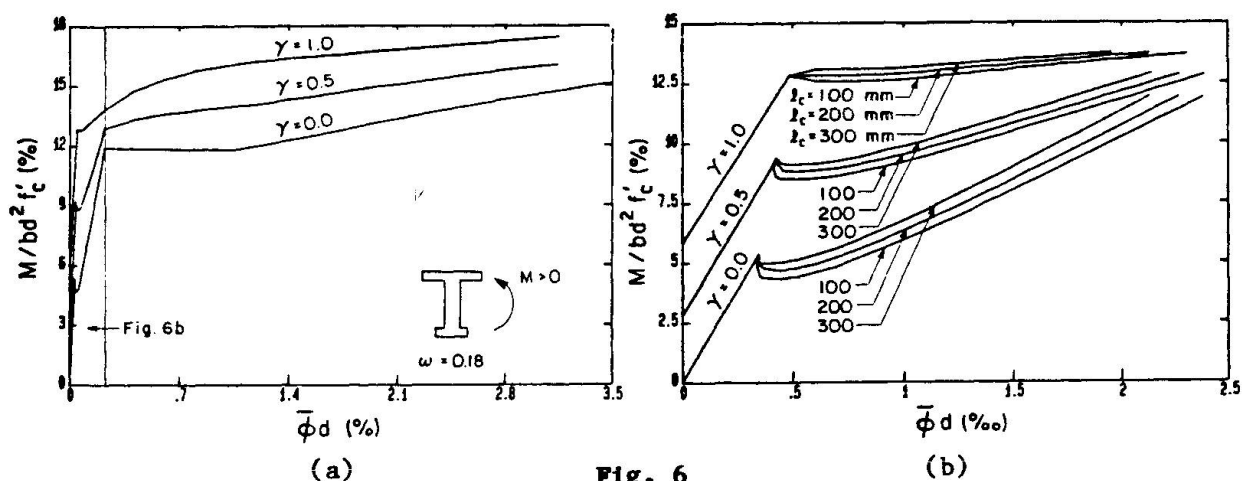
$\bar{k} = 1$			SECTION A	SECTION B	SECTION C	SECTION D
$\omega$	$\gamma$	$l_c$				
0.12	0.5	200	•	•	•	•
0.18	0.0	100	•			
		200	•			
		300	•			
	0.5	100	•			
		200	•	•	•	•
		300	•			
	1.0	100	•			
		200	•			
		300	•			
0.24	0.5	200	•	•	•	•
0.30	0.5	200	•	•	•	•

STIRRUPS #10 AT 300 mm IN ALL CASES

### 3.3 Influence of $\gamma$ and $l_c$ on the $M - \bar{\phi}$ Constitutive Law

The influence of parameters  $\gamma$  and  $l_c$  for Section A and  $\omega = 0.18$  is shown in the diagrams of Fig. 6. The basic differences in the behaviour of R.C. ( $\gamma = 0$ ), P.P.C. ( $\gamma = 0.5$ ) and P.C. sections may be summarized as follows:

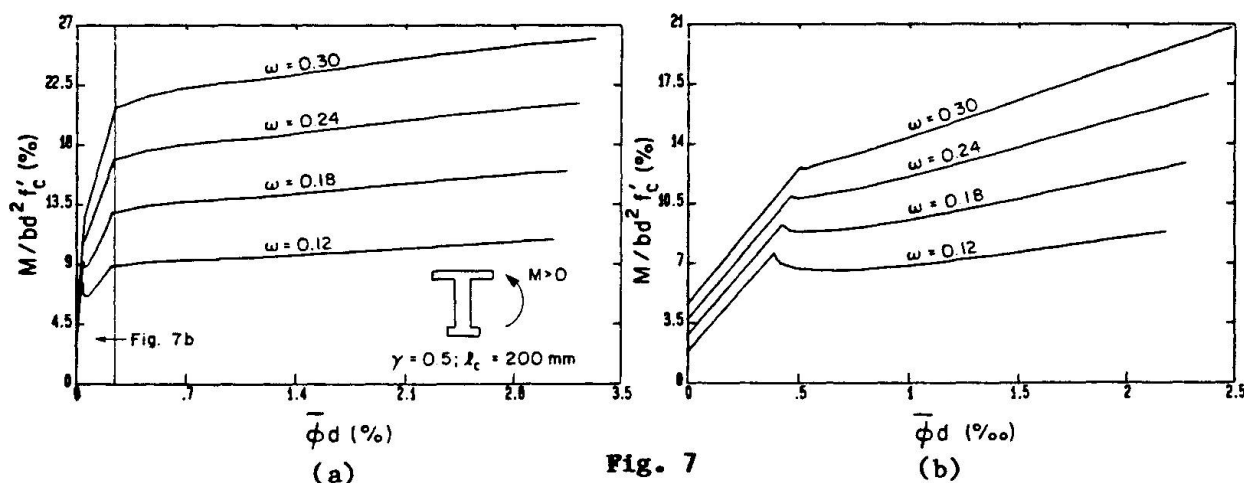
- the stiffness of the first state is practically constant, but the cracking moment and curvature increase with the amount of prestressing;
- the transition from the first to the second state is characterized by a sudden drop of the moment, which is larger for small  $\gamma$  values;
- for the second state, section stiffnesses decrease with higher  $\gamma$  values;
- increases of the crack spacings  $l_c$  correspond to smaller moment drops at the onset of cracking and to increases of the tension stiffening effects;
- for the R.C. section ( $\gamma = 0$ ), the transition from the second to the third state takes place at  $\epsilon_s = \epsilon_{sy} = 0.2\%$ , and is sharper than for the P.P.C. or P.C. sections ( $\gamma > 0$ ); for the P.C. section the transition point is no longer well defined;
- the third state is essentially characterized by the strain hardening of the section, with a more pronounced initial yield plateau for the R.C. section ( $\gamma = 0$ );
- for the P.C. and R.C. sections, the ultimate moments are the same; for the P.P.C. section with the same  $\omega$ , the ultimate moment is smaller because, as the prestressing still governs the behaviour, the mild steel reinforcement cannot develop its ultimate strength;
- the ultimate curvature is much larger for the R.C. than for the P.C. and P.P.C. sections because of the correspondingly higher maximum strain of the mild steel;
- as expected, the crack spacing  $l_c$  has only a negligible influence on the third state.



### 3.4 Influence of $\omega$ on the $M - \bar{\phi}$ Constitutive Law

The influence of  $\omega$  for Section A, with  $\gamma = 0.5$ , may be seen from Fig. 7:

- the stiffness of the first state is practically constant, while the cracking moment and curvature increase with  $\omega$ ;
- the drop of the moments at the onset of cracking increases for decreasing  $\omega$  values;
- the stiffnesses of the second state increase with  $\omega$ ; for the lower  $\omega$  value investigated ( $\omega = 0.12$ ) after the moment drop, the cracking moment value is again reached only for a curvature equal to more than three times the cracking curvature;
- the yielding moments and curvatures increase with  $\omega$ ;
- the stiffness in the third state are practically independent of  $\omega$ , while the ultimate moments and curvatures increase with  $\omega$ .



### 3.5 Influence of the Section Shape on the $M - \bar{\phi}$ Constitutive Law

The influence of the section shape when  $\omega = 0.18$  and  $\gamma = 0.5$  may be seen from Fig. 8:

- the stiffnesses in the first state and the cracking moment and curvature values are strongly affected by the section shape;
- sections with a flange in tension exhibit the highest moment drops at the onset of cracking because of the correspondingly largest losses of inertia; no discontinuities are noted for the rectangular and T sections under positive moments;



- for I sections the moment drop in the second state is as high as 15%, and the cracking moment value is again reached only at a curvature of about 3.5 times the cracking curvature;
- the slope of the curves in the second state is practically independent of the section shape, as it essentially depends on  $\omega$ ;
- the stiffnesses at the third state are also practically constant;
- sections with compression flanges exhibit higher ultimate moments and curvatures than the rectangular section and the T section under negative moment;
- the behaviour at the advanced second and third states is governed by flange-to-web-width ratios: a similar behaviour is noted for the T and I sections under positive moment (identical  $b_f/b_w$ ), and for the rectangular and T section under negative moment; the non-symmetric I section under negative moment exhibits an intermediate behaviour.

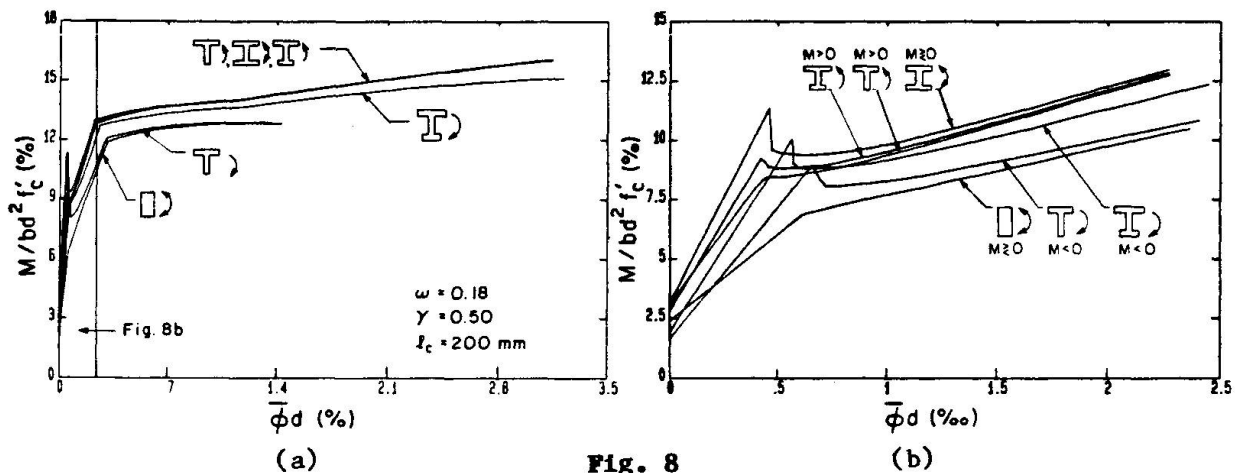


Fig. 8

### 3.6 Ductility Factor $\bar{\phi}_u/\bar{\phi}_y$

The following remarks are made with reference to Fig. 9:

- for the wide-flanged sections, the ductility factor is practically independent of  $\omega$  and has a value of about 14;
- the rectangular and T section under negative moment exhibit the lowest ductility, which is strongly affected by  $\omega$  values;
- ductility factors of non-symmetrical I sections under negative moment assume intermediate values to the above cases;
- it is noted from Fig. 6 that ductility factors are reduced by increases of  $\gamma$  value and are almost independent of the crack spacings  $l_c$ .

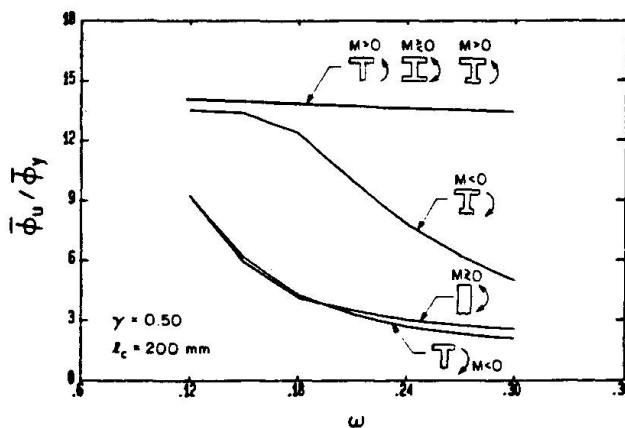


Fig. 9



## 4. CONSTITUTIVE LAW AND BEHAVIOUR OF STRUCTURAL CONCRETE

### 4.1 R.C. versus P.P.C. and P.C.

The basic differences between R.C., P.P.C. and P.C. sections can be summarized as follows:

- P.P.C. and P.C. sections are characterized by an increasingly higher cracking resistance;
- R.C. and P.C. sections can reach the same ultimate moment, whereas the same moment cannot be reached by P.P.C. sections (Section 3.3);
- R.C. sections are more ductile than P.P.C. and P.C. sections.

### 4.2 State I

- The behaviour is basically linearly elastic up to cracking. The cracking resistance increases, while the elastic stiffness slightly decreases, with increasing amounts of prestressing. This trend is noted for all section shapes.
- For high  $\omega$  values, the real transition from the first to the second state occurs for moments slightly higher than the cracking moment, because of the resistance of the reinforcement to crack opening.
- For nonlinear analysis purposes, a perfectly elastic model up to the first cracking (neglecting the slight nonlinearity and the effective value of the transition moment) can be adopted without introducing appreciable errors and loss of generality or consistency.

### 4.3 State II

- The transition from the first to the second state is characterized by a sudden moment drop of up to 15% for I and T sections under negative moment. This drop becomes smaller for higher  $\omega$  and  $\gamma$ , for sections under positive moment, and becomes negligible for rectangular and T sections.
- The stiffnesses at the second state increase with  $\omega$ , decrease for larger  $\gamma$ , and are practically independent of the section shape.
- The tension stiffening effect increases with better bond behaviour of the reinforcement and with the crack spacing.
- Due to the high moment and curvature discontinuity at the onset of cracking and at the early second state, a reliable model for nonlinear analysis must account for the tension stiffening effect and the crack propagation.
- A linear approximation of the second state is valid only for rectangular or T sections under positive moment.

### 4.4 State III

- For R.C. and lightly prestressed P.P.C. sections, the transition from the second to the third state is clearly identified and corresponds to the yielding of the mild steel. For P.C. sections, the transition is characterized by a gradual change of stiffness and a yielding point is no longer clearly identified.
- The third state is characterized by strain-hardening, with the exception of an initial plastic behaviour for R.C. sections.
- R.C. and P.C. sections with the same  $\omega$  may develop the same ultimate moment. In general, P.P.C. sections cannot reach the same moment.
- The ductility is mainly governed by  $\omega$  and by the shape of the section. It is higher for flanged sections and lower for high  $\omega$  values.
- A linear approximation of the third state appears reasonable for P.C. and highly prestressed P.P.C. sections. In the transition zone from the second to the third state, a nonlinear behaviour must be assumed if no arbitrary transition point is chosen.

## 5. CONCLUSIONS

This study has enabled the analytical derivation of the moment-curvature constitutive law for R.C., P.C. and P.P.C. flexural sections under quasi-static loading, starting with the description of stress-strain relations of constitutive materials. Consideration of tension-stiffening effects over elements of variable lengths (equal to the crack openings) allows a better understanding of the section behaviour at and after cracking. Generation of the constitutive law is automatically performed by a computer program (MOCURO) that combines the positive features of similar codes during the first and last behaviour states [10,4]:

- (a) realistic prediction of material response;
- (b) general application to R.C., P.C. and P.P.C.;
- (c) historical, complete description through all loading states.

Parametric studies on the effects of the amount of prestressing, the total reinforcement index, the cross-section shape, and the crack spacing on the flexural response have yielded results within the expected ranges and tend to confirm the reliability of the model.

Further investigations, currently in progress, consist of applying the developed model to the analysis of hyperstatic structures of reinforced, prestressed and partially prestressed concrete. The purpose of these investigations is to achieve the highest possible accuracy for the lumped-plasticity approach to nonlinear analysis [17], and to assess its capabilities with regard to both structural engineering research and practice. Indeed, this approach may help clarify some outstanding problems such as: the hyperstatic effects of prestressing, moment redistribution in the cracked range, realistic stiffness evaluation at service and inelastic moment redistribution. Also, a relatively simple, automated code, that uses standard-type input and predicts the complete nonlinear response, may become a valuable tool for structural concrete designers.

## ACKNOWLEDGEMENTS

The financial support of the Natural Sciences and Engineering Research Council (NSERC) of Canada under Grant A4789, and of the NATO Division of Scientific Affairs under Grant 524/83, which made possible the research reported in this paper, is gratefully acknowledged.

## REFERENCES

- [1] Sargin, M., "Stress-Strain Relationships for Concrete and the Analysis of Structural Concrete Sections," SMD Study No. 4, University of Waterloo, Waterloo, Ontario, 1971, 167 pp.
- [2] Sargin, M., Ghosh, S.K. and Cohn, M.Z., "A Computer Program for the Nonlinear Analysis of Reinforced Concrete Sections," SMD Report No. 23, University of Waterloo, Waterloo, Ontario, 1973, 43 pp.
- [3] Cohn, M.Z. and Ghosh, S.K., "Ductility of Reinforced Concrete Sections," IABSE Publications, Vol. 32, No. 2, 1973, pp. 51-81.
- [4] Cohn, M.Z. and Bartlett, M., "Nonlinear Flexural Response of Partially Prestressed Concrete Sections," ASCE Journal of the Structural Division, Vol. 108, No. ST12, 1982, pp. 2747-2765; also SM Paper No. 168, Solid Mechanics Division, University of Waterloo, Waterloo, Ontario, 1981, 55 pp.
- [5] Rao, P.S., "Die Grundlagen zur Berechnung der bei statisch unbestimmten Stahlbetonkonstruktionen im plastischen Bereich auftretenden Umlagerungen der Schnittkräfte," Deutscher Ausschuss für Stahlbeton, Heft 177, W. Ernst & Son, Berlin, 1966.
- [6] Aparicio, A.C. and Arenas, J.J., "Evolution up to Failure of Continuous Prestressed Concrete Bridge Decks," IABSE Acta Periodica, No. 3/81, P-44/81, August 1981.

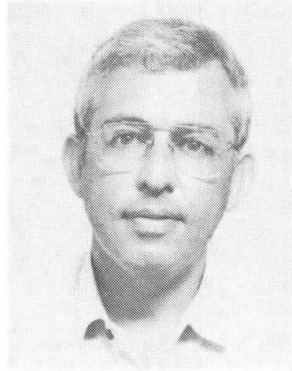


- [7] Aguado, A., Murcia, J. and Mari, A., "Nonlinear Analysis of Concrete Structures by the Imposed Deformations Method. Comparison with Experimental Results," IABSE Colloquium on Advanced Mechanics of Reinforced Concrete, Delft, The Netherlands, 1981, Final Report, IABSE Working Commissions Reports, 1981, pp. 255-262.
- [8] Appleton, J., Camara, J. and Almeida, J.F., "Elastoplastic Analysis and Design of Partially Prestressed Concrete Beams," International Symposium on Nonlinearity and Continuity in Prestressed Concrete, Preliminary Publication, Vol. 2, University of Waterloo, Waterloo, Ontario, 1983, pp. 77-106.
- [9] Giuriani, E., "Le curvature di travi in cemento armato tenso e presso-inflesse nel primo e secondo stadio," Studi e Ricerche, Corso di Perfezionamento per le Costruzioni in Cemento Armato F.lli Pesenti, Politecnico di Milano, Vol. 1, 1979.
- [10] Giuriani, E. and Riva, P., "Effetti della fessurazione sui legami Momenti-curvature delle travi parzialmente precomprese," Studi e Ricerche, Corso di Perfezionamento per le Costruzioni in Cemento Armato F.lli Pesenti, Politecnico di Milano, Vol. 7, 1985.
- [11] Giuriani, E., "Theoretical Analysis of the Early Second Stage in R.C. Beams," CEB - Bulletin d'Information, No. 153, April 1982, pp. 91-116.
- [12] Cohn, M.Z., "Some Problems of Partial Prestressing", Partial Prestressing from Theory to Practice, Proceedings NATO ARW, Paris, France, June 18-22, 1984, Vol. I, Chapter 2, Martinus Nijhoff Publishers, Dordrecht, The Netherlands, 1986, pp. 15-66.
- [13] Cohn, M.Z., "Continuity in Prestressed Concrete", Partial Prestressing from Theory to Practice, Proceedings NATO ARW, Paris, France, June 18-22, 1984, Vol. I, Chapter 8, Martinus Nijhoff Publishers, Dordrecht, The Netherlands, 1986, pp. 189-256.
- [14] Cohn, M.Z. and Franchi, A., "STRUPL: A Computer System for Structural Plasticity," J. of the Structural Division, ASCE, Vol. 105, No. ST4, April 1979, pp. 789-804.
- [15] Cohn, M.A., Erbatur, F. and Franchi, A., "STRUPL: User's Manual," University of Waterloo Press, Waterloo, Canada, 1981, 231 p.
- [16] Cohn, M.Z., Erbatur, F. and Bhat, P.D., "Computer Analysis of Reinforced Concrete Structures," ACI Journal, Vol. 64, No. 1, February 1983, pp. 28-32.
- [17] Cohn, M.Z. and Krzywiecki, W., "Nonlinear Analysis System for Concrete Structures: STRUPL-1C," Engineering Structures, 1987 (to appear).
- [18] Giuriani, E., "Experimental Investigation on the Bond-Slip Law of Deformed Bars in Concrete," IABSE Colloquium on Advanced Mechanics of Reinforced Concrete, Final Report, Delft, 1981, pp. 121-142.
- [19] Giuriani, E., "On the Effective Axial Stiffness of a Bar in Cracked Concrete," Bond in Concrete, ed. Bartos, Applied Science Publishers, London, 1982, pp. 107-126.
- [20] Giuriani, E. and Rosati, G., "Ricerca sperimentale su elementi di c.a. soggetti ad una singola fessura. Studio dei rami instabili e del legame momenti-curvature," Studi e Ricerche, Corso di Perfezionamento per le Costruzioni in Cemento Armato F.lli Pesenti, Politecnico di Milano, Vol. 6, 1984.
- [21] Kelly, P.F., "Flexural Stiffeners Considerations in Reinforced Concrete Buildings," M.A.Sc. Thesis, University of Waterloo, Waterloo, Ontario, Canada, 1986.
- [22] ASTM Specifications, A416, A615-76a.
- [23] Vos, E. and Reinhardt, H.W., "Influence of Loading Rate on Bond Behaviour of Reinforcing Steel and Prestressing Strands," Matériaux et Constructions, Vol. 15, No. 85, 1982.

## **Focal Points Model for Uniaxial Cyclic Behaviour of Concrete**

Modèle des points focaux pour le comportement du béton sous charge cyclique uniaxiale  
Brennpunktmodell für das einachsige zyklische Verhalten von Beton

**David Z.  
YANKELEVSKY**  
Senior Lecturer  
Technion  
Haifa, Israel



David Z. Yankelevsky joined the faculty at Technion in 1976, following a period of seven years in professional practice. He received his D.Sc. in 1979 from Technion. His research interests include nonlinear behaviour of R.C., earthquake response, impact response of structures and soil-structure interaction.



**Hans W. REINHARDT**  
Professor  
Darmstadt Univ. of  
Technology  
Darmstadt, FRG

Hans W. Reinhardt graduated from Stuttgart University in 1964. After research and teaching activities in Stuttgart and Chicago, he joined Delft University in 1975 where he has been head of the concrete section of the Stevin laboratory. In 1986 he accepted a position at Darmstadt University. Main research areas are impact behaviour of concrete, testing methods in structural engineering, modelling of cementitious materials, and demountable concrete structures.

### **SUMMARY**

A new one-dimensional model for random cyclic compression and tension in plain concrete is developed. The model determines several geometrical loci in the uniaxial stress-strain plane that govern the unloading-reloading curves in the softening range. The model allows the prediction of unloading-reloading curves by simple graphical means without further calculations.

### **RÉSUMÉ**

Un modèle nouveau est développé pour des cas de charges aléatoires répétés à la compression et tension du béton non armé. À l'aide du modèle, quelques lieux géométriques sont déterminés dans le plan des contraintes et déformations uniaxiales qui servent à la construction des courbes de déchargement et rechargement dans la région de dégradation. Le modèle permet la prédiction simple de courbes de déchargement et rechargement avec des moyens graphiques et sans calcul supplémentaire.

### **ZUSAMMENFASSUNG**

Ein neues eindimensionales Modell für willkürliche wiederholte Druck- und Zugbelastungen von unbeehrtem Beton wurde entwickelt. Mit Hilfe des Modells werden einige geometrische Orte in der einachsigen Spannungsdehnungsebene bestimmt, die zur Konstruktion der Entlastungs-Wiederbelastungskurven im Entfestigungsbereich dienen. Das Modell erlaubt somit die einfache Vorhersage von Entlastungs-Wiederbelastungskurven mit graphischen Mitteln ohne weiteren Rechenaufwand.



## 1. INTRODUCTION

An unconfined concrete element which is subjected to random cyclic uniaxial compression or tension loading is considered. Quite a large variety of models are available for compressive loading, being based on the theory of elasticity [e.g. 5,7,9,13], theory of plasticity [e.g. 6,7,18], plastic fracturing approach [e.g. 2] and the endochronic theory of plasticity [e.g. 3]. There also exist simplified models some of which are mathematical descriptions of test results e.g. [9,12,17].

Considerably less effort has been given to model the relatively new experimental results of tensile loading [e.g. 11,14,15,16,20]. Most of the models propose a description for the envelope curve and only a few introduce a simplified formulation for the unloading-reloading cycle [10,16,20].

Examination of many test results on concrete samples subjected to monotonic and especially cyclic loading, both in compression and in tension, has clearly shown that there exist some common geometrical properties in the uniaxial strain plain. Several fixed points are determined, and denoted as focal points, with aid of which the complete loading-unloading history may be reproduced. The approach has been examined with respect to many test data and shows very good agreement. It may be formulated as a material law and be implemented in a computer code. The geometrical interpretation yields a further advantage that the cyclic loading-unloading history may be reproduced graphically without any computations.

## 2. EXPERIMENTAL STRESS-STRAIN CURVES

### 2.1 Compressive Loading

The monotonic stress-strain curve shows linear behaviour up to about 30 % of the strength  $f_c$ , and nonlinear behaviour at higher stresses. Concrete softens until a peak stress is reached at a strain  $\epsilon_0$  as a result of microcracks propagation. At larger strains a descending part of the stress-strain curve is observed.

The envelope curves for different cyclic loading histories have been found to fit, with a reasonably small scatter, with the monotonic curve. The unloading curve from that envelope gradually softens with continuing unloading and changes in strain are more pronounced at low stress levels. The reloading curve reverses curvature during increasing stresses and intersects with the unloading curve at the "common point limit" [12]. Cycling within a certain bounding loop lowers down the common point and within several cycles it stabilizes at the lower "stability limit". Starting unloading at larger strains shows smaller stiffnesses and larger strain changes.

### 2.2 Tensile Loading

The concrete sample behaviour under tensile loading is usually expressed in a stress vs. displacement relationship. The displacement is the total elongation of the microcracked zone, as measured by extensometers of certain length. The monotonic stress-displacement curve in tension behaves linearly up to about 80 % of the tensile strength  $f_t$ , with a tangent modulus of elasticity similar to that in compression. At higher stresses concrete softens considerably until the tensile strength  $f_t$  is reached at a displacement  $\delta_0$ . At larger displacements a wide softening range is observed, which is characterized by a descending branch.



Only a limited amount of test data has been reported in literature on deformation controlled tensile tests in general and on cyclic tests in particular. The work that has been carried out at the Stevin laboratory [8,14,15] has covered various load histories through which stresses during unloading varied between the envelope to either low tensile stress level, low compression or higher compression, as may be seen in Fig. 1. For all load histories the envelopes were found to be similar to the monotonic curve in tension, and a unique envelope curve may be assumed.

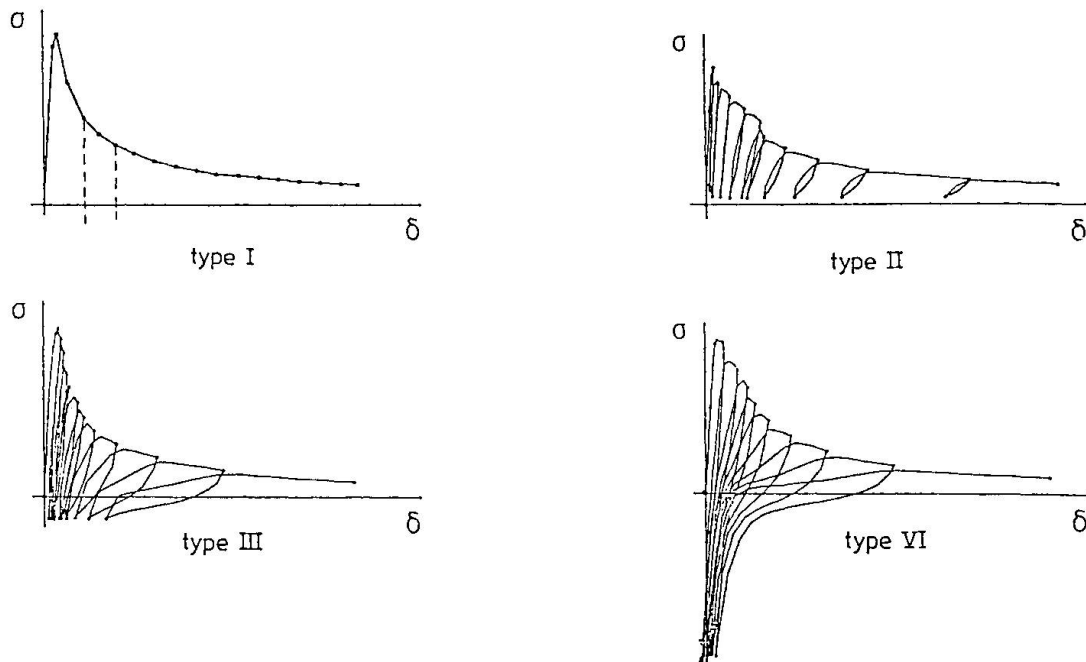


Fig. 1: Experimental Load Histories in Cyclic Tension.

During unloading the curve softens and around a zero stress level stiffness becomes very small and large displacements are involved. When the compressive stress increases, at further unloading, the curve stiffens up again (see Fig.1).

### 3. THE FOCAL POINTS MODEL

#### 3.1 Model Concept

The cyclic stress-strain or stress-displacement curves, both in compression and in tension, exhibit a decreasing stiffness with unloading. The curve softens considerably when stresses drop close to zero and large plastic strains are developed. If unloading starts at a larger strain, the softening will be more pronounced. That trend resembles to rays originated at a low stress and strain level, on which lie those unloading curves. A similar observation relates to the reloading curves.

The model defines several geometrical loci in the uniaxial stress-strain or stress-displacement plane. These points are defined as "focal points" [19,20]. The focal points coordinates are independent on a specific cycle and are given as functions of the envelope parameters.





### 3.2 Model Rules for Compressive Loading

To obtain any cycle in compression, six focal points C1-C6 are defined (Fig. 2). Five of them are placed along the tangent to the envelope curve at the origin, and the sixth is placed on the strain axis.

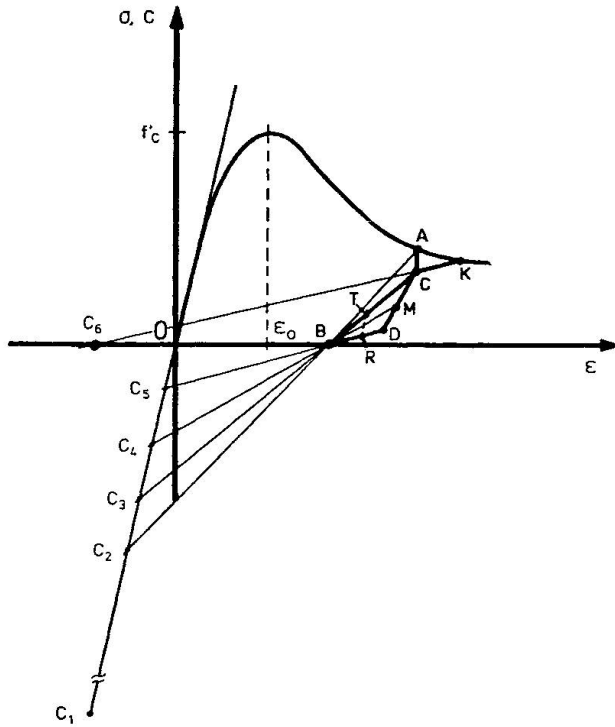


Fig. 2: Focal Point Model for Cyclic Compression

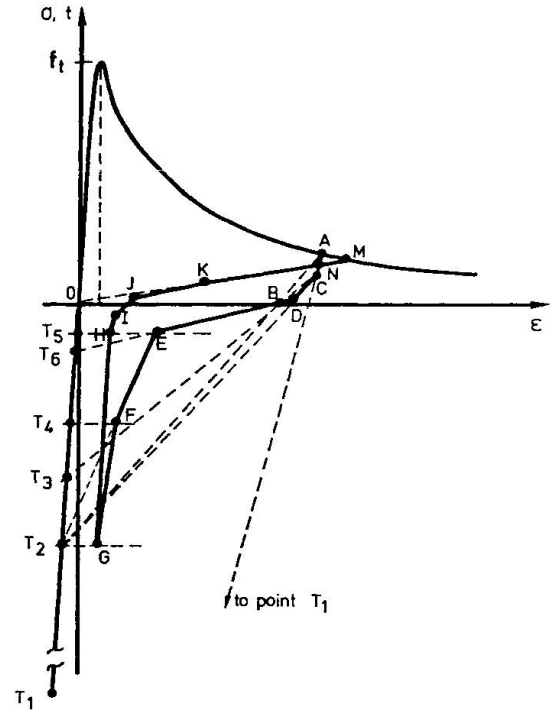


Fig. 3: Focal Point Model for Cyclic Tension

The focal points stress coordinates are expressed as function of the uniaxial compression strength (negative stresses mean compression):

$$\begin{aligned} c_1 &= 3 \cdot f'_c & c_4 &= 0.47 \cdot f'_c \\ c_2 &= f'_c & c_5 &= 0.2 \cdot f'_c \\ c_3 &= 0.75 \cdot f'_c & c_6 &= 0.0; \epsilon_{C6} = -\epsilon_0 \end{aligned}$$

The unloading curve, starting from point A on the envelope, is idealized by the piecewise linear curve A-C-D-B (Fig.2). Point B is the intersection of the line connecting point A and focal point C<sub>2</sub>. Line A-C is parallel to the stress axis, and point C is obtained by the intersection of this line with the line connecting focal point C<sub>3</sub> and point B. Point D is the intersection of lines C-C<sub>1</sub> and C-B.

The reloading curve is idealized by B-C-K. Point K is the intersection of line C-C<sub>6</sub> with the envelope.

Point C is the common point and point M, which is the intersection of C<sub>4</sub>-B with C-D, is the stability limit.

### 3.3 Model Rules For Tensile Loading

An average tensile strain is defined as the tensile elongation per unit gage length, and the experimental stress-displacement curve may be transformed into a stress-strain curve in tension. In this coordinate system any cycle may be obtained with aid of seven focal points: point O (the coordinate origin), points  $T_1$ - $T_5$ , which are placed along the tangent to the envelope curve at the origin, and point  $T_6$ , the coordinates of which depend on the strain at which unloading starts (Fig. 3).

All focal points, except for focal points  $T_6$ , are fixed in the stress-strain coordinate system and independent on a certain cycle. Their stress coordinates are expressed as function of the uniaxial tensile strength  $f_t$  (negative stress means compression):

$$\begin{aligned} t_0 &= 0.0 & t_3 &= -0.75*f_t \\ t_1 &= -3*f_t & t_4 &= -0.5*f_t \\ t_2 &= -f_t & t_5 &= -0.125*f_t \end{aligned}$$

The coordinates of focal point  $T_6$  are  $T_6 [\epsilon_A/2, -0.075*f_t]$ , where  $\epsilon_A$  is the strain at point A on the envelope, at which unloading starts.

The unloading curve in tension, which starts at point A on the envelope, is idealized by the piecewise linear curve A-C-D-B and continues in the compression range along the curve B-E-F-G. Point B is the intersection with the strain axis of line A- $T_2$ . Point C is the intersection of lines  $T_1$ -A and  $T_3$ -B. Point D is the intersection of lines  $T_2$ -C and  $T_6$ -B. Point E has the stress level as focal point  $T_5$ . Point F has the stress level of focal point  $T_4$  and is placed along  $T_2$ -E. Point G lies along  $T_1$ -F and has the stress level of focal point  $T_2$ .

Reloading will follow the elastic stiffness (slope O- $T_1$ ) as long as unloading has not reached the stress level of focal point  $T_5$  (line G-H in Fig. 3).

If reloading starts at point G, the reloading curve will be idealized by the piecewise linear curve G-H-I-J-K-M. The segment I-J is parallel and equal in length with segment C-D. Segment J-K is parallel to D-E where point K lies on O-N. Point N lies on A-C and its stress level is 85% of the stress at point A. Line O-N intersects with the envelope at M. If reloading starts at a lower compressive stress than  $-f_t$ , then that point on the unloading curve will be denoted H.

## 4. COMPARISONS WITH TEST RESULTS

At the present stage, the model assumes a given envelope, which coincides with the monotonic curve. The cycle starts from and returns to the given envelope. Once the envelope is known to coincide with the experimental one, comparisons may be made between experimental cycles and the focal point model cycles.

### 4.1 Tests of Cyclic Compression

The focal points model has been compared with various test results in which the sample is loaded in uniaxial cyclic compression. Fig. 4 shows comparison with a test performed by Karsan & Jirsa [12], and Fig. 5 compares the model prediction with test results of Okamoto [1]. In these figures the predictions have been obtained graphically and good correspondence is obtained.



More comparisons of the focal points model with characteristics of the cyclic behavior in compression have been made [19]. The model predictions of the common point limit, the stability limit, the residual plastic strain and the point at which the reloading curve meets with the envelope, have been compared with both various test data and empirical expressions. Those comparisons show very good agreement.

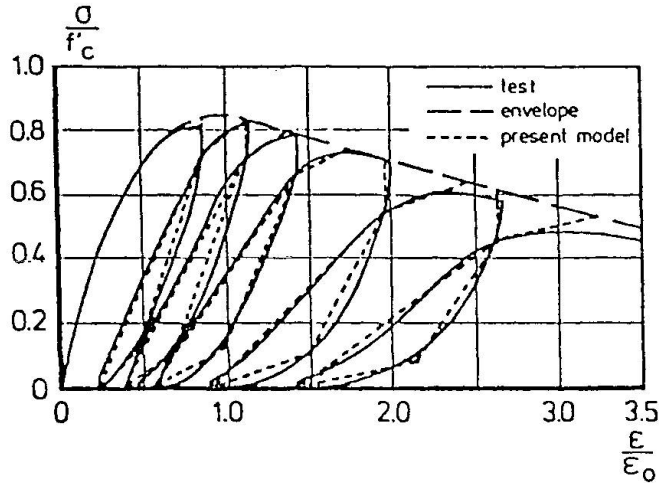


Fig. 4: Comparison with Test Results by Karsan & Jirsa [12]

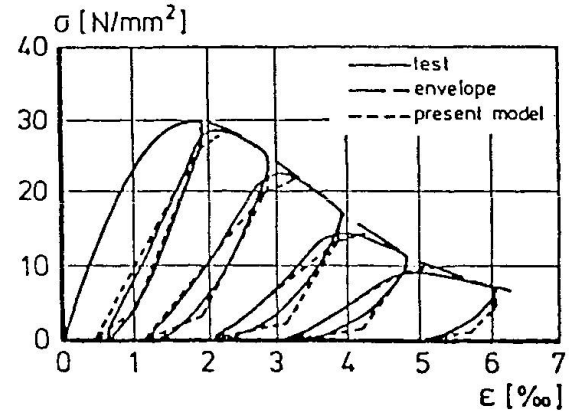


Fig. 5: Comparison with Test Results by Okamoto [1]

#### 4.2 Tests of Cyclic Tension

Comparisons of the focal point model with test results obtained at the Stevin Laboratory, Delft University of Technology, are shown in Fig. 6-7. Fig. 6 shows the cyclic tensile tests in which unloading goes to slight compression and Fig. 7 shows the cyclic tensile tests, in which unloading reaches a compression level that is equal to the tensile strength  $f_t$ . The focal point model cycles are found to be in good agreement with the measured cycles, although their shape is rather complex. The predicted cycles may be obtained either graphically or through a mathematical subroutine which follows the model rules. More comparisons appear in [20] and all of them show good correspondence with test results.

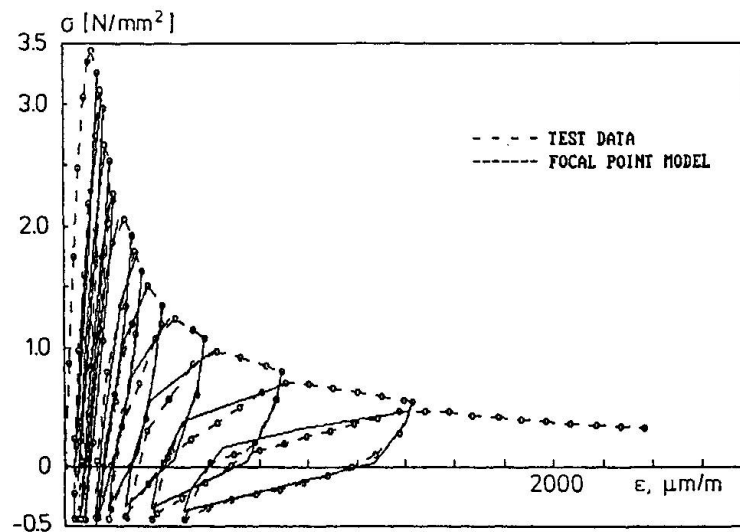


Fig. 6: Comparison with Tensile Cyclic Tests Type III

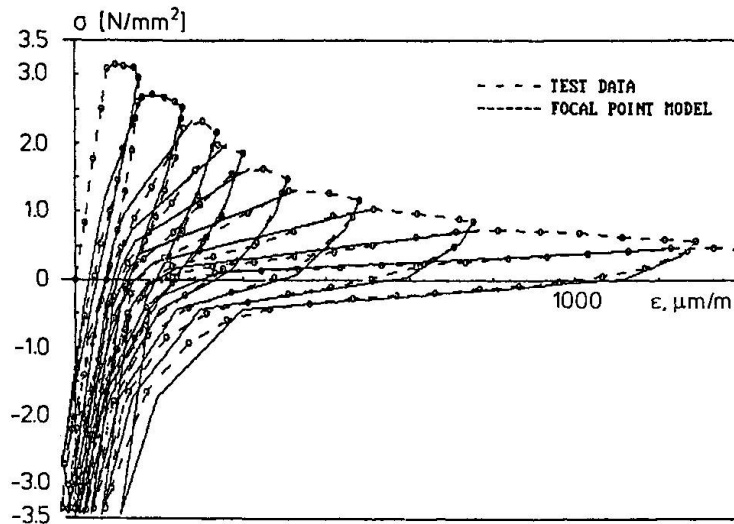


Fig. 7: Comparison with Tensile Cyclic Tests Type IV

## 5. SUMMARY AND CONCLUSIONS

A new one-dimensional model for random cyclic compression and tension is proposed. The model provides a set of rules to follow the cyclic uniaxial response of concrete once the envelope curves are given. The model determines a set of focal points with aid of which the complete piecewise linear unloading-reloading cycle, starting at a given point on the envelope, may be reproduced. The focal point model may be used graphically, with no accompanied calculations, or mathematically, following a subroutine in which the model rules are implemented.

The model has been compared with a variety of test results, in compression, in tension and in tension unloaded to compression and it is found to compare well with those tests. The model enables a more realistic representation of the complex behaviour of concrete in compression-tension and might be implemented in computer codes.

## REFERENCES

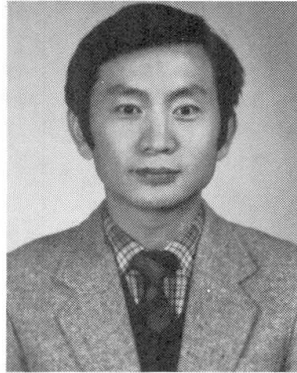
1. AOYAMA, H. and NOGUCHI, H., "Mechanical Properties of Concrete Under Load Cycles Idealizing Seismic Actions". State of the Art Report, AICAP-CEB Symposium on Structural Concrete Under Seismic Actions, Rome, May 1979
2. BAZANT, Z.P., and KIM, S.S., "Plastic Fracturing Theory for Concrete", Journal of the Engineering Mechanics Division, ASCE, Vol.105, No.EM3, June 1979, pp. 407-428.
3. BAZANT, Z.P., and BHAT, P., "Endochronic Theory of Inelasticity and Failure of Concrete", Journal of the Engineering Mechanics Division, ASCE, Vol. 102, No. EM4, April 1976, pp. 701-722.



4. BAZANT, Z.P., and CEDOLIN, L., "Blunt Crack Band Propagation in Finite Element Analysis", ASCE, Journal of the Engineering Mechanics Division, Vol. 105, No. EM2, April 1979, pp. 297-315.
5. CEDOLIN, L., CRUTZEN, Y.R.J., and DEI POLI, S., "Triaxial Stress-Strain Relationship for Concrete", Journal of the Engineering Mechanics Division, ASCE, Vol. 103, No. EM3, June 1977, pp.423-439.
6. CHEN, W.F., "Plasticity in Reinforced Concrete", McGraw-Hill Book Company, New-York, 1981
7. CHEN, W.F., and SALEEB, A.F., "Constitutive Equations for Engineering Materials", Vol. 1-"Elasticity and Modelling", Vol. 2-"Plasticity in Reinforced Concrete", McGraw-Hill Book Company, New-York, 1981
8. CORNELISSEN, H.A.W., HORDIJK D.A., and REINHARDT, H.W., "Experiments and Theory for the Application of Fracture Mechanics to Normal and Lightweight Concrete", Proc. Int.Conf. on Fracture Mechanics of Concrete F.H. Wittmann-Editor, Elsevier, Amsterdam 1985.
9. DARWIN, D., and PECKNOLD, D.A., "Nonlinear Biaxial Stress-Strain Law for Concrete", Journal of the Engineering Mechanics Division, ASCE, Vol. 103, No. EM2, Apr. 1977, pp . 229-241
10. GOPALARATNAM, V.S., and SHAH, S.P., "Softening Response of Plain Concrete In Direct Tension". Journal of the American Concrete Institute Vol.82, No. 3,May 1986, pp. 310-323
11. HILLERBORG, A., "Numerical Methods to Simulate Softening and Fracture of Concrete", Fracture Mechanics of Concrete, G.C. Sih and A. Ditomasso-Editors, Martinus Nijhoff Publishers, The Hague, 1985.
12. KARSAN, I.K., and JIRSA, J.O., "Behaviour of Concrete Under Compressive Loadings", Journal of the Structural Division, ASCE, Vol. 95 No. ST 12, Dec. 1969, pp. 2543-2563
13. OTTOSEN, N.S., "Constitutive Model for Short Time Loading Concrete", Journal of the Engineering Mechanics Division, ASCE, Vol. 105, No. EM1, Feb.1979, pp. 127-141.
14. REINHARDT, H.W., CORNELISSEN, H.A.W., and HORDIJK, D.A. "Tensile Tests and Failure Analysis of Concrete", Journal of Structural Engineering Division, ASCE, Vol. 112, No. 11, pp.2462-2477
15. REINHARDT, H.W., "Fracture Mechanics of an Elastic Softening Material Like Concrete", HERON, Vol. 29, No. 2, 1984, pp.1-42
16. ROTS, J.G., NAUTA, P., KUSTERS, G.M.A., and BLAAUWENDRAAD, J. "Smeared Crack Approach and Fracture Localization in Concrete", HERON Vol. 30, No. 1, 1985
17. SINHA, B.P., GERSTLE, K.H., and TULIN, L.G., "Stress-Strain Relation for Concrete Under Cyclic Loadings", Journal of the American Concrete Institute, Vol. 61, No. 2, Feb. 1964, pp. 195-211.
18. SUIDAN, M., and SCHNOBRICH, W.C., "Finite Element Analysis of Reinforced Concrete", Journal of the Structural Division, ASCE, Vol. 99 No. ST 10, Oct. 1973, pp. 2109-2122.
19. YANKELEVSKY, D.Z., and REINHARDT, H.W., "Uniaxial Cyclic Behaviour of Concrete in Compression", Journal of the Structural Division, ASCE, Vol.113 (1987), No. 2, pp.228-240
20. YANKELEVSKY, D.Z., and REINHARDT, H.W., "Uniaxial Cyclic Behaviour of Concrete in Tension", Accepted for Publication, J. Struct. Div. ASCE, 1987

**Rate-Dependent Constitutive Theory of Concrete in Tension**  
Théorie constitutive dépendant de ratios pour le béton en traction  
Geschwindigkeitsabhängiges Werkstoffgesetz für Beton unter Zugbelastung

**Byung Hwan OH**  
Assist. Professor  
Seoul National Univ.  
Seoul, Korea



Byung Hwan Oh, born 1950, received his Ph.D. degree in civil engineering at Northwestern University, Evanston, Illinois. His research interests include the nonlinear analysis of concrete structures, inelastic behavior, fracture, cracking, fatigue behavior, bond characteristics, constitutive relations, and structural reliability of structures.

#### SUMMARY

A realistic nonlinear constitutive model which can describe the dynamic tensile behavior of concrete is presented. The model is obtained by generalizing a rate-independent nonlinear tensile stress-strain relation for concrete. The static tensile behavior of concrete is modeled on the basis of the concept of microcrack planes. The affinity and shape transformations are employed to model the effect of strain-rate. The material parameters are characterized in terms of the strain-rate magnitude. The present theory is compared with the dynamic tensile test data available in the literature.

#### RÉSUMÉ

L'article présente un modèle constitutif réaliste et non-linéaire, du comportement dynamique du béton en traction. Le modèle est obtenu en généralisant une relation contrainte-déformation du béton à la traction pour un ratio indépendant non-linéaire. Le comportement statique du béton à la traction est exprimé dans un modèle sur la base du concept de plans de micro-fissures. L'affinité et la transformation de la forme sont utilisées pour modéliser l'effet du ratio de déformation. Les paramètres du matériaux sont caractérisés en termes d'amplitude du ratio de déformation. L'équation proposée permet de prédire l'augmentation de la résistance à la traction suite à l'augmentation du ratio de déformation.

#### ZUSAMMENFASSUNG

Der Beitrag behandelt ein wirklichkeitsnahes nichtlineares Werkstoffgesetz für das Stossverhalten von Beton unter Zugbelastung, wobei der Ansatz von Mikrorissebenen verwendet wird. Affinitäts- und Formtransformationen werden gebraucht um den Einfluss der Dehngeschwindigkeit zu modellieren. Nach einem Vergleich von Theorie und Versuchsergebnissen wird eine Beziehung für den Einfluss der Dehngeschwindigkeit auf die Zugfestigkeit vorgeschlagen.



## 1. INTRODUCTION

The mechanical behavior of concrete under dynamic loads induced from earthquakes, impacts, air blasts, wind gusts, and ocean waves is very complicated. In fact, the stiffness of material may significantly depend on the rate of loading under these conditions. The dynamic behavior of concrete in tension has been studied by Hatano[6], Suaris and Shah[8], Zielinski et al[10], and several other investigators. These outstanding studies have mainly focussed on the experimental aspects of concrete under high rates of tensile loadings.

Recently, Bazant and Oh[1] have developed a model to predict the strain-rate effect of concrete in compression. However, no model of this type exists to describe the dynamic behavior of concrete in tension. The purpose of this paper is, therefore, to propose a realistic model which can describe the dynamic tensile behavior of concrete. The model is obtained by generalizing a rate-independent nonlinear constitutive model for concrete in tension.

## 2. CONSTITUTIVE MODEL FOR STATIC TENSION

To develop a model to predict the dynamic tensile behavior of concrete, it is first necessary to clarify the static tensile behavior. Recently, Bazant and Oh[2, 3] have proposed a rate-independent nonlinear constitutive model which can describe the static tensile behavior of concrete. This model considers that there exist certain weak planes within the material in which the stress relief due to microcracking takes place as a function of the stress and strain on each particular plane. It is then assumed that the orientations of the weak planes are distributed uniformly. The total strain tensor,  $\epsilon_{ij}$ , is considered as a sum of an elastic strain tensor  $\epsilon_{ij}^{el}$  and an inelastic strain tensor,  $e_{ij}$ , in which the latin lower-case subscripts refer to cartesian coordinates  $x_i$  ( $i = 1, 2, 3$ ). The rheological model for this theory is depicted in fig. 1. The theory may be summarized as follows[2].

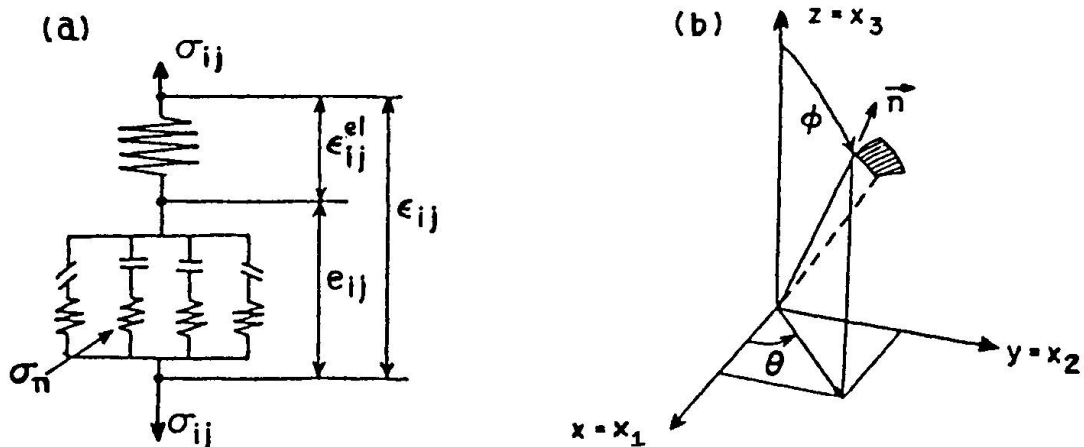


Fig. 1 (a) Rheological Model for concrete  
(b) Spherical coordinate system.

$$d\sigma_{ij} = D_{ijkl} d\epsilon_{kl} \quad (1)$$

in which

$$D_{ijkl} = [C_{ijkl}^{el} + (B_{ijkl})^{-1}]^{-1} \quad (2)$$

$$C_{ijkl}^{el} = \frac{1}{9K} \delta_{ij} \delta_{kl} + \frac{1}{2G} \left( \delta_{ik} \delta_{jl} - \frac{1}{3} \delta_{ij} \delta_{kl} \right) \quad (3)$$



$$B_{ijklm} = \int_0^{2\pi} \int_0^{\pi/2} n_i n_j n_k n_l n_m f'(e_n) \sin\phi d\phi d\theta \quad (4)$$

Here  $\delta_{ij}$  = Kronecker delta,  $K$  = bulk modulus,  $G$  = shear modulus, and  $C_{ijklm}^{el}$  = elastic compliances corresponding to  $\epsilon_{ij}^{el}$ .

The function  $f(e_n)$  of Eq. 4 must be capable of describing the microcracking behavior of concrete. The simple and desirable expressions for this behavior are adopted as [2, 3]

$$\sigma_n = E_n \epsilon_n e^{-(K \epsilon_n^p)} \text{ for } \epsilon_n > 0, \sigma_n = E_n \epsilon_n \text{ for } \epsilon_n \leq 0 \quad (5)$$

Where  $E_n$ ,  $k$ , and  $p$  are material parameters which are functions of concrete strength  $f'_c$ . It was found from this study that the average value of  $E_n = 5,322 \sqrt{f'_c}$ ,  $k = 4.07 \times 10^8 / \sqrt{f'_c}$ , and  $p = 2$ , where  $f'_c$  is given in N/mm<sup>2</sup>. Note here that the expression in Eq. 4 must be evaluated numerically. The numerical integration formulas for this purpose have been developed by the author and described in detail in ref. 4.

### 3. TENSILE STRESS-STRAIN RELATION WITH STRAIN RATE EFFECT

We now need to generalize the rate-independent constitutive model to include the effect of strain-rate. Recently, Bazant and the author [1] have developed a strain-rate dependent nonlinear constitutive theory for concrete in compression. This theory is extended here to model the dynamic tensile behavior of concrete. It was found from experiments [8] that the effect of strain rate is more sensitive in tension than in compression. This fact must be reflected in modeling the dynamic tensile behavior.

The shape of the uniaxial stress-strain curve of concrete largely depends on the strength. Generally, the peak portion of the curve is flatter for a lower strength concrete and becomes sharper for a higher strength concrete. This nature may be characterized by the parameter  $r$  [1].

$$r = \frac{E \epsilon_p}{\sigma_p} \quad (6)$$

in which  $\sigma_p$  = peak stress,  $\epsilon_p$  = strain at peak stress, and  $E$  = initial elastic modulus. The parameter  $r$  represents the ratio of strain at peak stress to the elastic strain corresponding to this stress. The general stress-strain curve may, therefore, be characterized by three basic parameters, i.e.,  $\sigma_p$ ,  $E$ , and  $r$ .

It was found from previous study [1] that the parameter  $r$  depends on the strength  $f'_c$ . This relation may be written as  $f'_c = f_1(r)$ . Since the elastic modulus  $E$  of concrete is known as a function of  $f'_c$  strength, one may reasonably write that  $E = f_2(r)$ .

Since the constitutive equation expressed in Eq. 1 is a function of current strain, stress, and concrete strength, this relation may be rewritten as

$$d\sigma_{ij} = D_{ijklm}[\epsilon, \sigma; f_1(r)] d\epsilon_{km} \quad (7)$$

For the given value of  $r = r^*$ , these constitutive relations will yield the peak stress  $f_1(r^*)$ , and initial tangent modulus  $f_2(r^*)$ .

It is now needed to make a transformation that preserves the value  $r^*$  but changes the peak stress and the initial elastic modulus. The affinity transformations may be applied for this purpose. Namely, the strain values are replaced by  $a\epsilon$  and the stress values by  $b\sigma$ . Therefore, Eq. 7 may be written as



$$b \, d\sigma_{ij} = D_{ijkl} [a \, \epsilon, b \, \sigma; f_1(r^*)] a \, d\epsilon_{kl} \quad (8)$$

It is noted here that the parameter  $r$  is not affected by such transformations. However, the peak stress,  $f_1(r^*)$ , and the initial elastic modulus,  $f_2(r^*)$ , will be transformed to the following values.

$$\sigma_p^* = \frac{1}{b} f_1(r^*), \quad E^* = \frac{a}{b} f_2(r^*) \quad (9)$$

The transformation coefficients  $a$  and  $b$ , may now be determined from Eq. 9.

$$b = \frac{f_1(r^*)}{\sigma_p^*}, \quad a = \frac{E^*}{f_2(r^*)} b \quad (10)$$

The following formulas have been obtained by fitting the available dynamic tensile test data[6, 8, 10].

$$g(\dot{\epsilon}) = \frac{1 - \dot{\epsilon}^{1/8}}{2.2 + 3.2 \dot{\epsilon}^{1/8}} \quad (11)$$

$$r^* = 2.09 - 0.0215 \sigma_{po} + g(\dot{\epsilon}) \quad (12)$$

$$\sigma_p^* = [1.95 - 3.32g(\dot{\epsilon})] \sigma_{po} \quad (13)$$

in which  $\dot{\epsilon}$  = strain rate, given in strain per second, and  $\sigma_{po}$  = uniaxial static strength in N/mm<sup>2</sup>. It is noted here that the formulas in Eqs. 11-13 differ from those for dynamic compression because the effect of strain rate is more sensitive in dynamic tension[8]. This is probably due to the fact that the concrete cracking influences greatly the strain rate sensitivity.

As mentioned previously, the relation  $f'_c = f_1(r)$  is formalized here from the test data as follows.

$$f_1(r^*) = (110 - 46r^*) \quad (14)$$

$$f_2(r^*) = 4,740 \sqrt{f_1(r^*)} \quad (15)$$

in which  $f_1(r^*)$  and  $f_2(r^*)$  are expressed in N/mm<sup>2</sup>, and  $f_2(r^*)$  is obtained from the relation between the elastic modulus and the compressive strength.

The behavior of concrete under initial stage may be characterized by the compliance function,  $J(t, t')$ , which is defined as the strain at time  $t$  produced by a constant unit stress acting since time  $t'$ [5]. The appropriate form for the compliance function of concrete may be written as[5]

$$J(t, t') = \frac{1}{E_o} [1 + \phi_o(t - t')^n] \quad (16)$$

in which  $\phi_o = \phi_1(t'^{-m} + \alpha)$ ,  $E_o$  = asymptotic modulus. The typical values of the material parameters are  $m = 1/3$ ,  $n = 0.1$ ,  $\phi_1 = 5$ ,  $\alpha = 0.03$ ,  $E_o = 1.5E_{28}$  where  $E_{28}$  = standard 28-day elastic moduls. It was shown the Eq. 16 gives reasonable values even for the rapid loading[5]. Since the aging of concrete during rapid loading is negligible, the effective modulus, defined as  $E_{eff} = 1/J(t, t')$ , may be efficiently used to model the concrete behavior. One may, therefore, take the initial elastic modulus  $E^*$  as the effective modulus for load duration equal to the time to reach strain  $0.05\epsilon_p$ . Since the peak strain  $\epsilon_p$  is about 0.0002 for concrete in tension, the load duration  $(t - t') = 0.05\epsilon_p / \dot{\epsilon} = (1 \times 10^{-5} / \dot{\epsilon})$  days  $\approx (1/\dot{\epsilon})$  seconds. Therefore one may write

$$E^* = \frac{1}{J(t, t')} \approx \frac{E_o}{1 + \phi_o(\dot{\epsilon})^{-n}} \quad (17)$$

Since the static uniaxial tension test is normally conducted at  $\dot{\epsilon} \approx 2 \times 10^{-6}$  / sec as indicated by Hatano et al[6], the value  $E$  for static tension may be expressed as  $E = E_0 / [1 + \phi_0 (2 \times 10^{-6})^{-n}]$ .

The dynamic tensile behavior of concrete may now be described through Eqs. 1, 8-9. One may finally write the constitutive relations as

$$d\sigma_{ij} = D_{ijkl}(\epsilon, \sigma, \dot{\epsilon}) d\epsilon_{kl} \quad (18)$$

#### 4. COMPARISONS WITH TEST DATA

The rate-dependent tensile stress-strain relation derived in the previous section has been compared with the existing dynamic tensile test data for concrete.

Fig. 2 shows the comparison of the uniaxial tensile stress-strain curves obtained for different strain rates by Hatano[6] in which the solid lines indicate the results from the present theory and the dashed lines indicate the test data. It can be seen that the tensile strength of concrete is greatly increased with the increase of strain rate.

It was possible to obtain from the present study a prediction formula for the dynamic uniaxial tensile strength of concrete. The formula obtained is

$$f_{td} = [1.95 - 3.32 \left( \frac{1 - \dot{\epsilon}^{1/8}}{2.2 + 3.2 \dot{\epsilon}^{1/8}} \right)] f_{to} \quad (19)$$

in which  $f_{td}$  = dynamic tensile strength, and  $f_{to}$  = static tensile strength.

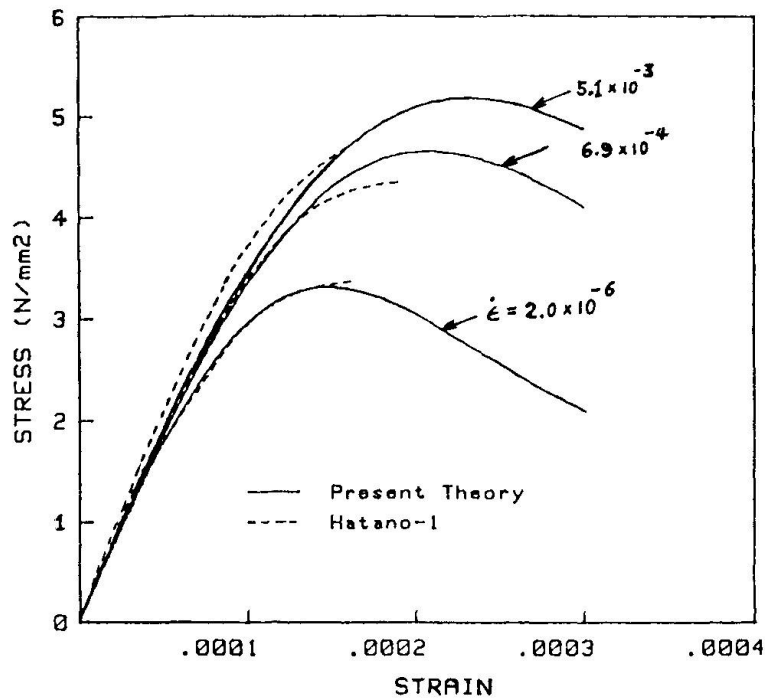


Fig. 2 Comparison of present theory with the dynamic tensile tests

#### 5. CONCLUSION

The rate-dependent nonlinear constitutive relation for concrete in tension is proposed. The model is obtained by generalizing a recently developed, rate-independent nonlinear tensile constitutive relation for concrete. The static tensile behavior is modeled on the basis of the concept of micro-crack planes which may be considered to be uniformly distributed within the concrete.



The affinity and shape transformations are used to include the effect of strain rate. The present theory, which can model the dynamic tensile behavior of concrete, is compared with the test data available in the literature. The model adequately predicts the dynamic tensile properties of concrete and allows more realistic dynamic analysis of concrete structures.

#### References

1. Bazant, Z.P., and Oh, B.H., Strain-Rate Effect in Rapid Triaxial loading of concrete, *Journal of the Engineering Mechanics Division, ASCE*, Vol. 108, No. EM5, Oct. 1982, pp. 764-782.
2. Bazant, Z.P., and Oh, B.H., Microplane Model for Progressive Fracture of Concrete and Rock, *Journal of the Engineering Mechanics, ASCE*, Vol. 111, No. 4, 1985, pp. 559-582.
3. Bazant, Z. P., and Oh, B. H., Microplane model for Fracture Analysis of Concrete Structures, *Proc., Symp. on The Interaction of Nonnuclear Munitions with Structure*, U.S. Air Force Academy, Colorado Springs, May 1983, pp. 49-55.
4. Bazant, Z.P., and Oh, B.H., Efficient Numerical Integration on the Surface of a Sphere, *"Zeitschrift fur angewandte Mathematik und Mechanik (ZAMM)"*, Leipzig, Germany, 1985.
5. Bazant, Z.P., and Panula, L., Prediction of Time-Dependent Deformations of Concrete, *Material and Structures*, Paris, France, Parts, I and II, Vol. 11, No. 65, 1978, pp. 307-328, Parts III and IV, Vol. 11, No. 66, 1978, pp. 415-434, Parts V and VI, Vol. 12, No. 69, 1979.
6. Hatano, T., Dynamic Behavior of Concrete under Impulsive Tensile Load, *Technical Report: C-6002*, Central Research Institute of Electric Power Industry, Japan, 1960.
7. Hatano, T., and Tsutsumi, H., Dynamic Compressive Deformation and Failure of Concrete under Earthquake Load, *Proceedings of the 2nd World Conference on Earthquake Engineering*, Science Council of Japan, Tokyo, Japan, Vol. 111, 1960, pp. 1963-1978.
8. Suaris, W., and Shah, S.P., Properties of Concrete Subjected to Impact, *Journal of the Structural Engineering, ASCE*, Vol. 109, No. 7, July, 1983, pp. 1727-1741.
9. Watstein, D., Effect of Straining Rate on the Compressive Strength and Elastic Properties of Concrete, *American Concrete Institute Journal*, Vol. 49, No. 8, Apr., 1953, pp. 729-744.
10. Zielinski, A.J., Reinhardt, H. W., and Kormeling, H. A., Experiments on Concrete under Uniaxial Impact Tensile Loading, *Materiaux et Constructions*, Vol. 14, No. 80, 1981, pp. 103-112.

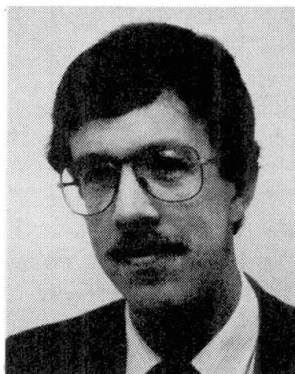
## Time-Dependent Shear Transfer of Cracked Reinforced Concrete

Béton fissuré soumis à des charges de cisaillement de longue durée

Das zeitabhängige Schubverhalten von gerissenem Stahlbeton

**Jerome FRÉNAV**

Research Engineer  
Delft Univ. of Techn.  
Delft, The Netherlands



Jerome Frénay, born 1956, received his M.Sc. degree from Delft Univ. of Techn. in 1980. Since 1982 he has been involved in research on cracked plain and reinforced concrete at the Stevin Laboratory in Delft.

### SUMMARY

Recent experimental results are presented which show the displacement behaviour of a single crack in reinforced concrete. The push-off specimens used were subjected to sustained shear loading. The time-dependent shear transfer has been described quasi-statically with regard to the effects of aggregate interlock according to Walraven's model as well as dowel action of the reinforcing bars. The implementation of the observed phenomena in non-linear finite element programs is demonstrated qualitatively.

### RÉSUMÉ

Des résultats expérimentaux récents montrent l'évolution d'une fissure unique dans du béton armé. Les éprouvettes ont été soumises à des charges de cisaillement de longue durée. La résistance au cisaillement dans le temps est considérée comme étant quasi-statique. L'explication se trouve dans l'effet d'interpénétration des granulats suivant le modèle de Walraven ainsi que l'effet de goujon de l'armature. L'interprétation du phénomène observé par un programme non-linéaire d'éléments finis est illustrée.

### ZUSAMMENFASSUNG

Neue Versuchsergebnisse zeigen das Verformungsverhalten eines einzigen Risses in bewehrtem Beton. Die Proben wurden durch eine Dauerschubbelastung beansprucht. Die zeitabhängige Schubtragfähigkeit wird quasi-statisch beschrieben. Für eine theoretische Erklärung werden sowohl die Kornverzahnung als auch die Dübelwirkung der Bewehrungsstäbe berücksichtigt. Die Übertragung dieser Phänomene in nicht-lineare Finit-Element-Programme wird qualitativ erläutert.



## 1. INTRODUCTION

As a result of the increase in scale and complexity of new structures, advanced numerical methods are being used for design purposes. These methods take account of the non-linear behaviour of cracked reinforced concrete. Whereas in the case of bending the behaviour of reinforced concrete has been extensively investigated, there is still a lack of knowledge and modelling in the case of shear forces, especially when the concrete is cracked.

As an example of a heavily loaded complex structure an offshore production platform may be taken which rests on the sea bed. The substructure consists of a caisson subdivided into several compartments by means of concrete shear walls. Usually a dense and high-strength concrete is used with mean cylinder strengths ranging from 40 to 60 N/mm<sup>2</sup>. Due to differential settlements and temperature gradients (for example storage of hot oil in the compartments) cracks may form. Also considerable redistribution may take place causing shear displacements along existing cracks. There is a need to analyse the behaviour of these cracks under various types of loading in order to design safely and cost-effectively. This paper will deal with experimental investigations carried out on reinforced concrete specimens with a single crack, which were subjected to sustained shear loading. A physical explanation for the observed time-dependent crack displacements is based on Walraven's rough crack model [1] for plain concrete and on existing dowel action formulas for the reinforcing bars crossing the crack plane. These models should be adapted to sustained shear loading conditions. Moreover, attention will be paid to the numerical implementation of this research into finite element programs. This study is supported by the Netherlands Centre for Civil Engineering Research, Codes and Specifications (CUR).

## 2. STATIC SHEAR STRENGTH

For the actual research program [2] shear loading tests were carried out on push-off specimens similar to those used by Walraven [1]. See Figure 1. The dimensions of the crack plane were 120mm x 300mm. In order to prevent premature failure and to improve the gradual introduction of the external force into the cracked shear plane, the bottom and top of the specimen have been post-tensioned transversely.

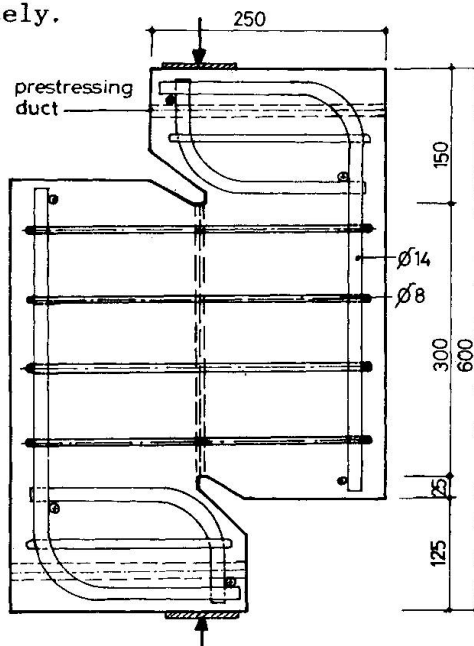


Fig. 1. Push-off specimen used for the shear tests [1,2,3].

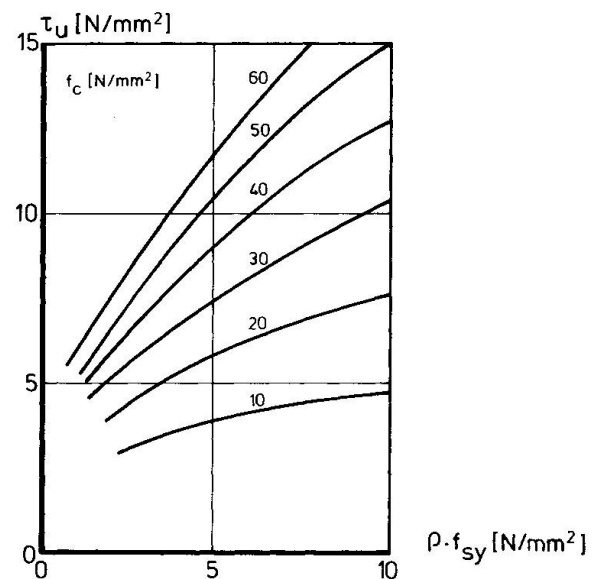


Fig. 2. Static shear strength according to formula (1).

For the series of sustained tests the static shear strength  $\tau_u$  was taken as a calibration value. A formula for  $\tau_u$  has been derived based on four sources [1-4]. The initial crack width of the push-off specimens was between 0.01 and 0.10mm. Concrete cylinder strengths varied from 17 to 60 N/mm<sup>2</sup>. River gravel aggregates were used having a maximum particle size  $D_{max} = 16-32$ mm. The bar diameter of the stirrups ranged between 8 and 16mm and the value of  $\rho f_{sy}$  lay between 0.35 and 12.32 N/mm<sup>2</sup>. After analysing a total number of 88 static tests [5] an empirical expression was found:

$$\tau_u = \alpha (\rho f_{sy})^\beta \quad [\text{N/mm}^2] \quad (1)$$

in which:  $\alpha = 0.878 f_c^{0.406}$   
 $\beta = 0.167 f_c^{0.303}$  with  $f_c$  in [N/mm<sup>2</sup>]

Formula (1) is shown graphically in Figure 2. The average ratio of measured and calculated  $\tau_u$ -values is 1.001 with a coefficient of variation of less than 11%.

### 3. SHEAR TRANSFER IN CRACKED CONCRETE UNDER SUSTAINED LOADING

#### 3.1 Experimental variables

Recently, experiments were carried out on 32 push-off specimens for sustained shear loading conditions. Only a few details of the testing program [2] will be given. The main variables were:

- *cube compressive strength of the concrete*  
 $f_{cc} = 51$  or  $70$  N/mm<sup>2</sup>, which corresponds to cylinder strengths  $f_c$  of 43 and  $60$  N/mm<sup>2</sup> respectively for an assumed strength ratio  $f_c/f_{cc} = 0.85$ . The two mixes contained Portland cement B and glacial river aggregates having a 16mm maximum diameter and a grading curve according to Fuller. Both a medium-strength and a high-strength concrete were investigated. Usually cracks will be initiated in the bond zone between the aggregate particles and the cement matrix. For high-strength concrete cracks were expected to extend predominantly through the aggregates. This should result in different mechanisms of shear transfer. However, no significantly different crack patterns were observed with regard to the percentage of fractured particles in the crack plane [2];
- *normal restraint stiffness*  
Embedded 8mm diameter reinforcing bars were used. The reinforcement ratios were  $\rho = 0.0112$ ,  $0.0168$  or  $0.0224$ , realised by 4, 6 or 8 stirrups respectively, all perpendicularly crossing the crack plane. The yield strength of the deformed bars was  $f_{sy} = 460$  and  $550$  N/mm<sup>2</sup> respectively;
- *initial crack width  $w_0$*   
The initial crack width ranged between  $w_0 = 0.01-0.05$  mm;
- *sustained shear stress level  $\tau/\tau_u$*   
 $\tau = 5.7-11.5$  N/mm<sup>2</sup>, i.e. 45%-89% of the static shear strength  $\tau_u$ .

#### 3.2 Testing procedure

The specimens were cured in a fog chamber (19°C: 95% RH) for 22 days. Next, they were stored in the laboratory (20°C: 50% RH). Tests started when the concrete had reached an age of 28 days. Prior to the shear test each specimen was pre-cracked in a vertical position. The average remaining crack width was the initial crack width. After application of the shear loading at a loading rate of about  $0.02$  N/mm<sup>2</sup> per second, the displacements parallel and perpendicular to the shear plane were recorded periodically. The load was sustained for at least 91 days. After unloading the displacements were measured during the following 25 days, after which a static failure test was carried out.





### 3.3 Statistical analysis of test results

Mean values of the measured crack widths  $w$  and the parallel displacements  $s$  can be presented as functions of the duration of load application  $t$ . The overall displacements consist of instantaneous values  $w_{e1}$  and  $s_{e1}$  (at  $t=0$  hrs) plus the time-dependent increments  $w_c(t)$  and  $s_c(t)$ . According to Fig. 3, it follows that:

$$\begin{aligned} t \geq 0 \text{ hrs} : w(t) &= w_{e1} + w_c(t) \quad [\text{mm}] \\ s(t) &= s_{e1} + s_c(t) \quad [\text{mm}] \end{aligned} \quad (2)$$

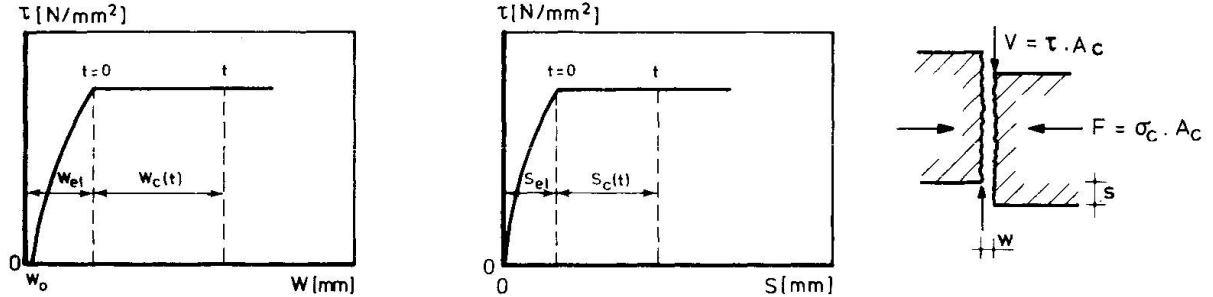


Fig. 3. Definitions of instant and creep displacements as functions of  $\tau$  and  $t$ .

Due to the small displacement increments and their observed scatter, the instantaneous and the time-dependent displacements were statistically described as functions of the experimental variables by multiple regression analysis [2,6]. Also, the effect of scatter of the experimental variables (e.g. variations in concrete strength) on the displacement response could be quantified. Extrapolation to non-tested circumstances is possible to a certain extent. An empirical formula has been derived for the crack width [6]:

$$w(t) = \alpha_1 (\tau/\tau_u)^2 + \alpha_3 (\tau/\tau_u)^4 \cdot \rho f_{sy} \quad [\text{mm}] \quad (3)$$

with values:  $30 \leq f_{cc} \leq 75 \text{ N/mm}^2$

$4 \leq \rho f_{sy} \leq 12 \text{ N/mm}^2$

$0.60 \leq \tau/\tau_u \leq 0.90$  provided that  $\tau > 3 \text{ N/mm}^2$

in which  $\alpha_1$ - $\alpha_4$  are non-linear functions of compressive strength and time of load application. A similar formula has been derived for  $s(t)$ .

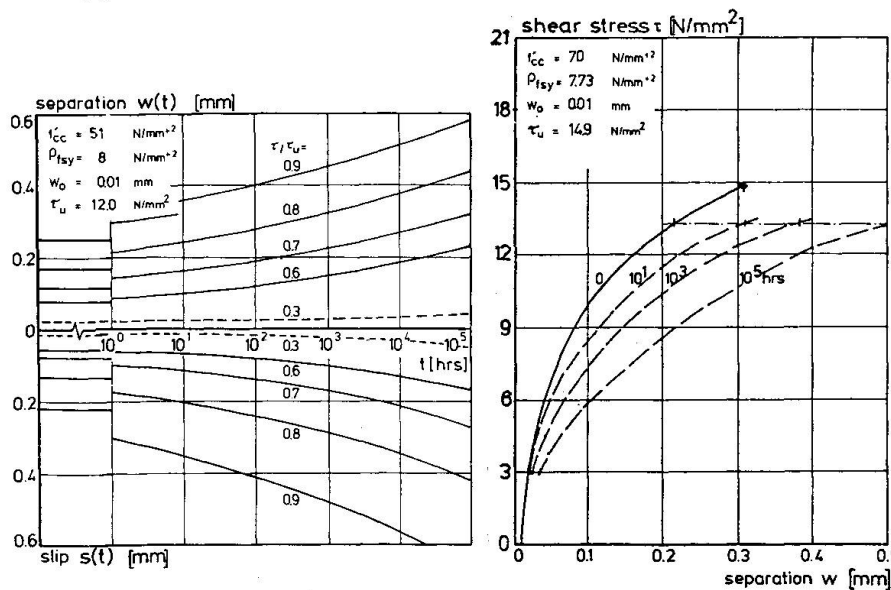


Fig. 4.  $w(t)$  and  $s(t)$  curves for  $\rho f_{sy}=8 \text{ N/mm}^2$ ;  $f_{cc}=51 \text{ N/mm}^2$ .

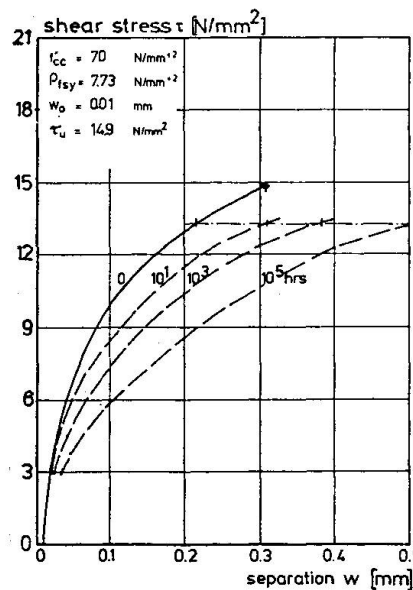


Fig. 5.  $\tau$ - $w(t)$  curves for  $\rho f_{sy}=7.73 \text{ N/mm}^2$ ;  $f_{cc}=70 \text{ N/mm}^2$ .

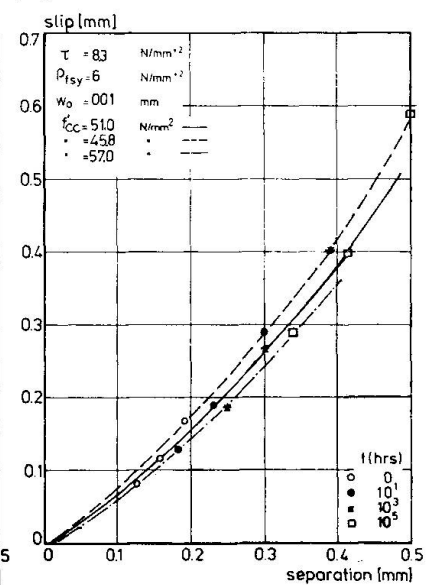


Fig. 6.  $s(w)$ -curves for  $\tau=8.3 \text{ N/mm}^2$ ; variation of  $f_{cc}$ .

Equation (3) is worked out in Figs. 4 and 5. It can be seen that there is a significant effect of the shear stress level  $\tau/\tau_u$  on the instantaneous and the time-dependent displacements. At low stresses, for instance  $\tau/\tau_u = 0.30$ , the time-dependent displacements are small within the first  $10^4$  hours. With the aid of equation (3), creep coefficients  $\varphi_w = w_c(t)/w_{e1}$  and  $\varphi_s = s_c/s_{e1}$  can be calculated [6]. Examples of the crack opening curves are given in Fig. 6; a variation of the concrete strength considerably influences the displacement behaviour [2]. For a safe physical basis a model should be provided which accounts for the most likely shear transfer mechanisms, i.e. aggregate interlock and dowel action.

#### 4. PHYSICAL MODELLING OF SHEAR TRANSFER

##### 4.1 Static shear loading

The external shear force  $V$  causes a shear stress  $\tau = V/A_c$ , which is transferred in the crack plane by both dowel action  $\tau_d$  of the bars and by aggregate interlock  $\tau_a$  of the opposing crack faces of the plain concrete.

##### Aggregate interlock

For static shear loading the aggregate interlock mechanism has been described by the rough crack model of Walraven [1]. Concrete is modelled as a two-phase material consisting of rigid spherical aggregate particles embedded in a cement matrix. As far as normal-strength concrete is concerned the preformed crack will run into the matrix along the surface of the aggregate particles.

If a shear stress  $\tau_a$  is applied to the cracked concrete specimen, the crack opening increases and the rigid spheres of one crack face are pushed into the matrix material of the opposing crack face; see Figure 7. The required normal stress  $\sigma_a$  is obtained by embedded reinforcement or by external restraint rods.

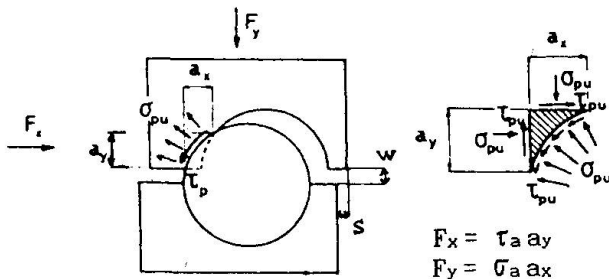


Fig. 7. Contact area between matrix and matrix material [1].

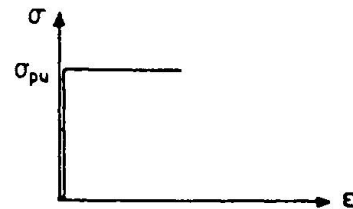


Fig. 8. Rigid-plastic behaviour of matrix material [1].

The total projected contact areas are  $A_x = \sum a_x$  and  $A_y = \sum a_y$ . For a unit surface area of the crack, the equilibrium condition can be formulated:

$$\begin{aligned} \tau_a &= \sigma_{pu} (A_y + \mu A_x) & [N/mm^2] \\ \sigma_a &= \sigma_{pu} (A_x - \mu A_y) & [N/mm^2] \end{aligned} \quad (4)$$

The rough crack model implies that there is a unique relation between the displacements  $w$  and  $s$  of the crack and the corresponding stresses  $\tau_a$  and  $\sigma_a$ . The shear stress as well as the normal stress are both functions of  $A_x$  and  $A_y$  (which can be analytically calculated: for a given mix proportion these areas depend on the shear displacements  $w$  and  $s$ ), of the matrix strength  $\sigma_{pu}$  and of the coefficient of friction  $\mu$  of the matrix material. It follows that  $\tau_{pu} = \mu \cdot \sigma_{pu}$ . Empirical values of  $\mu$  and  $\sigma_{pu}$  were derived from static shear tests on plain concrete push-off specimens [1]:

$$\sigma_{pu} = 6.39 f_{cc}^{0.56} \quad [N/mm^2] \quad \text{and} \quad \mu = 0.40 \quad [-] \quad (5)$$



### Dowel action

The ultimate dowel force  $F_{du}$  of a reinforcing bar, which will be reached for a sufficiently large parallel displacement  $s > w_0$  of the crack faces, is given by [7]:

$$F_{du} = 1.3 d_{bar}^2 \sqrt{f_{cc} f_{sy}} \quad [N] \quad (6)$$

The maximum shear stress due to  $n$  bars is then:  $\tau_{du} = n \cdot F_{du} / A_c$ . The total shear stress is the sum of the two components  $\tau_a$  (aggregate interlock) and  $\tau_{du}$  [3]:

$$\tau = \tau_a + \gamma_d \tau_{du} \quad [N/mm^2] \quad (7)$$

in which  $\gamma_d = \tau_d / \tau_{du} = \sqrt{1 - (\sigma_s / f_{sy})^2}$  takes account of the yield criterion [8]. Now, a stepwise overview of the calculation procedure can be given if the crack opening curve is assumed to be known:

- for given crack displacements  $w$  and  $s$  the corresponding stresses  $\sigma_a$  and  $\tau_a$  in the plain concrete are computed by means of the equations (4)-(5);
- equations (6)-(7) provide the contribution of the embedded reinforcing bars;
- if  $\sigma_s = \sigma_a / \rho > f_{sy}$  then in eq. (7)  $\tau_a$  should be multiplied by  $\gamma_a = f_{sy} / \sigma_s$ . This means that an equal reduction of  $\sigma_a$  and  $\tau_a$  is proposed [3].

### 4.2 Sustained shear loading

In a first attempt to analyse theoretically the sustained shear tests it is assumed that  $\tau_a$  and  $\tau_d$  are both affected by the same damage parameter  $\lambda(t) < 1$ . This parameter takes account of the influence of the sustained loading period upon the concrete compressive strength.

$$\tau = \lambda(t) (\tau_a + \gamma_d \tau_{du}) \quad [N/mm^2] \quad (8)$$

Combining the equations (4)-(8) with  $\rho = n \pi d_{bar}^2 / (4 A_c)$  leads to:

$$\tau = \lambda(t) f_{cc}^{0.67} [4.42 (A_y + \mu A_x) + 0.84 \rho \gamma_d \sqrt{f_{sy}}] \quad [N/mm^2] \quad (9)$$

The values of  $\lambda$  were calculated for the complete test series using the time-dependent crack opening curves - as presented in Fig. 6 - as the input data. For  $t = 0$  the sustained shear stress was just applied; it was found that  $\lambda = 1.077$  with a coefficient of variation of 8.9%. In fact  $\lambda$  should be 1.0. This calculation discrepancy could be due to the load-controlled application method used [2], whereas Walraven's specimens were loaded displacement-controlled [1].

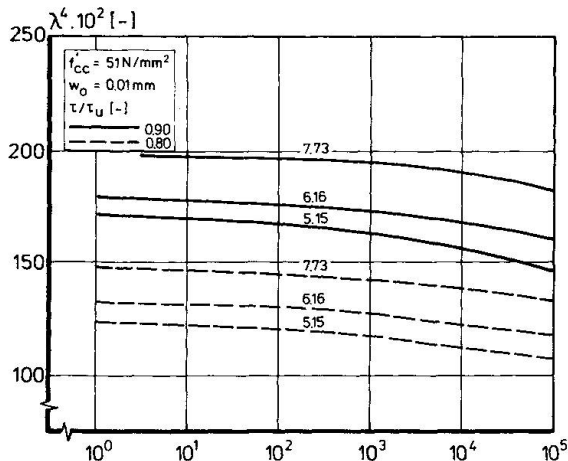


Fig. 9. Development of  $\lambda^4$  as a function of  $t$ .

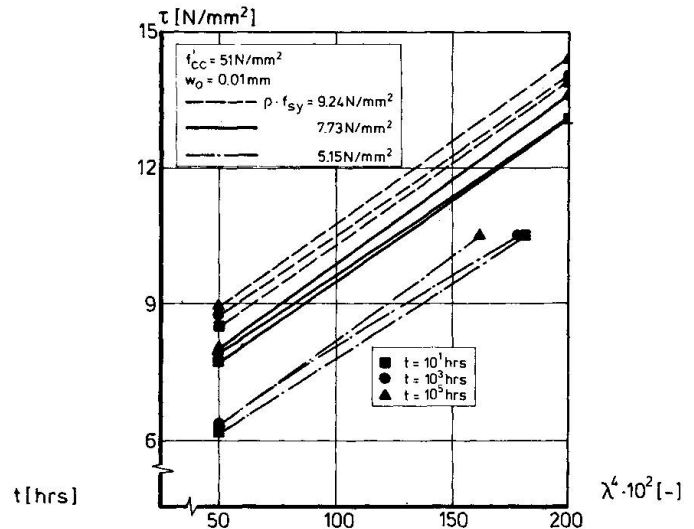


Fig. 10. Development of  $\lambda^4$  as a function of the sustained shear stress  $\tau$ .

For  $f_{cc} = 51 \text{ N/mm}^2$  and  $t = 10^0 - 10^5$  an empirical relation was found statistically for the damage parameter with  $D_j = C_{1j} + C_{2j} \cdot \ln(t) + C_{3j} [\ln(t)]^2$  for  $j = 1, 2, 3$  and 4:

$$\lambda(t) = \sqrt[4]{0.01 [D_1 + D_2 \rho f_{sy} + (D_3 + D_4 \rho f_{sy}) (\tau/\tau_u)]} \quad [-] \quad (10)$$

The average ratio of calculated and empirically found  $\lambda^4$ -values is 1,017 with a coefficient of variation of 12.4%. A few examples of the development of  $\lambda^4$  are presented in Figs. 9 and 10. As a result of the development of  $\lambda(t)$  the dowel force will gradually decrease. Note that  $f_{cc}$  and  $\mu$  are kept constant in this analysis. An increase of  $f_{cc}$  (due to hydration) or  $\mu$  would reduce the  $\lambda$ -values.

## 5. NUMERICAL IMPLEMENTATION

### 5.1 Static shear loading

Pruijssers [9] used the measured static crack behaviour for the smeared crack concept. For this purpose one incremental stress-strain relation is needed describing the behaviour of both the uncracked and the cracked concrete sections. Cracks develop in a direction perpendicular to the principal tensile stress  $\sigma_{nn}$ . Once the static tensile strength  $f_{ct}$  has been reached, at first a band of microcracks forms. In Fig. 11,  $\zeta$  is defined as the tension softening factor or the normal retention factor. For the partially cracked area  $\zeta = E_t \cdot (\epsilon_{nn} - \epsilon_u) / (E \cdot \epsilon_{nn})$ .

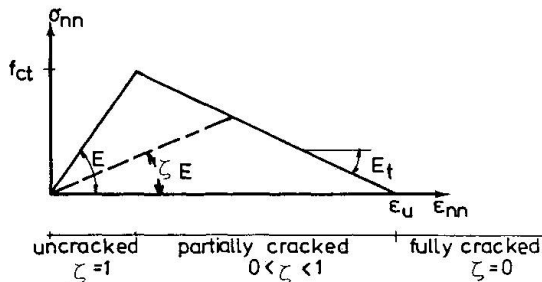


Fig. 11. Tensile stress-strain relation [9].

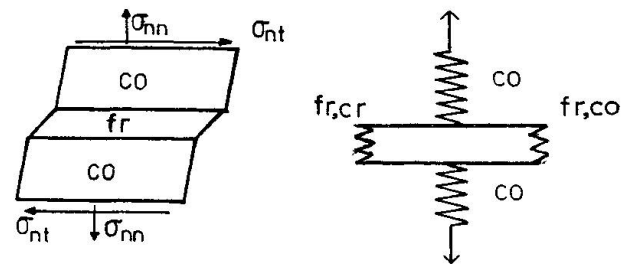


Fig. 12. Rheological model of the fracture zone [9].

The deformation of an element can be modelled by the contribution of the uncracked and cracked concrete sections. See Fig. 12. The fracture zone (fr) is divided into two parts: a fully cracked part (fr,cr) with  $\zeta=0$  and an uncracked part (fr,co). Using the model of Figure 11 the incremental stress-strain relation for each section of the element can be described. For the uncracked section (co) and the uncracked part of the fracture zone (fr,co) the incremental stress-strain relations are governed by Young's modulus  $E$ , Poisson's ratio  $\nu$ , and  $\zeta$ . For the cracked part of the fracture zone (fr,cr) the two-dimensional stiffness matrix has four coefficients which can be deduced from the rough crack model of Walraven [1,3,9]. Finally, a stiffness matrix for the complete element can be found.

### 5.2 Sustained shear loading

Now, the crack displacements will increase depending on the level and the time-duration of the shear loading. In Fig. 12 the gradual weakening of the concrete can be expressed by adding dashpots placed in series with the springs which represent the uncracked and the cracked part of the fracture zone. For the uncracked part of this zone, the material degradation can be formulated by reducing Young's modulus. Concerning the cracked part damage parameters  $\lambda_\mu$  and  $\lambda_\sigma$ , as reported in Section 4.2, can take account of changes in concrete strength and friction coefficient. This converts equation (4) into:

$$\begin{aligned} \tau_a &= \lambda_\sigma \cdot \sigma_{pu} (A_y + \lambda_\mu \cdot \mu A_x) \quad [\text{N/mm}^2] \\ \sigma_a &= \lambda_\sigma \cdot \sigma_{pu} (A_x - \lambda_\mu \cdot \mu A_y) \quad [\text{N/mm}^2] \end{aligned} \quad (11)$$

The development of the theoretical model will be a subject of further study.



## 6. CONCLUSIONS

Some conclusions can be drawn:

- Cracked concrete exhibits time-dependent crack sliding and crack opening under sustained shear loading. The magnitude depends strongly on concrete quality, reinforcement ratio and stress level. In the range which has been investigated all these effects are non-linear.
- The variation of concrete strength has a considerable effect on the time-dependent crack displacements.
- Time-dependent shear transfer can be modelled by the use of a damage parameter  $\lambda$  affecting both the aggregate interlock and the dowel action mechanism. The time dependency of the concrete compressive strength and the coefficient of friction should be further quantified.
- Time dependent shear displacements under service loads seem to be small.

## 7. NOTATION

Unless otherwise stated, the dimensions are N, mm or N/mm<sup>2</sup>.

$d_{bar}$	-diameter of reinforcing bar	$A_c$	-area of shear plane [mm <sup>2</sup> ]
$f_c$	-cylinder compressive strength	$C_{ij}, D_j$	- coefficients [-]
$f_{cc}$	-cube compressive strength	$V$	-shear force
$f_{sy}$	-yield strength of steel	$\lambda$	-damage parameter [-]
$s$	-parallel displacement (or:slip)	$\zeta$	-normal retention factor [-]
$s_c$	-slip increment	$\mu$	-friction coefficient [-]
$s_{el}$	-instantaneous slip	$\rho$	-reinforcement ratio [-]
$t$	-load application period [hours]	$\sigma_{pu}$	-yield strength of matrix material
$w$	-crack width (or:separation)	$\tau$	-shear stress
$w_c$	-separation increment	$\tau_a$	-shear stress due to aggregate interlock
$w_{el}$	-instantaneous separation	$\tau_d$	-shear stress due to dowel action
$w_o$	-initial crack width	$\tau_u$	-static shear strength
$A_x, A_y$	-projected contact areas [mm <sup>2</sup> ]		

## 8. REFERENCES

1. Walraven, J.C., Reinhardt, H.W.: Theory and experiments on the mechanical behaviour of cracks in plain concrete and reinforced concrete subjected to shear loading, Heron, No. 26, 1981,
2. Frénay, J.W.: Shear transfer across a single crack in plain and reinforced concrete under sustained loading, Stevin Reports 5-85-5/6/7/13, Delft University of Technology, 1985.
3. Pruijssers, A.F., Liqui Lung, G.: Shear transfer across a crack in concrete subjected to repeated loading, Stevin Report 5-85-12, Delft University of Technology, 1985.
4. Hofbeck, J.A., Ibrahim, I.O., Mattock, A.H.: Shear transfer in reinforced concrete, ACI-Journal, No. 2, 1969, pp. 119-128.
5. Walraven, J.C., Frénay, J.W., Pruijssers, A.F.: Influence of concrete strength and load history on the shear friction capacity of concrete members, PCI-Journal, Vol. 32, No. 1, 1986, pp. 66-84.
6. Frénay, J.W.: Behaviour of a single crack in concrete subjected to sustained shear loading. Empirical formulae for the crack displacements, Stevin Report 5-86-11, Delft University of Technology, 1986.
7. Rasmussen, B.H.: The bearing capacity of a dowel cast in concrete, Technical University of Denmark, 1962.
8. Vintzeleou, E.N., Tassios, T.P.: Mathematical models for dowel action under monotonic and cyclic conditions, Magazine of Concrete Research, No. 134, 1986, pp. 13-22.
9. Pruijssers, A.F.: Description of the stiffness relation for mixed-mode fracture problems in concrete using the rough crack model of Walraven, Stevin Report 5-85-2, Delft University of Technology, 1985.

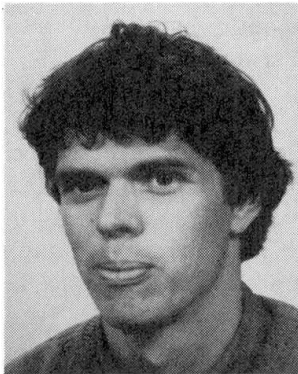
## Significance of Crack Models for Bond-Slip Studies

Valeurs des modèles de fissuration pour les études adhérence-glisement

Die Bedeutung von Rissmodellen für Verbundstudien

### Jan G. ROTS

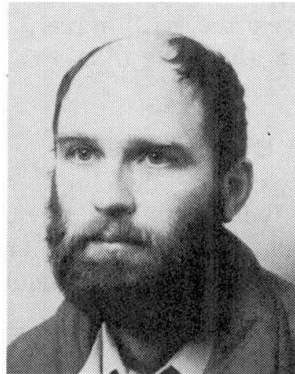
Research Engineer  
Delft Univ. of Techn.  
Delft, The Netherlands



Jan Rots, born 1958, graduated from Delft University of Technology in 1983. Since 1983 he has been involved in a research project in the field of concrete mechanics.

### Ger M.A. KUSTERS

Research Manager  
TNO-IBBC  
Delft, The Netherlands

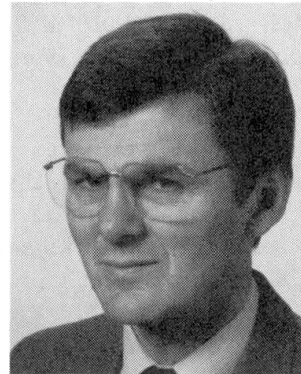


Ger Kusters, born 1948, graduated from Delft University of Technology, Faculty of Mechanical Engineering in 1976. Since 1974 he has been involved in the development of the DIANA finite element package at the Institute TNO for Building Materials and Structures. Being a research manager since 1980 he is presently head of the DIANA research group.

### Johan

### BLAAUWENDRAAD

Professor  
Delft Univ. of Techn.  
Delft, The Netherlands



Graduated from Delft University in 1962. Joined TNO in 1964 and Rijkswaterstaat in 1971. Professor in Civil Engineering since 1979.

## SUMMARY

The bond-slip phenomenon in reinforced concrete is investigated using finite elements and an elastic-softening crack model. Computational examples demonstrate the capability of this approach for predicting bond-slip related cracks such as primary cracks, secondary cracks and longitudinal splitting cracks. Attention is furthermore drawn to 'tau-delta' curves and their possible non-uniqueness. The paper is concluded by a more practical example involving the application of bond-slip interface elements.

## RÉSUMÉ

La phénomène adhérence-glisement dans le béton armé est étudié à l'aide des éléments finis et d'un modèle de fissuration élastique souple. Des exemples de calcul démontrent la capacité de cette approche à prédire les fissures dues à cette situation adhérence-glisement, telles que fissures primaires, secondaires et longitudinales. L'attention est attirée sur les courbes 'tau-delta' et sur leur éventuelle non-unicité. L'article conclut par un exemple pratique comportant l'application d'éléments d'interface adhérence-glisement.

## ZUSAMMENFASSUNG

Der verschiebbare Verbund im Stahlbeton wird mit Hilfe von Finiten Elementen und einem elastischen Entfestigungsmodell untersucht. Beispiele zeigen die Fähigkeiten des Modells in Bezug auf die Voraussage von Primär- und Sekundärrissen und Längsspaltissen. Schubspannungs-Verschiebungskurven werden kritisch beleuchtet, vor allem hinsichtlich ihrer Nicht-Eindeutigkeit. Der Beitrag wird mit einem Beispiel aus der Praxis abgeschlossen.





## 1. INTRODUCTION

Bond-slip in reinforced concrete is known to be closely related to, or even stronger, caused by cracking. This was probably first emphasized by Goto [13], who presented experimental results on tension-pull specimens, revealing the existence of primary cracks surrounded by cone-shaped secondary cracks (Fig. 1a). While the primary cracks are generally visible at the outer surface, the secondary cracks are formed internally behind the ribs of the (deformed) reinforcing bar at both sides of a primary crack. In some cases one may also observe longitudinal splitting cracks, the importance of which depends on the precise ratio of concrete cover versus bar dimensions (Fig. 1b). Secondary cracks and longitudinal splitting cracks are generally considered as being the dominant factors contributing to bond-slip.

Experimental measurements of bond-slip and bond-slip related cracks have been the subject of much controversy, primarily because of the significant scatter emerging from different specimen configurations and different testing techniques, e.g. [1,10,11]. Within this context computational models may be helpful for investigating bond-slip behaviour, especially when we consider the progress which has been recently made in the field of fracture mechanics and crack models for concrete.

The purpose of this paper is to apply this increased knowledge of concrete cracking to the bond-slip problem. To this end, the crack model developed within DIANA [6,18] has been applied to a tension-pull configuration and the focus is placed on obtaining a detailed resolution of primary cracks, secondary cracks and longitudinal splitting cracks. The paper is concluded by a more practical example involving the application of special bond-slip elements [9,19] in addition to cracking options.

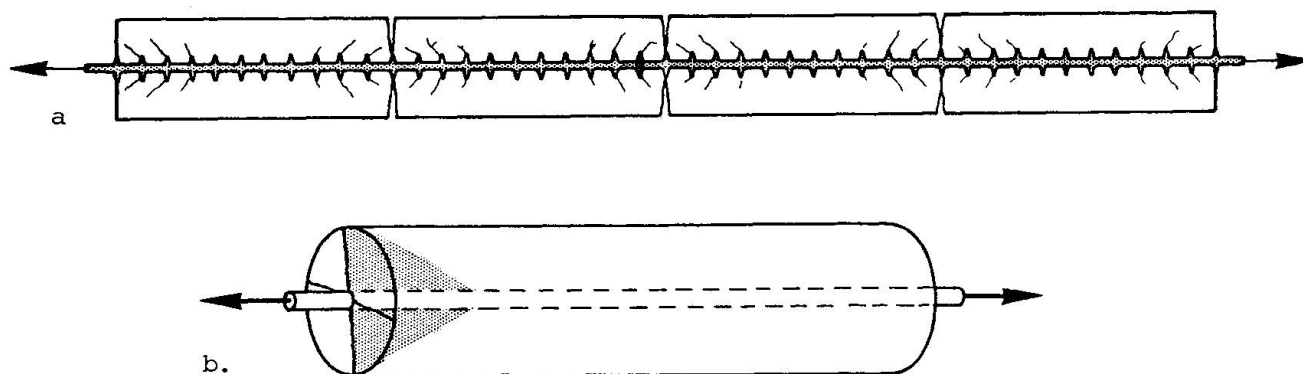


**Fig. 1.** Crack formation in tension-pull configuration.

(a) primary and secondary cracks, (b) longitudinal cracks.

## 2. CRACK MODEL

The crack model adopted was based on a decomposition of the total strain into a concrete part and a crack part. This procedure has the notable advantage that it allows crack behaviour to be treated separately from the behaviour of the intact concrete between the cracks (de Borst & Nauta [6], Rots et al. [18]). In this paper a linearly elastic model has been assumed for the concrete and a softening model for the crack, so that we arrive at an elastic-softening model for the cracked concrete.

The softening was assumed to occur in mode-I and was controlled by three parameters, viz. the uniaxial tensile strength  $f_{ct}$ , the mode-I fracture energy  $G_f$  and the shape of the softening diagram. In this paper a non-linear tensile softening function [17] has been adopted. The



tensile strength and the fracture energy  $G_f$  were assumed to be fixed material constants and provisions were included to correctly release the fracture energy over the given crack band width  $h$  which is related to the particular finite element configuration [2]. A constant crack shear modulus was inserted to control mode-II crack sliding behaviour. This technique corresponds to the use of a constant shear retention factor  $\beta$  [18].

Multi-directional cracking in an integration point was modelled according to the ideas of Litton [15] and de Borst & Nauta [6]. For axi-symmetric configurations like tension-pull specimens this option is essential as it allows us to simultaneously detect one or more tangential cracks as well as a radial splitting crack. It is further noted that the crack model includes a crack closing and re-opening option in the form of a secant unloading/reloading branch.

### 3. COMPUTATIONAL SET-UP

This paper considers a tension-pull specimen, which consists of a center-placed reinforcing bar surrounded by a cylinder of concrete. The particular dimensions correspond to a portion of the specimen tested by Broms & Raab [4], which also served as a basis for a numerical study by Ingraffea et al. [14]. The axi-symmetric finite element configuration is shown in Fig. 2 and consists of quadratic elements which have been integrated using nine-point Gauss quadrature. The concrete elements have been rigidly connected to the steel elements in order to simulate the mechanical interlock between the ribs of the (deformed) reinforcing bar and the concrete. In doing so, pure slip along the steel-concrete contact surface has been neglected. In addition, possible local "crushing" in front of the steel ribs has been neglected, which seems to be justified since confinement in the form lateral compression was lacking. As a consequence, the computations aim at explaining bond-slip solely via elastic deformation, secondary cracking and longitudinal cracking.

The elastic properties of the concrete were assumed to be: Young's modulus  $E_c = 25000 \text{ N/mm}^2$  and Poisson's ratio  $\nu = 0.2$ . The crack parameters were taken as: tensile strength  $f_{ct} = 2.8 \text{ N/mm}^2$  (with a slight perturbation for the Gauss-points near midlength of the specimen), fracture energy  $G_f = 50 \text{ J/m}^2$ , crack band width  $h = 8.46 \text{ mm}$  and shear retention factor  $\beta = 0.5$ . The reinforcing bar was given a Young's modulus  $E_s = 200000 \text{ N/mm}^2$  and a yield stress  $\sigma_y = 400 \text{ N/mm}^2$ . The specimen was analysed under direct displacement control of the end-face of the reinforcing bar, using a modified Newton-Raphson incremental-iterative procedure.

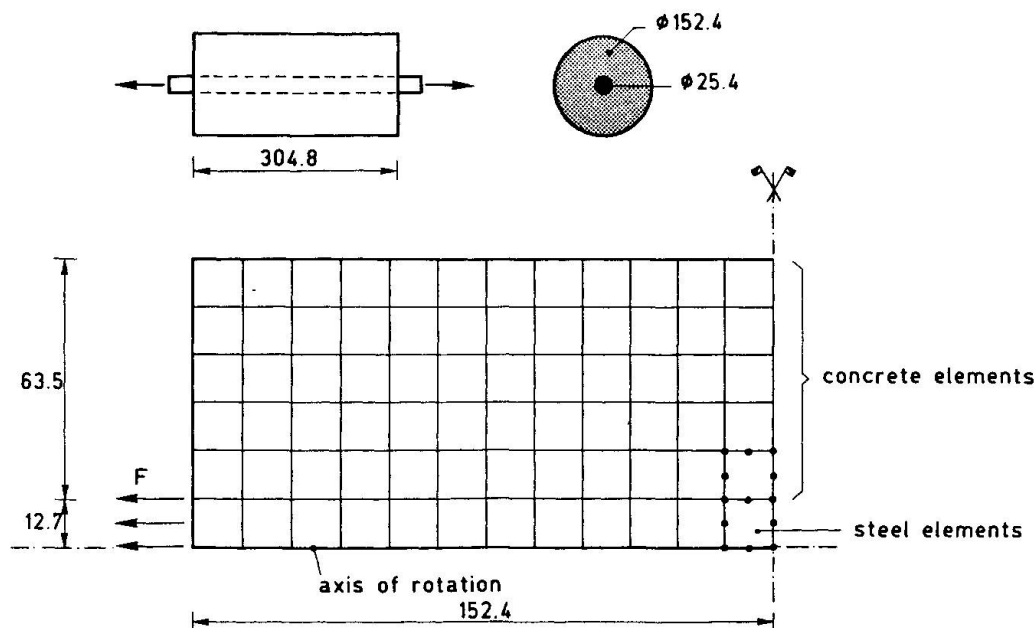


Fig. 2. Finite element idealization of tension-pull specimen.



#### 4. CONE-SHAPED SECONDARY CRACKS

The analysis progressed as shown in Figs. 3 and 4, giving the crack patterns and the corresponding incremental deformations at key-events. Initially, secondary cracks form at the location where the steel exits the concrete (Figs. 3a and 4a). On subsequent loading, these cracks propagate and additional secondary cracks nucleate further from the specimen end-face. At a certain load level also the tensile stress at midlength of the specimen reaches the tensile strength, which results in the unstable formation of a localized primary crack (Figs. 3b and 4b). Beyond this stage additional secondary cracks nucleate in response to the free surface provided by the primary crack, just like they did in response to the free end-face (Figs. 3c and 4c). Consequently, a number of Gauss-points display not only one but two secondary cracks, crossing each other. Formation of the "second" secondary crack was mostly accompanied by closing of the existing secondary crack.

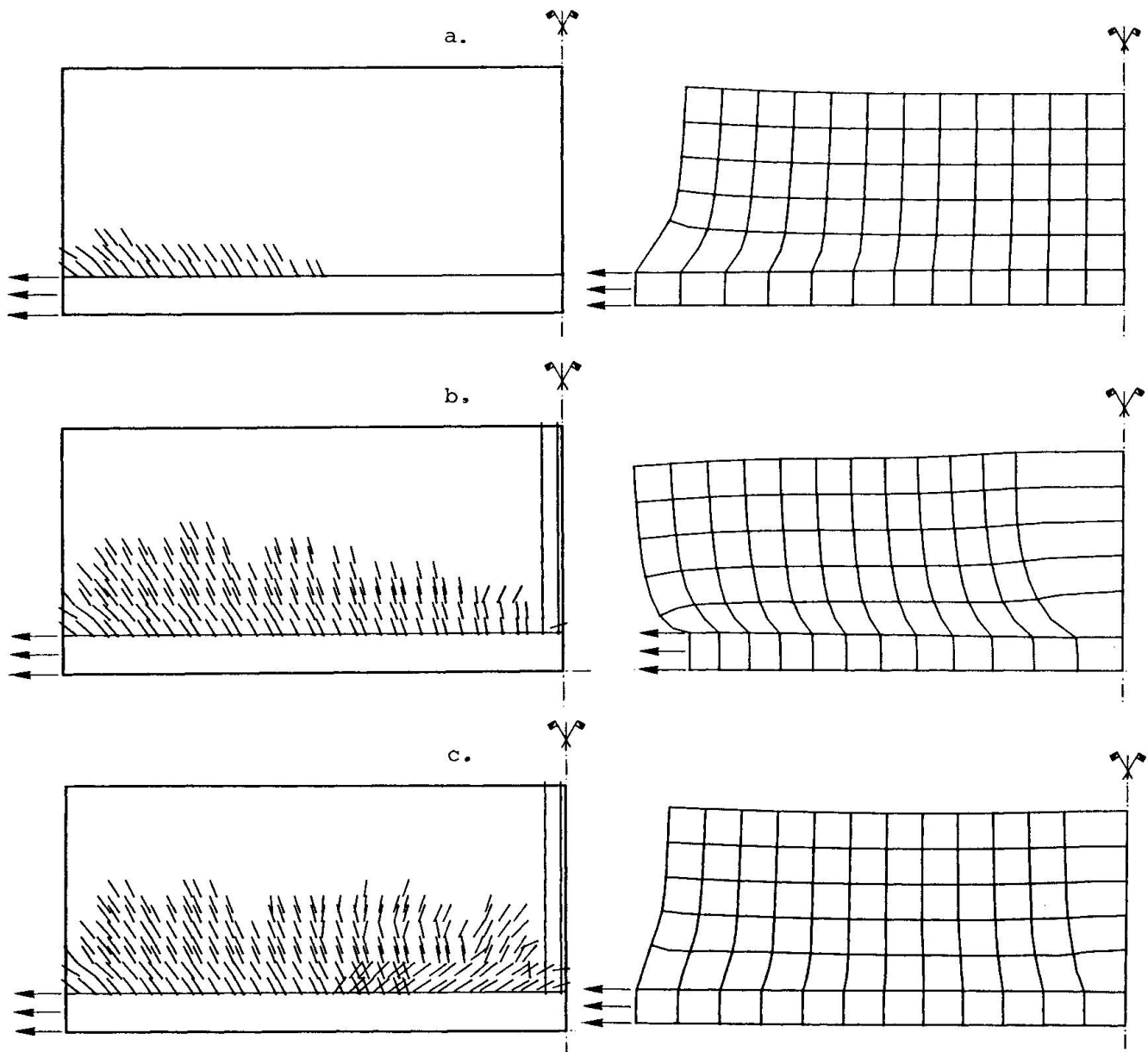


Fig. 3. Tangential crack pattern.

Fig. 4. Incremental deformations.

(a)  $u_A = 0.02\text{mm}$ , prior to primary cracking, (b)  $u_A = 0.06\text{mm}$ , at primary cracking, (c)  $u_A = 0.10\text{mm}$ , beyond primary cracking.

The above mechanisms turn out to be in line with the experimental findings by Goto [13]. A discrepancy is that the computational result exhibits a rather diffuse pattern of secondary cracks, while in the experiments the tiny secondary cracks localized behind each rib of the steel bar. This discrepancy is due to the mesh adopted, which is too coarse to model the action of individual ribs. Further computational details, such as the impact of the various crack parameters on secondary crack formation are given in [19]. It appeared that not only the mode-I fracture parameters, but also the shear retention factor  $\beta$ , controlling the amount of stress rotation after crack initiation, and the inter-crack threshold angle [8], controlling the inclination between multi-directional cracks, played a crucial role. Improvements of the crack model regarding these issues are currently worked out, e.g. [20].

## 5. PRIMARY CRACKS

Fig. 4b indicates that primary cracking occurs in the form of a sudden, brittle type of fracture which is highly localized. The primary crack involves a drastic redistribution of the stresses within the specimen. In fact, the specimen is predicted to be halved into two sub-specimens, the behaviour of each of which is a copy of the original specimen.

This sudden transition from the one equilibrium state to a different equilibrium state is not free from complications. This becomes manifest if we plot the load-elongation response, which shows a local limit point followed by a sudden drop of the load, as shown in Fig. 5. Obviously, we are dealing with a "snap-back" [5,7,8], which can also be deduced from Fig. 4b revealing relaxation of the steel bar upon primary crack formation. In the present study the snap-back was passed by temporarily switching-off the iterations, allowing the load to drop suddenly. For a more elegant way to solve this problem one should resort to advanced solution techniques which control the opening displacement of the primary crack rather than the end-displacement of the reinforcing bar (de Borst [7,8]).

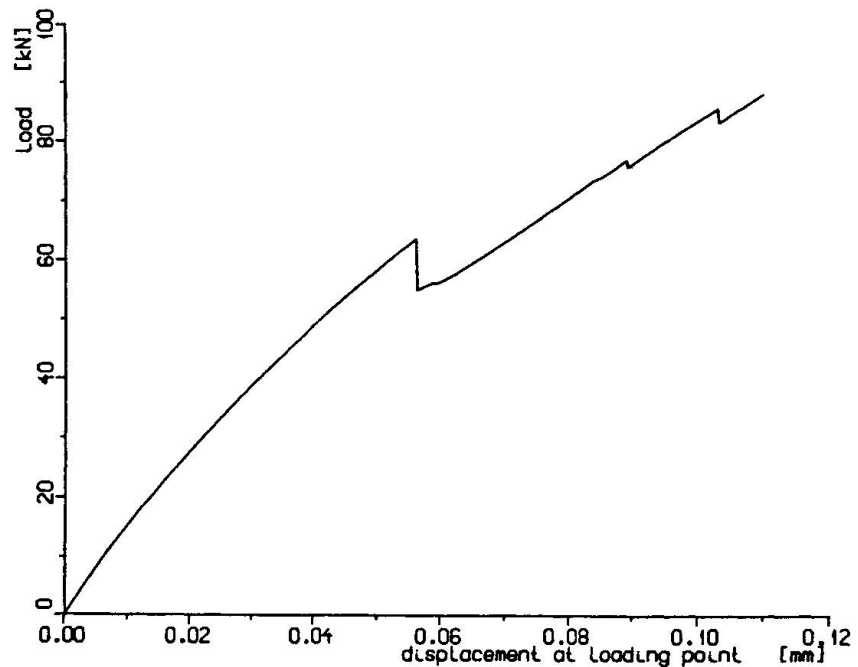
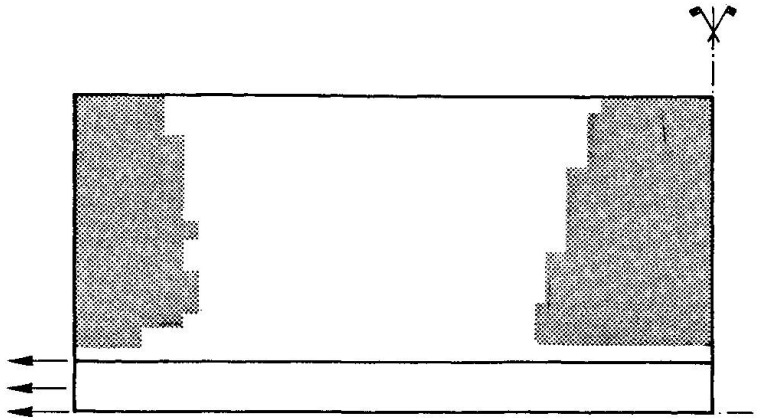


Fig. 5. Load versus end-displacement reinforcing bar.

It is interesting to note that the above phenomena not only adhere to computational predictions, but also to experimental research, where primary cracks have been repeatedly referred to as being "unstable" (e.g. Goto [13]).

## 6. LONGITUDINAL SPLITTING CRACKS

In addition to the tangential primary and secondary cracks the specimen is predicted to have longitudinal splitting cracks, as shown in Fig. 6. These cracks occur near the free surfaces of the specimen. Our experience is that the inclusion of a longitudinal cracking option is essential because this type of crack formation correctly limits the compressive strut action in the concrete cones radiating from the steel ribs.



**Fig. 6.** Region in which longitudinal (radial) splitting cracks have developed. (axi-symmetric analysis).

Because of the axi-symmetric idealization, the longitudinal cracks in Fig. 6 are smeared out over the circular cross-section. As a consequence, it was impossible to model localization of these cracks. From experiments it is known that such localizations occur, as shown in Fig. 7 which was obtained using holographic interferometry [3]. To circumvent this deficiency of the model, the specimen was re-analysed using a fully 3-dimensional configuration with a 3D-variant of the crack model. One quarter of the cross-section was modelled and perturbations of strength properties were used. Indeed, this analysis turned out to be capable of predicting a localized longitudinal splitting crack, as shown in Fig. 8.



**Fig. 7.** Localized splitting cracks at end-face, experimentally [3].

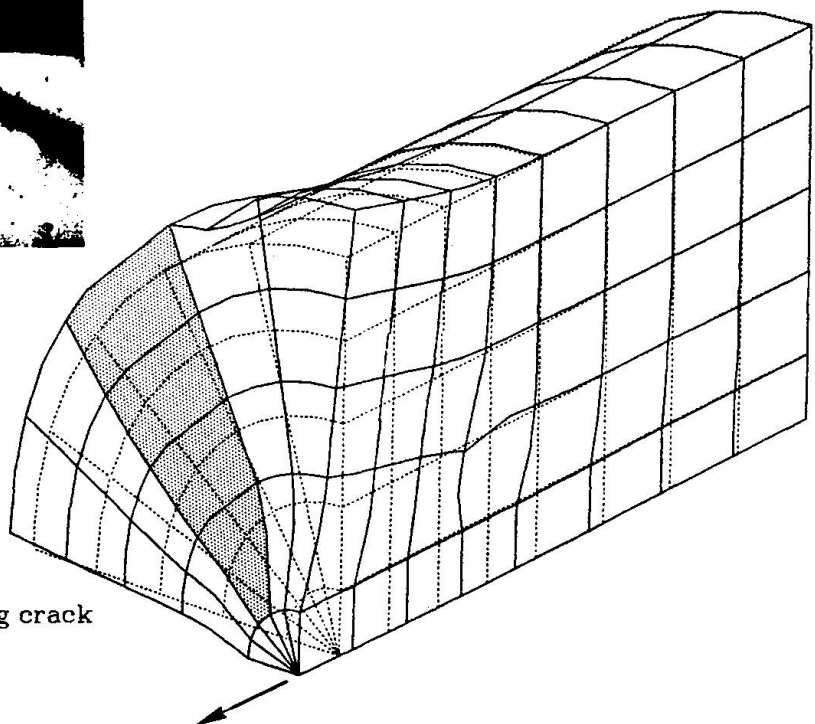


**Fig. 8.** Localized splitting crack for 3D analysis.

## 7. TAU-DELTA CURVES

Bond-slip research has been primarily directed towards the experimental determination of "tau-delta" curves, with tau being the bond shear traction and delta being the slip between concrete and reinforcement (e.g. [1,10,11]). In a similar way, the computational outcome allows such curves to be recorded, which is exemplified by Fig. 9 giving the tau-delta curve for point A some distance away from the reinforcing bar. The curve shows fair qualitative agreement with experimental measurements, which indicates that bond-slip in reinforced concrete can be at least partially explained from the underlying concrete and crack properties.

It should be noted that the location of the measuring point A does not seem to have been uniquely defined in literature, which explains some of the scatter encountered in tau-delta curves. We have also monitored the bond shear traction and the bond-slip for different points further away from the specimen end-face than point A, and the resulting curves indeed turned out to differ markedly from Fig. 9. It is therefore concluded that a tau-delta curve is a non-unique *structural* property rather than a unique *material* property. It is a challenge to investigate these effects by means of additional computational research. Together with the available experimental data this may contribute to the development of a sound bond-slip model which is independent of boundary conditions, specimen dimensions and so on. At present, attempts in this direction are being made (e.g. [12]).

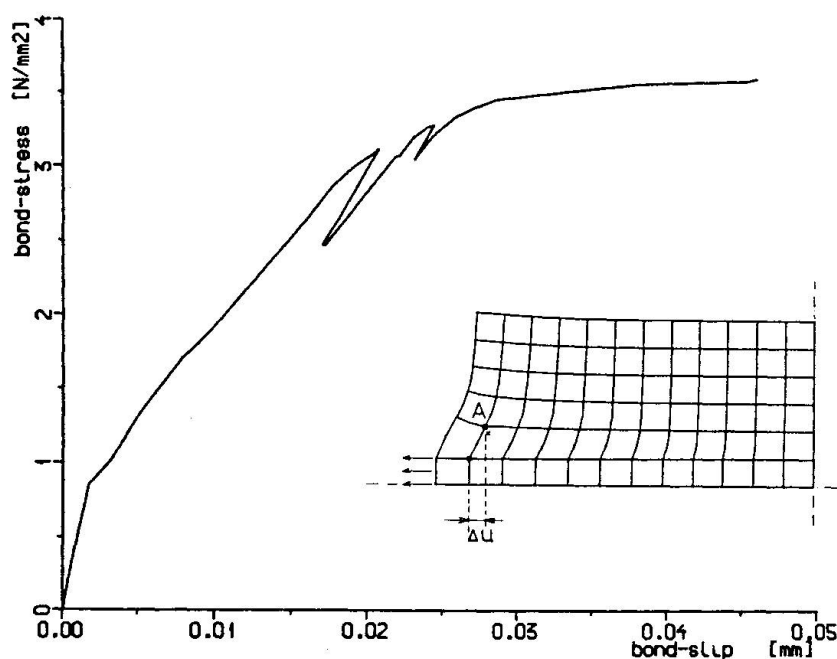


Fig. 9. Local bond-stress vs. bond-slip curve for point A.

## 8. BOND-SLIP ELEMENTS

Although bond-slip is known to be one of the dominant factors governing the non-linear behaviour of concrete structures, it appears that most practical finite element computations are still being performed under the assumption of overall perfect bond [16]. However, considering the above analyses it seems natural to lump the bond-slip contribution due to cracking into an interface element, which can be subsequently inserted for general purposes. This idea was followed by a number of researchers [16], and a particular result obtained before [19] will be reviewed here. It concerns a reinforced concrete beam which fails in bending. A bilinear bond stress-slip law was used for the interface elements and an elastic-softening model for the concrete. For details of the mesh and the material properties the reader is referred to [19].



Fig. 10 gives a comparison between the crack pattern obtained with perfect bond and the pattern obtained with bond-slip elements. The inclusion of bond-slip not only appears to enhance strain-localization, but it also yields a smooth and undistorted crack pattern in the neighbourhood of the reinforcement. In contrast, the perfect bond assumption may give rise to distortions and spurious checkerboard patterns, as was demonstrated before in e.g. [5,18]. Our experience is that the inclusion of bond-slip is essential for finding a detailed resolution of stress and strain fields in the vicinity of the reinforcement. Perfect bond tends to homogenize stress and strain fields and therefore conflicts with the delicate fracture mechanics treatment of individual cracks. In this case it may be better to resort to global tension-stiffening techniques rather than tension-softening techniques.

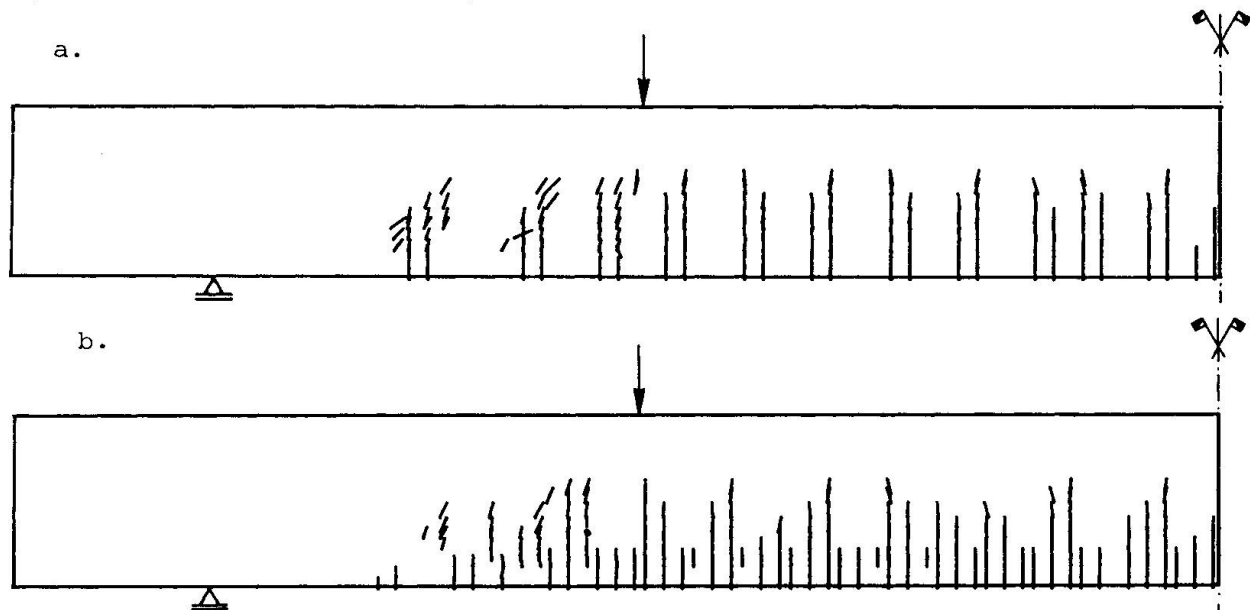


Fig. 10. Crack pattern for reinforced beam.

(a) bond-slip included, (b) overall perfect bond.

## 9. CONCLUDING REMARKS

The bond-slip phenomenon in reinforced concrete has been explained by means of computational crack models. A finite element approach using elastic-softening material laws was shown to be capable of simulating primary cracks, secondary cracks and longitudinal cracks which accompany bond-slip. The method was demonstrated to be capable of predicting "tau-delta" relationships, which can be subsequently implemented into special bond-slip interface elements for predicting the overall response of reinforced concrete structures. An example thereof has been presented.

It is remarked that similar studies have been undertaken before in 1980 by De Groot, Kusters & Monnier [9], using a less far evolved crack model and more simple solution strategies. They repeatedly reported numerical divergence and related problems, which indicates that the increase of knowledge of concrete cracking and solution procedures over the past few years has significantly enhanced the possibilities of non-linear finite element codes. Bond-slip research may take advantage of that.

## ACKNOWLEDGEMENTS

Computational results for this paper were obtained with the DIANA finite element environment of the Institute TNO for Building Materials and Structures (TNO-IBBC). Support from Mr. R. de Borst, Mr. J.C.M. Jansen, Mr. P. Nauta, Mr. F.C. de Witte and other colleagues from the DIANA-group of TNO-IBBC is gratefully acknowledged. The research was supported financially by the Netherlands Technology Foundation (STW) and by CUR-committee A26 "Concrete Mechanics".

## REFERENCES

1. BARTOS P. (Ed.), Bond in concrete. Applied Science Publishers, London, 1982.
2. BAZANT Z.P. & OH B.H., Crack band theory for fracture of concrete. RILEM Mat. and Struct. 16, No. 94, 1983, pp. 155-177.
3. BERANEK W.J., Experimental techniques for the analysis of deformation. Documentation-Page 119, Inst. TNO for Building Mat. & Struct., Delft, april 1980 (in Dutch).
4. BROMS B.B. & RAAB A., The fundamental concepts of the cracking phenomenon in reinforced concrete beams. Report 310, Dept. Struct. Eng., Cornell Univ., Ithaca, NY, 1961.
5. CRISFIELD M.A., Snap-through and snap-back response in concrete structures and the dangers of underintegration. Int. J. Num. Meth. Eng. 22, 1986, pp. 751-768.
6. DE BORST R. & NAUTA P., Non-orthogonal cracks in a smeared finite element model. Eng. Comput. 2, 1985, pp. 35-46.
7. DE BORST R., Non-linear analysis of frictional materials. Dissertation, Delft Univ. of Technology, Delft, 1986.
8. DE BORST R., Computation of post-bifurcation and post-failure behavior of strain-softening solids. Comp. & Struct. 25, No. 2, 1987, pp. 211-224.
9. DE GROOT A.K., KUSTERS G.M.A. & MONNIER Th., Numerical modelling of bond-slip behaviour. HERON 26, No. 1B, 1981.
10. DORR K., Bond behaviour of ribbed reinforcement under transverse pressure. Final Report IASS Symp. Darmstadt (G. Mehlhorn et al. Eds.), Werner-Verlag, Düsseldorf, Vol. 1, 1978, pp. 13-24.
11. GERGELY P. (Ed.), Proc. ACI Symp. Interaction between Steel and Concrete, J. Am. Concrete Inst. 76, Nos. 1 and 2, 1979.
12. GROENEVELD H., Computation of bond-experiments with DIANA. Internal Report, Inst. TNO for Building Mat. & Struct., 1986.
13. GOTO Y., Cracks formed in concrete around deformed tension bars. J. Am. Concrete Inst. 68, 1971, pp. 244-251.
14. INGRAFFEA A.R., GERSTLE W.H., GERGELY P. & SAOUMA V., Fracture mechanics of bond in reinforced concrete. J. Struct. Eng. 110, 1984, pp. 871-889.
15. LITTON R.W., A contribution to the analysis of concrete structures under cyclic loading. Dissertation, Univ. of California, Berkeley, Calif., 1974.
16. NILSON A.H. et al. (Eds.), ASCE State-of-the-Art Report on Finite Element Analysis of Reinforced Concrete. ASCE, New-York, 1982.
17. REINHARD, H.W., CORNELISSEN, H.A.W. & HORDIJK D.A., Tensile tests and failure analysis of concrete, J. Struct. Engng. 112, No. 11, 1986, pp. 2462-2477.
18. ROTS J.G., NAUTA P., KUSTERS G.M.A. & BLAAUWENDRAAD J., Smeared crack approach and fracture localization in concrete. HERON 30, No. 1, 1985.
19. ROTS, J.G., Bond-slip simulations using smeared cracks and/or interface elements. Research Report, Struct. Mech. Group, Dept. of Civil Engng., Delft Univ. of Technology, Delft, November 1985.
20. ROTS, J.G. & DE BORST R., Analysis of mixed-mode fracture in concrete, J. Engng. Mech., ASCE, 1987.



Leere Seite  
Blank page  
Page vide

## **Modelling of Bond**

Modélisation de l'adhérence  
Modellierung des Verbundes

**Mato DRAGOSAVIC**  
Civil Engineer  
TNO-IBBC  
Delft, The Netherlands



Mato Dragosavic, born 1928 in Yugoslavia, got his civil engineering degree at Delft University. Since 1961 he is a scientific-research member of IBBC-TNO, having been involved in various projects of bond research ever since. Since 1980 he has been carrying out the project presented here (physical accent), together with Hans GROENEVELD (computational accent).

### **SUMMARY**

In micro-mechanic calculations of reinforced structural concrete it is necessary to treat bond explicitly. The corresponding bond-element and bond-model are described in this paper. The model is based on theoretical considerations and experimental observations of the bond zone. Two expressions are given for the model: one in material terms as usual, the other in periferic (stress/slip) relations. Numerical implementation into finite-element-program DIANA is discussed briefly.

### **RÉSUMÉ**

Dans les calculs micro-mécaniques de béton armé, il est nécessaire de traiter l'adhérence de façon explicite. L'élément d'adhérence et le modèle y relatif sont expliqués dans l'article. Le modèle est fondé sur des considérations théoriques et des observations expérimentales dans la zone de l'adhérence. Deux expressions sont présentées pour ce modèle: l'une en des termes matériels, l'autre en relations d'adhérence (contrainte/glisement) périphériques. L'application numérique dans le programme DIANA est discuté brièvement.

### **ZUSAMMENFASSUNG**

In mikro-mechanischen Berechnungen des konstruktiven Stahlbetons muss der Verbund explizit betrachtet werden. Das betreffende Verbundelement und Verbundmodell werden in diesem Artikel beschrieben. Das Modell beruht auf theoretischen Betrachtungen und experimentellen Beobachtungen. Zwei Ausdrücke für das Modell werden vorgestellt: einmal in Materialkennwerten, wie üblich, zum anderen als Beziehung zwischen Verbundspannung aus Stabumfang und Verschiebungen. Die numerische Anwendung im Finite-Element-Programm DIANA wird kurz diskutiert.



## 1. INTRODUCTION

Bond is an essential property in reinforced structural concrete, influencing the behaviour and the bearing capacity of a structure, in particular of many crucial structural details. In macro-mechanic calculations the bond is processed implicitly: in terms of anchoring length of the reinforcement, crack width, tension stiffening, etc. In micro-mechanic calculations an explicit model is required.

In micro-mechanic finite-element-program DIANA, a simplified model has already been defined to process bond. That model expressed an axial bond stress/slip constitution, but was unable to honour relevant radial components introduced by the bond zone [1, 2]. A follow-up project of study and experiments is carried out to provide a better one.

This project started with definition of a bond zone around a reinforcing bar, with the inner diameter equal to the nominal diameter  $\varnothing$  of the bar and the outer diameter twice as large. Over a limited axial length, the bond zone is considered as a bond-element. This length is facultatif; for didactic reason it can be here assumed equal to the bar diameter. In other words: a bond-element is a hole cylinder, with the inner diameter  $\varnothing$ , the outer diameter  $2\varnothing$  (thus thickness  $0,5\varnothing$ ), and the axial length  $\varnothing$  (Figure 1).

The behaviour of a bond-element was studied:

- theoretically, based on constitution of concrete and adhesion, in particular with respect to deformation-controlled post-failure behaviour, and
- experimentally, by series of tests where the behaviour of the bond zone was measured under various practical conditions (cracking of the surrounding concrete, cyclic and sustained loading).

Some results (with an accent on the experimental ones) have already been presented in [3]. A final report on the experiments is given in [4]. Further results (with the accent on the modelling) are briefly discussed in this paper; more information will be given in a final report [5].

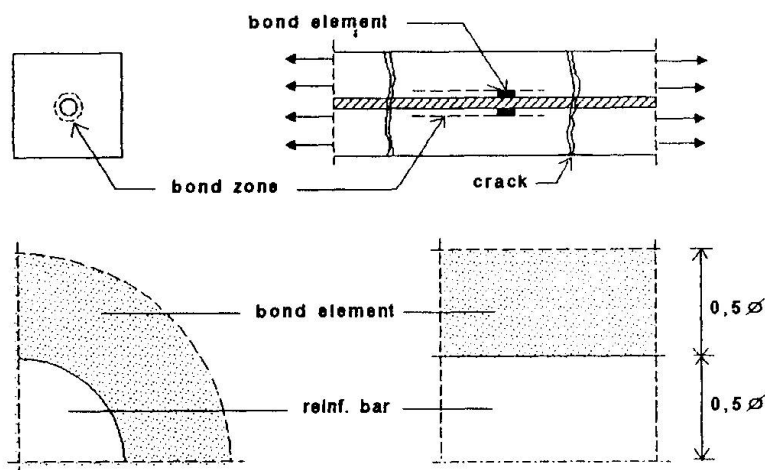


Fig. 1 Bond element

## 2. TWO VERSIONS OF MODELLING

When with respect to element mesh acceptable, the bond-element as defined in 1. will be considered as one mesh element; compatible with the bar element inside, the concrete element(s) outside and the bond elements aside.

With respect to the constitution of the bond-element, being the bond-model required, various appearances of the model are considered here, depending on the aims involved (Figure 2).

When the model is defined in material terms as for a concrete model usual, it is indicated as a "material" model. For more reasons it is also significant to define the model in periferic constitution only; than it is indicated as a "periferic" model.

bond model concept, terms	material terms	periferic terms
fysical concept	BOND MODEL fysical , material	BOND MODEL fysical , periferic
numerical concept	BOND MODEL numerical , material	BOND MODEL numerical , periferic

Fig. 2 Appearances of the bond model

The relevant periferic variables are (Figure 3):

- the axial and radial stress components ( $\tau$  and  $\sigma$  respectively) in the inner surface of the bond-element (in the outer surface  $0.5\tau$  and  $0.5\sigma$  are assumed),
- the axial and radial displacements ( $\Delta$  and  $\nabla$  respectively) of the outer surface of the bond-element with respect to the bar axis, and the bar contraction  $\nabla_s$ .

A distinction shall also be made between a "fysical" model and a "numerical" one. A fysical model aims to describe the real behaviour as close as possible, without simplifications which a numerical program might require. With these simplifications committed, the model is called the numerical model. It is evident that a numerical model is program-dependent; suggestions will be given here for DIANA.

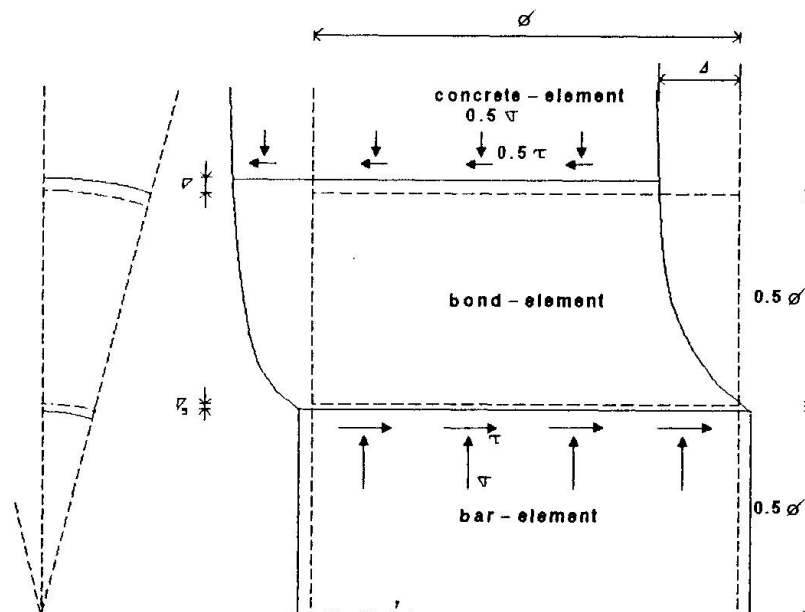


Fig. 3 Periferic stress/displacement components:  $\tau$ ,  $\sigma$ ,  $\Delta$ ,  $\nabla$



### 3. BASIC ASPECTS

From the definition of the bond-element it is obvious that it consists of concrete. The reason to require another model for bond is that attention must be paid to specific features:

- adhesion between concrete and the bar,
- stress concentrations at bar ribs,
- post-failure damages and deformations of the concrete, and
- peculiar loading in bond.

The concrete-to-steel adhesion strength is inferior to the concrete tensile strength. Thus, a bond-element behaves as an orthotropic body with a weak plane. After the adhesion failure the frictional capacity is very limited and another mechanism is necessary to resist bond of deformed bars.

After the adhesion failure, stress concentrations occur at the ribs. But the stresses are much higher and the deformation much larger there, then from the assumed uniformly distributed  $\tau$  over the rib distance would follow.

Because of the adhesion failure and the stress concentrations, post-failure stage of concrete occur at low values of  $\tau$ , too. Equilibria are still possible due to the deformation-controlled situation of the bond zone, but the damages and deformations are excessive in relation to those of pre-failure.

The loading in bond, i.e. history and level of  $\tau$ , is very different with the loading of a structural member in mind. Because of tensile axial stresses in tensile zone of a member, and the difference in radial contraction of the bar and concrete, the adhesion failure or concrete tensile failure occur at a very low (or even zero) value of  $\tau$ . Due to a (sudden) appearance of a crack,  $\tau$  suddenly becomes all values possible, depending on the crack distance.

A cyclic or sustained loading of a (cracked) member, should have a tremendous influence (cyclic of sustained creep) on the bond where post-failure stages already occurred. But this is tempered as tremendously by the deformation-controlled condition (relaxation and redistribution). Because of that, the usual fatigue or creep parameters, defined for constant (amplitudes of)  $\tau$  do not fit for bond.

More in detail the above aspects and their consequences for modelling of bond will be shown in [5].

### 4. PHYSICAL BOND-MODEL

#### 4.1 Material version

It follows from paragraph 3 that the bond-model is similar to that for concrete. The conformity is evident because of the concrete involved, the difference is understood from the specific features mentioned.

Suppose the adhesion strength is  $\xi_1$  times the concrete tensile strength, and after the adhesion failure  $\xi_2$  times the rib distance is resisting  $\tau$  (so,  $1/\xi_2$  higher stresses occur at the ribs). Such an element, with the concrete having a nominal tensile strength  $f_{ct}$  and a nominal compressive strength  $f_{cc}$ , behaves (rough about) as a concrete with a tensile strength  $\xi_1 f_{ct}$  and a compressive strength  $\xi_2 f_{cc}$ . With respect to other uncertainties even may be assumed that a bond-element behaves as concrete one with by  $\xi \ll 1.0$  reduced concrete grade. Due to uncertainties, cyclic and sustained loading can be treated the same way: by further reduction of  $\xi$ .

Reduction factors  $\xi_i$  to various parameters of the concrete model separately are being studied, comparing them with the experimental results. Up to now the bond-model can be assumed as a concrete-model with reduced concrete grade only. Values of about  $\xi = 0.4$  for a first loading and  $\xi = 0.3$  for (long time)

cyclic or sustained loading promise reasonably good results. Corresponding envelopes in Mohr-diagram and uniaxially presented deformations are drawn in Figure 4.

The variables of the bond-model remain the infinitesimal (principal) stresses and strains, as for a material model usual.

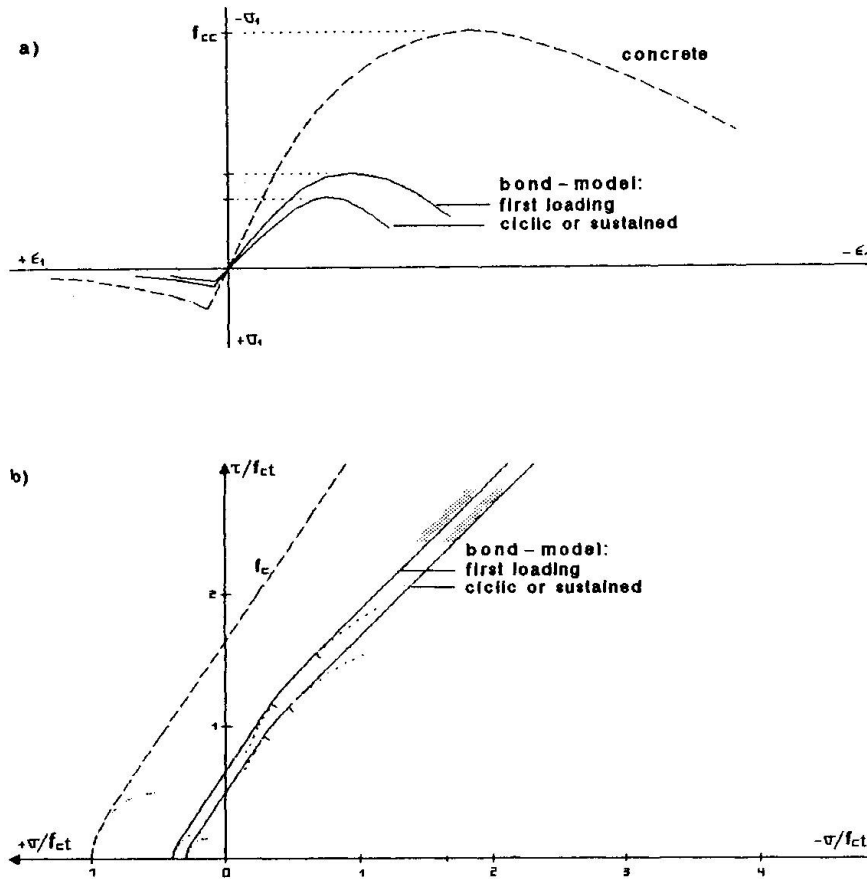


Fig. 4 Fysical bond-model, in material terms:  
a) uniaxial constitution  
b) Mohr envelop

#### 4.2 Periferic version

In principle, the periferic bond model is exactly the material one, but transformed into the periferic components as mentioned before. But, because of:

- imperfections of the material model,
- numerical complications of the transformation, and
- direct comparability of the periferic model with the experimental results,

the periferic model is here defined independently. By comparing the periferic model with the material one on one side, and with the experimental results on the other, both models can be improved, too (Figure 2).

It is easy to understand that the  $\tau/\Delta$  relation is very similar with an artan-function. So it can be written:

$$\tau = \tau_{oo} \frac{\text{artan } \Delta}{0.5 \pi} \quad \dots \dots \text{for } \nabla = 0$$

For practical values of  $\nabla$ , the  $\tau/\nabla$  relation is approximated by



$$\tau = \tau_{oo} \left( 1 - \frac{\arctan N(\nabla + \nabla_s)}{0.5 \pi} \right) \dots \dots \text{for } \Delta = \infty$$

Together for  $\tau/\Delta, \nabla$  (see Figure 5a,b):

$$\tau = \tau_{oo} \left( \frac{\arctan D\Delta}{0.5 \pi} \right) \left( 1 - \frac{\arctan N(\nabla + \nabla_s)}{0.5 \pi} \right)$$

$D$ ,  $N$  en  $\tau_{oo}$  are parameters to be defined. A first comparison with the experimental results gave  $\tau_{oo} \approx 20 \text{ N/mm}^2$  (seems very little dependent on the concrete grade, due to dominant post-failure behaviour), with  $D \approx 30 \text{ 1/mm}$  and  $N = 300 \text{ 1/mm}$  (for deformed bars). Further comparative calculations may result in better values (or will approve these ones).

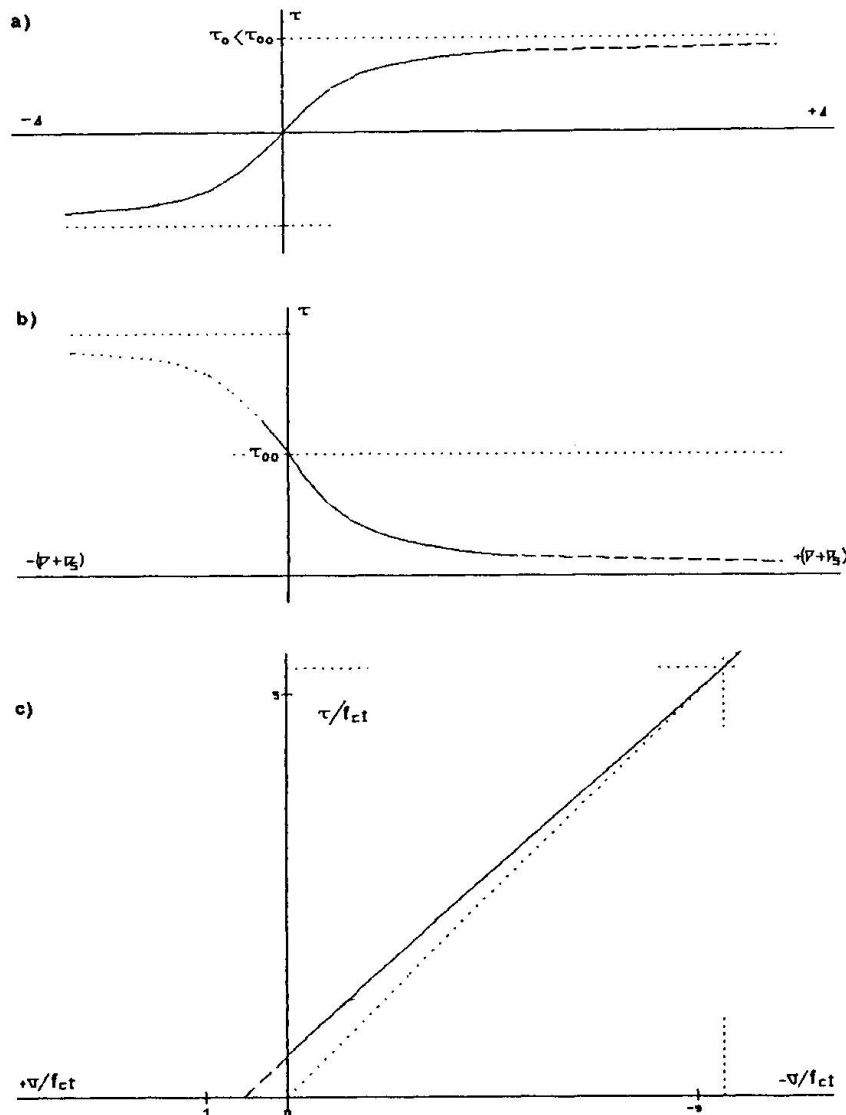


Fig. 5 Physical bond-model, in periferic terms

a)  $\tau/\Delta$     b)  $\tau/(\nabla + \nabla_s)$     c)  $\tau/\sigma$

An equation similar to  $\tau/\Delta, \nabla$  can be written for  $\sigma/\Delta, \nabla$ ; but it appeared from the theoretical and experimental results that approximately (Figure 5c):

$$\sigma = 0.5 f_{ct} - \tau \frac{f_{cc} + f_{ct}}{f_{cc}}$$

For  $\tau > f_{ct}$  can even be accepted:



$$\sigma = - \tau$$

Axial concrete stresses can be neglected within the bond zone (mind the post-failure stages when concrete tension is inferior). Tangential stresses are inferior, too (as already assumed with  $0,5 \tau$  and  $0,5 \sigma$  in the outer surface, paragraph 2). Thus, the periferic variables as applied and the parameters  $D$ ,  $N$  and  $\tau_{oo}$  are sufficient to complete the periferic model.

## 5. NUMERICAL BOND-MODEL

### 5.1 Material version

In DIANA, the parameters of the model for concrete are [2]:

- Mohr-Coulomb envelop, with a cohesion  $c$  and a friction angle  $\theta$ , both adapted for dominant compression,
- cut-off criterion with a tensile strength  $f_{ct}$ , suitable for dominant tension;
- stiffness ratios  $E$  and  $\mu$  for pre-failure
- yield rule beyond the Mohr-coulomb envelop, and softening terms beyond the cutt-off;
- additional parameters related to cracking.

An obstacle to the numerical bond-model in material terms is the incompatibility of the numerical concrete model in compression and tension. Another one is the dominance of post-failure stages, when  $E$  and  $\mu$  are irrelevant and the flow rule is not very satisfactory.

As long as the concrete model remains as now, it has not much sense to add the bond factors  $\xi_i$  very exactly. A reduction of the concrete grade as mentioned in 4.1 with  $\xi_1 \approx 0.4$  and  $\xi \approx 0.3$ , can be applied. A better definition of the post-failure constitution is necessary, however.

### 5.2 Periferic version

The fysical model can be applied, but DIANA requires an incremental approximation of the artan-functions. At a level  $\tau_k$ ,  $\sigma_k$ ,  $\Delta_k$ ,  $V_k$  follows ("d" assigns an increment):

$$\begin{array}{rcl} \tau & = & \tau_k + \begin{array}{cc} K_{11} & K_{12} \\ K_{21} & K_{22} \end{array} \cdot \begin{array}{c} d\Delta \\ dV \end{array} \\ \sigma & & \end{array}$$

The partial derivates  $K_{11} \dots K_{22}$  can easy be calculated from the equations in 4.2 because for any (artan  $X.x$ ), with  $X = D$  or  $N$ , and  $x = \Delta_k$  or  $V_k$ :

$$\frac{d(\text{artan } X.x)}{dx} = \frac{X}{1 + (X.x_k)^2}$$

Herewith the bond part of the model is defined. For the bar inside the bond element, with the axial steel stress  $\sigma_s$ , Young-modulus  $E_s$  and axial strain  $\epsilon_s$ , follows simply:

$$\sigma_s = E_s \cdot \epsilon_s$$

Evident is the relation  $\tau_k/\sigma_s$  over an incremental bar length  $d\ell$ :

$$\tau_k \cdot \pi \varnothing \cdot d\ell = d\sigma_s \cdot \frac{1}{4} \pi \varnothing^2 \quad \text{or:} \quad \tau_k = \frac{1}{4} \varnothing \cdot \frac{d\sigma_s}{d\ell}$$

For  $V_s$  holds:  $V_s = \mu_s \epsilon_s \cdot 0.5 \varnothing$

Evident is also that with the bond model as given here, the obstacles mentioned in 5.1 are passed by. Uncertainties of the values of  $D$ ,  $N$  and  $\tau_{oo}$  remain instead, and a adequat numerical bond-element is to be defined.



## 6. FINAL REMARKS

With the model(s) proposed, the parameters as the crack distance from a bond-element, eventual external compression perpendicular to the reinforcing bar etc., are avoided. Such parameters would be in contradiction with a model, too.

The results presented in this paper will be checked and improved by comparative calculation of the behaviour measured in the experiments mentioned before. Such calculations are only incidentally carried out until this paper.

It is evident that a numerical model is dependent on the capacity and sophistication of a finite-element-program. With better programs, the model(s) for bond can be improved, too. For three- or two-dimensional application a further adaption of the axissymmetrical model is required.

## REFERENCES

1. DE GROOT A.K., KUSTERS G.M.A., MONNIER Th., Numerical modelling of bond-slip behaviour. HERON, Vol. 26 - 1981 - No. 1B.
2. VAN MIER J., a.o., Examples of Non-Linear Analysis of Reinforced Concrete Structures with DIANA.  
IBBC-TNO Report No. BI- - (draft)
3. DRAGOSAVIĆ M., GROENEVELD H., Bond Model for Concrete Structures. Proceedings of the Intern. Conf. on Computer Aided Analysis and Design of Concrete Structures. Split (YU), 1984. Pineridge Press, Swansea, UK.
4. DRAGOSAVIĆ M., GROENEVELD H. Concrete Mechanics - Bond. Part II: Experimental Research. IBBC-TNO Report No. BI-87-19 (1987)
5. DRAGOSAVIĆ M. et al, Concrete Mechanics - Bond. Part I: Fysical Behaviour and Constitutive Consequences. IBBC-TNO Report No. BI-87-18 (1987) (in preparation).

## Tests of Size Effect in Pull-Out of Reinforcing Bars from Concrete

Influence de la dimension lors de l'extraction des barres d'armatures du béton  
Versuche zum Masstabseinfluss auf das Verbundverhalten von Bewehrungsstäben

### Zdenek P. BAZANT

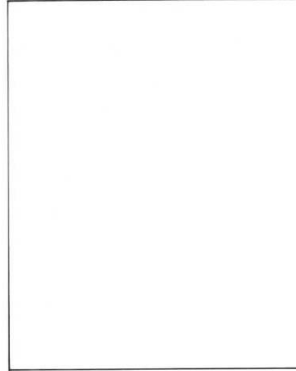
Prof. of Civil Eng.  
Northwestern University  
Evanston, IL, U.S.A.



Born and educated at Prague, Dr. Bazant joined the faculty of Northwestern University in 1969, where he has been professor since 1973 and served as Structural Engineering Coordinator and as Director of the Center for Concrete and Geomaterials.

### Siddik SENER

Visiting Scholar  
Northwestern University  
Evanston, IL, U.S.A.



### SUMMARY

The paper gives a brief preliminary report on pull-out tests of geometrically similar specimens of very different sizes. The test results indicate a significant size effect which can be described by Bazant's approximate size effect law.

### RÉSUMÉ

L'article donne un bref rapport préliminaire d'essais d'extraction de spécimen géométriquement semblables mais de dimension très différentes. Les résultats d'essais montrent un effet très important de la dimension qui peut être décrit comme la loi de l'effet de la dimension approximative de Bazant.

### ZUSAMMENFASSUNG

Das Ziel dieses Beitrags ist, einen kurzen Bericht über Ausziehversuche an geometrisch ähnlichen Probekörpern verschiedener Größe zu geben. Die Ergebnisse zeigen einen deutlichen Masstabseinfluss, der mit dem Modell von Bazant beschrieben werden kann.



### Introduction

The pull-out failure of reinforcing bars embedded in concrete is known to be a brittle failure in which the maximum load decreases after its peak value rather than remaining constant. For this type of failure, theoretical analysis shows there should be a significant size effect, such that the nominal stress at failure decreases as the specimen size increases. Although the fracture mechanics aspects of pull-out failures have been pointed out by various authors, e.g., by S. P. Shah and A. Ingraffea, and the presence of fracture mechanics type size effect have been suspected, no test data which would clearly document this effect have apparently been obtained so far. Experimental verification requires testing specimens that are geometrically similar and a brief preliminary report on such tests which were carried out at Northwestern University is the purpose of this paper.

### Tests and Their Evaluation

The test specimen was a cube with a steel bar embedded in it, parallel to one edge of the cube and sticking out at the center of one face. The sides of the cubes tested were  $d = 1.5$  in., 3 in., and 6 in., and the reinforcing bars were scaled in proportion to the size of the cubes, having nominal diameters 0.125 in., 0.25 in., and 0.5 in. respectively (1 in. = 25.4mm). The yield strength of steel was 60,000 psi (1 psi = 6895 N). The embedment lengths were 0.5 in., 1 in., and 2 in., respectively, which ensured the specimen to fail before the yielding of the bars could occur. One specimen of each size was cast from the same batch of concrete. The concrete mix ratio of water:cement:sand:-gravel was 0.6:1:2:2, by weight. The maximum gravel size was  $d_a = 0.25$  in., and the maximum sand grain size was 0.132 in. The aggregate was crushed limestone, and the sand was a siliceous river sand. The aggregate and sand were air-dried prior to mixing. Portland cement C150, of ASTM Type 1, with no admixtures, was used. Companion cylinders of 3 in. diameter and 6 in. length were cast from each batch of concrete. The mean compression strength of these cylinders after standard 28-day moist curing was  $f'_c = 6,650$  psi. The cubes were removed from their plywood forms 1 day<sup>c</sup> after casting and were subsequently cured in a moist room of relative humidity 95% and temperature 78°F for 28-days. Then the tests were made in a 60-ton Baldwin frame modified as a servo-controlled closed loop machine with an MTS controller. The ends of the steel bars were gripped in the machine, and the reaction was provided by a square sleeve made of split reinforcing bars as shown in Fig. 2, the sides of these squares being 0.5 in., 1 in., and 2 in. for the small, medium and large sizes. These reaction square sleeves were glued to concrete by epoxy shortly before testing.

Orangun et al. [1] developed for the bond strength the formula:

$$v_u = k_1 [1.22 + 3.23 C/d_b + 53d_b/\ell_d] \sqrt{f'_c} \quad (1)$$

in which  $v_c$  = 28-day bond strength in psi,  $C$  = minimum clear cover of concrete in inches,  $\ell_d$  = embedment length in inches,  $d_b$  = nominal bar diameter in inches,  $f'_c$  = standard 28-day cylinder strength of concrete in psi, and  $k_1$  = an empirical<sup>c</sup> coefficient. According to Bažant's approximate size effect law for failures due to distributed cracking, this formula may be extended as follows:

$$v_u = C_1 k_1 \left(1 + \frac{d_b}{\lambda_0 d_a}\right)^{-1/2}, \quad C_1 = (1.22 + 3.23 \frac{C}{d_b} + 53 \frac{d_b}{\ell_d}) \sqrt{f'_c} \quad (2)$$

in which  $d_a$  = the maximum size of aggregate and  $\lambda_0$  = a coefficient

characterizing the center of the transition from failures dominated by plastic limit analysis to failures dominated by linear elastic fracture mechanics. The formula of Orangun et al., yielded better agreement with the present test results than other formulas such as that of ACI [5] or of Aboona [6]. The nominal bond strength given by Eq. 2 is defined as  $v_u = T/s\ell_d$ , where  $T$  = maximum tensile force in the bar and  $s$  = nominal surface area of the reinforcing bar embedded in concrete.

Eq. 2 can be algebraically rearranged to a linear plot in which  $Y = (C_1/v_u)^2$  is plotted versus  $X = d_b/d_a$ . The present test results, listed in Table 1, are plotted in this manner in Fig. 3 (left). The optimum fit can be obtained by linear regression, and the regression parameters are given in the figure along with the coefficient of variation of the vertical deviations from the regression line  $w_{y|x}$ , the correlation coefficient  $r$ , and the coordinates  $X$  and  $Y$  of the data centroid. Based on linear regression, one may then plot the diagram of  $\log(v_u/C_1)$  versus  $\log(d_b/d_a)$ , as shown in Fig. 3 on the right. The test results in these plots represent the individual tests made. If the averages for each size are plotted, the scatter is of course considerably reduced.

### Conclusions

Despite the significant scatter of the test results, probably inevitable in this type of test, the size effect is clearly apparent. Although the test results cannot be said to validate the applicability of the size effect law, they are nevertheless described by this law adequately.

Acknowledgment. - Financial support for the theoretical research which underlies the present approach was received from U. S. Air Force Office of Scientific Research under Contract No. F49620-87-C-0030DEF with Northwestern University, monitored by Dr. Spencer T. Wu.

### References

1. ORANGUN, C. D., JIRSA, J. O., and BREEN, J. E., A Re-evaluation of Test Data on Development Length and Splices, ACI Journal, 74, pp. 114-122, 1977.
2. BAŽANT, Z. P., Size Effect in Blunt Fracture: Concrete, Rock, Metal, ASCE Journal of Engineering Mechanics, 110, pp. 518,535, 1984
3. BAŽANT, Z. P., Mechanics of Distributed Cracking, Applied Mechanics Reviews 39, May, No. 5, pp. 675-705, 1986.
4. BAŽANT, Z. P., Fracture Energy of a Heterogeneous Brittle Material and Similitude, Preprints, RILEM-SEM Int. Conf. on Fracture of Concrete and Rock, held in Houston, 1987, ed. by S. P. Shah and S. Swartz, Publ. by Soc. of Exper. Mechanics - in press, 1987.
5. ACI Committee 318, Building Code Requirements for Reinforced Concrete, ACI, Detroit, pp. 87, 1983.
6. ABOONA, L. R., Development of a Design Type Solution for Predicting the Ultimate Shear Force in Reinforced Concrete Beams, M.S. Thesis, Northwestern University, Evanston, Illinois, U.S.A., 1985.

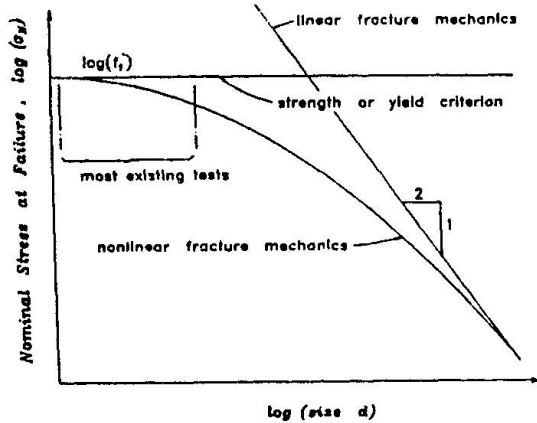


Fig. 1 - Size Effect Law

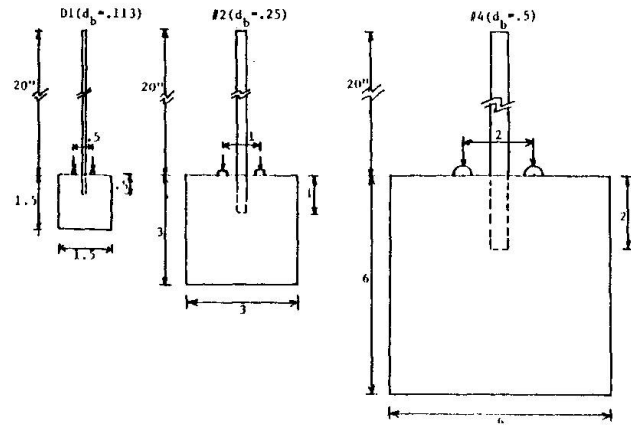


Fig. 2 - Specimen Geometry

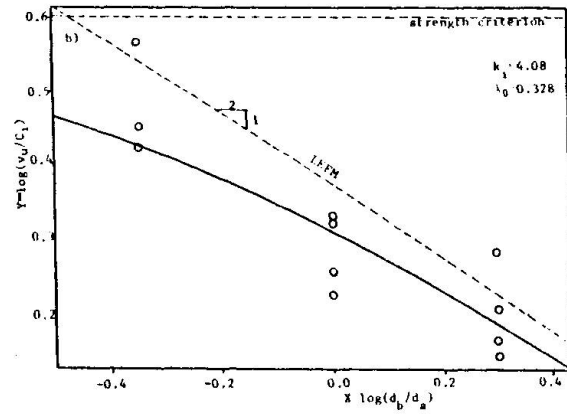
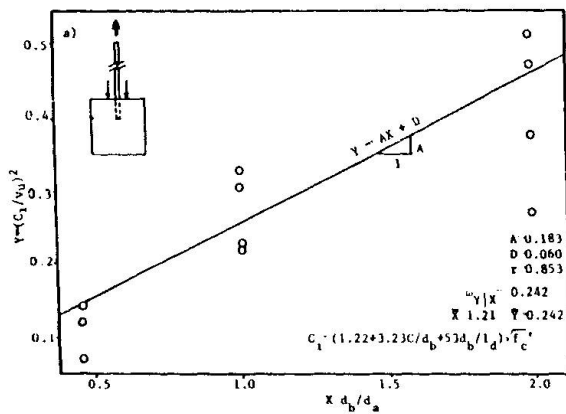


Fig. 3 - Size Effect Observed in pullout Tests

Table 1. Pullout Test Results

Beam No	$d_b$ in.	$l_d$ in.	$d_a$ in.	$f'_c$ psi	$P_u$ p
A1	.5	2.	.25	6650	5040
A2	.5	2.	.25	6650	4801
A3	.5	2.	.25	6650	5592
A4	.5	2.	.25	6650	6624
A5	.25	1.	.25	6650	1512
A6	.25	1.	.25	6650	1800
A7	.25	1.	.25	6650	1836
A8	.25	1.	.25	6650	1560
A9	.113	0.5	.25	6650	502
A10	.113	0.5	.25	6650	468
A11	.113	0.5	.25	6650	656